

FUNDAMENTAL HYDROGEN TRANSFER STUDIES IN COAL LIQUEFACTION: UNDERSTANDING THE ANSWERS AND QUESTIONS.

JA Franz, DM Camaioni, MS Alnajjar, T Autrey,* JC Linehan
Pacific Northwest Laboratory

The goal of our research is to quantitatively understand mechanisms of hydrogen transfer pathways between coal-like structures. Understanding the differences between the various hydrogen shuttling mechanisms will yield valuable insight into the fundamental chemistry of coal hydrolification. We have combined experimental model compound studies with theoretical approaches to gain a quantitative understanding of the hydrogen transfer process involving donor solvents that promote the scission of strong bonds and prevent retrograde reactions. Mechanistic modeling has been utilized for the development of a global model for predicting rates of bond scission for one-, two- and three-ring diarylmethanes. The model is tested by thermal model compound studies with labeled donor solvents. Ab initio studies have been utilized to obtain activation parameters for the novel radical hydrogen transfer pathway, and semi-empirical methods have been used to investigate trends within families of both hydrogen transfer and hydrogen abstraction pathways.

Keyword. Hydrogen Transfer.

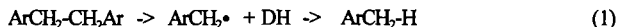
Introduction.

The classical model of coal hydrolification has evolved from assuming a passive role for hydrogen donor solvents trapping free radicals formed from the thermolysis of labile bonds, to a model that predicts an active role for hydrogen donor solvents participating in the scission of thermal stable bonds.

Fundamental approaches utilizing model compound studies have provided the impetus for evolution of this model as they provide strong evidence for the importance of hydrogen donor solvents in the scission of strong bonds.¹⁻¹⁰ The philosophy of basic research in coal hydrolification is to gain an understanding of structure-reactivity relationships. Understanding why a change in structure results in a change in reactivity will lead to an intelligent approach to improving hydrogen transfer reactions that control both bond-cleaving and bond-forming reactions.

A simplified picture of the units that hold the structures of coal together is summarized in Scheme I. Thermally labile bonds can cleave homolytically to form stabilized radicals (1); arenes linked by longer alkyl chains can decompose by β -scission following hydrogen abstraction (2); and thermal stable diarylmethanes can be cleaved by β -scission following hydrogen transfer from solvent molecules (3). The goal of our research is to understand the role of hydrogen transfer pathways from donor solvents to coal model structures that can result in the scission of this class of strong carbon-carbon bonds.

Scheme I.



The role of donor solvent in both the homolysis pathway (1), and the radical scission pathway (2) is generally to trap the incipient radicals to prevent retrograde reactions. On the other hand, the donor solvent participates in promoting the scission of strong diarylmethane carbon-carbon bonds (3).

Several of the model compound studies have focused on identifying and quantifying the competing mechanisms that have been postulated to be important hydrogen transfer steps between aromatic structures. The common denominator of all these works is the dynamic exchange of hydrogen transfer reactions between arene structures. This is not surprising, given the early studies that showed deuterium from labeled solvents can be transferred throughout the coal.^{11,12} Hydrogen from the donor solvent, hydrogen gas, and/or from the coal itself is thoroughly scrambled throughout the system. The goal of liquefaction is to have the hydrogen scramble to the appropriate locations to promote bond scission. Thus a fundamental understanding of what controls the hydrogen transfer pathways, from a donor to a receptor, can provide beneficial guidance for experimental process development.

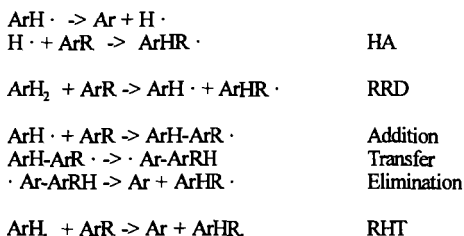
Consideration of both the kinetic and the thermodynamic factors of hydrogen transfer to diarylmethanes leads to two simple questions. *Is hydrogen transfer to the ipso position a necessary requirement for bond scission?* Direct hydrogen transfer to the ipso position of a

substituted aromatic ring is both sterically and thermodynamically less favorable than addition alpha to the substituent. *How can we break only the bonds we want to break?* We want to cleave diarylmethanes and leave the alkyl groups alone to increase the formation of liquids and prevent the formation of light gases.

Thermolysis Questions.

Fortunately, an understanding of structure reactivity relationships can lead to some insight to answer these questions. McMillen and Malhotra^{1d} have reviewed four possible non-ionic mechanisms of hydrogen transfer that could be responsible for the scission of diarylmethane C-C bonds, summarized in Scheme II: (1) free hydrogen atoms (HA), a two-step pathway involving the scission of a hydrogen from a hydroaryl solvent radical followed by addition to the diarylmethane; (2) reverse radical disproportionation (RRD), involving the transfer of a hydrogen atom from the dihydroarene solvent; (3) addition transfer elimination (ATE), involving a multi-step addition of the solvent radical to the diarylmethane, followed by hydrogen transfer, and elimination; and (4) radical hydrogen transfer (RHT), involving the transfer of a hydrogen atom from a solvent radical to the diarylmethane.

Scheme II.



Clearly, there is no lack of potential pathways to make diarylmethanes look like weak bonds; an understanding is needed of what pathways are important under a given set of conditions, and how to optimize the transfer of hydrogens to the appropriate positions that promote bond scission.

These free radical hydrogen transfer pathways are separated into two categories. Because of the product-like (RRD) and reactant-like (HA) nature of the transition state of these two pathways, the activation parameters can be estimated. On the other hand, because of the intermediacy of the transition state of the RHT and ATE hydrogen transfer pathways, the activation parameters are not so easily predicted. For these hydrogen transfer reactions, computational approaches will be necessary to investigate the structure reactivity relationships.¹³ The difficulty in assigning a barrier to these pathways has resulted in some debate as to the significance of the RHT hypothesis.^{4d,e} Although the RHT pathway was suggested to operate under a limited set of conditions,^{1c} it has often been invoked as an important pathway for the scission of a large variety of conditions.¹⁴

Regardless of the pathway, hydrogen is transferred to the arene structures in the presence of donor solvents. In our current work we are concerned with the fate of adding hydrogen, by any pathway, to a nonipso position and if this can result in the scission of strong carbon-carbon bonds.

We have attempted to devise an experiment to quantify how many hydrogen transfers are required to induce bond scission in diarylmethanes. Thermolysis studies of 1,2'-dinaphthylmethane (1,2'-DNNM) in a perdeuterated donor solvent mixture, dihydroanthracene(d_{12})/anthracene(d_{10}) results in the scission of the diarylmethane to yield both naphthalene and methylnaphthalene (ca. 5% conversion, 100 minutes, 400°C). Analysis of the products and reactants by GCMS reveals several interesting observations. The most obvious is the reduction of anthracene by the dihydroanthracene as we previously observed.^{4f} Reduction of the 1,2,3,4-positions of anthracene occurs by a series of RRD and hydrogen abstraction steps. Analysis of the remaining 1,2'-DNNM shows more deuterium incorporation into the diarylmethane than was expected from exchange at the benzylic positions. Therefore, hydrogen (labeled as deuterium in this experiment) is transferred to the arene rings of the diarylmethane from the donor solvent without the scission of any carbon-carbon bonds. Analysis of the product naphthalene shows that, on average, more than one deuterium is incorporated in the naphthalene cleavage product. If direct ipso hydrogen transfer was the only operating hydrogen transfer mechanism, only one deuterium would have been detected in the naphthalene product. However, because more than one deuterium per scission product was detected, something in addition to ipso displacement must be competing.

This should not be surprising if the probability of adding a hydrogen to the ipso

position is considered versus the probability of adding a hydrogen to any other position. To illustrate, consider the case of hydrogen transfer by a reasonably selective mechanism (RRD or RHT), to the ipso position of diphenylmethane. Several factors reduce the probability of ipso hydrogen addition (Figure I). One source of discrimination between the ipso and nonipso positions is the steric bulk of the donor, either a dihydroarene (RRD) or a dihydroaryl radical (RHT). Additional thermodynamic factors are against ipso addition. The adduct formed by addition of hydrogen γ or β to the ipso position yields a tertiary radical that is more stable than the secondary radical formed by addition to the ipso position. Finally, consideration of statistics suggests there are several more nonipso positions, 2,3,4,5 or 6-position. A conservative estimate suggests addition of a hydrogen atom to the nonipso position will occur ten times more frequently than addition to the ipso position. It could even be argued that there is a higher probability that the "less selective" free hydrogen atom pathway will more likely add to the ipso position of a substituted arene because this pathway is least affected by the steric or the thermodynamic constraints.

If, as we have argued, the hydrogen is more likely to be transferred to a nonipso position, to understand the complete picture we must understand the fate of the nonipso hydrogen addition adduct. A more complete scheme of hydrogen transfer, including the addition to nonipso positions, is shown in Figure II. Depending on the reaction conditions, there are two possibilities for the nonipso adduct. At higher donor (dihydroarene) concentrations it is possible to trap the adduct. Abstraction from the solvent to produce a reduced arene, path (e), results in lowering the bond energy of the diarylmethane to the ballpark of the thermally labile diarylethane type bonds.¹⁵ At low donor (dihydroarene) concentration, scission of the hydrogen atom will dominate the radical termination pathways. In this case, although we may not have started with a free hydrogen atom, we may need to account for free hydrogen atom chemistry for a complete picture.

If the nonipso adduct is not trapped something must be done to make efficient use of the hydrogen atom donated from the solvent mixture. One approach that has been used at low donor concentrations is to add a good hydrogen atom trap. Hydrogen atoms add to arenes more readily than abstract from dihydroarenes.^{1b,7a} If anthracene is added to the reaction mixture, the hydrogen can be stored for re-use. Radical disproportionation of the hydroaryl radical generates a dihydroarene donor solvent.

It remains to be determined if the excess deuterium observed in the 1,2'-DNM thermolysis studies is due to bond scission by the reduction (pathways b, e, and f) shown in Figure II or due to inefficient hydrogen transfer (pathways b, and d, or RHT, in competing with ipso addition). Answering these questions will provide additional insight into improving the efficiency of hydrogen transfer and best utilization of hydrogen donor solvents.

Catalysis Questions.

It has also been reported that iron catalysts promote the scission of diarylmethanes at lower temperatures than thermal solvent pathways.¹⁶ We have found that alkylarenes are reduced with no apparent loss of the alkyl group. For example, we have found that the catalytic reaction of 1-methylnaphthalene in dihydrophenanthrene results in the formation of 1-methyltetralin; no naphthalene scission product was detected. On the other hand under the same reaction conditions, 1-benzyl naphthalene and its derivatives yield only scission products with no apparent reduction.

Studies investigating the relative rates of bond scission in a series of diphenylmethanes suggest a mechanism that may involve either a two-step, electron transfer followed by reduction of the radical center or a proton transfer from the catalyst to the substituted arene (Figure III). A mechanism involving ipso hydrogen transfer from the catalyst to the arene is tentatively ruled out because we would have observed little selectivity between the scission of either the methyl or the benzyl substituent if hydrogen transfer to the ipso position were rate limiting.¹⁷ We prefer the two-step electron transfer-hydrogen atom transfer mechanism to generate the intermediate cation. Compared to the radical mechanism where the loss of a benzyl radical is only ca. 10 kcal/mol lower than loss of methyl radical, there is a substantial difference in scission by the ionic pathway. The difference between scission of a benzyl cation and scission of a methyl cation could be as high as 70 kcal/mol.

Wei et al.¹⁸ have compared the decomposition of dinaphylethane with the decomposition of dinaphthylethane. A similar mechanism could be proposed for their hydrocracking catalyst. They only detected scission when a stabilized leaving group was present, e.g. dinaphthylmethane to naphthalene and methylnaphthalene. In the absence of a stabilized leaving group, e.g. dinaphthylethane, they observed mostly reduction, tetralin derivatives.

Conclusions.

Hydrogen transfer is extremely dynamic. It is hard to imagine a magic catalyst or smart solvent that can selectively add a hydrogen to the ipso position of a diarylmethane.

Hydrogen will be transferred by one or more pathways several times before finally promoting scission of strong bonds.

We have attempted to answer two questions in our recent work: (1) Is hydrogen transfer to the ipso position a necessary requirement for bond scission? and (2) How can we break only the bonds we want to break? We have outlined a multistep hydrogen transfer scheme, given the high probability of nonipso hydrogen transfer, that results in a reduced diarylmethane adduct capable of homolytic scission at coal liquefaction temperatures. Both the catalytic ionic pathways and the thermal reduction pathways permit the scission of stabilized benzylic radicals without requiring the scission of less stabilized alkanes.

ACKNOWLEDGMENT

This work was supported by the U.S. Department of Energy, Office of Basic Energy Research, Chemical Sciences Division, Process and Techniques Branch under Contract DE-AC06-76RLO 1830.

References

- (a) Malhotra, R.; McMillen, D. F. *Energy Fuels* **1990**, *4*, 184. (b) Malhotra, R.; McMillen, D. F. *Energy Fuels* **1993**, *7*, 227. (c) McMillen, D. F.; Malhotra, R.; Tse, D. S. *Energy Fuels* **1991**, *5*, 179. (d) McMillen, D. F.; Malhotra, R.; Chang, S.-J.; Fleming, R. H.; Ogier, W. C.; Nigenda, S. E. *Fuel* **1987**, *66*, 889.
- Derbyshire, F. J.; Varghese, P.; Whitehurst, D. D. *Fuel*, **1982**, *61*, 859.
- Stein, S. E. *Acc. Chem. Res.* **1991**, *24*, 350. (b) Manka, M. J., S. E. *J. Phys. Chem.* **1984**, *88*, 5914. (c) Billmers, R.; Griffith, L. L.; Stein, S. E. *J. Phys. Chem.* **1986**, *90*, 517.
- (a) Autrey, T.; Franz, J. A.; Camaioni, D. M.; Ferris, K.; Gleicher, G. J. *Coal Science Proceedings, International Conference on Coal Science*, **1991**, 239. (b) Autrey, T.; Gleicher, G. J.; Camaioni, D. M.; Franz, J. A. *Am Chem Soc, Div Fuel Chem. Preprints*, **1991**, (36)2, 521. (c) Autrey, T.; Franz, J. A. *Am Chem Soc, Div Fuel Chem. Preprints*, **1990**, (35)2, 381. (d) Camaioni, D. M.; Autrey, S. T.; Franz, J. A., *J. Phys. Chem.*, **1993**, *97*, 5791 (e) Autrey, S. T.; Camaioni, D. M.; Ferris, K.; Franz, J. A. *Coal Science Proceedings, International Conference on Coal Science*, **1993**, 336. (f) Autrey, T. Albom-Cleveland, E., Camaioni, D. M. Franz, J. A. *Fuel Preprints* **1994**, 39(3) 627-631. (g) Autrey, S. T.; Albom-Cleveland, E.; Camaioni, D. M.; Franz, J. A. submitted to *Energy Fuels*.
- Dabbagh, H. A.; Shi, B.; Davis, B. H.; Hughes, C. G. *Energy Fuels* **1994**, *8*, 219
- (a) Smith, C. M. and Savage, P. E. *Energy Fuels* **1994**, *8*, 545. (b) Smith, C. M. and Savage, P. E. *Energy Fuels* **1992**, *6*, 195.
- (a) Owens, R. M.; Curtis, C. W. *Energy Fuels* **1994**, *8*, 823. (b) Bedell, M. W.; Curtis, C. W. *Energy Fuels* **1991**, *5*, 469.
- Buchanan, A. C.; Britt, P. F. *Energy Fuels* **1993**, *7*, 331. Poutsma, M. L. *Energy Fuels* **1990**, *4*, 113.
- Kofi, O. -A.; Stock, L. M.; Zabransky, *Energy Fuels* **1988**, *2*, 511.
- Bockrath, B. C.; Schroeder, K. T.; Smith, M. R. *Energy Fuels* **1989**, *3*, 268.
- King, H. -H.; Stock, L. M. *Fuel*, **1982**, *61*, 257.
- Franz, J. A.; Camaioni, D. M. *Fuel*, **1984**, *63*, 990.
- (a) Franz, J. A.; Ferris, K. F.; Camaioni, D. M.; Autrey, S. T. *Energy Fuels* **1994**, *8*, 1016. (b) Camaioni, D.M., Autrey, S. T. Franz, J. A. *Fuel Preprints* **1994**, 39(3) 638-642. Washington, D.C., August 21-26 **1994**. (c) Donald M. Camaioni, S. Torn Autrey, and James A. Franz. *Petroleum Preprints* August 21-26, **1994** - Washington, DC
- (a) Sakanishi, K.; Towata, A.; Mochida, I.; Sasaki, M. *Energy Fuels* **1988**, *2*, 802. (b) Schulten, H.-R.; Marz, A.; Dyla, P.; Simmleit, N.; Muller, R. *Energy Fuels* **1989**, *3*, 481. (c) Shin, S.-C.; Baldwin, R. M.; Miller, R. L. *Energy Fuels* **1989**, *3*, 71. (d) Dhawan, J. C.; Legendre, R. C.; Posey, S. M. *Fuel* **1991**, *70*, 30. (e) Fixari, B.; Le Perchec, P. *Fuel* **1989**, *68*, 218.
- The BDE of 1,2'-DNN is ca. 80 kcal/mol. The BDE of the reduced 1,2'-DNN is ca. 52 kcal/mol. This results in a half live of xx minutes at 400 C.
- Linehan, J.C., Matson, D.W.; Darab, J.G.; Autrey, S.T.; Franz, J.A.; and Camaioni, D.C., Presented at the American Chemical Society Meeting in Washington, D.C., August 21-26 **1994**.
- An alternative explanation for the apparent selectivity between the methyl and benzyl radical scission would be if the surface stabilized the ipso adduct enough to slow down the rate of methyl radical scission so that back hydrogen atom transfer to the catalytic surface would compete.
- Wei, X.-Y.; Ogata, E.; Futamura, S.; Kamiya, Y. *Fuel Processing Technology*, **1990**, *26*, 135.

FIGURE I.

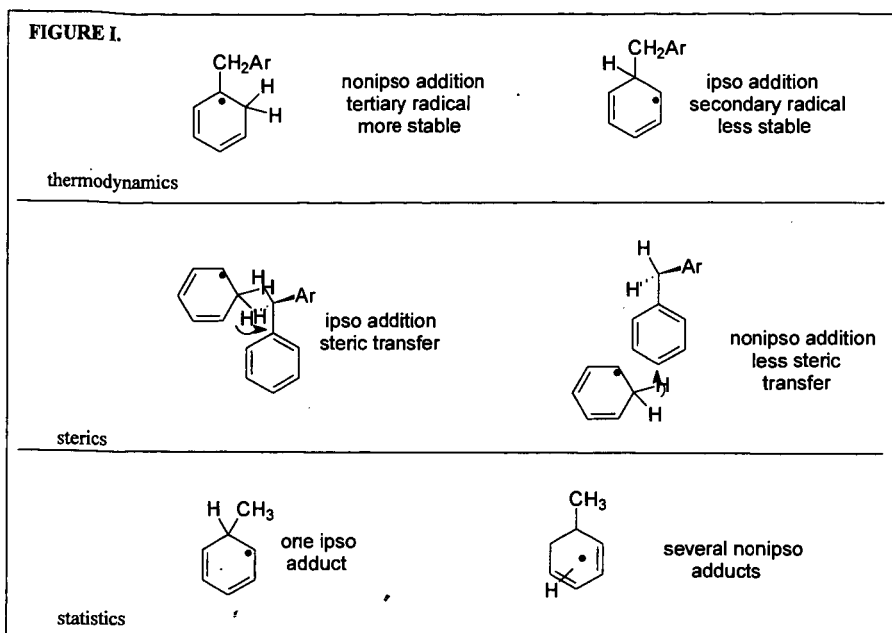


FIGURE II

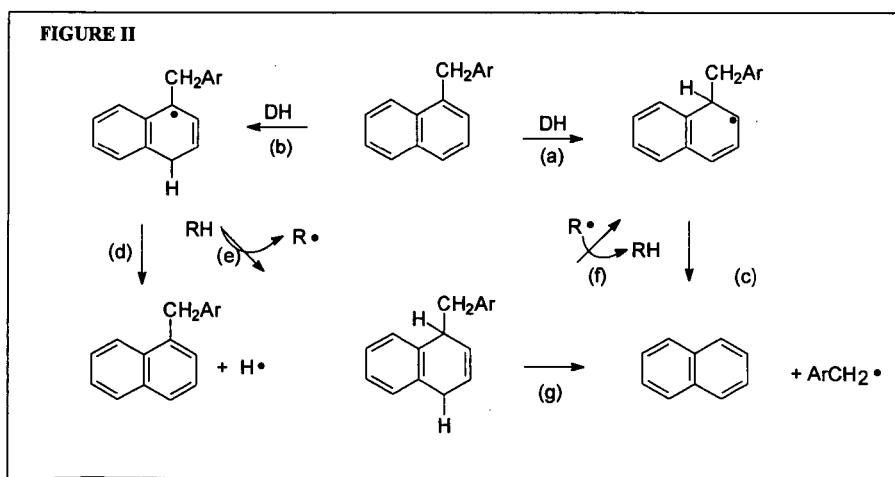
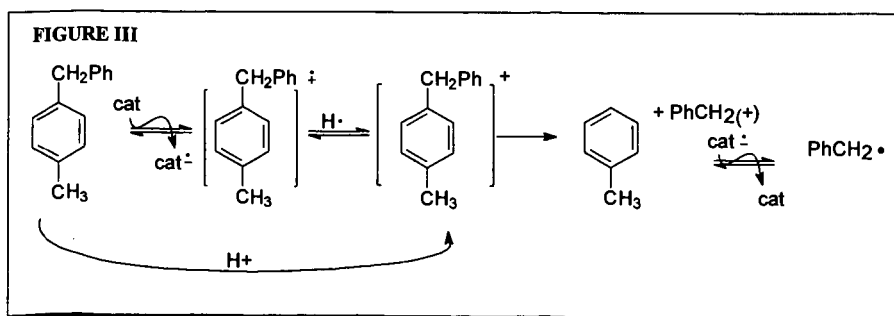


FIGURE III



HYDROGEN TRANSFER DURING DIRECT COAL LIQUEFACTION WITHOUT HYDROGEN OVERPRESSURE

Geoff M. Kimber
Center for Applied Energy Research
3572 Iron Works Pike
University of Kentucky
Lexington, KY 40511-8433
(formerly with British Coal 1965-93)

Keywords: Coal, Liquefaction, Solvent

INTRODUCTION

Since the late 1960s, the British Coal Corp. has been concerned with the development of two coal liquefaction processes, both of which depend upon a liquid solvent at low pressure to extract the coal. The first of these was designed to extract a precursor suitable for the manufacture of electrode coke (1). In the second process, the extraction step was modified by the introduction of hydrogen donors into the solvent and employed as the first stage of a two-stage liquefaction process (Liquid Solvent Extraction, LSE) whose net products were distillate transportation fuels(2). Pilot plants of about a ton per day for each process have been built and operated successfully.

This paper is primarily concerned with the LSE process and will consider the significance and effects of solvent hydrogen transfer on the performance and operation of the first stage, its influence on subsequent process steps, and on the overall process.

LSE PROCESS DESCRIPTION - A schematic of the process is shown in Fig. 1

Coal is dried, pulverised and slurried with a hydrogen donor recycle solvent. This solvent, which is a mixture of aromatic and hydroaromatic hydrocarbons is produced within the process and is entirely coal-derived.

The coal slurry is pressurised to 20 bar, preheated to the reaction temperature of 410°C and fed to a digester in which up to 95% of the coal is dissolved. The use of elevated pressure in this stage is to prevent undue vapourisation of the solvent. During the digestion process, hydrogen is donated from the solvent to the coal structure as it breaks up, stabilizing the lower molecular weight fragments and preventing retrograde reactions. The resulting digest contains dissolved coal ('extract'), residual coal solids and the mineral matter originally present in the coal.

The digest is cooled to 300°C, reduced in pressure and filtered to remove the mineral matter and the undissolved coal. The filtrate, which is solids free and has a very low ash content (i.e. less than 0.1%), is known as 'coal extract solution'. The filter cake is washed with a low boiling fraction of the solvent, which displaces the coal extract solution trapped within the voidage of the cake. Residual wash oil is in turn recovered by vacuum drying the filter cake. This washing and drying procedure minimises the loss of extract and solvent with the cake.

In the second stage, the coal extract solution is pressurised, typically to 210 bar, mixed with hydrogen gas, preheated and fed to ebullated bed hydrocracking reactors. These reactors operate at temperatures in the range 400 - 450°C. Standard oil industry heavy residuum hydrosulphurisation catalysts can be used.

The product from hydrocracking is distilled to recover the recycle solvent (boiling above 300°C) and to give three main products: LPG, naphtha (boiling below 180°C) and mid-distillate (boiling range 180-300°C). In addition, a by-product pitch stream (nominally boiling above 500°C) is taken off, although most of the material in this boiling range is recycled as part of the solvent. The remaining by-product streams contain light hydrocarbon gases, predominantly methane and ethane, and heterogases. An appreciable proportion of the oxygen originally present in the coal is emitted as CO₂, reducing the overall hydrogen consumption.

In addition to the process configuration described above, several alternative processing options have been examined which may be appropriate under some economic conditions. The pitch by-product may be fed to a delayed coker to recover additional distillate and to produce a premium grade coke which is an excellent starting material for the preparation of graphites and carbon electrodes. The rehydrogenation of the recycle solvent to replace the hydrogen donated to the coal during digestion may be carried out in a separate reactor on a fraction of the solvent recovered by distillation from the filtrate. Finally, if saturated hydrocarbon (which are not hydrogen donors) build up in the solvent, a portion of the solvent may be fed to a 'satcracker' in which the saturated compounds are thermally cracked to lower boiling liquids and gases.

The main features of the LSE press which distinguish it from other two-stage direct liquefaction processes are therefore the low pressure first stage and the removal of solids by filtration, both of which reduce capital costs. All coals except anthracites can be processed, although some energy penalties are associated with the use of lignites.

Over the past 25 years the British Coal team of workers have built up expertise in the various unit operations, based partly on practical plant experience and partly on more fundamental laboratory studies, mainly but not solely with bituminous coals.

Although it became apparent that each stage of the process affected the others, this paper will now concentrate on the dissolving (or extraction) stage and in particular upon hydrogen transfer and retrogressive reactions therein.

The aim of most current coal liquefaction processes is to produce distillate fuels in high yield and thus much effort has been expended in trying to minimise retrogressive reactions which eventually lead to coke formation. In contrast in the Electrode-coke process (Fig. 2) maximising the quantity and quality of extract derived coke was the aim; it is thus relevant to review some of the studies of this process to assist understanding of retrogressive reactions.

DIGEST VISCOSITY

Studies of the changes in slurry viscosity during extraction process have shown that, regardless of temperature and solvent to coal ratio, the same general time-dependent pattern was observed(3) for bituminous coals, Fig. 3.

Starting from the slurry (A) there is an initial rise in viscosity (Zone B) which takes place rapidly at all temperatures studied, reaching a peak within a few minutes, possibly within seconds. The peak viscosity in this region is at least five times that of the untreated slurry. Comparison between the physical state of a slurry which consists of 20-25% rigid particles in a fluid (anthracene oil), with that of a digest of large polymers, formed from the dissolving coal, and intimately dispersed within the same fluid, enables the change in viscosity during digestion to be appreciated. It is also known that the coal particles themselves swell prior to their disintegration and this phenomenon too is thought to contribute to the viscosity increase.

After reaching a peak the digest viscosity drops continuously over a period of about 20-30 mins., (Zone C) a time found to be independent of temperature. However, the minimum viscosity reached at the end of this zone was temperature dependent, the higher the temperature the lower the viscosity. This result indicates more extensive depolymerisation at higher digestion temperatures. Furthermore, the initial rate of viscosity reduction was found to increase markedly with increasing temperature. At the lower temperatures studied, the rates of change of viscosity over the same viscosity range can be compared reasonably accurately. The time taken for the viscosity to decrease from 2.5 to 1.5 cP (measured at 250°C) was 20 mins. at 380°C and 5 mins. at 400°C. From these data, an activation energy of 60 kcal/g mole can be calculated, indicative of a process involving the breaking of moderately strong chemical bonds. It was considered that the kinetics observed were the result of the combination of several reactions; however, the cause of the reduction of viscosity is attributed solely to the depolymerisation (i.e. reduction in molecular weight) of the coal extract.

After about an hour (total time) the viscosity then begins to increase again, independently of temperature (Zone D). The polymerisation reactions occurring in this zone which cause the second viscosity increase obviously started before the end of depolymerisation stage and it is the combination of these two reactions that controls the position of the minimum at the end of Zone C. The rate of increase of viscosity is not greatly enhanced between 380 and 420°C indicating a low activation energy for this process which is consistent with polymerisation reactions.

Finally, the reduction in viscosity during Zone E is explained as due to the growth of mesophase in which the higher molecular weight coal extract components are concentrated into many small areas within the remaining fluid which is of lower viscosity, hence creating a relatively dilute continuous phase. The end of zone E represents a slurry of coal extract mesophase in solvent.

It was also realised that beyond Zone E and under exceptionally severe conditions, the whole digest, including solvent, would coke and thus the viscosity would rise again; this is definitely a zone that there is every incentive to avoid in any process!

Assessments of coke properties confirmed that by employing digestion times much longer than those necessary for extraction there was some improvement in final coke quality, presumably because the mesophase liquid crystals had been given time to grow before coking became too advanced. Such a step is now known to be essential to the formation of graphitisable carbons.

The quinoline insolubility of the slurry or digest shows an initial reduction (Zone B & C) as the coal is taken into solution. It then rises in a manner consistent with a 2nd order, polymerisation reaction, i.e. more rapidly as the solvent to coal ratio is reduced.

Several lessons and questions which are relevant to coal liquefaction in general emerge from these studies of the electrode coke process.

(1) to minimise retrogressive reactions then, all other things being equal, a high solvent to coal ratio should be used. In process development there are often strong pressures from design and costing engineers to reduce the amount of recycling solvent which has to be handled for a given coal throughout. Those applying these pressures rarely take into account that small improvements in the overall conversion to liquid products could be more valuable than the cost of increasing the solvent to coal ratio substantially; this is particularly so if the solvent doesn't all have to be distilled.

(2) similarly, as soon as extract is taken into solution it should be diluted with the other liquid phase (i.e. solvent). Presumably small particle size would help in this respect as would agitation that resulted in high particle Reynolds numbers.

(3) if conditions that produce some coking occur somewhere in the process after extraction (e.g. in preheaters or on catalyst surfaces) then is it better to allow those species that polymerise more rapidly to do so in the extraction stage, as they will be removed along with the residual coal (e.g. in the subsequent solid-liquid separation step-by filtration in the LSE process), thereby increasing the life of catalyst and preheater.

(4) what is the relative ease of hydrogenation and hydrocracking of molecules that are truly in solution compared with the same species arranged in mesophase liquid crystals? In other words is the irreversible point in inevitable coke formation at the liquid crystal ordering stage or after further polymerisation?

(5) the presence of hydrogen, either as H_2 or in hydrogen donor solvents, is well known to reduce the rate of carbon (strictly it is still only a semi-coke) deposition on catalysts and to dramatically reduce viscosity. This does not mean however that hydrogenated extract doesn't polymerise or form mesophase. Indeed given suitable conditions, bigger and better liquid crystals can be formed resulting in excellent needlecoke because the hydrogenation reactions help to remove some of the heteratoms thereby reducing the steric hindrance to perfect alignment of aromatic layers. This is desirable if coke is aimed to be the end product but the formation of micron-sized mesophase spheres in the digester, perhaps due to imperfect mixing or just exhaustion of hydrogen donors in the solvent, could cause problems in the solids separation stage due to their plastic deformable nature.

LIQUEFACTION AND H-TRANSFER

The term coal conversion is used with different meanings and can cause confusion. It can mean the extent of conversion into liquid and gas, a secondary solvent, quinoline, cresol or THF, being used to determine the insoluble organic matter (IOM). In other cases conversion is defined as the yield of liquids boiling below say 450°C.

It is reasonably well accepted that little coal will dissolve in most solvents below 200°C (although work with NMP with and without CS_2 can give extensive solution of some coals (4)). However at the temperature of most liquefaction processes, i.e. around 400°C, the majority of most coals (except anthracite) can be taken into solution. Using phenanthrene or recycled anthracene oil without hydrogen over pressure, up to 80% of bituminous coal appears in the filtrate. Much of the extract can be insoluble in THF and some, even insoluble in quinoline which implies molecular weights in excess of 2000.

Is this conversion? One could say that the coal has merely been reconstituted without its mineral matter and some of its macerals, e.g. the inertinite. To support this is the fact that the softening point of such pure extracts is over 300°C, i.e. only a little lower than of the coal; it takes the addition of about 2% hydrogen to reduce the extract softening point to around 150°C (e.g. as in the SRCI process or as has been observed when using tetralin as solvent(7)).

The amount of coal taken into solution is enhanced by the presence of hydrogen, either from a donor solvent or as gas. The molecular weight of the extract is reduced as has just been mentioned, but whether this is instantaneous or caused by a sequential reaction is open to discussion. Is it that the extra taken into solution when donor hydrogen is available is due to the avoidance of very rapid retrogressive reactions by some thermally produced radicals, as is perhaps suggested by recent work, (5), or is it that the hydrogen is contributing directly to the dissolution reaction?

Whatever the reason, there is no doubt that more coal appears in solution when hydrogen donors are available, and that for a given coal the extra conversion is dependent on the amount of hydrogen transferred. Thus it seems reasonable to assume, for the purposes of process development and reactor design, that until proven otherwise, there are two discrete steps i.e. coal solution and liquid

phase hydrocracking of the coal extract. In some process designs it all happens in a single reactor whereas in LSE for example the first reactor is primarily for dissolution and the second reactor for hydrocracking. Specific conditions can be chosen for each reactor, rather than the necessary compromise when a single reactor system is used.

COAL EXTRACT QUALITY

Increasing extraction to the maximum possible extent would be desirable if all the coal molecules taken into solution were identical. But bearing in mind the variation of the hydrogen contents of the macerals that make up the bulk coal (e.g. 7% in liptinite to under 4% in some of the so-called "inertinite" that can be dissolved) this is unlikely to be even an approximation of the truth. In deciding whether maximum extraction is the optimum the most important properties of the coal extract molecules are their rate of hydrocracking and the consequent yield of desired product (i.e. gasoline rather than gas), and the hydrogen consumption needed to achieve this. Whilst experimental measurements of the amount of coal going into solution can be quickly and accurately determined experimentally the same cannot be said for the hydrocracking properties just mentioned.

In studies (6) of the reactivities of coal extract solutions, samples were made from different coal preparation plant streams, in which both mineral matter and maceral distribution varied. Although extents of dissolution varied with inertinite content by as much as 10% differences in hydrocracking could not be distinguished because of experimental reproducibility. These coal samples were far from pure macerals so it cannot be concluded yet that there aren't differences between maceral extracts from the same coal. All other things being equal, which is rarely the case in coal science, one would consider it desirable to have a high liptinite content in the feed coal because of its high hydrogen content. Unfortunately a lot of this hydrogen is in alkyl groups and probably results in higher yields of less valuable gaseous products.

Overall it should be mentioned that advantage could be taken of modern dense media coal cleaning technology in a commercial liquefaction plant with the clean fraction going to liquefaction and the middlings fraction to utilities. As shifts of small amounts in the extent of conversion (whether it be to extract or to finished products) have very significant effects on plant economics, it is still desirable to do further work quantifying the magnitude of any difference between maceral extracts.

SOLVENT QUALITY

In any plant the solvent has to be recycled and thus although useful studies can be performed using pure compounds and doing once-through i.e. single cycle, experiments, eventually recycle must be studied. Whilst the biggest change takes place over the first recycle, changes can continue for a long time as the solvent becomes truly process-derived. Monitoring and then controlling these changes can present a big challenge.

In experimental work a 102% solvent mass recovery should be aimed for to allow for overall losses that are likely to occur even with the most rigorous housekeeping. If there is a slight solvent surplus then it can be converted into lighter products without much effect on plant economics; if there is a solvent deficit the process isn't viable.

In most liquefaction processes, including LSE, the process solvent consists of material boiling above 300°C and includes some above 500°C (which is extract that is not 'converted' during hydrocracking). From studies with various pure compounds and process solvents particularly hydrogenated phenanthrenes and pyrenes, it has been concluded that di- and tetra hydro-derivatives are the most reactive and that they are preferred to the extensively hydrogenated species (i.e. the hexa or octa hydro-derivatives). It is thus preferable to have every molecule hydrogenated to a small extent rather than a few heavily hydrogenated species. As the maximum amount of hydrogen transferred to the coal during extraction is only 1 - 2% of coal, this represents less than 1% on a solvent basis (equivalent to that which can be provided by di-hydro species of aromatics boiling between 300°C and 500°C). The levels of hydrogen donors should of course be above the minimum so that even at the end of the digestion stage there is still a concentration of hydrogen donors available to cap further radicals that are formed by continuing albeit slower thermal cracking of coal and extract molecules.

Not all the hydrogen donated by the solvent reaches the desired recipient, i.e. the extract. About a tenth ends up as molecular hydrogen and represents an inefficiency. If catalyst is present it merely enhances solvent dehydrogenation and thus increases the yields of IOM and hydrogen. The hope that catalyst might enable hydrogen to be released from the solvent at an appropriate rate to match coal radical formation has not been realised. This is perhaps yet another indication of the difficulty of having coal, hydrogen and catalyst and maybe solvent simultaneously present at the same reaction site.

MONITORING RECYCLE SOLVENT

While proton NMR has proved extremely useful for monitoring short term changes during dehydrogenation (i.e. extraction) and rehydrogenation it is, however, not so good for estimating absolute concentrations of hydroaromatics. Generally, the use of NMR is limited for tracking if there is the possibility of slow long term changes in the solvent composition. In plant operations another reason to aim for 102% solvent recovery is as a way of limiting the build up of undesirable trace species in the solvent.

It is also necessary to have a method of determining if the extracting power of the solvent is decreasing *before* the point is reached when plant filter cake yields rise and other operational problems due to insufficient hydrogen transfer set in. Remedial action, e.g. by increasing hydrogenation or sat-cracking, would then have a chance of recovering the situation.

Early in the LSE project this need was especially pressing in convincing a potential sponsor that the LSE process could cope with their lignite and the author promised to devise such a test in time for the recycle run due to take place a few months later. So was born SDI, or Solvent Dissolving Index to give it its full name.

The test (7) involves diluting by a known amount a sample of the solvent with a non-hydrogen donor (usually, but not necessarily, naphthalene) so that there are less hydrogen donors than required to ensure maximum extraction when a mini-bomb test is done with this diluted process solvent.

Tests for the particular coals in use with well characterised solvents enable calibration graphs to be constructed Fig. 4 & 5 in which nominally an SDI of 10 means that there are just enough hydrogen donors to ensure maximal extraction

In practice it was found that a certain margin above this minimum was desirable, i.e. 3 or 4 but the SDI fulfilled its major objective of enabling the changes in recycle solvent donor properties to be confidently monitored. As with testing coals the best test of a solvent is to perform an actual extraction.

Non distillate fractions of recycle solvents (i.e. pitch) were shown to be excellent solvents, those with softening points under 200°C having SDI's greater than 10. Such pitches have little hydrogen donor ability and contain plenty of coke precursors so that when used alone extractions reduce if severe digestion conditions are used (i.e. above 420°C). However, as they are normally diluted with distillate material this is rarely a problem and keeping a certain level of pitch in the recycling solvent became generally regarded as advantageous, helping to keep everything in solution, being intermediate in MW etc between solvent and extract, but compatible with both.

At almost the opposite extreme are the light end saturates which are basically not hydrogen donors. The alkanes which usually represent about a quarter of these are thought to be formed directly from the coal. For Point of Ayr coal this is about 0.3% coal (8) whereas for the lignites it can be much greater. The others, i.e. naphthenes, are formed in the hydrotreatment stage and once formed are difficult to dehydrogenate, as was found in many attempts to achieve this catalytically. It was found, however, that if only aromatics and naphthenes were present then the naphthenes did donate some hydrogen and extraction levels above that expected from the pure aromatics were achieved (9). However, hydroaromatics donate their hydrogen first and the naphthenes later, if at all. Various ways of trying to utilise this interesting effect were considered but none proved practical.

CONCLUSION

In order to achieve maximal coal extractions and to minimise retrogressive reactions of the extract, the recycle solvent must be in adequate supply and of the right properties, i.e. good hydrogen donor ability as well as good physical solvent properties.

It is noteworthy that during the 70's and 80's other liquefaction process developers, who without exception used high pressure hydrogen during extraction, gradually came round to the view that having a 'good' solvent present made their processes work better, i.e. "hydrogen donor species could reach places that ordinary (gaseous) hydrogen could not".

REFERENCES

1. G.M. Kimber, 11th Pittsburgh Int. Coal Conf., Sept. 1994. pp. 188-192.
2. S.A. Moore, G.M. Kimber and M.D. Gray, 8th Pittsburgh Int. Coal Conf. Oct. 1991, pp. 747-52.
3. G.O. Davies, F.J. Derbyshire and G.M. Kimber, ECE Symposium Proceedings Dusseldorf, Jan. 1976.
4. J.W. Zondlo, P.G. Stansberry, and A.H. Stiller, 15th Pittsburgh Int. Coal Conf., Sept. 1993, pp. 379-383.

5. J.R. Gibbins, G.M. Kimber, A. F. Gaines, and R. Kandiyoti, Fuel 70 (3), March 1991, pp. 380-5.
6. S.A. Moore, EEC Final Repot, En3V oo54 UK(H) 1991.
7. G.M. Kimber, and G.O. Davies, I. Chem. Eng. Symposium, Energy Production Processes, London, April 1988, pp. 14.
8. G.M. Kimber, Proc. Int. Conf. Coal Science, 1985, pp. 106-9.
9. J.W. Clarke, T.D. Rantell and C.E. Snape, Fuel 63 (1984) pp. 1476-78.

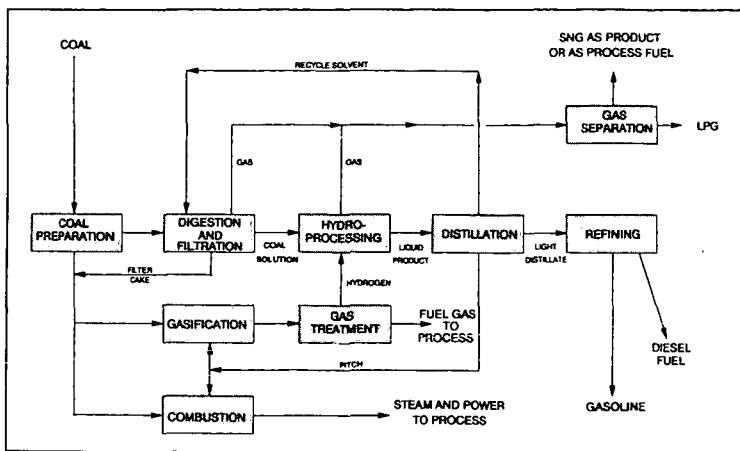


Figure 1 The Liquid Solvent Extraction Process

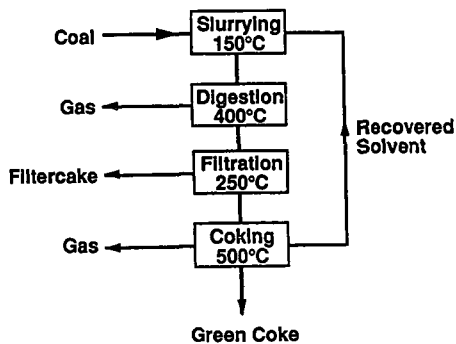


Figure 2. Electrode Coke Process

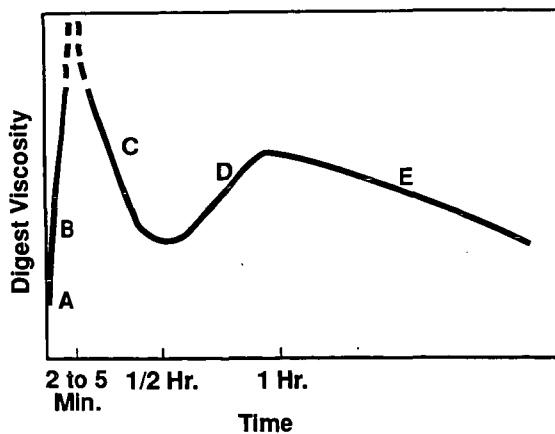


Figure 3. Effect of Digestion Time on Viscosity

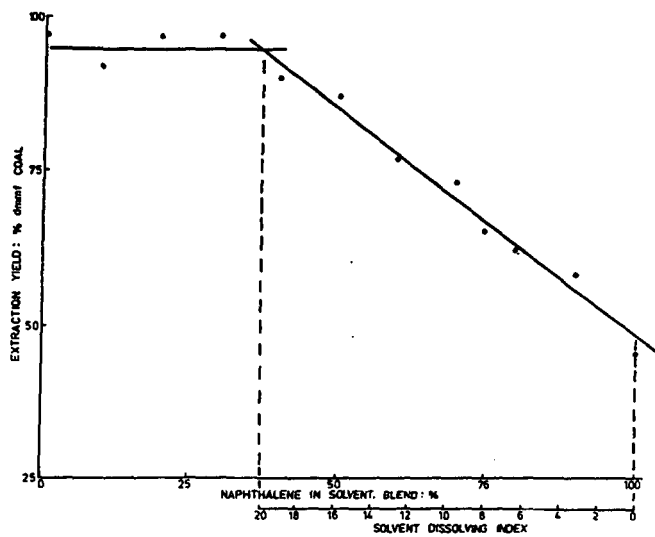


FIGURE 4. SDI CALIBRATION FOR THE LIGNITE

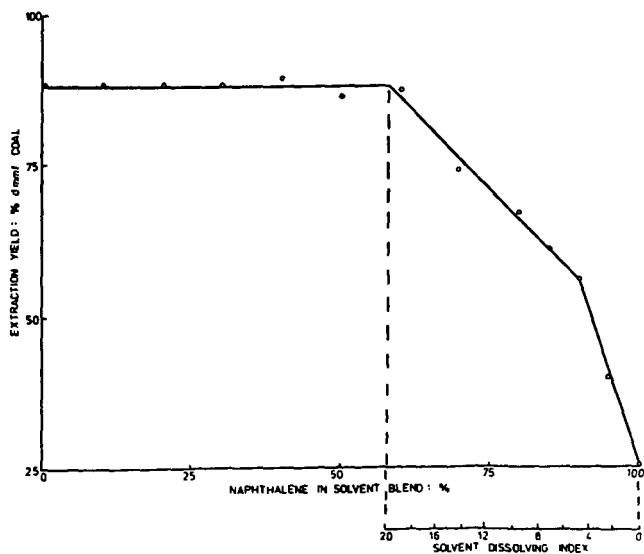


FIGURE 5. SDI CALIBRATION FOR THE BITUMINOUS COAL

THE ROLE OF RECYCLE OIL IN DIRECT COAL LIQUEFACTION PROCESS DEVELOPMENT

F. P. Burke
CONSOL Inc., Research and Development
4000 Brownsville Road
Library, PA 15102

Keywords: Coal, Liquefaction, Recycle Oil

ABSTRACT

It has long been recognized that use of a recycle oil is a convenient and perhaps necessary feature of a practical direct coal liquefaction process. The recycle oil performs a number of important functions. It serves as a vehicle to convey coal into the liquefaction reactor and products from the reactor. It is a medium for mass and heat transfer among the solid, liquid, and gaseous components of the reactor inventory. It can act as a reactant or intermediate in the liquefaction process. Therefore, the nature of the recycle oil can have a determining effect on process configuration and performance, and the characterization of recycle oil composition and chemistry has been the subject of considerable interest. This paper discusses recycle oil characterization and its influence on the industrial development of coal liquefaction technology.

EARLY GERMAN TECHNOLOGY

In the early 1900s, Bergius used a petroleum "heavy oil" as a vehicle to slurry coal in batch and continuous unit liquefaction experiments.¹ The German technology utilized in the 1940s was based on further development of the Bergius-Pier process, and utilized high temperature and pressure (750 K, 300 atm) and an inexpensive (and relatively low-activity) iron oxide catalyst (red mud) in a liquid (slurry) phase reactor. The recycle solvent was a distillate from gas phase hydrogenation of the slurry-phase reactor overheads. Although this technology anticipated the dispersed catalysts under development today, the process employed a high reaction severity, rather than seeking to minimize reaction severity by improved catalyst or solvent activity.

CONSOL SYNTHETIC FUELS PROCESS

In the 1960s, Consolidation Coal Company sought to improve on the performance of the German liquefaction technology by utilizing more active supported-metal hydrogenation catalysts in fixed bed reactors. To overcome catalyst deactivation problems, the coal dissolution and catalytic conversion steps of the two-stage CONSOL Synthetic Fuels (CSF) process² were separated by an interstage deashing step. The coal dissolution step was non-catalytic, and carried out at a relatively low temperature to produce an "extract" suitable for catalytic upgrading. The process was designed to produce a distillate hydrogen donor solvent in the second stage.³ The role of recycle solvent was explored in bench-scale tests supported by mass spectrometric and ¹H- and ¹³C- nuclear magnetic resonance analysis of the recycle solvent.⁴ This work showed that, although the recycle oil increased in molecular weight upon recycle, it became less aromatic (Table I). Recycle oil characterization was used to indicate the approach of the process operation to steady state, and revealed the important effect of solvent characteristics on other process operations, particularly solids separation.

SOLVENT REFINED COAL PROCESS

In the mid-1970s, interest grew in the development of a process to convert coal into a fuel-oil substitute for use in oil-fired electric utility boilers. The Solvent Refined Coal (SRC) process was piloted by Gulf at Ft. Lewis, WA,⁵ and by Southern Company Services (and later EPRI) at Wilsonville, AL.⁶ The objective of the process was to solubilize coal under hydrogen, but in a non-catalytic reaction, so that the ash-forming minerals, including pyrite, could be removed by physical means. Some organic sulfur removal also was expected. The deashed products were distilled to yield the SRC product and a distillate recycle solvent. One objective was to produce only enough distillate to remain in solvent balance. This would ensure the maximum yield of the desired SRC product, while minimizing hydrogen consumption.

Because the SRC process was designed as a thermal distillate-recycle process (perhaps aided by the catalytic effect of the coal ash), the operating conditions had to be chosen to achieve satisfactory coal conversion, SRC yield, and desulfurization, while maintaining an adequate yield of recycle solvent. In practice, this proved to be a difficult balance to achieve. Higher reaction temperature

tended to improve coal conversion and reduce SRC sulfur, but increased gas make at the expense of recycle solvent and SRC yield.⁷

In addition, because the distillate yield in the SRC process was low (typically, less than 5 wt % MAF coal), the replacement rate of the recycle solvent was low, and changes in solvent composition over time were difficult to assess. Because it was run at relatively constant conditions for long periods of time, and because of its size, the 6 TPD Wilsonville pilot plant became an excellent source of coal liquefaction data and samples for assessing the longer term effects of coal liquefaction on recycle oil quality. In 1977 and 1978, we obtained three relatively large and representative samples of the recycle distillate from Wilsonville for use in bench-scale liquefaction research. Some of the solvents were catalytically hydrogenated in a bench scale unit. These samples were the basis for an extensive characterization effort,⁸ which included ¹H-NMR and ¹⁹F-NMR (for phenol determination following derivatization), GC/MS, FIMS, reverse phase liquid chromatography, and empirical tests of solvent quality.

As the distillate recycle solvent in the SRC-I process evolved (Tables 2 and 3), it increased in total hydrogen content, but was lower in molecular weight, more aliphatic, and more phenolic. The practical consequence, as indicated by the microautoclave solvent quality tests, was that it lost hydrogen donating ability. The underlying structural changes were revealed by the NMR and FIMS data. The overall decrease in aromaticity was totally at the expense of the condensed aromatic structures; uncondensed aromatic hydrogen actually increased. The increase in aliphatic hydrogen appeared in both cyclic and aliphatic regions initially, but as the solvent further evolved, the cyclic aliphatic hydrogen decreased. The apparent loss of hydrogen donor activity under kinetic control (KIN test) was associated with the decrease in condensed aromatic hydrogen. The decrease in conversions at the EQ conditions, designed to measure donor hydrogen content, was associated with the ratio of cyclic to alkyl aliphatic hydrogen. FIMS analysis (Figures 1 and 2) showed that catalytic hydrogenation of the more aromatic solvent (8/77 sample) converted aromatics to hydroaromatics and improved solvent quality. Although solvent evolution increased hydrogen content (and alkyl tetralin) by an amount similar to catalytic hydrogenation, it decreased the concentration the aromatics and the corresponding hydroaromatics.

SELECTIVE RECYCLE AS AN IMPROVED LIQUEFACTION OPTION

The research on the evolution of the SRC distillate solvent clearly indicated the importance of higher molecular weight hydroaromatics as hydrogen donor solvent components. However, the low distillate yield in the SRC process provided few options for improving the situation, leading to the conclusion that recycle of vacuum bottoms, or a vacuum-bottoms component, would be necessary to maintain solvent quality⁹. This concept was tested by separating the SRC into "light" and "heavy" components and using the light SRC (LSRC) as a component of the recycle solvent in bench scale and microautoclave liquefaction experiments.⁹ In the microautoclave experiments, the LSRC was added to the Wilsonville solvent sample during 4/78. The addition of LSRC improved solvent quality at the "kinetic" conditions (Table 4), but decreased conversion at the "Equilibrium" conditions indicating that it contained active hydrogen donors, but not in large concentration. The improvement seen at the EQ conditions under hydrogen pressure were somewhat surprising and the degree of improvement was remarkable. These results clearly indicated that this non-distillate oil was capable of facilitating gas phase hydrogen utilization for coal conversion in the absence of an added catalyst.

THE ROLE OF PARAFFINS IN SOLVENT QUALITY

Not all solvent quality effects can be ascribed to the activity and concentration of hydrogen donors. There has been a tendency to think in terms of "average" structures in describing coal and coal products. However, coal liquids are much more heterogeneous than an average structure might suggest. One feature of solvent quality that the FIMS data failed to reveal was the concentration of straight-chain and branched paraffinic components in recycle oils; FIMS is relatively insensitive to paraffins. In one case, the recycle distillate from a Wilsonville ITSL run with subbituminous coal produced a 47% wax yield upon ketone dewaxing; 12 wt% of the recycle distillate consisted of n-paraffins.¹⁰ Simple physical removal of this wax fraction increased the solvent quality in the EQ microautoclave test from 71% to 87%.

SINGLE STAGE CATALYTIC LIQUEFACTION

The H-Coal process employs a single ebullated-bed reactor to convert coal to distillate products. In PDU and pilot plant development, a relatively high reaction temperature (825-840 °F) and resid recycle were used to achieve high

conversion while minimizing reactor residence size. Compared to the SRC process, H-Coal approached a steady state recycle composition quickly¹¹ because of the higher turnover rate of the recycle oil components. The process solvent increased in aromaticity and phenolic -OH content with run time, corresponding to catalyst deactivation. Characterization of the recycle oil during the PDU runs was used to determine the approach steady state composition. The results indicated that the residual recycle components, particularly the preasphaltenes, reached a consistent composition relatively early in the run, but the degree of hydrogenation of the recycle distillate decreased throughout the run. This suggested that the rate of catalyst deactivation was relatively more rapid for the larger resid molecules than for the smaller distillate molecules.

INTEGRATED TWO-STAGE LIQUEFACTION

The idea of separating the coal dissolution and catalytic upgrading functions was further evaluated in the development of the Lummus Integrated Two-Stage Liquefaction Process. The Lummus ITSL process used a short-residence-time (SRT), high temperature (850 °F) coal conversion stage, followed by anti-solvent deashing. The deashed oil was converted to liquid products in an expanded-bed catalytic reactor (LC-Finer), which was operated at a lower temperature (720-750 °F) than the H-Coal reactor. The recycle oil from the second stage contained distillate and unconverted resid. Because of the thermal first stage, solvent quality was an important factor in process performance. The reactor configuration also provided an opportunity to investigate the separate roles of catalytic and thermal reactions in direct liquefaction. Comparison of the process oil characteristics in the Lummus ITSL process to those from single-stage H-Coal process were particularly instructive.¹² The results showed that hydrogen donor solvent quality was a key to coal conversion in the SRT first stage, and promoted thermal resid conversion in both stages. The lower temperature of the LC-Finer, compared to that of the H-Coal reactor, produced a more highly hydrogenated resid that underwent considerable thermal conversion in the short-residence-time, high temperature first stage. The temperature of the LC-Finer also contributed to the maintenance of distillate solvent quality by minimizing cracking and isomerization reactions that could remove hydroaromatics and their precursors (Table 5). Most of the development work for ITSL was done with mid-continent bituminous coals, and a limitation was revealed when the process was applied to subbituminous coals. Despite the good solvent quality, coal conversion was kinetically limited, necessitating the use of a longer residence time in the first stage reactor. The Lummus work also demonstrated that interstage deashing was not necessary to maintain catalyst activity, because catalyst activity loss was primarily a function of carbon deposition, which occurred regardless of the presence of solids.

Extensive further development work was done on the two-stage process at the Wilsonville pilot plant, in a wide variety of configurations.¹³ The Wilsonville operators concluded that it was necessary to use a dispersed iron oxide catalyst to achieve satisfactory conversions with subbituminous coal. Essentially all of the work with bituminous coals was done with two ebullated-bed catalytic reactors in series. Moderate reactor temperatures, low space velocities, and high catalyst replacement rates (relative to H-Coal), and close-coupling of reactor stages (i.e., no interstage deashing) resulted in improved yields, product quality, and selectivity. The use of a critical solvent deasher (ROSE-SR) unit allowed considerable flexibility in controlling recycle composition. The plant employed high recycle rates of heavy distillate (>750 °F IBP), resid, and unconverted coal to reduce the required per-pass conversion level. The result of these changes was a departure from the original two-stage concept of separating thermal coal dissolution and resid upgrading. Most of the feed to the first stage was recycled resid.

Subsequent work has shown that the insoluble organic matter (IOM) in the recycle resid from Wilsonville is reactive for further conversion, and methods to improve solvent quality by dewaxing and hydrogenation are being evaluated.¹⁴ This work will provide the opportunity to better define the role of recycle solvent quality in the current generation of two stage catalytic liquefaction processes.

CONCLUSIONS

This paper was not intended as a comprehensive review of the subject of recycle oil chemistry, but rather as a perspective on the changing perception of the role of recycle or solvent-mediated phenomena in direct liquefaction process development. In the earlier US work on direct liquefaction, the goal of separating the thermal coal dissolution and catalytic distillate production steps led to process configurations that relied on hydrogen donor solvents for coal conversion. Research showed that the distillate recycle solvents which evolved under mostly

thermal conditions were poor hydrogen donors, but that selective recycle of higher molecular weight components improved both donor content and activity. When it was realized that interstage deashing had little practical benefit, conversion of the coal in a catalytic first stage diminished the perceived need for an active hydrogen donor solvent. For subbituminous coals, donor solvent hydrogen alone did not appear to be adequate to achieve satisfactory conversions, leading to the use of dispersed catalysts, greater reaction severity, and solids recycle. However, the improvements of two-stage liquefaction came at the expense of reduced space velocity and increased catalyst usage. Current research is looking to replace the supported-catalyst systems with dispersed catalysts that offer higher selectivity and activity, while avoiding the capital cost of a supported-catalyst system. As this research and development continues, it will be important to understand and evaluate the role of vehicle solvents, and to look for opportunities to utilize solvent-mediated reactions as part of an overall strategy for reducing the cost of producing liquids from coal.

ACKNOWLEDGEMENT

The work discussed in this paper was supported by the CONSOL Inc., the U.S. Department of Energy, and the Electric Power Research Institute. I am indebted to many colleagues, particularly those at CONSOL, DOE, EPRI, HRI, the Wilsonville Advanced Liquefaction Test Facility, and Lummus-Crest for their contributions to this work.

1. Bergius, F., German Patent No. 301,231, August 9, 1913.
2. Gorin, E.; Kulik, C. J.; Lebowitz, H. E. *Ind. Eng. Chem. Process Des. Dev.* 1977, 16 95.
3. Curran, G. P.; Struck, R. T.; Gorin, E. *Ind. Eng. Chem. Process Des. Dev.* 1967, 6, 166.
4. Kleinpeter, J. A.; Jones, D. C.; Dudd, P. J.; Burke, F. P. *Ind. Eng. Chem. Process Des. Dev.* 1979, 18, 535.
5. Pittsburgh and Midway Coal, "Solvent Refined Coal (SRC) Process, Annual Report, 1976", DOE Report FE-496-131 (May 1977).
6. Lewis, H. E.; Weber, W. H.; Usnick, G. B.; Hollenack, W. R.; Hooks, H. W. "Solvent Refined Coal (SRC) Process. Operation of Solvent Refined Coal Pilot Plant at Wilsonville, Alabama. Annual Technical Progress Report, January-December, 1976", DOE Report No. FE-2270-15 (June 1977).
7. Styles, G. A.; Weber, W. H.; Basu, A. "Short Residence Time Studies Utilizing the Dissolver Preheater at the Wilsonville SRC Pilot Plant", Proceedings, EPRI Contractor's Conference on Coal Liquefaction, Palo Alto, May 1978.
8. Burke, F. P.; Winschel, R. A.; Pochapsky, T. C. "Composition and Performance of Distillate Recycle Solvents from the SRC-I Process", *Fuel* 1981, 60, 563.
9. Kleinpeter, J. A.; Burke, F. P. "Conventional and Short Residence Time Coal Liquefaction Using Selective Product Recycle", Proceedings, EPRI Contractor's Conference on Coal Liquefaction, Palo Alto, May 1979.
10. Winschel, R. A.; Robbins, G. A.; Burke, F. P. "Improvement in Coal Liquefaction Solvent Quality by Dewaxing", *Fuel* 1987, 66, 654.
11. Burke, F. P.; Winschel, R. A. "Slurry Recycle Oil Composition and Process Performance in H-Coal PDU Operations", Proceedings, Sixth Annual EPRI Contractor's Conference, Palo Alto, May 1981.
12. Winschel, R. A.; Burke, F. P. "Process and Product Oil Characterization in Two Stage Coal Liquefaction", Proceedings, Eighth Annual EPRI Contractor's Conference on Coal Liquefaction, Palo Alto, May 1983.
13. Lee, J. M.; Vimalchand, P.; Cantrell, C. E.; Davies, O. L. "Major Accomplishments at the Advanced Coal Liquefaction Test Facility at Wilsonville", DOE Liquefaction Contractors' Review Conference, Pittsburgh, September 1992.
14. Derbyshire, F. J. "Improved Coal Liquefaction through Enhanced Recycle Distillate Quality", Proceedings, DOE Coal Liquefaction Contractors' Conference, September 1993.

Table 1. Proton Distributions of Recycle Solvents in the CSF Process

	H-Distributions, Normalized			
	Aromatic	Alpha	Beta	Gamma
Cycle 1	50	39	9	2
Cycle 2	49	35	12	3
Cycle 3	43	37	16	4
Cycle 4	40	37	16	6

Table 2. Characterization of Recycle Solvents from Wilsonville SRC-I Operations

Sample Date	Hydrogen, wt%						Solvent Quality	
	Total	Aromatic		Aliphatic		- OH meq/g	KIN	EQ
		Condensed	Uncond	Cyclic	Allyl			
8/77	8.0	2.15	0.90	1.96	2.99	1.23	81.4	76.5
4/78	9.0	1.31	0.95	2.29	4.45	1.51	76.5	74.4
10/78	8.9	1.21	1.09	1.99	4.61	1.66	75.4	67.4
Hydro (8/77)	6.9	1.89	0.83	2.54	3.64	0.68	80.9	85.8

Table 3. Comparison of Wilsonville Solvents by FIMS

	Differences, mol % of total liquid	
	Batch VI - Batch I	Hydro - Batch I
Naphthalene	-0.9	-2.1
Tetralin/Indans	4.8	3.1
Mass 178	-3.1	-1.5
Hydro Mass 178	-1.9	2
Mass 202	-1.1	-0.6
Hydro Mass 202	-0.7	1.3
Carbazole	-0.1	
Quinolines		-1.1
Hydroquinolines		0.3
Indanols	1.3	-1.4
Phenols	5.9	-0.2

Table 4. Effect of Kerr-McGee Light SRC addition on Wilsonville solvent quality (4/78 sample)

LSRC wt%	H2 psig cold	Solvent Quality	
		KIN	EQ
0	0	76.5	74.4
25	0	79.1	73.7
50	0	88.6	65.5
25	1000	85.6	82.8
50	1000	87.6	86.2

Table 5. Comparison of Lummus ITSL (Run 2SCT9) and H-Coal (PDU Run 9) Recycle Distillates

	Concentration, wt%	
	ITSL	H-Coal
Aromatics	12	8
n-Alkyl Aromatics	10	20
Hydroaromatics	31	8
Cyclo-Penta Arom	6	18
n-Alkanes	1	6

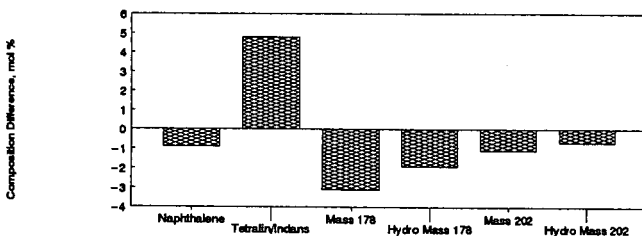


Figure 1. FIMS Comparison: Batch VI - Batch I.

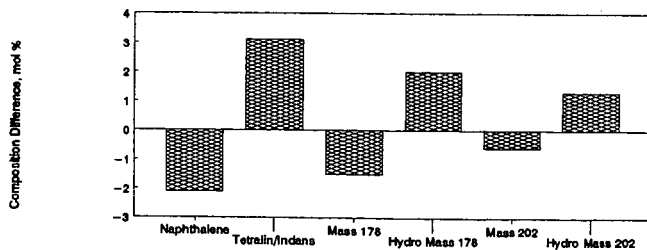


Figure 2. FIMS Comparison: Hydro I - Batch I.

THE ROLE OF THERMAL HYDROGEN-TRANSFER PROCESSES IN CATALYTIC COAL LIQUEFACTION

Donald F. McMillen and Ripudaman Malhotra
Molecular Physics Laboratory
SRI International, Menlo Park, CA 94025

Keywords: Liquefaction mechanisms, bond cleavage, iron-catalysts

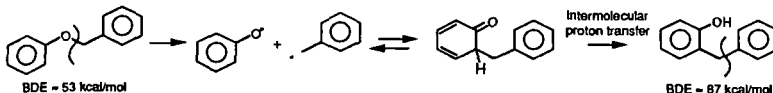
INTRODUCTION

The complexity of coals and their liquefaction products unavoidably means that no "model compound" system can be found that even remotely approaches the real coal in behavior, without also approaching it in intractability of chemical analysis. Notwithstanding these limitations, much has been learned by detailed examination of coal liquefaction phenomenology in light of the behavior of "model" or surrogate structures under liquefaction conditions. Recently we have reviewed¹ some of our own research and other related work that highlights some of what has been learned following this approach. That review summarizes some of the limitations of the formerly accepted weak-bond scission view of donor-solvent coal liquefaction, along with the improved interpretation that emerges when the role of solvent-mediated H-transfer in *actively* promoting bond scission is considered. In addition, the preceding papers in this symposium have highlighted various hydrogen-transfer mechanisms and some key features (and questions) that have evolved during the development of direct coal liquefaction processes.

In this paper, we attempt to build on the background of model compound studies and process development results. We begin by emphasizing two points that have sometimes been lost in discussions of radical reaction mechanisms of hydrocarbon structures. First, high-temperature reactions of coals are not necessarily limited to processes that are purely free-radical: the polar functional groups on coals make it very likely in fact that reactions involving charge separation (i.e., "ionic" reactions) can play some key roles in high temperature coal conversion processes. Second, we assert "thermal" and "catalytic" reactions should *not* be considered as two separate realms of the universe, but as classes of reactions that are *both* important in virtually all catalytic liquefaction processes. Bearing these two points in mind, we then briefly examine some data from the recent literature in an attempt to gain new insight about how cleavage intermediates on iron-based catalyst surfaces may relate to those present in the bulk donor solvent.

IONIC REACTIONS IN BOND-FORMATION AND BOND-CLEAVAGE

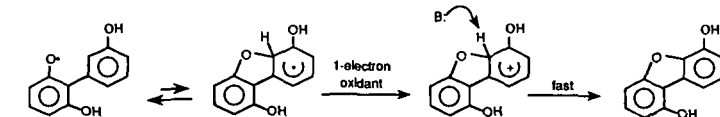
Potential Role of Charged Species and Proton Transfer in Retrograde Reactions. Contrary to the common perception, simple radical recombination reactions are not good candidates for the retrograde processes that plague coal liquefaction, because radical recombination will involve the most stabilized radicals, to generate only the weakest bonds. However, a major exception to this generalization is the case of phenoxy- or other aryloxy radicals. In this case we have suggested¹ that successful retrogression is possible because the highly unstable intermediates generated by ring-recombination of aryloxy radicals are able to rapidly tautomerize through facile intermolecular proton-transfer reactions,² thus locking the original unstable recombination into place. This suggestion is illustrated in Scheme 1 with benzylphenyl ether, and its validity is supported by the reports in the literature³ that the presence of scavengers can decrease, but not easily eliminate, the formation of benzylphenol.



Scheme 1. Retrograde Reaction via Phenoxy Radical Recombination and Rapid Tautomerization.

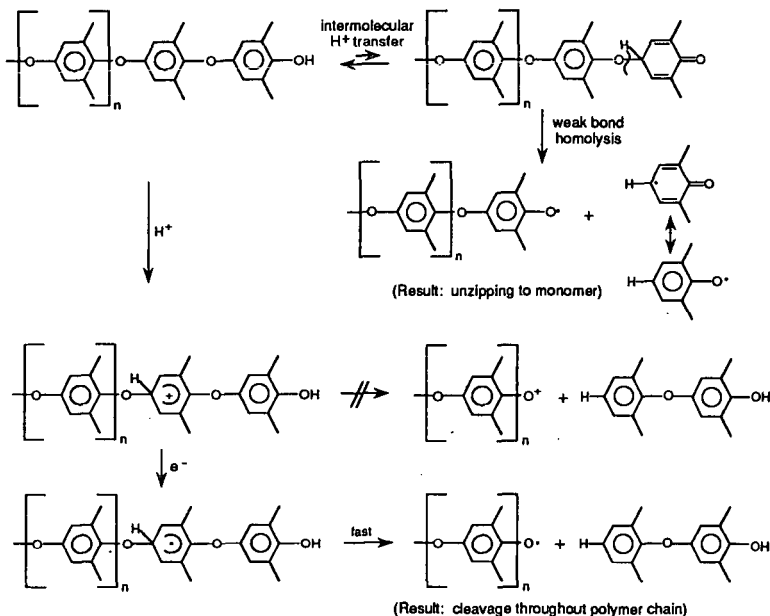
This reaction is one example of interplay between radical and ionic reactions, a phenomenon that may be commonly important in the retrograde processes of oxygen-containing coal structures.

Retrograde Reaction Facilitated by Electron- and Proton- Transfer. The presence of one or more phenolic groups can also promote retrograde reactions that begin with radical addition to an aromatic system. Here removal of the ipso hydrogen is likely enabled not by the relatively high acidity of a keto structure such as in Scheme 1 above, but by the fact that ortho- or para -OH groups on the ipso radical may facilitate its oxidation to the corresponding cation. The cation is very acidic, and can lose a proton extremely rapidly, as suggested⁴ for the products observed in the retrograde reactions of dihydroxyarenes and illustrated in Scheme 2.



Scheme 2. Suggested Completion of Retrograde Reaction by One-Electron Oxidation and Proton Loss.

Bond Cleavage Promoted by Electron- and Proton Transfer. Ten years ago, Solomon and Squire showed⁵ that pyrolysis of poly(2,6-)xlenol in the inlet of a field ionization mass spectrometer results in a rapid, apparently autocatalytic process at about 380°C, yielding a series of oligomers consisting primarily of monomer through hexamer. The carbon-oxygen bond strength in this polymer is about 77 kcal/mol,⁶ far too high to react by simple homolysis at a substantial rate at 400°C. The decomposition of the polymer appears to be predominantly, *but not exclusively*, an unzipping process, since the monomer is in moderate excess over higher oligomers until the final stages of the decomposition process. The reaction is autocatalytic, accelerating as the phenolic products accumulate. Since the reaction proceeds even in the absence of a donor solvent, generation of the main products (which is a reduction process) must be fed by hydrogen from some minor product(s), presumably non-volatile charry material. These factors lead us to suggest the dual-pathway mechanism shown in Scheme 3.



Scheme 3. Suggested Cleavage of Polyxlenol via Proton- and Electron Transfer.

The unzipping process by which the terminal units cleave off to form xlenol is almost certainly the reverse of the phenoxyphenol cleavage we reported some years ago, i.e., the reverse of the retrograde reaction shown in Scheme 1 above. However, reaction via the keto tautomer is not the only significant bond cleavage process, since the homolysis of the much weaker⁷ (ca. 40 kcal/mol) cyclohexadienone-oxygen bond would be about 10^7 times faster (on a per-molecule of original enol starting-material basis) than reaction of the original aryl-oxygen bonds in the polymer. If we consider reaction of polymeric structures of $n \approx 100$, we should still see cleavage of the end units dominating by a factor of about 10^5 . In fact, for most of the reaction, the monomer dominates over the small oligomers in the product mixtures by factors of only two to three. The degree of accelerated bond cleavage observed here for even the internal aryl-oxygen bonds is far greater than that which has been observed for simple H-atom transfer to diaryl ether from a good donor solvent.⁸ Clearly either this reaction mixture is an unusually good source of free H-atoms, which are reactive enough to readily cleave even simple diphenyl ether structures, or there is something about a phenyl ring with ether linkages in both the 1- and the 4- positions that make it quite susceptible to other cleavage pathways.

We suggest the additional bond cleavage pathway to be considered for internal aryl-O linkages in the polymer chain is the proton-transfer, electron-transfer process also shown in Scheme 3. The rationale here is that oxygen substitution on an aromatic ring system facilitates protonation at certain positions, and electron transfer to the protonated segment results in a net H-transfer, bringing about rapid bond cleavage. Protonation at a carbon bearing an oxygen would itself not readily result in cleavage of the C-O bond, since that would involve elimination of a disfavored aryloxy cation. However, electron transfer following the proton transfer would give the ipso-substituted radical, for which β -scission should then be very facile. In the polymer, there are two oxygens connected to each ring. While one of them deactivates protonation at the ipso position, the other, which is para to that position, promotes it. The para oxygen would also promote simple H-atom transfer, but such H-atom transfer from a good donor solvent to substituted naphthalenes and naphthols is known to be accelerated by factors of only about ten,⁴ whereas here oxygen substitution has accelerated cleavage by many orders of magnitude (as compared to diphenyl ether itself).

It is of course speculative to suggest electron transfer without an identified eT agent, but we are not concerned here with electron transfer near room temperature, but at much higher temperatures, and to a positively charged species. The proton transfer that precedes electron transfer could in fact be facilitated by the high acidity of the very class of keto-form retrograde intermediates shown in the examples given in Scheme 1 above. The net result of the proton-transfer, electron-transfer sequence shown in Scheme 3 is an H-atom transfer. The indirect sequence would of course have significance only if it serves to supplant a kinetically hindered direct H-atom transfer, such as radical hydrogen-transfer (RHT) process, that could otherwise not account for the observed cleavage rates.

To summarize the situation for cleavage of the polyxylenol, two cleavage pathways evidently become operative as coal liquefaction temperatures are approached. One, which cleaves off terminal units that have free phenolic groups, almost certainly occurs through ionic tautomerization to a weakly bonded keto form that undergoes rapid homolysis. The second cleaves O-aryl bonds to internal units that have no free -OH groups. The latter process could involve free H-atoms, but more likely we suggest, involves a proton-transfer, electron-transfer process.

The examples shown in Schemes 1 through 3 demonstrate that heteroatom linkages and functional groups are quite likely to bring ionic reactions into play, often in combination with free radical reactions. In the discussion of iron sulfide catalysis that follows, we take as a starting point the corollary expectation that reactions promoted by iron-oxygen-sulfur surfaces might well involve, even for substrates containing no heteroatoms, the formation of ionic or charge-separated species.

THE ROLE OF THERMAL REACTIONS IN CATALYTIC CONVERSION

It is sometimes said that "thermal" reactions, i.e., donor-solvent-coal interactions, become irrelevant as processes evolve towards more effective use of catalysts. This view is first, clearly not correct, and second, belies the potential value of an understanding of thermal process as a basis for addressing the nature of those processes that are clearly catalytic.

A prime example of thermal reactions playing a key role in a "catalytic" process comes from the field of catalytic resid upgrading (including coal-oil coprocessing). Here, it is well recognized⁹ that the factor having the largest impact on distillate conversion is temperature, and that the distillate generation processes are primarily thermal, rather than catalytic. Thus, even though the feedstock in this case is (at process temperatures) a liquid, and has nominal access to catalyst surfaces, most of the reactions that make distillate actually occur in the bulk reaction medium, remote (in molecular terms) from the catalyst surfaces. Thermal distillate formation is in overall terms essentially a disproportionation process, presumably proceeding to a large degree through Rice-Herzfeld H-abstraction— β -scission chemistry. The distillate materials are derived mainly from the aliphatic portions of the resid molecules, which as they fragment to an alkane-alkene mixture, act as a hydrogen "sponge" and place a severe hydrogen demand on the portions of the resid molecules that are already hydrogen poor. In the absence of more readily available sources of hydrogen, this demand is satisfied by utilizing hydrogen made available from the aromatic centers of the resid molecules, thus driving those PAH towards coke.

Since the distillate formation is largely thermal, it follows that the coke formation that is driven by it is probably also thermal, occurring remote from the catalyst surface. Although the key role of the catalyst is to limit coke formation, what occurs remote from the catalyst surface can only be impacted *indirectly* by the catalyst, that is by "thermal" reactions between the reaction medium and the coke precursors. Thus the essence of catalytic resid upgrading can be summarized by saying it is relatively easy to derive a large fraction of the potential distillate by simply raising the temperature; the key to a more efficient process essentially involves finding the most effective way to supply hydrogen via H₂, catalyst, and reaction medium, thus limiting formation of coke. In other words, efficient, high space-velocity resid conversion requires optimization of the complementary operation of catalytic *and* thermal reactions. Similar arguments can be made for some stages of coal liquefaction.

CLEAVAGE INTERMEDIATES ON IRON- AND IRON SULFIDE SURFACES.

Another sense in which coal-solvent, or "thermal" reactions are relevant to catalytic coal liquefaction lies in current attempts to learn more about the species on iron sulfide catalyst surfaces. These surfaces are now known¹⁰ to promote coal liquefaction and dealkylation of substituted aromatics via intermediates that involve transfer, in some manner, of only a single hydrogen. How might the surface-bound species be similar to (or different from) the intermediates involved in pure solution-phase hydrogenolysis? Are these surface species likely to be free-radical, or is there enough ionic and/or semiconductor character in the critical crystal surfaces or edges to facilitate the formation of charged species?

Several years ago, Wei et al.¹⁰, and more recently, Davis and coworkers,¹¹ and Linehan, et. al.,¹² have used model compounds to study the hydrogen exchange and/or C-C bond cleavage promoted by Fe or FeS surfaces. Their results all provide strong evidence for bond cleavage following transfer of a single hydrogen. The data of Wei et al. indicate that even at 300°C and in the presence of 1450 psi H₂, reaction of 1,1'-dinaphthylmethane is almost exclusively to produce naphthalene and 1-methylnaphthalene, with very little di- or tetra-hydronaphthalene derivatives. These

researchers consider that the intermediate in the cleavage reaction is a surface-bound ipso radical,¹⁰ generated by H-atom transfer to produce intermediates exactly analogous to those involved in solvent-mediated hydrogenolysis. However, the examples discussed above, where the presence of only a few heteroatoms in the coal structure bring ionic reactions into play, should make us alert to the possibility that the surface of an ionic solid may also be promoting reactions that involve electron transfer or charged intermediates.

The nature of the intermediates on various iron surfaces are of particular interest for two very important reasons. First, although cleavage is facile at 300°C for displacement of resonance stabilized radicals¹⁰ (or perhaps cations), displacement of unstabilized radicals appears not to occur even at 400°C.¹² Clearly transfer of a single hydrogen to bring about cleavage of very strong methylene bridges between two aromatic clusters is rapid, whereas displacement of bridges of two or more atoms, where the departing fragment is not resonance stabilized, essentially does not occur on these catalysts. Thus, these surfaces evidently will not cleave diarylethane linkages, but these are in any case weak bonds that will homolyze readily during liquefaction. These surfaces will also not serve to cleave bridges of three or more atoms, but such linkages are susceptible to cleavage via H-abstraction— β -scission. The catalysis will also not cause displacement of simple alkyl groups. Thus, it is clear that such catalysts have the potential to use hydrogen to cleave those linkages it may be most important to cleave, leaving the more labile linkages of two or more atoms to less "expensive" routes (or to occur at a more convenient time), and leaving totally untouched the simple alkyl groups whose displacement would only result in hydrogen consumption and the unwanted formation of methane or other light hydrocarbon gases.

The second reason why these intermediates are of practical interest derives from the fact that the hydrogen needed for the cleavage does not have to come, at least during the coal dissolution step, from high pressure hydrogen. Linehan et al. report¹² using 9,10-dihydrophenanthrene, rather than H₂ gas, as the source of surface hydrogen for model compound studies testing their dispersed iron catalysts. This result is very interesting, because researchers have from time to time explored the possibility of catalytic use of donor hydrogen, sometimes called "transfer hydrogenation." However, what has most often been found is that under conditions with no hydrogen overpressure, typical coal liquefaction catalysts, which of course are usually good hydrogenation catalysts, serve simply as an open valve for rapid dehydrogenation of the donor solvent, while providing very little catalytic aid to the liquefaction itself. Clearly what is needed is a catalyst that allows relatively facile H-transfer from a hydroaromatic to the catalyst surface, but does not allow facile recombination to H₂ and dissociation. In the simplest terms, this would merely require a catalyst or conditions under which the dissociatively adsorbed hydrogen has sufficiently low coverage (and/or low mobility) to limit recombination, but enough coverage to be active in causing single H-atom transfer to positions on aromatic clusters bearing linkages. Since the requirements for low coverage and high activity tend to be conflicting, a balance providing real-world catalytic utility may be difficult to find. Thus it is likely that an effort to substantially accelerate selective catalytic cleavage under conditions where there is no hydrogen overpressure will need to be aided by a better picture of the critical surface-bound species and their reactivity.

Examination of the data of Davis and coworkers¹¹ reveals an observation parallel to the exclusive displacement of resonance-stabilized groups, namely that isotopic exchange of aromatic hydrogens (e.g., on 1-methylnaphthalene), occurs without loss of a methyl fragment. However, this is not what would generally be expected were the surface intermediate an ipso-radical species. As shown in Table 1, the estimated rates of either unimolecular H-atom elimination or bimolecular removal of H-atoms via interaction with solution-phase species are substantially lower than estimated rates of methyl radical elimination (assuming that the thermodynamics of H-atom loss are essentially the same as those for solution-phase ipso-radical species). The differences would be even greater for elimination of ethyl radicals and other non-benzylic fragments.

Ades et al. have suggested¹³ that the iron-sulfide-catalyzed cleavage of the model compound bibenzyl-naphthylmethane involves one-electron oxidation to the radical cation, which then cleaves directly (preferentially giving a naphthyl- and a bibenzylmethyl fragment). However, Penn and Wang¹⁴ have shown that generation of bona fide radical cations, either in solution or in the gas phase, leads preferentially to cleavage of the weakest bond in the original molecule (in this case the bibenzyl linkage) or secondarily to cleavage that gives the most stabilized benzylic fragment (in this case a naphthylmethyl fragment). This contrasts with the observed FeS-catalyzed cleavage, which gives preferential cleavage *between* the methylene linkage and the naphthalene ring.

Autrey et al., in one of the preceding papers in this symposium,¹⁵ also invoke one-electron oxidation, but not direct cleavage of the radical cation. They suggest the inability of the cleavage intermediate to eliminate a simple alkyl fragment may reflect that fact that it actually is a cationic species resulting from electron transfer to the surface, followed by H-atom transfer to the substrate to generate the ipso-cation. Such a species might well exhibit the high selectivity observed for elimination of a benzylic fragment, as compared to a methyl fragment. However, this would be tantamount to an acid-cracking process, for which molybdenum and iron sulfide surfaces are not generally known. Furthermore, a mechanism involving elimination of benzylic cations (from either cation or radical-cation intermediates) would have to account for the absence of transalkylation products by invoking what amounts to a hydride transfer to the benzylic cation before it departs the surface. Thus it appears to us that neither direct cleavage of a radical cation nor formation and cleavage of an acid cracking intermediate offer very satisfactory explanations of the observed bond cleavage.

A partially satisfactory rationalization can be achieved by noting that application of the estimated cleavage rates (Table 1) to surface species requires qualification. The zeroth-order assumption of little change in the thermodynamics of the surface-bound species, relative to the same species in solution, is clearly an oversimplification. Preferential adsorption on the surface of course means stabilization, relative to the bulk solution-phase species. This stabilization will make more difficult the unimolecular elimination of a methyl radical, which will be less strongly bound on the surface than the larger and more polarizable ipso-intermediate. On the other hand, the heat of adsorption of H-atoms on the catalyst surface will very likely be more than that for the ipso intermediate, thus facilitating exchange of the H-atom back to the surface. Thus, by considering, at least in qualitative terms, the relative impacts of surface adsorption on the various species, we can achieve a gross rationalization of the observed fragmentation behavior on iron catalyst surfaces, as compared to that which has already been quantified in the gas phase and/or bulk solution.

Additional support for a surface-bound radical intermediate may lie in the details of the isotopic exchange results briefly described above. Dabbagh et al. report¹¹ not only the total extent of exchange, but also the fraction of total deuterium found at positions 2 through 8 on the 1-methylnaphthalene recovered from the high-temperature exchange and also from a lower temperature (100°C) acid-catalyzed exchange. The deuterium distributions, as shown in Table 2, are very similar in the two cases, *except* for the deuterium content at the position ortho- to the 1-methyl group.

The high temperature, surface-promoted exchange results in only ~9% of the deuterium being located at the 2-position, very similar to the 3-, 6-, and 7- positions, which are the least reactive in the molecule. In contrast, under acid-catalyzed exchange conditions, the 2-position has 30% of the deuterium, almost as much as the most reactive (4-) position. We tentatively conclude that the rapid exchange at the inherently unreactive 2-position under acidic conditions reflects marked stabilization by methyl of the partial positive charge at the 1-position that results from proton attack. In contrast, the minimal enhancement (by 1-methyl substitution) of iron-catalyzed exchange at the 2-position suggests that exchange there occurs via H-atom transfer, since the benefits of creating a tertiary radical center are *much* less than the benefits of creating a tertiary carbocation. This difference is illustrated by the relative enthalpy costs for generating secondary and tertiary cations and radicals ($\Delta\Delta H^\circ_{298}[\text{cation-parent alkane (g)}]$ is 16 kcal/mol greater for generation of the isopropyl cation than for generation of the t-butyl cation [from the respective alkanes], whereas the difference is only 2-3 kcal/mol for generation of the secondary and tertiary radicals¹⁰).

Although the above rationalization of observed cleavage selectivity and H-exchange patterns may remove any compelling need to invoke the generation and decomposition of positively charged hydrocarbon species on the iron surface, we believe the possibility of ionic intermediates should still be kept in mind. It is imprudent to simply assume that decomposition that is aided by adsorption on a surface that is even modestly ionic, and/or has some semiconductor character, does not involve either electron transfer or the formation of charged species. To the extent that the catalytically active surfaces (or edges) are not pure sulfides, but are some class of much more ionic mixed oxysulfides, or to the extent that iron vacancies (as often invoked for pyrrhotite) are present to provide the surface with electron donor/acceptor properties, the possibility of charged intermediates needs to be considered. Moreover, given the inability, via prior- or post- analysis of the inorganic phase, to make definitive statements about the nature of the active catalyst under the *actual reaction conditions*, more systematic use of model compound variations to probe the nature of these catalysts is clearly in order. For instance, the possibility of reaction via cationic intermediates, such as that argued against above, could be further tested by comparing the catalytic decomposition of diarylmethanes to their diaryl ether analogs. Decomposition to give aryloxy cations should be distinctly less favored than decomposition to give arylmethyl cations, whereas decomposition to give aryloxy radicals would if anything be more favored than in the hydrocarbon analog.

There is also a fourth possibility that needs to be considered for these catalytic bond cleavages, namely that *net* H-atom attack might result from 1-electron reduction, followed by proton transfer to the radical ion. Although one-electron reduction is not such an obvious candidate with an iron-deficient surface like pyrrhotite that should show better acceptor, rather than donor, properties,¹³ the exact surface (or edge) properties of a nominal pyrrhotite catalyst under reaction conditions are hardly well known. Such an electron-transfer, proton-transfer sequence could call into play both the electronic properties of the iron sulfide and the weakly acid character of surface sulfhydryl groups¹⁷ to provide a catalyzed route to net H-atom transfer.

Suffice it to say at this point that (1) some species on the iron-oxygen-sulfur surface is bringing about selective C-C bond cleavage while utilizing hydrogen obtained from a donor solvent, (2) to do this without gross dehydrogenation of the solvent to H₂ could be very valuable, and (3) understanding the relationship between these surface species and the ipso-radical intermediates responsible for hydrogenolysis in the bulk donor solvent could be key to optimizing and exploiting such reactions.

SUMMARY AND CONCLUSIONS

Heteroatom functional groups, namely phenolic and ether oxygen, very likely play a key role in coal conversion by facilitating rapid transfer of hydrogen as a proton, both to promote bond cleavage and also to allow strong-bond formation. This proton-transfer may sometimes involve uncharged acidic species, such as keto-forms of phenols, which are common recombination intermediates, and sometimes cations that are formed by one-electron oxidation of radicals. The cleavage of certain oxygen-substituted diaryl ether structures, such as polyxylenol, may be promoted by protonation and reductive electron transfer, followed by facile elimination of an aryloxy radical fragment.

Thermal reactions of donor solvent and coal structures are relevant to catalytic processes first in the sense that these two classes of reactions can operate in a very complementary fashion. Two key examples are catalytic hydrotreatment of heavy oil and coal-oil coprocessing. In these two cases, improved use of catalyst allows higher operability temperature limits that make more effective use of thermal distillate generation processes.

Thermal reactions are also relevant to catalytic processes in the sense that the understanding of thermal bond cleavage processes that has been acquired in the last ten years provides a background for learning about the structure of intermediates on catalyst surfaces. Reexamination of data in the recent literature for model compound cleavage on iron sulfide surfaces results in the following observations.

- The observed products are *not* consistent with those generated from cleavage of bona-fide radicals cations, either in the gas phase or in solution.
- The observed bond cleavage, while consistent in itself with that known to occur for acid cracking, does not result in the transalkylation products commonly seen for solution-phase acid-catalyzed dealkylation.
- The H-exchange that occurs at un-substituted positions, which in all likelihood results from the same type of attack as does the ipso-displacement of linkages, shows a pattern consistent with H-atom, rather than H⁺, attack.
- The increased selectivity for displacement of resonance-stabilized (e.g., benzylic) fragments, and the increased ratio of H-loss/methyl-loss, relative to the observed gas-phase or bulk-solution behavior, can be qualitatively rationalized by expected relative adsorption strengths on the catalyst surfaces.
- The data as yet provide no direct evidence about the possibility that *net* H-atom transfer could proceed by I-electron reduction, followed by proton transfer to the radical ion. Such a sequence could be facilitated by both the electronic properties of the iron sulfide and the weakly acid character of surface sulphydryl groups.

ACKNOWLEDGMENT

The work discussed in this paper has been primarily supported, through various contracts, by the U.S. Department of Energy, with additional support from the Electric Power Research Institute. The authors are particularly indebted to many colleagues, who over the years, have contributed support and constructive criticism to our efforts to help improve the collective understanding of coal liquefaction mechanisms.

REFERENCES

1. Malhotra, R.; McMillen, D. F. *Energy & Fuels*, **1993**, *7*, 227.
2. Tupitsyn, I. F.; Komarov, V. I. *Reakts. Sposbn. Org. Soedin.*, **1969**, *6*, 616.
3. Poutsma, M. L., "A Review of Thermolysis Studies of Model Compounds Relevant to Processing of Coal," Oak Ridge National Laboratory Report ORNL/TM-10637, **1987**, p. 95.
4. McMillen, D. F.; Chang, S. -J.; Fleming, R. H.; Laine, R. M.; Malhotra, R.; Nigenda, E.; Ogier, W., "Effect of Amine Solvents and Oxygen Functionalities on Coal Liquefaction," Final Report EPRI Research Project 2147-5 **1985**, p. 6-17.
5. Squire, D. R.; Solomon, P. R.; DiTaranto, M. B., "Synthesis and Study of Polymer Models Representative of Coal Structure - Phase II", Final Report, Gas Research Institute, August, **1985**, p. 92-93.
6. McMillen, D. F.; Golden, D. M., "Hydrocarbon Bond Dissociation Energies," *Annu. Rev. Phys. Chem.*, **1982**, *22*, 497.
7. McMillen, D. F.; Ogier, W. C.; Ross, D. S., *J. Org. Chem.* **1981**, *46*, 3322.
8. McMillen, D. F.; Malhotra, R.; Chang, S.-J.; Fleming, R. H.; Ogier, W. C.; Nigenda, S. E. *Fuel* **1987**, *66*, 889.
9. a. Savage, P. E.; Klein, M. T.; Kukes, S. G., *Fuel*, **1988**, *2*, 619.
b. Khorasheh, F.; Rangwala, H. A.; Gray, M. R.; Dalla Lana, I. G., *Energy & Fuels*, **1989**, *3*, 716.
c. Miki, Y.; Yamadaya, S.; Oba, M.; Sugimoto, Y., *J. Catal.* **1983**, *83*, 371.

10. Wei, X.-Y.; Ogata, E.; Futamura, S.; Kamiya, Y. *Fuel Process. Technol.* **1990**, *26*, 135.
11. a. Dabbagh, H. A.; Shi, B.; Davis, B. H.; Hughes, C. G. *Energy & Fuels*, **1994**, *8*, 219.
b. Shi, B.; Guthrie, R. D.; Davis, B. H. *Energy & Fuels*, **1994**, *8*, 1268.
12. a. Linehan, J. C.; Matson, D. W.; Darab, J. G.; Autrey, S. T.; Franz, J. A.; Camaioni, D. M. *Am. Chem. Soc. Div. Fuel Chem. Preprints* **1994**, *39*(3), 720.
b. Matson, D. W.; Linehan, J. C.; Darab, J. G.; Buehler, M. F. *Energy & Fuels*, **1994**, *8*, 10.
13. Ades, H. F.; Companion, A. L. Subbaswamy, K. R. *Energy & Fuels*, **1994**, *8*, 71.
14. Penn, J. H.; Wang, J.-H. *Energy Fuels*, **1994**, *8*, 421.
15. Franz, J. A.; Camaioni, D. M.; Alnajjar, M. S.; Autrey, T.; Linehan, J. C. *Am. Chem. Soc. Div. Fuel Chem. Preprints* **1995**, *40*, XXX.
16. Lias, S. G.; Bartmess, J. E.; Liebman, J. F.; Holmes, J. L.; Levin, R. D.; Mallard, W. G. *J. Phys. Chem. Ref. Data* **1988**, *17*, Suppl. 1, 1-816.
17. Shan, H.-Y.; Satterfield, C. N. *Ind. Eng. Chem. Proces. Dev.* **1984**, *23*, 20.

Table 1
Estimated Rates of Unimolecular and Bimolecular Loss of Methyl Radical and
H-atoms from 1-Methylnaphthalene Hydroaryl Radical Intermediates

Loss Process	Estimated Rate Constant (s ⁻¹)
Me• Elimination	1 X 10 ⁴
H• Elimination	3 X 10 ³
H-Loss by RD ^a .	<1 X 10 ²
H-Loss by RHT ^b .	≤3 X 10 ³

- a. Pseudo-first-order rate constant for H-loss by radical disproportionation, where [R•]_{tot} is assumed to be dominated by the α-tetralyl radical, and is estimated to be less than 10⁻⁷ M in 90% naphthalene/10% tetralin.
- b. Pseudo-first-order rate constant for H-loss by radical hydrogen-transfer, based on [naphthalene] = ~5M, and on a lower limit for RHT intrinsic activation energy of 17 kcal/mol.

Table 2
Substitution Patterns for Catalysis of Deuterium Exchange by Stainless Steel or
Homogeneous Acids, from Data of Dabbagh et al.

1-Methylnaphthalene Ring Position	% of Total Aromatic Deuterium	
	SS-Catalyzed @ 385°C	Acid-Catalyzed @ 100°C
2	9	30
3	5	11
4	47	35
5	17	11
6,7	5	6
8	17	14

COAL SLURRY pH STUDIES

Karl S. Vorres
Chemistry Div., Bldg. 211
Argonne National Laboratory
Argonne, IL 60439

ABSTRACT

Coal slurry pH values can be used to characterize coals. pH values depend on the coal, time since slurry preparation, contact with gas atmosphere, particle size, and stirring. Measured values reflect a sequence of reactions probably including: carbon dioxide absorption by water from the air, wetting of the coal (pH may be affected by the elemental composition of the mineral matter), and further equilibration with species in the water. The pH initially drops as carbon dioxide is absorbed, then rapidly increases as the coal is wetted, and then slowly decreases as some reactions with species in the water take place.

INTRODUCTION

Coal slurry pH values are used to characterize samples. It has been suggested as a means to indicate the degree of oxidation or weathering. The measurement procedure is similar to that used for soil samples (1). The usual procedure calls for the addition of a weighed quantity of coal and water (1:2), stirring well, and measurement of the pH of the liquid above the settled coal after a time period of one half hour.

The stirring is intended to quickly wet the hydrophobic coal particles so that they will be suspended in the slurry rather than remain on the surface of the mixture. The waiting period before the measurement implies a dynamic situation and an approach to a steady state pH value. This paper is intended to describe some of the changes which take place during the course of the period from the beginning of the mixing to several hours afterward. Several reactions are apparent from the changes which have been observed.

The wetting involves an interaction with the surface of the coal particles. The effect on pH includes at least dissolution of soluble acidic or basic species, interaction with surface acidic or basic functional groups, interaction with acidic or basic surface sites or areas. Oxidation can change the surface of the mineral as well as the organic parts of the coal, and can be expected to affect the pH. Some of these potential effects may be deduced from changes in the progression of pH with time for a sample.

EXPERIMENTAL

An Orion Model EA940 pH meter was used with an Accumet pH electrode. The electrode was calibrated with standard buffers of pH 4, 7 and 10. A two point method was used depending on the range of pH values involved in the experiment. Typically calibration was done at pH 7 and 10. Distilled and de-ionized water was used.

The coal samples were taken from the Argonne Premium Coal Sample Program set. Both -100 and -20 mesh samples were used. Water/coal ratios of 2-32 to 1 were obtained by mixing an ampule of 5 grams of -100 or 10 grams of -20 mesh coal with varying amounts of water. For some experiments a polyethylene plug (machined to fit inside the pyrex beaker and center the electrode in a snug-fitting hole) was used to limit the access to the atmosphere. For deaerated water experiments, the water was prepared by bubbling a stream of nitrogen through the stirred water for a minimum of 30 minutes. In one experiment, nitrogen gas was passed over the coal-containing equipment in a plastic enclosure. A magnetic stirrer was used in a number of experiments.

Sealed ampules were opened at the beginning of the experiment, weighed, water added and weighed, and mixed with a glass stirring rod or magnetic stirrer. Data were recorded on a IBM microcomputer at 15-20 second intervals. The computer data were analyzed using Lotus 123.

RESULTS AND DISCUSSION

A typical result for a Pittsburgh high volatile bituminous coal is shown in Figure 1. Initially the pH decreases as the water is stirred and affected by the atmosphere. As the coal is added the pH increases to a maximum value and then slowly decreases again. This general behavior pattern has been observed for most of the coal samples.

The initial decrease is believed to be due to the dissolution of carbon dioxide from the air, formation of carbonic acid, and ionization to provide hydronium and bicarbonate ions. The increase on addition of coal involves an interaction with the surface accessible to the water. This interaction consumes hydronium ions. The final slow decrease in pH may be again due to interaction with the carbon dioxide in the air.

The initial reaction with coal gives a series of maximum values. The value of the maximum does not correlate with carbon content or others of the organic elemental composition.

A series of runs with Illinois #6 (Ik) indicated the effects of several values and produced a range of values for the maximum pH. For the -100 mesh samples run in pyrex beakers, the maxima were in the range 9.75-9.80. If a stainless steel beaker was used instead (250 ml) the maxima were in the pH range 9.65-9.71. These results were obtained over a water/coal ratio range of 2/1 to 32/1. However, for the -20 mesh sample with a water/coal ratio of 4, the pH range was lower, 9.61-9.76, with a value of 9.53 for the stainless steel beaker. The high values were obtained when the magnetic stirrer was off in the early stages of the run. Stirring introduced a limitation to the maximum pH, probably due to the incorporation of carbon dioxide from the atmosphere. Aerating or de-aerating the water had little effect on the maximum pH as both gave 9.72. Interestingly, a sample which had no gas bubbled through gave pH 9.67.

The run with equipment blanketed with nitrogen and de-aerated water gave the pH 9.76 which was higher than other stirred runs.

The effect of stirring speed was notable at low coal concentrations. Apparently, more rapid stirring gives a higher maximum pH.

In an effort to understand the reason for the increase in pH on the addition of coal to water, a series of materials were stirred with water. It was apparent that graphite did not behave like the coal, unless it was assumed that the behavior was like an extremely high rank coal. However the addition of titanium dioxide, as an example, gave a behavior very reminiscent of the plot of pH versus time for the coal samples. This observation would indicate that the pH may be due to the effect of various mineral constituents in the sample.

CONCLUSIONS

The measured pH value of a given coal slurry will depend on the parameters of the experiment, including water/coal ratio, stirring speed, particle size, and coal rank.

The addition of coal to water produces a series of pH changes. Initially, the drop in pH corresponds to the addition of carbon dioxide to the slurry. A subsequent increase appears to be related to inorganic constituents in the coal. A long term decrease in pH is assumed due to continued interaction with carbon dioxide.

The maximum pH depends on the interaction of the concentration of carbon dioxide, and the concentration of the mineral matter in the slurry.

ACKNOWLEDGMENT

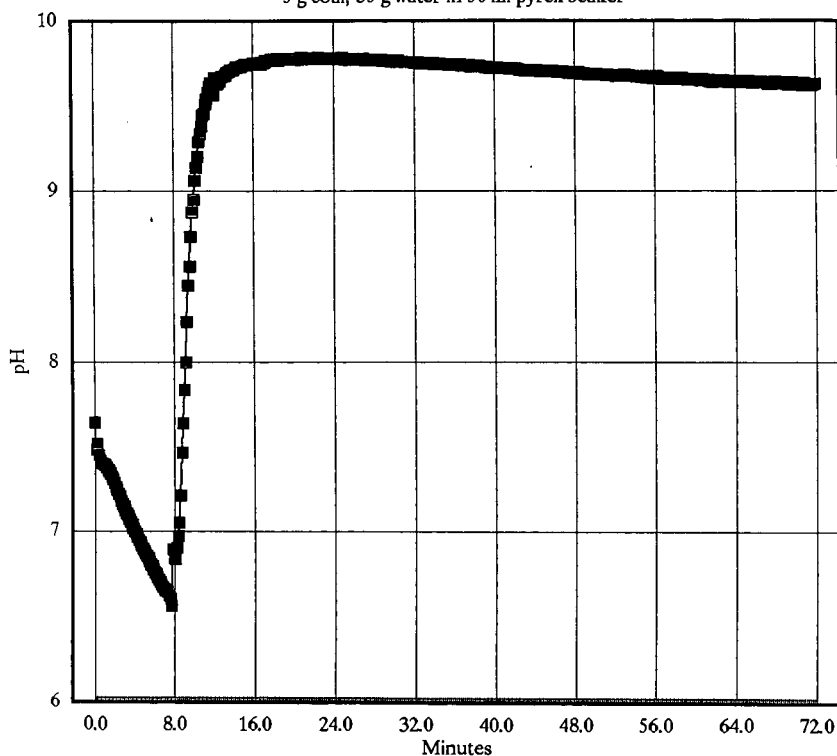
The author gratefully acknowledges the support of the U. S. Department of Energy, Office of Fossil Energy for financial support, and the staff at the Pittsburgh Energy Technology Center for help with this program.

REFERENCES

1. Methods of Soil Analysis, Part 2, Chemical and Microbiological Properties, ed. C. A. Black, Amer. Soc. of Agronomy, Madison, WI 1965, pp. 915-920.

Fig. 1, pH of PI-100 mesh Slurry

5 g coal, 35 g water in 50 ml pyrex beaker



PI922A94.wk3
ck

ADSORPTION ENTHALPIES FOR HYDROCARBONS ON WYODAK COAL SURFACES
BY INVERSE GAS CHROMATOGRAPHY

Amy S. Glass
Department of Chemistry
University of Dayton
Dayton, OH 45469-2357

(Keywords: Wyodak coal, coal surfaces, inverse gas chromatography)

Introduction

Studies of coal surface interactions are important for understanding how technologically important reagents interact with coal. Thermodynamic data provide a quantitative means to assess the interactions between reagents and coal. Knowledge of interaction strengths for solutes with coal surfaces should enable the design of more effective coal reaction strategies and lead to better utilization of coal as fuel and chemical feedstock.

In addition, studies of coal surface thermodynamics provide information about the structure and chemistry of coal. An important advantage with surface thermodynamic data is that they are not complicated by processes in bulk coal. For example, surface data are free of mass transport effects and intermolecular coal-coal associations which may exist in the bulk. Surface interaction data therefore provide a direct measure of the interaction between the solute and coal for a single specific type of chemical or physical property of the coal.

We recently developed the technique of inverse gas chromatography (IGC) for obtaining coal surface thermodynamics.¹ Solute molecules are carried past coal packed into a stainless steel tube. IGC provides a means to discriminate against the diffusion of solutes into bulk coal and thus enables the measurement of surface adsorption thermodynamics for polar and nonpolar molecules with coal surfaces. Coal IGC data are collected in the Henry's Law region of the adsorption isotherm, so the data represent interactions with the coal at infinite dilution surface coverage.

The present paper reports surface thermodynamic data for Wyodak coal surfaces. Because the coal is from the Argonne Premium Coal Sample Bank, it is intended that the interactions at this surface provide a benchmark for interactions of solutes with a low rank, high oxygen content coal. In the present work, it has been found that the Wyodak surface has relatively weak (low exothermicity) adsorption enthalpies with saturated hydrocarbons (alkanes) but quite strong (highly exothermic) interactions with alkenes and aromatic adsorbates. Recently, Ahsan et al. reported calorimetric data for aromatics with original and with citric acid washed (CAW) Wyodak coal.² These workers observed that citric acid washing of Wyodak coal caused heats of immersion (ΔH_{imm}) for the coal in aliphatic acids to decrease while ΔH_{imm} in aryl sulfonic acids increased. In contrast, CAW caused no changes in the ΔH_{imm} of Illinois No. 6 coal in these acids. Nishioka observed that alkylation or washing in 2N HCl caused a drastic increase in the swelling ratio of the pyridine insoluble portion of a Wyoming subbituminous coal.³ These changes were not observed for a higher rank Illinois No. 6 coal. He ascribed the changes in the Wyoming coal to the reduction of strong ionic forces in the coal by HCl or by the tetrabutyl ammonium salt which acts as a catalyst in the alkylation procedure. The existence of strong ionic forces in low rank coal is supported by the results of the present work. These forces make themselves felt in the unusually exothermic interactions of unsaturated hydrocarbon adsorbates with the Wyodak coal surface.

Theory

IGC differs from analytical GC in that in IGC the emphasis is on stationary phase properties as opposed to properties of the injected solute. In IGC, the retention volume serves as a measure

of the interaction strength between the single, pure injected solute and the stationary phase. The interaction is most straightforward in the regime of linear chromatography. In this regime, the retention volume represents the Henry's Law constant for the solute-stationary phase interaction. If the retention volume is sensitive to the surface of the stationary phase, then the Henry's Law constant expresses the equilibrium interaction between the injected solute and the stationary phase and gives the equilibrium constant for surface adsorption, K_s .⁴ This relationship is expressed by equation 1.

$$K_s = \frac{V_s}{RT} \quad (1)$$

where V_s is the retention volume per unit adsorbate gas pressure and per unit accessible surface area, S , of the stationary phase ($V_s = V_N/SRT$ where R is the ideal gas constant, T is the column temperature, and V_N is the retention volume corrected for pressure drop across the column.) The van't Hoff equation gives the enthalpy from the temperature dependence of the equilibrium constant. For equilibrium surface adsorption at infinite dilution surface coverage, the van't Hoff equation gives the isosteric adsorption enthalpy, q_{st} , as the slope of a plot of the natural logarithm of the retention volume over temperature vs. inverse temperature. Equation 2 is the defining equation:

$$\frac{d(\ln V_N/T)}{d(1/T)} = \frac{-q_{st}}{R} \quad (2)$$

Plots of $\ln(V_N/T)$ vs. $1/T$ were used to determine the isosteric adsorption enthalpies for saturated and unsaturated hydrocarbons on Wyodak coal surfaces.

Experimental

The procedure and apparatus for IGC of coal surfaces have been described previously.¹

Adsorbate liquids were obtained from Aldrich at the highest purities available and were used without further purification. They were admitted to the vacuum manifold for injection after at least 3 freeze-pump-thaw cycles. Adsorbate gases were obtained from Aldrich or from Matheson in the highest purities available and were admitted to the vacuum manifold directly. Wyodak coal (-20 mesh) was obtained from the Argonne Premium Coal Sample bank. The coal was sieved to 40/60 mesh and packed into 1/8 inch O.D. stainless steel tubes about 100 cm in length. The columns were heated in helium at 150°C or at 250°C for at least a week until the GC baseline stabilized. Significant weight loss (~30%) was observed. In order to eliminate the large dead volume these columns were repacked using coal which had been previously heated at 115°C in vacuum.

Retention volumes were determined from the first moments of the GC peaks. Van't Hoff plots were constructed using data obtained at temperature intervals of 5 to 10° over at least a 30° temperature range. At least 5 retention volumes were obtained at every temperature. The errors in the adsorption enthalpies were 7% or lower. Data for Illinois No. 6 coal are taken from reference 1.

Results and Discussion

Figure 1 shows plots of the isosteric adsorption heat, q_{st} , vs. the electronic volume polarizability of the adsorbates, α'_v , for *n*-alkane adsorbates on two different rank coals, an Illinois No. 6 bituminous coal and a Wyodak subbituminous coal.¹ Data for propene and 1-butene are also shown for the Illinois No. 6 coal. The lower plot is for alkanes on Wyodak coal and the upper plot is for alkanes on Illinois No. 6 coal. Both coals were heated at 150°C in helium. These plots demonstrate that these two coals have different dispersive surface interactions with alkanes. The Illinois No. 6 coal has more exothermic adsorption heats with alkanes, demonstrating that it has a more polarizable surface than

the Wyodak coal. Dispersive surface tensions, γ_s^d , have also been determined for the two coals, and are $\gamma_s^d=104 \text{ mJ/m}^2$ for Illinois No. 6 and $\gamma_s^d=25.2 \text{ mJ/m}^2$ for Wyodak.^{1,5} These data demonstrate that Wyodak coal possesses a relatively low energy surface, similar to those found for polymers such as polyethylene.⁶ This conclusion supports the idea that Wyodak coal has surface properties which are similar to those of its precursor, a polymeric cellulosic type of material. On the other hand, Illinois No. 6 coal possesses a higher energy surface, similar to those found for carbonaceous materials.⁶ As seen from the center plots, heating to 250°C or extracting either of the coals results in a surface with similar adsorption heats for alkanes. The adsorption heats for n-alkanes on both of these modified surfaces are similar to heats for alkanes on graphitized carbon black.⁴ The plot for Illinois No. 6 coal also shows data for two alkenes, propene and 1-butene. On Illinois No. 6 coal, alkene adsorbates have interactions which depend on adsorbate electronic polarizability (α') in the same way as the alkanes.

In Figure 2, adsorption heats for alkanes on Wyodak coal heated at 150°C and at 250°C are replotted. However, in Figure 2, these data are plotted vs. (total) volume polarizability, α' , whereas in Figure 1, they are plotted against electronic volume polarizability, α'' . For alkanes, $\alpha'=\alpha''$, because these adsorbates only interact with the surface via induced dipole-induced dipole (London dispersion) forces. Also plotted in Figure 2 are adsorption heats for alkene and aromatic adsorbates on Wyodak coal. For alkenes, there is an additional induction contribution to α' . This contribution may make itself felt if there exists a dipole or Coulomb force at the surface which is capable of inducing a dipole in the adsorbate (Debye force).

Interpretation of the data for alkenes on the 250°C-heated coal appears relatively straightforward (Figure 2). The alkene adsorbates on this surface have q_s 's which depend on the total volume polarizability, α' , in the same way as the alkanes. (Alkenes on the 250°C-heated Wyodak surface have ~1.5-2.0 kcal/mol additional interaction with this surface over that expected from electronic polarizability (α'') alone.) Apparently, alkenes interact with this surface according to their total volume polarizabilities, α' . As seen from Figure 2, benzene has a somewhat stronger interaction with the 250°C-heated Wyodak coal surface than expected based on α' .

The data for alkenes on the 150°C-heated Wyodak surface appear to be more complex. (See Figure 2.) Propene and 1-butene have higher adsorption heats by ~3-4 kcal/mol with this surface than expected based on α' . It may be fortuitous that these adsorbates give adsorption heats on the 150°C-heated coal surface which equal those expected based on α' for the 250°C-heated coal surface.

Comparing the adsorption heats for alkenes on Illinois No. 6 coal (Figure 1) with those for alkenes on Wyodak coal (Figure 2) shows that there is an additional type of force operating at the Wyodak surface which produces more exothermic interactions with alkenes and aromatics. Ionic forces exist in low rank coals.³ At a surface, the presence of small cationic charges augments the adsorption heats with molecules that contain additional electron density in double, triple, or aromatic bonds.⁴ Such effects are observed for hydroxylated silica and for zeolite surfaces.⁴ Silica contains a cationic proton while zeolites contain Na⁺, Ca²⁺, etc. ions. The existence of ionic forces at the Wyodak coal surface would explain the more exothermic adsorption heats with alkene and aromatic compared to alkane adsorbates. Studies are underway to explore the nature of these forces at the surfaces of original and modified Wyodak coal surfaces.

Acknowledgement

This work was supported by a Fellowship from the University of Dayton Research Council.

References

1. Glass, A. S.; Larsen, J. W. *Energy Fuels* 1994, 8, 629-636.
2. Ahsan, T.; Wu, J. H.; Arnett, E. M. *Fuel* 1994, 73, 417-422.
3. Nishioka, M. *Fuel* 1993, 72, 1725-1731.
4. Kiselev, A. V.; Yashin, Y. I. *Gas-Adsorption Chromatography*; Plenum: New York, 1969.
5. Glass, A. S., unpublished data.
6. Zisman, W. A. *Contact Angle, Wettability, and Adhesion*, ACS Adv. Chem. Ser. No. 43; American Chemical Society: Washington, DC, 1964; pp. 1-51.

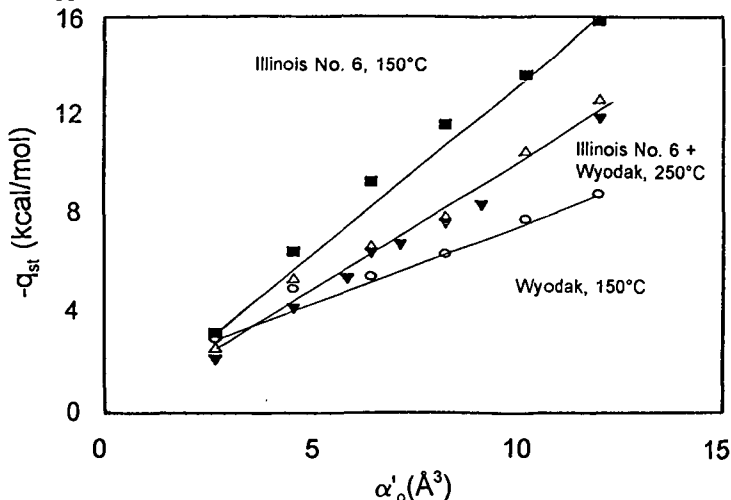


Figure 1. Isosteric adsorption heat (q_{st}) vs. electronic volume polarizability (α'_o) for hydrocarbons on Wyodak and Illinois No. 6 coal surfaces. \blacksquare =alkanes on Illinois No. 6 heated at 150°C. \blacktriangledown =alkanes on Wyodak heated at 150°C. \circ =alkanes on Wyodak heated at 150°C. For \blacksquare , \blacktriangledown , \circ adsorbates are (from left to right): methane, ethane, propane, *n*-butane, *n*-pentane, *n*-hexane; \blacktriangledown =alkanes and alkenes on Illinois No. 6 coal extracted in tetrahydrofuran and heated at 150°C. For \circ adsorbates are: methane, ethane, cyclopropane, propane, propene, 1-butene, *n*-pentane, *n*-hexane. All coals heated in helium.

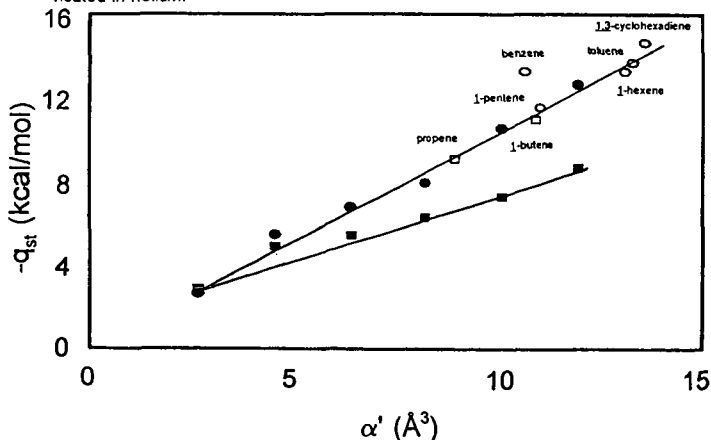


Figure 2. Isosteric adsorption heat (q_{st}) vs. volume polarizability (α') for hydrocarbons on Wyodak coal surfaces. \blacksquare =alkanes on Wyodak heated at 150°C. \bullet =alkanes on Wyodak heated at 250°C. \square =alkenes on Wyodak heated at 150°C. \circ =alkenes and aromatics on Wyodak heated at 250°C. For \blacksquare and \bullet adsorbates are: methane, ethane, propane, *n*-butane, *n*-pentane, *n*-hexane. For \square adsorbates are propene and 1-butene. For \circ adsorbates are 1-pentene, 1-hexene, 1,3-cyclohexadiene, benzene, and toluene.

AIR OXIDATION-INDUCED EFFECT ON THE PYROLYSIS BEHAVIOR OF A SUBBITUMINOUS COAL FROM SOUTHERN ALASKA

Olayinka I. Ogunsola and Michael Downing
Mineral Industry Research Laboratory
School of Mineral Engineering
University of Alaska Fairbanks
Fairbanks, Alaska 99775-7240

Keywords: Alaskan low-rank coals; TGA; oxidation

ABSTRACT

A subbituminous coal from Beluga coalfield, Alaska was oxidized in air at 120°C for about 8 days. The pyrolysis behavior of the raw coal and oxidized samples was determined using a Perkin-Elmer Series 4 thermogravimetric analyzer (TGA). The TGA pyrolysis behavior of partially demineralized raw and oxidized samples was also conducted to investigate any accompanying effect of demineralization. Results obtained indicate a decrease in the maximum decomposition rate and apparent reactivity and an increase in activation energy of devolatilization of the coal when it was air oxidized. The effect was found to be less significant in the demineralized coal.

INTRODUCTION

The complex and heterogeneous nature of coal has made understanding of its structure very difficult. Oxidation is one of the methods of evaluating the physical and chemical structural properties of coal. Considerable emphasis has been placed on oxidation as a means of understanding coal chemistry[1]. Efforts have also been made to conduct studies in order to address some practical implications of oxidation on coking and agglomerating potentials[2] and ignition, and spontaneous combustion characteristics of coal[3-5].

Many studies have been conducted on coal oxidation, review of which has been given in the literature[6-8]. From these previous studies, impact of oxidation on the coal properties that are of practical significance to coal beneficiation and utilization has been established. For example, chemical changes that occur during coal oxidation affect flotation behavior of stockpiled run of mine coal and the coking potential of the stockpiled products[9].

In addition to the effect of atmospheric oxidation of coal on its properties, beneficiation, quality and utilization, coal oxidation in a stream of air has been used to enhance production of humic acids, which are used as fertilizers, from coal[3,10-13]. The materials produced during atmospheric coal oxidation depends on the rank, type, and nature of the coal and on the oxidation conditions (e.g. temperature and period of oxidation)[10,13]. While studies have been conducted on the production of humic acid from oxidized British coal[3], Spanish coals[10], European brown coals[12], and Alaskan coals[13], no study has been conducted to address the effect of atmosphere oxidation on the pyrolysis behavior of Alaskan coals. The effects of thermal upgrading on the performance of an interior Alaska low-rank coal during pyrolysis (an important stage of coal utilization processes) have only been recently studied[14]. About half of the U.S. coals are located in the state of Alaska[15]. Alaskan coals, which are estimated at about 5.5 trillion tons[15], are of Cretaceous and Tertiary age[16] and are mainly of low rank[17].

This paper discusses the results of a preliminary study on the effect of air oxidation and demineralization on the devolatilization behavior of Beluga subbituminous coal using thermogravimetric analysis (TGA) technique. Decomposition characteristics and reactivity of oxidized and unoxidized coal samples were obtained.

EXPERIMENTAL

The coal sample used in this investigation was a subbituminous C coal from Beluga field, west of Anchorage, Alaska. Analytical characteristics of the coal are summarized in Table 1.

The bulk coal sample was collected in lump size from the mine and taken to the laboratory in plastic bag contained in steel metal container under nitrogen. The coal sample was crushed to pass through 60 mesh. The minus 325 mesh size fraction was sieved off. The 60 x 325 mesh fraction was split into 4. One split of the sample was partially demineralized, one split was oxidized while another split of each sample was used for the analytical characterization.

Prior to oxidation, one split of the sample was partially demineralized according to the method used by Estevez, et al.[10]. This was achieved by suspending the coal in 0.5N HCl (1:10 w/v) for one hour at ambient temperature with continuous mechanical stirring. The partial demineralization was done in order to evaluate the catalytic effect (if any) of the mineral matter on oxidation[10].

The demineralized and undemineralized coal samples were oxidized at a temperature of 120°C for a period of about eight days in an air forced circulation oven. The pyrolysis behavior of the raw and oxidized coal samples was investigated using a Perkin-Elmer TGS-4 thermogravimetric analyzer. About 5 mg sample was scanned from 350°C to 950°C at a rate of 20°C/min. under nitrogen gas flowing at a rate of 80 cc/min. A series of runs was conducted before the actual runs to obtain the best conditions for excellent reproducibility. Reproducibility was best at the experimental conditions used. Sample was purged for about 15 minutes in nitrogen prior to run.

Thermograms and differential thermograms of the samples were obtained from which data, such as decomposition regions, pyrolysis rate, activation energy and thermal reactivity, were obtained and/or calculated.

RESULTS AND DISCUSSION

Figure 1 shows the thermograms/differential thermograms (TG/DTG) for the raw Beluga coal used in this study. Two distinct weight loss regions, one at about 119°C and the other at about 343°C can be observed for the unoxidized coal. Corresponding TG/DTG curves were obtained for the oxidized demineralized (BDX8) sample and the oxidized undemineralized sample. Table 2 shows the rate of weight loss at the two regions and the temperature at which they occur for the feed and treated samples. The first weight loss region, which is attributed to loss of moisture, occurred at a slightly lower temperature for the oxidized coal than the raw coal. Partial demineralization appears to reduce the extent of decrease in the temperature at which the first region occurs as shown by the results on Table 2. The second weight loss region, which indicates onset of primary decomposition and entails primary devolatilization, occurred at 343°C for the raw coal and at 329°C and 331°C, respectively for the undemineralized oxidized and demineralized oxidized samples. Also, shown on Table 2 is the maximum devolatilization rate which occurred at the second region. It could be observed from the results on Table 2 that oxidation of the Beluga coal decreased its maximum decomposition rate from about 0.181 mg/hr/mg to about 0.156 mg/hr/mg. The maximum devolatilization rate of the coal was only decreased to 0.17 mg/hr/mg when the coal was demineralized prior to oxidation. Although the decomposition kinetics of coal are very complex [18-19], some useful kinetic information such as the activation energy was obtained. Apparent activation energies of decomposition over 475°C - 800°C temperature range were obtained for the raw and treated coal samples from the Arrhenius equation plotted in Figure 2, for the raw coal, oxidized coal, and oxidized demineralized coal, on the assumption that thermal decomposition was a first order that followed the relationship:

$$-dw/dt = kw \quad (1)$$

where dw/dt = instantaneous rate of weight loss, w = undecomposed decomposable matter, and k = specific reaction rate. The reaction rate was then related to the Arrhenius equation by

$$\ln k = \ln A - E_a/RT \quad (2)$$

where A = the frequency factor, R = the universal gas constant, E_a = activation energy and T = absolute temperature.

Values of k were obtained at various temperatures by using data from TG and DTG curves. The apparent activation energies for the raw coal and the oxidized undemineralized and oxidized demineralized samples were determined from plots of $\ln k$ versus $1/T$, shown in Figures 2. The activation energy of the coal was increased by about 50% from 16.9 KJ/mol to about 26 KJ/mol when it was oxidized for eight days as depicted by the results on Table 2. Little or no change in activation energy was observed when the coal was demineralized prior to oxidation. Apparent activation energy of the raw coal in this study appears to be lower than those reported by others [19] for other coals of similar rank. However, activation energy of thermal decomposition of coal has been reported to be as low as 20 KJ/mol [20]. Maximum decomposition rate has been related to thermal reactivity of coal [19, 21-23]. From a kinetic view point the maximum decomposition rate is related to the reactivity R by

$$R = 1/w_i (dw/dt)_{\max} \quad (3)$$

where w_i = initial weight of coal (mg) and $(dw/dt)_{\max}$ = maximum loss rate (mg/min).

Table 2 gives the value of reactivity for the raw coal and treated samples. A slight decrease in the reactivity of the coal could be observed when the coal was demineralized and oxidized for eight days. A more significant decrease in the reactivity occurred when the coal was not demineralized prior to oxidation as illustrated on Table 2.

CONCLUSIONS

The thermal reactivity and apparent activation energy of the Alaskan subbituminous C coal have been found to be affected by oxidation in air at a temperature of 120°C. A decrease in reactivity and a corresponding increase in apparent activation energy have been observed when the coal was oxidized for eight days. Demineralizing the coal prior to oxidation was found to reduce the effect of oxidation on both thermal reactivity and apparent activation energy.

REFERENCES

1. Elliott, M.A. in 'Chemistry of Coal Utilization', John Wiley & Sons, New York, USA, 1981, p. 455-460.
2. Kalema, W.S. and Gavalas, G.R. *Fuel* 1987, 66, 158.
3. Swartz, D., Hall, P.J. and Marsh, H., *Fuel* 68, 1989, 868.
4. Painter, P.C., Snyder, R.W., Pearson, D.E. and Kwong, J., *Fuels* 1980, 59, 282.
5. Liotta, R., Brown, G. and Isaacs, J., *Fuels* 63, 1984, 935.
6. Berkowitz, N. "An Introduction to Coal Technology," Academic Press, New York, 1979, p. 96.
7. Andersen, N.F. and Hamza, H.A., "The Characterization of Oxidized Coal-A Review," Proc. CIC Symp., Halifax, Nova Scotia, 1981, p. 117.

8. Barkowitz, N., "Atmospheric Oxidation of Coal," in Sampling, Selection, Aging, and Reactivity of Coal, (Klein, ed.), John Wiley and Sons Inc., New York, 1989, pp. 217-289.
9. Mikula, R.J., Axelson, D.E., and Michaelian, K.H., "Oxidation and Weathering of Stockpiled Western Canadian Coals," CANMET Divisional Report ERP/CRL 85-105(OP-3), 1985.
10. Estevez, M., Juan, R., Ruiz, C. and Andres, J.M. Fuel 69, 1990, 57.
11. Juan, R., Ruiz, C., Andres, J.M. and Estevez, M., Fuel 69, 1990, 61.
12. Unarov, T., Zh., Pobedonostseva, O.I. and Pobedorostseva, N.I., Solid Fuel Chem. 15(4), 1981, 35.
13. Ogunsola, O.I. and Rao, P.D., Fuel 72, 1992, p. 1121.
14. Ogunsola, O.I. and Rao, P.D., "Effect of Thermal Treatment on the Pyrolysis Behavior of Alaskan Low-Rank Coals," Proc. Ninth Annual Int. Pittsburgh Coal Conference, Pittsburgh, p. 509, 1992.
15. Merritt, R.D. and Hawley, C.C., "Map of Alaska's Coal Resources," Alaska DNR Special Report 37, 1986.
16. Youtcheff, J.S., "Characterization of Alaskan Coals-Evaluation of their Liquefaction Behavior," MIRC Report No. 72, p. 366, 1986.
17. Rao, P.D., Walsh, D.E., Willson, W., and Li, Yu-Fu, "Characterization of Hydrothermally and Evaporatively Dried Coals and Char Products from Usibelli Subbituminous C Coals," Paper Presented at the Low Rank Fuel Symposium, Billings, Montana, May 20-23, 1991.
18. Kasperski, K.H. and Ogunsola, O.I., Thermal Analysis of Nigerian Coals Using Thermogravimetry, Presented at the 24th Annual Conf. of Canadian Institute of Chemical Engineers, Halifax, Nova Scotia (1989).
19. Cummings, J.W., Reactivity Assessment of Coals Using a Weighted Mean Activation Energy, Fuel 63 (1984), 1436.
20. Anthony, D.B. and Howard, J.B., Coal Devolatilization and Hydrogasification, AIChE J. 27 (1976), 625.
21. Jenkins, R.G., Nandi, S.P. and Walker, P.L., Jr., Reactivity of Heated Treated Coals in Air at 500°C, Fuel 52 (1975), 288.
22. Mahajan, O.P. and Walker, P.L., Jr., Reactivity of Heat Treated Coals, in C. Karr (Ed.), Analytical Methods for Coal and Coal Products Vol. II, Academic Press, Inc., 1978, pp. 465-494.
23. Leslie, I.H., Jost, M., and Kruger, C.H., Measured and Predicted Char Reactivity of Three U.S. Coals, Combustion and Flames 78 (1989), 195.

TABLE 1. Characteristics of Beluga coal

<u>Beluga Coal</u>	
Proximate analysis: (wt/%, ASTM equilibrium moisture basis)	
Moisture	24.40
Ash	7.71
Volatile matter	33.72
Fixed carbon	34.18
Ultimate analysis: (wt/%, ASTM equilibrium moisture basis)	
Carbon	46.73
Hydrogen	6.88
Nitrogen	0.71
Sulfur	0.18
Oxygen	37.79
Heating Value (MJ/kg)	18.84

TABLE 2. Summary of Results

	Raw Coal BxO	Oxidized Coal for 8 days, Bx8	Oxidized demineralized coal for 8 days, Bdx8
Peak Temperature of Region 1, (°C)	119	110	113
Peak Temperature of Region 2, (°C)	343	329	331
Weight Loss Rate at Region 1, (Mg/Min)	0.028	0.022	0.019
Weight Loss Rate at Region 2, (Mg/Min)	0.181	0.156	0.170
Maximum Decomposition Rate, (Mg/Min)	0.181	0.156	0.170
Temperature of max. dw/dt, (°C)	343	329	331
Apparent Reactivity, daf, (Mg/hr/mg)	2.43	1.98	2.06
Activation Energy, (KJ/mol *k)	16.90	25.98	16.7

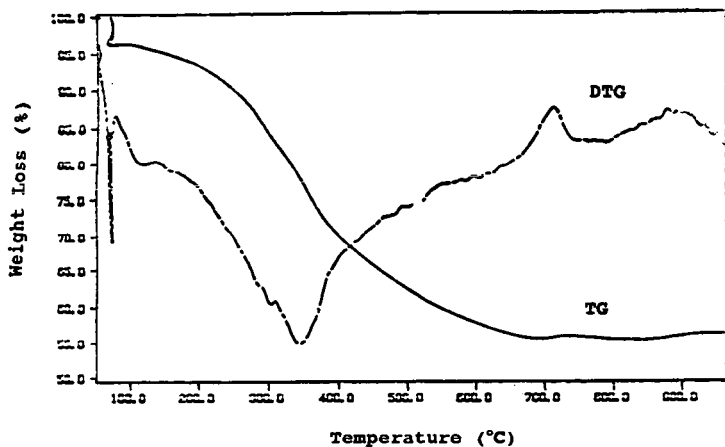


Figure 1. Thermograph of Raw Coal

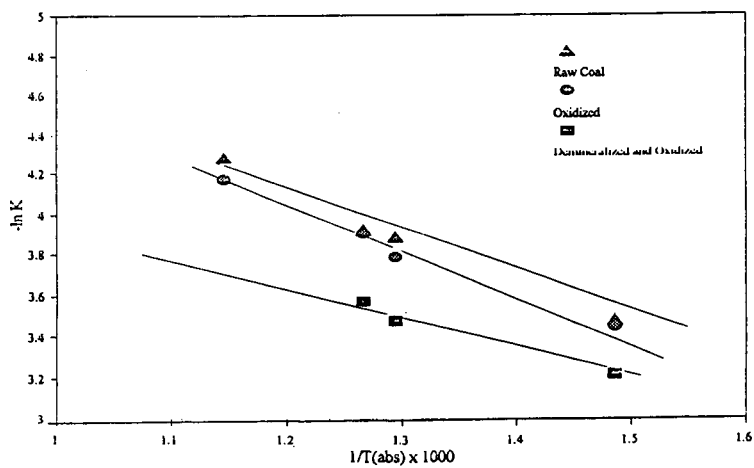


Figure 2. $-\ln K$ verses $1/T$ (abs. $\times 1000$)


P.S. Virk and V.J. Vlastnik
Department of Chemical Engineering
M. I. T., Cambridge, MA 02139

KEYWORDS: Thermolysis, Reaction Paths, Kinetics, Demethylation, Hydrogen Transfer.

INTRODUCTION

Motivation. This work on thermolysis of 9-methyl-anthracene, abbr 9MA, is a part of our continuing studies of methylated acenes, that mimic the chemical moieties found in complex fossil materials of engineering interest. Also, since 9MA is a primary product of 9,10-dimethyl-anthracene, abbr 910DMA, thermolysis [1, 2], it was hoped that information regarding the former might buttress our understanding [3] of 910DMA thermolyses at high conversions.

Previous Work. The earliest work we could find on 9MA thermolysis was by Pomerantz [4], who reported its half-life to be ~ 25000 s at $T = 400$ C for an initial concentration $[9MA]_0 \sim 0.15$ mol/l, with anthracene, abbr ANT, as the major product, accompanied by lesser amounts of 1- and 2-methyl-anthracenes, abbr 1MA, 2MA, and 9,10-dihydro-anthracene, abbr DHA. Subsequently, in a brief experimental and mechanistic study of 910DMA thermolysis at $310 < T < 390$, conducted in the present authors' laboratory, Pope [5] pointed out that 9MA can give rise to two delocalized radicals,


HMA9* and HMA10*, of which only the latter can propagate the demethylation pathway to ANT. Most recently, Smith & Savage [6] have pyrolysed 9MA at $350 < T < 400$ using $[9MA]_0 \sim 0.09$ mol/l. Their decomposition kinetics were ~ 20 -fold faster than those reported by Pomerantz [4] and they detected dimethyl-anthracenes, abbr DMAs, among the products, in addition to the ANT, 1MA, 2MA and DHA previously found.

Outline. We first describe the experiments and present results for the concentration histories, product selectivities, and kinetics observed during 9MA thermolysis. Reaction pathways for the decomposition of 9MA are then inferred from the major products observed, and their ratios. Finally, a free-radical mechanism comprizing 22 elementary steps is proposed for 9MA thermolysis at low conversions, and shown to accommodate many of the experimental observations.

EXPERIMENTAL

Conditions. Table 1 summarizes conditions for, and results obtained from, the present experiments. The first column of this table refers to 9MA substrate and its second to 910DMA, the latter serving as a basis for later comparisons. The upper portion of Table 1 summarizes conditions for the experiments, listing the model substrates, their structures and the ranges of temperatures, holding times and initial concentrations studied, as well as the temperatures at which light gases were analysed. Thermolyses were conducted in batch reactors, volume 0.6 ml, made from 1/4" stainless steel Swagelok parts. The reactors were charged with weighed amounts of biphenyl (internal standard) and substrate (9MA) totalling 0.30 g, sealed and placed in an isothermal, fluidized-sand bath for the appropriate holding times, after which they were quenched in ice-water, and their contents extracted into methylene chloride. Reactor contents were in the liquid phase during all experiments.

Assays. Gaseous and liquid thermolysis products were identified and analyzed by GC, augmented by GC/MS. All gas peaks were identified by injections of standards. Most liquid products were identified by injections of standards with some minor liquid products identified by determining their masses by GC/MS and relating their retention times to those of known molecules. Heavy thermolysis products, mostly dehydrogenated dimers of the substrates, were identified by GC/MS. For example, in 9MA thermolyses, the MS of a prominent late GC peak showed a molecular ion at mass 382 and a fragment at mass 191, suggestive of a bibenzyl, dehydrogenated dimer of 9MA called 9MAD. Product assay trains developed for 9MA substrate using the preceding GC and GC/MS techniques typically identified ~ 15 reaction products. Identified products accounted for $> 70\%$ of the reacted mass at substrate fractional conversions $0.2 < X < 0.8$. Experimental details are available [7].

RESULTS AND DISCUSSION

Histories. Fig. 1 chronicles the concentration histories of substrate and products during thermolysis of 9MA at $T = 370$ C and $[C]_0 = 0.82$ mol/l, using arithmetic coordinates of absolute mols J of either substrate or product present in the reactor versus reaction holding time t in seconds. Part (a), upper panel, shows that the substrate 9MA decayed monotonically, with half-life $t^* \sim 23000$ s. The products formed, in order of their abundance, were ANT, various dimethyl-anthracenes, abbr ALL DMAs, methane CH₄, 1MA, 2MA, and trimethyl-anthracenes, abbr TMA. Part (b), lower panel, details histories of the individually identified dimethyl-anthracene isomers and several 9,10 dihydro- species. The DMAs include 9,10-DMA (major), and 1,10-, 1,9-, and 2,9- + 3,9-DMA, while the hydrogenated species are DHMA (major), DHDMA, and DHA. The formation of DMAs and DHMA products concurrent with ANT shows that during 9MA thermolysis, methylation and hydrogenation always occur in parallel with demethylation. It is also interesting that the isomers 1MA and 2MA both arose subsequent to ANT, which suggests that they formed from methylation of ANT rather than from the isomerization of 9MA.

Selectivities. Fig. 2 depicts the preceding product history data as selectivity diagrams, with ordinate of product selectivity $S = \text{mols J produced/mol of substrate 910DMA decomposed}$, and abscissa of substrate fractional conversion X . Parts (a), upper panel, and (b), lower panel, show that the products formed at low conversions, $X < 0.30$, were ANT, DMAs, DHMA, and CH_4 with selectivities respectively $S = 0.30, 0.20, \sim 0.10$ and 0.05 . With increasing conversions, to $X \sim 0.60$, the selectivity to ANT increased somewhat, to $S \sim 0.35$; the DMAs showed a shallow maximum, $S \sim 0.20$ at $X \sim 0.4$ and then declined slightly; DHMA declined sharply, to $S \sim 0.03$ at $X \sim 0.6$, and CH_4 increased monotonically, to $S \sim 0.15$ at $X \sim 0.6$. The sum of the selectivities of all identified liquid products (squares) was ~ 0.75 over the major range of conversions, $0.2 < X < 0.6$, from which the selectivity of unidentified, mostly heavy, product formation is inferred to be ~ 0.25 .

Kinetics. 9MA decomposition kinetics are illustrated in Fig. 3. Part (a), upper panel, is a log-log plot of decay half-life t^* versus initial concentration $[9\text{MA}]_0$ at fixed temperature. The data, spanning 1.5 decades of $[9\text{MA}]_0$, describe a line of slope $-1/2$, which implies that the decomposition was of $3/2$ order wrt substrate. Part (b), bottom panel, is an Arrhenius type of semi-log plot, showing decay half-life t^* versus the reciprocal of a scaled absolute temperature $\Theta = 0.004573 \cdot (T \text{ C} + 273.2)$. Here the data span almost two decades of t^* and lie on a line of slope ~ 46 , which latter is directly the activation energy of decomposition E^* , kcal/mol. The observed kinetics are summarized in Table I, which shows decay half-lives at $T = 370 \text{ C}$, orders wrt substrate, and Arrhenius parameters ($\log A, E^*$). Both the decompositions of 9MA and of 910DMA are of $3/2$ order wrt the substrate and exhibit activation energies $\sim 45 \text{ kcal/mol}$; their relative decomposition rates are roughly in the ratio $1 : 2$.

Product Ratios. The importance of each of the observed hydrogenation, methylation, and methane formation pathways relative to the dominant demethylation pathway can be assessed from the respective primary product ratios R , namely $R[\text{DHMA}/\text{ANT}]$, $R[\text{DMAs}/\text{ANT}]$ and $R[\text{CH}_4/\text{ANT}]$. Of these, the ratio of hydrogenation to demethylation $R[\text{DHMA}/\text{ANT}] \rightarrow 0.7$ at the lowest conversions, $X \rightarrow 0$, and then decreased rapidly to 0.05 ± 0.025 for $0.20 < X < 0.75$; this variation of $R[\text{DHMA}/\text{ANT}]$ versus X was essentially independent of initial concentration and temperature. Fig. 4(a), left panel, shows that the ratio of methylation to demethylation $R[\text{DMAs}/\text{ANT}] \sim 0.8 \pm 0.1$ for $X < 0.3$ at all temperatures while Fig. 4(b), right panel, shows that the ratio of methane formation to demethylation $R[\text{CH}_4/\text{ANT}] = 0.20 \pm 0.03$ for $X < 0.3$ at $T = 370 \text{ C}$. The sum $R[\text{DMAs}/\text{ANT}] + R[\text{CH}_4/\text{ANT}] \sim 1.0$ was close to unity, accounting for the methyl radicals implicitly associated with the demethylation pathway. Thus, at low substrate conversions, $\sim 1/5$ of all methyl radicals formed were quenched by hydrogen abstraction, forming methane gas, while $\sim 4/5$ were trapped by addition to the 9MA substrate, eventually appearing as DMAs. These results for 9MA substrate are in striking contrast to those for 910DMA [3], wherein $\sim 3/4$ of methyl radicals were quenched by hydrogen abstraction while $\sim 1/4$ were trapped by addition to the substrate. Since 9MA and 910DMA respectively possess 3 and 6 benzylic H-atoms per molecule, the observed $[\text{H-abstraction/addition}]$ ratios of $1/4$ versus $3/1$ show the methyl addition affinity of 9MA to be 6-fold greater than that of 910DMA. The greater methyl affinity of 9MA relative to 910DMA likely derives from the potency of its unsubstituted 10-position as an addition site.

Pathways. The foregoing observations lead to the 9MA decomposition pathways depicted in Fig. 5. Three primary pathways operate in parallel: (P1) Hydrogenation, to DHMA, (P2) Demethylation, to ANT, and (P3) Methylation, to 910DMA. Too, the demethylated acene product is associated with formation of methane gas CH_4 , and the scheme also includes formation of a heavy benzylic dimer of 9MA called 9MAD. Further, the primary demethylation and methylation products shown in the above scheme can be secondarily operated upon by a pathway triad analogous to the one from which they arose, leading, recursively, to the formation of a variety of methylated and hydrogenated acenes. This is evident in the appearance, at high conversions, of TMAs, a host of DMAs, 1MA and 2MA, as well as DHA and DHDMA (for clarity, these secondary products were omitted from Fig. 5). Pathway results are summarized in the bottom of Table I, which shows major product selectivities and ratios at $T = 370 \text{ C}$ and conversions $X = 0.05$ and 0.4 . Results for 9MA were akin to those obtained for 910DMA, but showed a two-fold greater selectivity to the methylated product, and also roughly two-fold greater ratios of hydrogenated/demethylated and of methylated/demethylated products at low conversions.

Mechanism. A possible mechanism for 9MA thermolysis is presented in Fig. 6, an elementary step "graph" constructed with substrate and all stable molecular products arrayed in the bottom row and unstable radical intermediates arrayed in the top row. Reaction "nodes", in the middle row, connect the individual species in the bottom and top rows with arrows indicating the initial direction of reaction (all reactions are reversible). Initiation reactions are denoted by solid interconnecting lines, propagation reactions by dashed lines and termination reactions by dotted lines. The 9MA substrate is in the middle of the bottom row, with light (propagation) products to its right and heavy (termination) products to its left. Consider first a subset of the full mechanism comprising reactions (R1-R10). This free-radical cycle is initiated by the bimolecular disproportionation of substrate (R1), an intermolecular hydrogen transfer reaction, to form the respectively dehydrogenated and hydrogenated radical species 9MA^* and $\text{HMA}10^*$. Of these, the latter can either abstract hydrogen from 9MA by (R2), to form DHMA product, or undergo a β -scission type of radical decomposition by (R3), forming ANT product and a methyl radical CH_3^* . The CH_3^* can either abstract H from 9MA by (R4), to form methane product, or add to 9MA by (R5), to form the dimethyl radical HDMA^* . The latter can then abstract H from 9MA via (R6) to form the observed 910DMA product. The cycle is terminated by the species 9MA^* and $\text{HMA}10^*$ engaging in both pure- and cross-combinations, (R7-R9), to form various dimeric products. $\text{HMA}10^*$

radical can also terminate by disproportionation, (R10), to form 9MA and DHMA. The foregoing portion of the full 9MA mechanism is evidently analogous to the 910DMA mechanism devised earlier [2, 3]. However, the 9MA substrate permits formation of an additional radical, HMA9*, which can engage in all the steps shown for HMA10* except for C-C bond scission, giving rise to steps (R11-R22) of the full mechanism. Thus substrate disproportionation by (R11) forms 9MA* and HMA9*, of which the latter can abstract hydrogen from 9MA by (R12), to form DHMA product. HMA9* can also form from H-transfer reactions (R16), between HDMA* and 9MA, and (R17), between HMA10* and 9MA, the latter causing radical isomerization. Finally, HMA9* can engage in a variety of termination reactions, including pure- and cross-combinations (R18, R19, R21) that form dimeric products, and disproportionations (R20, R22) that form 9MA and DHMA.

The proposed mechanism accounts for the major products, ANT, DMAs, DHMA, CH₄ and heavies, observed during the initial stages of 9MA thermolysis. Each of the observed triad of primary pathways, namely, P1 hydrogenation, P2 demethylation and P3 methylation, also arise naturally as limiting cases of the elementary step graph, with P1 comprising the sets [R1, R2, R7] and [R11, R12, R7], P2 the set [R1, R3, R4, R7] and P3 the set [R1, R3, R5, R6, R7]. The stoichiometry of these sets restricts the maximum selectivity of each major product to 1/3, which is of the magnitude of the highest selectivities actually observed. The mechanism also offers some theoretical insights. It suggests that the relative kinetics of hydrogenation to demethylation, (P1)/(P2), are controlled by the HMA9* and HMA10* radicals. The HMA10* radical propagates both hydrogenation (R2) and demethylation (R3), but HMA9* propagates only hydrogenation (R12). It follows that the pathway ratio (P1)/(P2) = [(R2)+(R12)]/(R3) for 9MA should exceed that for 910DMA, which has only a single radical carrier analogous to HMA10*. This accords with the observations in Table 1, which show (P1)/(P2) for 9MA almost twice that for 910DMA at low X. Further, the methylation to demethylation ratio, (P3)/(P2), is essentially governed by competition between methyl radical reactions (R4) and (R5), in which CH₃* either abstracts H from or adds to the 9MA substrate. In this regard, H-abstraction from 9MA should be less favoured than that from 910DMA by a statistical factor of 2, but 9MA possesses a potent unsubstituted 10-position in addition to all the unsubstituted positions present in 910DMA, so methyl radical addition to 9MA should be greatly favoured over that to 910DMA. Theoretically, therefore, the pathway ratio (P3)/(P2) for 9MA should exceed that for 910DMA. This accords with observations in Table 1 which show (P3)/(P2) for 9MA from 1.5 to 2 times that for 910DMA over the entire range of substrate conversions.

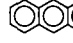
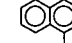
In future work it is hoped that the mechanism presented above will provide a basis for the further quantitative modelling and numerical simulation of 9MA and 910DMA thermolyses.

ACKNOWLEDGEMENT: This work was supported in part by Cabot Corporation, Boston, MA.

REFERENCES

- [1] Virk, P.S.; Vlastnik, V.J.: PREPRINTS, Div. of Fuel Chem., ACS, 37(2), 947 (1992).
- [2] Virk, P.S.; Vlastnik, V.J.: PREPRINTS, Div. of Petrol. Chem., ACS, 38(2), 422 (1993).
- [3] Virk, P.S.; Vlastnik, V.J.: PREPRINTS, Div. of Fuel Chem., ACS, 39(2), 546 (1994).
- [4] Pomerantz, M.; Combs Jr., G.L.; Fink, R.: J. Org. Chem., 45, 143 (1980).
- [5] Pope, J.M.: Ph.D. Thesis, Dept. of Chem. Eng., MIT, Cambridge, MA (1987).
- [6] Smith, C.M.; Savage, P.E.: A.I.Ch.E. J., 39, 1355 (1993).
- [7] Vlastnik, V.J.: Sc.D. Thesis, Dept. of Chem. Eng., MIT, Cambridge, MA (1993).

Table 1. Experimental Grid, Kinetics, and Major Product Selectivities and Ratios for Thermolyses of 9MA and 910DMA.

Substrate	9MA	910DMA	
Structure			
Experimental Grid			
Temperature, T C	315-409	315-409	
Holding Time, t s	450-57600	450-57600	
Initial Concentration, [C] ₀ , mol/l	0.082-2.06	0.082-2.47	
Gas Analyses at T C	370	335, 370	
Kinetics			
Decay Half-Life, t* s at T = 370 C	23000	9900	
Order wrt substrate	1.50	1.53	
Arrhenius Parameters (log A, E*)	(11.4, 46.4)	(10.6, 43.1)	
Product Selectivities at T = 370 C	X		
Demethylated	0.4	0.37	0.42
Methylated	0.4	0.22	0.10
Hydrogenated	0.05	0.03	0.06
Heavies	0.4	0.13	0.15
Product Ratios at T = 370 C	X		
[Hydrogenated/Demethylated]	0.05	0.43	0.21
	0.4	0.05	0.04
[Methylated/Demethylated]	0.05	0.69	0.35
	0.4	0.59	0.24

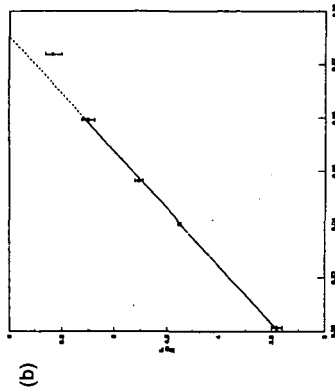
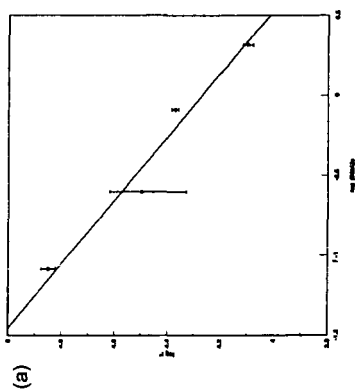


Fig. 3. 9MA thermolysis kinetics.
(a) Effect of $[9MA]_0$ at fixed $T = 370^\circ\text{C}$.
(b) Arrhenius diagram for fixed $[9MA]_0 = 0.82\text{ mol/l}$.

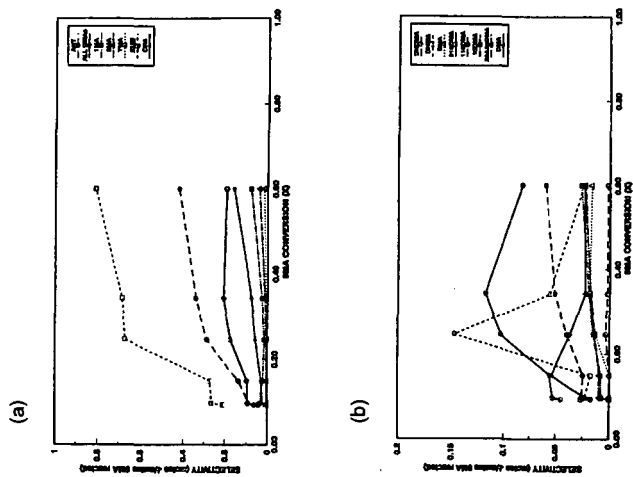


Fig. 2. Product selectivities for 9MA thermolysis at $T = 370^\circ\text{C}$, $[9MA]_0 = 0.82\text{ mol/l}$.
(a) ANT, DMAS, 1MA, 2MA, TMA, SUM, CH_4 .
(b) All other products.

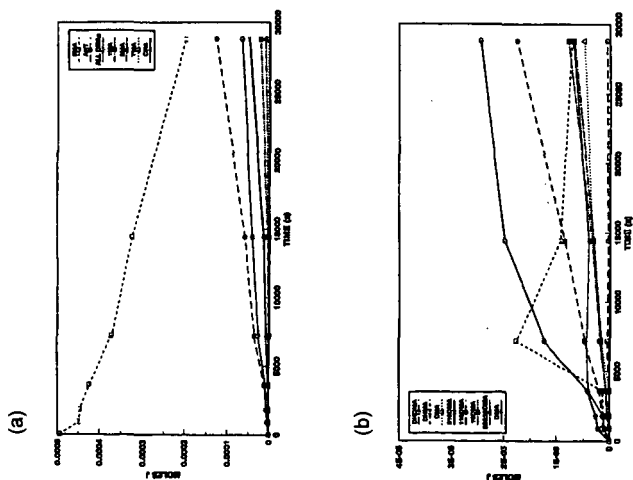


Fig. 1. Substrate and product histories for 9MA thermolysis at $T = 370^\circ\text{C}$, $[9MA]_0 = 0.82\text{ mol/l}$.
(a) 9MA, ANT, DMAS, 1MA, 2MA, TMA, CH_4 .
(b) All other products.

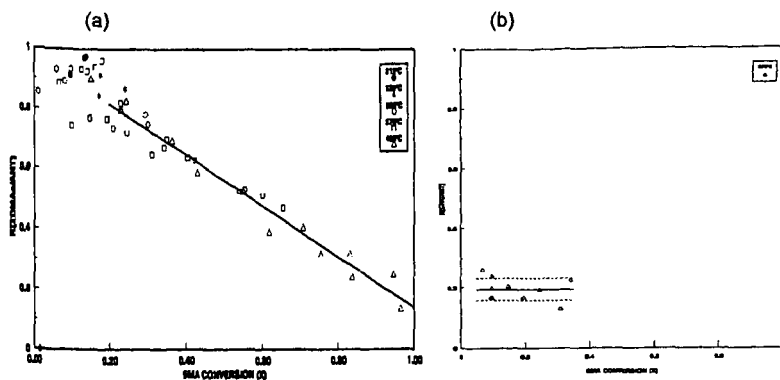


Fig. 4. Major product ratios in 9MA Thermolyses.
 (a) $R[DMA/ANT]$ at $T = 315$ to 409 C and $[9MA]_0 = 0.82$ mol/l.
 (b) $R[CH_4/ANT]$ at $T = 370$ C and $[9MA]_0 = 0.82$ mol/l.

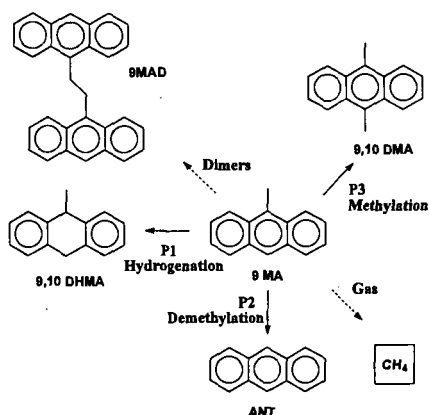


Fig. 5. Major pathways in 9MA thermolysis.

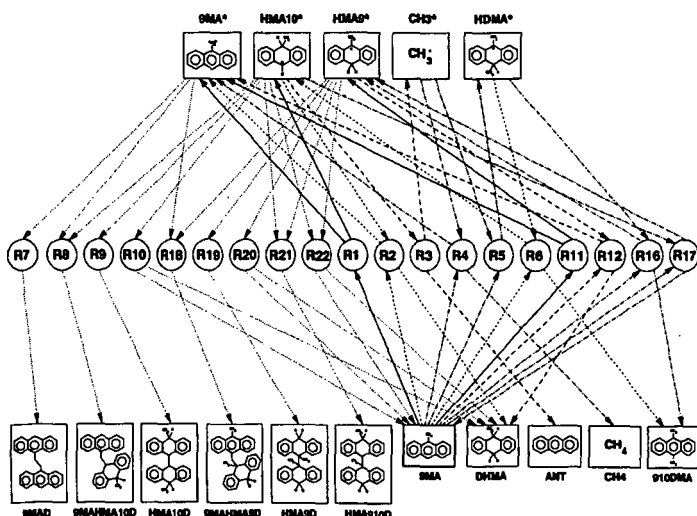


Fig. 6. Elementary step graph of 9MA thermolysis mechanism at low conversions.

CONVERSION OF WASTE POLYVINYL CHLORIDE (PVC) TO USEFUL CHEMICALS

T. Kamo, Y. Yamamoto, K. Miki, Y. Sato
National Institute for Resources and Environment
16-3, Onogawa, Tsukuba-shi, Ibaraki, 305, Japan

Keywords: PVC, Recycling, Pyrolysis, Liquefaction

INTRODUCTION

Developments of recycling technologies are expected one of the most important keys for saving energy and resources, and minimization impact for environment. For instance, combustion of waste for power generation and conversion of plastics into liquid fuels have been studying for thermal energy recycling ^{1), 2)}. However, PVC has been excepted from the most of these experiments. Because, heat of combustion of PVC is almost a half of other plastics', hydrogen chloride, which is produced at low temperature, corrodes the combustion chamber, and PVC causes coking reaction during pyrolysis of plastics.

Numerous investigations have been conducted on degradation of PVC. However, most of these experiments were done to improve heat resistance of PVC ^{3), 4)} or to study reaction mechanism of PVC degradation ^{5), 6)}. Pyrolysis of PVC into liquid products have been studying since 1960's from a view of environmental protection ^{7), 8), 9)}. Recently, Y. Maezawa et al. reported PVC was converted into oil at 600 °C with sodium hydroxide ¹⁰⁾. However, more than 50 % of hydrocarbon fraction of PVC was converted to residue and gas in their experiment. We are going to develop a new technology to convert of PVC into useful chemicals or liquid fuels at high efficiency by using hydrogen donor solvent.

In this experiment, we used PVC resin, because commercial PVC contain many other compounds as stabilizer. Chlorine in PVC was removed by pretreatment to prevent corrosion of an autoclave. We liquefied pretreated PVC resin in tetralin with some catalysts.

EXPERIMENTAL

Pre treatment of PVC: PVC resin was supplied Mitsubishi Kasei Vinyl Company. The PVC resin (100 g) was charged in a Pyrex flask (300 ml) and heated with nitrogen gas flowing. The samples were heated according to following temperature program, 200 °C (24 hours), 250 °C (24 hours) and 300 °C (24 hours). Finally, the samples were heated at 300 °C for 24 hours under vacuum. Weight of samples decreased less than 40 % of initial PVC resin after the pre treatment. Elemental analyses of original PVC resin and pretreated PVC resin were shown in Table 1. The pretreated resin still contained 2.8 % of chlorine.

Reaction procedure: Pretreated PVC resin (10.0 g) and tetralin (70.0 g) were charged into a 300 ml magnetic stirred autoclave. In order to study effects of catalysts on product distribution and content of remained chlorine in products, nickel - molybdenum catalyst for upgrading of petroleum (NiMo/Al₂O₃, 1.0 g) and sulfur (0.5 g), iron oxide (Fe₂O₃, 1.0g) and sulfur (0.5 g), Zeolite for FCC (1.0 g), and fine nickel powder (Ni, 1.0 g, diameter < 0.3 μm) were added in a few experiments. All reactions were carried out at 440 °C and 470 °C under an initial pressure of 6.9 MPa of hydrogen gas or nitrogen gas. Reaction products were separated residues and liquid products by filtration. The liquid products were vacuum distilled at 330 °C for 60 min. The vacuum bottoms were separated HS (hexane soluble) and HI (hexane insoluble) by hexane extraction. The residue and extracted products, HS and HI, were dried for one day at 110 °C under vacuum and weighted.

Analysis of products: Gas products were collected into a Teflon bag through 10% of sodium hydroxide aqueous solution and analyzed by gas chromatography (GASUKURO KOGYO, GC-312, molecular sieve 5A, molecular sieve 13X, Porapak N, gasukuro 54, and VZ-7). Liquid products were analyzed by gas chromatography (CARLO ERBA INSTRUMENTS, HRGC 5300) with capillary column (HP Ultra 1, 0.2 mm, 50m). Chlorine content in product was measured by total chlorine analyzer (Mitsubishi Kasei, TOX-10Σ).

RESULTS AND DISCUSSION

Product distributions from the pretreated PVC resins were shown Figure 1. Yields of each product were obtained by using an equation shown below. Oil yields were calculated from yields of gas, HS, HI and residue.

$$\text{yield(i)} = \frac{\text{weight of product (i)}}{\text{weight of hydrocarbon fraction in chlorine removed PVC}} \times 100$$

Yields of gas and residue were only 3 % and 13 % respectively at 440°C under nitrogen gas. Y. Maezawa et al.¹⁰⁾ reported that more than 50 % of hydrocarbon fraction in PVC was converted to gas and residue under conventional pyrolysis condition with sodium hydroxide. Remarkable decreases of yields of gas and residue observed in our experiment were caused by using hydrogen donor solvent. Product distribution from pretreated PVC indicates that hydrogen gas and NiMo/Al₂O₃ catalyst enhanced conversion of HS to oil and residue to HI at 440 °C. However, decomposition of HI to HS was not promoted in spite of presence of hydrogen gas and NiMo/Al₂O₃ catalyst. Yields of oil and HS increased with temperature significantly. Oil yield and HS yield were achieved to 40 % and 44 % respectively at 470 °C with NiMo/Al₂O₃ under hydrogen gas.

Methane, ethane, propane were produced mainly under our reaction condition. Production of methane increased particularly at 470 °C. Benzene, toluene and xylene (BTX) were produced as main liquid products from the pretreated PVC. Total yields of BTX were shown in Figure 2. Yields of these products increased with temperature significantly under hydrogen gas. These trends imply hydrogen gas enhanced production of BTX from pretreated PVC. Tetralin isomer, alkylated tetralin and tetralin dimmer were observed in the solvent after liquefaction. Productions of these compounds indicate hydrogen was transferred from tetralin very rapidly, isomerization and dimerization of tetralin radical were enhanced.

In order to show effects of various catalysts on pyrolysis of pretreated PVC, NiMo/Al₂O₃, iron oxide (Fe₂O₃), Zeolite and fine nickel powder were used. Product distributions of these catalysts were shown in Figure 3. Remarkable increases of oil yield or HS yield were not observed at 440°C. The NiMo/Al₂O₃ was most effective catalyst for pyrolysis of pretreated PVC.

Low chlorine contents of products are very important to use them as chemicals and liquid fuels. Chlorine contents of products from liquefaction were shown Figure 4. Chlorine contents of oil and vacuum bottom (HI+HS) were 25 ppm and 8 ppm respectively under nitrogen gas at 440 °C. These results show 99.9% of chlorine in pretreated PVC was removed by liquefaction. Chlorine contents of oil and HS+HI produced under hydrogen gas were lower than that of products obtained under nitrogen gas. Under hydrogen gas with NiMo/Al₂O₃, chlorine content of oil and HS+HI were only 2 ppm and 3 ppm respectively. Remarkable decreases of chlorine content were observed at 470 °C. Chlorine content decreased with severity of hydrogenation of products. These results imply chlorine was removed by hydrogenation reaction of products.

Effects of catalysts on chlorine content of HS+HI were shown in Figure 5. Iron oxide and fine nickel powder did not show remarkable effects on removal of

chlorine in products. On the other hand, zeolite inhibited removal of chlorine from products. This negative effect was estimated to be caused by strong acidity of zeolite.

SUMMARY AND CONCLUSION

PVC was heated under nitrogen gas to remove chlorine at 300 °C for 24 hours. Then, pretreated PVC was liquefied in tetralin at 440 °C and 470 °C for 60 minutes under an initial pressure of 6.9 MPa of hydrogen gas and nitrogen gas. Oil yield and HS yield were 40 % and 44 % respectively at 470 °C with NiMo/Al₂O₃ under hydrogen gas. Benzene, toluene and xylene were produced as main liquid product. Chlorine content in products decreased with temperature. Less than 3 ppm of chlorine was retained in oil and vacuum bottom (HS+HI) at 470 °C under hydrogen gas with NiMo/Al₂O₃. Hydrogen transferred from tetralin and hydrogen gas enhanced conversion of pretreated PVC to liquid products and removal of chlorine from products.

ACKNOWLEDGMENTS

We greatly thank T. Ueda, Japan PVC Association and H. Yamamoto, Mitsubishi Kasei Vinyl Company for supply PVC resin. We also acknowledge T. Imagawa, National Institute for Resources and Environment, Hydrosphere Environmental Protection Dept. for use of the total chlorine analyzer.

REFERENCE

- 1) D. S. Scott, S. R. Czernik, J. Piskorz and D. St. A. G. Radlein, *Energy & Fuels*, 4, 407 (1990).
- 2) R. C. Bailie, *Combustion*, 2, 13 (1974).
- 3) A. H. Frye and R. W. Horst, *J. Polym. Sci.*, 40, 419 (1959).
- 4) N. Bensemra, T. Van. Hoang, A. Guyot, M. Gay and L. Garette, *Poly., Deg. & Stab.*, 24, 89 (1989).
- 5) V. H. Tran, C. Carrigues, T. P. Nguyen and P. Molinie, *Poly. Deg. & Stab.*, 42, 189 (1993).
- 6) M. Rogstedt, and T. Hjertberg, *Macromolecules*, 25, 6332, (1992).
- 7) K. Saito and A. Kishi, Ichihashi, *The 2nd Japan Symposium on Thermophysical Properties*, 23 (1981).
- 8) Z. Mayer and J. Macromol. Sci., *Revs. Macromol. Chem.*, C10(2), 263 (1974).
- 9) S. Matsuzawa, T. Abe, H. Ando, O. Inomata and Y. Shimizu, *Bulletin of The National Research Institute for Pollution and Resources*, 4(1), 33 (1974).
- 10) Y. Maezawa, F. Tezuka, Y. Inoue, *Toshiba Review*, 49(1), 39 (1994).

Table 1 Elemental analyses of PVC and pretreated PVC

	C	H	O	Cl	H/C	O/C	Cl/C
PVC (resin)	38.64	4.81		56.53 ¹⁾	1.48		0.50
Pretreated PVC (300°C)	85.99	7.10		2.84	0.98		0.01

1) calculated (100 - C% - H%)

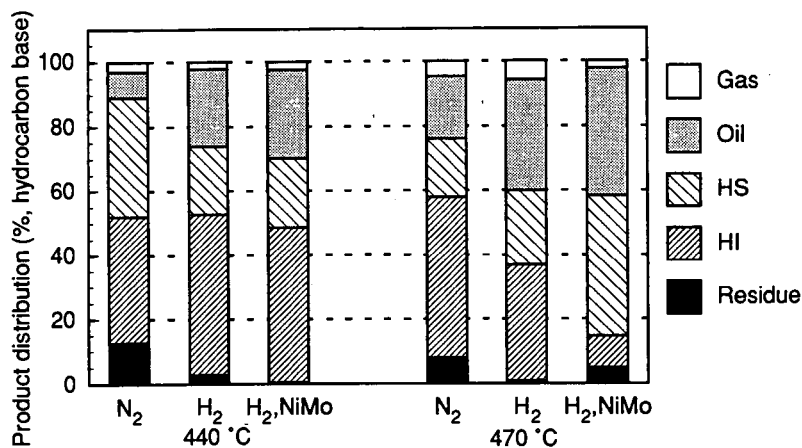


Figure 1 Distribution of products from pretreated PVC.

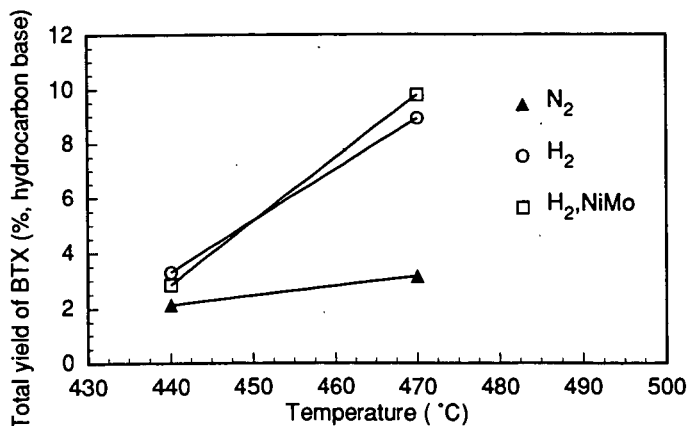


Figure 2 Total yield of benzene, toluene and xylene from pretreated PVC.

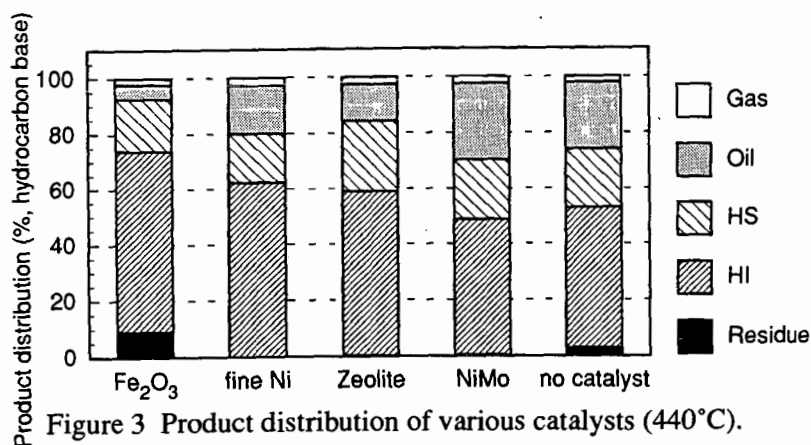


Figure 3 Product distribution of various catalysts (440°C).

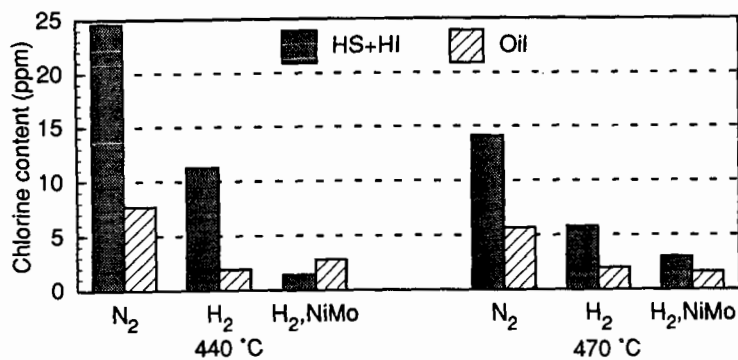


Figure 4 Chlorine content of oil and vacuum bottom (HS+HI).

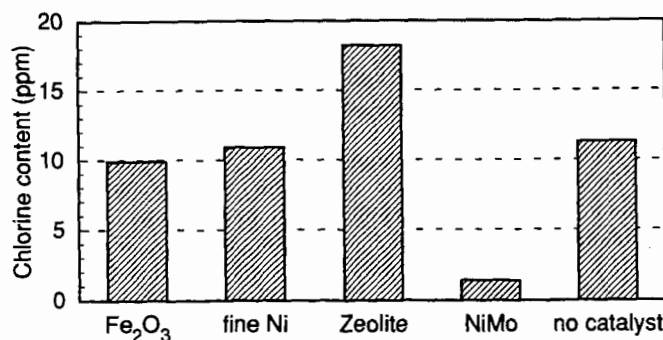


Figure 5 Effect of catalysts on chlorine content of vacuum bottom (HS + HI).

NON-FUEL USES OF COALS AND SYNTHESIS OF CHEMICALS AND MATERIALS

Chunshan SONG and Harold H. SCHOBERT

Fuel Science Program, 209 Academic Projects Building,
The Pennsylvania State University, University Park, Pennsylvania 16802

Keywords: Non-fuel use, Coal, Chemicals, Materials

ABSTRACT

This paper provides an account of our analysis of future needs for non-fuel uses of fossil fuels, particularly coal, and a discussion of possible routes for developing chemicals and materials. An overview of energy supply and demand in the world and the existing non-fuel uses of fossil fuels in the U.S. will be given first. The amount of energy used for non-fuel purpose is small compared with the amount of energy consumed by end users. Nevertheless, the non-fuel uses of fossil fuels may become more important in the future. The demonstrated coal reserves in the world are enough for consumption of over 220 years at the 1992 level, while the oil reserves are only about 40 times of the world's consumption level in 1992. Coal may become more important both as energy source and as the source of chemical feedstocks as we move into the 21st century. However, traditional non-fuel uses of coals (coke ovens and the coal tars) are diminishing rapidly. We will discuss the possible new processes for making both bulk and specialty chemicals and polymers and carbon materials from coals and liquids from coal liquefaction. Specific examples will be provided from work in progress in our laboratory, including conversion of coals and coal liquids to specialty chemicals, polymer materials, activated carbons, graphitic carbons, and electrode materials.

WORLD AND U.S. SUPPLY AND DEMAND OF FOSSIL FUELS

Table 1 summarizes energy supply and demand in the world and in the U.S., and the U.S. primary energy input into the electric utilities. The energy statistics data in this paper were derived from several recent DOE/EIA reports [EIA AER, 1993; AEO, 1994; IEO, 1994; IPSO, 1994; MER, 1993; QCR, 1994]. Fossil fuels are the dominant sources of energies for modern societies as well as chemicals and synthetic organic materials.

Currently the world consumes 66.9 million barrels of oils per day (mbpd) and 24.34 billion barrels per year (136.3 quadrillion Btu/year). According to the most recent report, the estimated crude oil reserves in the world are 999.1 billion barrels, with 66.3% in the Middle East region but only about 2.4% in the U.S. The world is consuming petroleum at a very fast speed. The sum of all the petroleum reserves in world is only 41 times the consumption in 1992.

As of 1992, the sum of all the known natural gas reserves in the world is 4375.8 trillion cubic feet, with about 40% in the former Soviet Union and only 3.8% in the U.S. The world total consumption in 1992 reached 74.7 trillion cubic feet, which is equivalent to 74.3 quadrillion Btu. The known reserves in the world are about 59 times the consumption level in 1992.

The worldwide coal consumption in 1992 is 5001 million short tons (4535.9 million metric tons), which is equivalent to 88.9 quadrillion Btu. The world coal reserves are 1145.3 billion short tons (1038.5 billion metric tons), with about 23.1% in the U.S. The world coal reserves are over 225 times the consumption level in 1992. In particular, coal is the most abundant fossil hydrocarbon resource in the U.S., and the U.S. coal reserves (265.2 billion short tons) are about 300 times the current domestic annual consumption. Coal is expected to become more important in the future both as energy source and as the source of chemical feedstocks.

OVERVIEW OF NON-FUEL USES OF FOSSIL FUELS

Table 2 shows the amount of fossil hydrocarbon resources used for non-fuel purposes. Non-fuel use of fossil fuels in the U.S. is small compared with the amount of energy consumed as fuels by end users. As shown in Table 2, the non-fuel use of fossil resources is overwhelmingly the use of petroleum products, primarily petrochemical feedstocks, asphalt and road oil, petroleum coke, and liquefied petroleum gases. Non-fuel use of coal is dominated by the coal carbonization to make metallurgical coke. The non-fuel use of natural gas includes making synthesis gas, olefins, and carbon blacks. In 1992, the 5.84 quadrillion Btu consumed for non-fuel uses of fossil fuels (including coals for coke production) represented 7.1% of total energy consumption in the U.S. (82.42 quadrillion Btu). Non-fuel use of petroleum is 13.2% of petroleum consumed in the U.S.

Status of U.S. Coal Production and Utilization. Figure 1 shows the profile of the U.S. coal production by type over the period 1960-1992. Currently U.S. coal industry employs about 120 thousand miners, and produces about 1 billion short tons (about 900 million metric tons) of coals

annually [NCA, 1993]. About 90% of the coals are consumed domestically. About 10% of coals mined in the U.S. are exported, and they are bituminous coals, including about 43 and 60 million short tons of steam coals and metallurgical coals, respectively [NCA 1993].

As shown Table 3, electric utilities are the dominant consumers of coals. In fact, their consumption grew from 177 to 780 million tons during 1960-1992 [Song, Schobert, Scaroni, 1994]. The percentage distribution of the domestic consumption in 1992 is as follows: 87.2% by utilities, 8.4% by industries, 3.8% by coke plants, and 0.6% by residential and commercial users. Coal accounted for about 80 % of all the fossil fuels consumed at electric utilities in 1992.

Non-fuel Uses of Coals. Existing non-fuel uses of coals include (1) high temperature carbonization of bituminous coal to make metallurgical coke; (2) gasification of coal to make synthesis gases and other chemicals; (3) use of coal in manufacturing other materials such as activated carbons, carbon molecular sieves (CMS) and production of phosphoric acid; (4) the use of coal tars from carbonization (and gasification) for making aromatic chemicals; and (5) the use of coal tar pitch for making carbon fibers and activated carbon fibers, and other related products.

Energy Policy Act of 1992. Non-fuel uses of coals have also been described under the Section 1304 of the National Energy Policy Act of 1992: The Secretary of Energy shall plan and carry out a program of research, development, demonstration, and commercial application with respect to technologies for the non-fuel use of coal, including (1) production of coke and other carbon products derived from coal; (2) production of coal-derived, carbon-based chemical intermediates that are precursors of value-added chemicals and polymers; (3) production of chemical feedstocks via coal treatment processes.

Non-fuel Use through Coal Liquefaction. It is expected that coal liquefaction could become a viable option sometime in the next century, for producing liquid transportation fuels as well as chemical feedstocks. Despite enormous strides in coal liquefaction research and development, coal-derived liquid fuels are still not economically competitive with petroleum. However, the economic analysis of the viability of coal liquefaction may well produce a different result if some coal-derived liquids, particularly aromatic and phenolic compounds, can be used for making value-added chemicals and polymer materials. Just as crude oils are also used for making petrochemicals, the liquids from coal liquefaction are expected to provide the needed organic chemicals, albeit in smaller amounts compared to their use as fuels.

The importance of promoting non-fuel uses of coal in conjunction with coal liquefaction in the future is also apparent from the following facts. In 1970 the daily petroleum production and consumption in the U.S. were 9.64 and 14.70 million barrels, respectively. However, the U.S. petroleum production decreased to 6.84 million barrels/day in 1993, whereas the consumption increased to 17.03 million barrels/day. The worldwide petroleum consumption also rose from 46.81 million barrels/day in 1970 to 66.93 million barrels/day in 1993, which is a 43% increase in 22 years. Currently, the U.S. petroleum consumption is about 24.6% of the world's total consumption, but U.S.'s petroleum reserves are only about 2.4% of the world's total reserves. The remaining crude oils in the existing reserves are getting heavier. For example, the average API gravity of crudes refined in the U.S. decreased from 33.8 to 31.8 during the 10 years between 1980 and 1990; related to this increase in density (decrease in API gravity) is a constant rise in the sulfur content of the crude oils, from 0.88 wt% in 1980 to 1.11 wt% in 1990 [Swain, 1991]. With the continuing decline in the resource and in the quality of crude oils, the processing of coal-derived oils in existing petroleum refineries may become economically viable sometime in the 21st century.

Liquids from coal liquefaction may be used as feedstocks for making organic chemicals and various carbon materials, in addition to their use for producing transportation fuels. Relative to heavy oils, the problems associated with refining coal-derived liquids are their higher contents of aromatics, particularly polycyclic aromatics, and higher contents of nitrogen- and oxygen-containing compounds. Sulfur removal does not seem to be such a technical problem, since it is thought that hydrodesulfurization is easier, chemically, than hydrodenitrogenation. In the context of the production of chemicals and specialty materials, however, the high contents of aromatics, phenolics, and nitrogen compounds may provide a practical application of the folk adage, "If life hands you a lemon, make lemonade." If the "lemon" is the problem of dealing with the oxygen and nitrogen compounds prior to conventional refining for fuel use, the "lemonade" may be the use of these compounds and their derivatives for making value-added chemicals and monomers for aromatic polymer materials.

SYNTHESIS OF CHEMICALS AND POLYMERS FROM COALS

Before 1945 about 75% of all the organic chemicals in the world were based on coal-derived liquids, but with the advent of vast petroleum resources in the world during the 1940s, crude oil gradually became dominant chemical feedstocks by 1960. Currently petroleum and natural gas account for more than 90% of the major industrial organic chemicals [Speight, 1991; Sheldon, 1983]. These resources are the primary sources of the seven basic organic chemical building blocks: ethylene, propylene, butadiene, benzene, toluene, the xylenes, and methanol. However, coal tars remain an important source of aromatic chemicals. The annual consumption of aromatic chemicals worldwide is about 25 Mt for benzene, toluene, and xylenes; and 5 Mt for naphthalene and three- and four-ring compounds [Murakami, 1987; Collin, 1985]. Coal tar accounts for about 15-25% of the BTX production and 95% of the larger aromatics.

The last two decades have witnessed enormous developments in various organic and carbon-based materials [Song and Schobert, 1993], and it is certain that the late 1990's and the 21st century will see significant further growth of these materials. Examples include engineering plastics, liquid crystalline polymers, high-temperature heat-resistant polymers, polymer membranes, graphitic carbon materials, carbon fibers, and activated carbon fibers. Many of the starting materials for monomers of the aromatic polymer materials are not readily available from petroleum.

Scheme I shows some important aromatic polymer materials [Song and Schobert, 1993]. Scheme II gives the structures of some important liquid crystalline polymers [Song and Schobert, 1993]. Due to the recent development of many aromatic polymer materials, there is a great demand for aromatic monomers. Since the U.S. production of coal tar, which is an important source for 1- to 4-ring chemicals (particularly 2- to 4-ring aromatics), has declined significantly in the past decade, there is a need for developing an alternative source of aromatic chemicals in the future. With the rapidly increasing engineering applications of aromatic compounds for polymer materials, the demands for many aromatics of one to four rings have increased in the recent past, and this trend is expected to continue into the 21st century. Thus an excellent opportunity exists to explore the potentials of developing value-added chemicals and specialty materials from coals and the liquids obtained from coal liquefaction.

As we have discussed in detail elsewhere [Song and Schobert, 1993], research on deriving coal-based chemicals from coal liquids can be viewed as an extension of coal liquefaction research. Development of value-added chemical products could both increase the economic viability of coal liquefaction and make coal liquids more competitive with petroleum because coal liquids contain many compounds not found in petroleum [Song et al., 1991, 1992; Lai et al., 1992; Zhou et al., 1992; Saini and Song, 1994]. In analogous fashion, the economic viability of processing heavy residual materials could also be strengthened if approaches were developed for their conversion into value-added chemical feedstocks as well as transportation fuels.

We suggest that two broad approaches can be taken for coal conversion into value-added chemicals. The first can be viewed as the indirect approach, analogous to the so-called "indirect" coal-to-chemicals conversion [Schobert, 1984]. The essence of the indirect approach would be the conversion of coals to liquids. Once the liquids were obtained, they would be subjected to appropriate separation or conversion operations to produce the chemical products of interest. However, separation of coal liquids into individual compounds is time consuming and expensive. An analogy from coal processing is the concept of combining short-contact-time liquefaction with catalytic dealkylation to produce aromatic hydrocarbon monomers [Song et al., 1989; Hirota et al., 1989]. The simplified aromatic compounds will then be used for making value-added products. The alternative, much bolder and of much higher risk, is the direct approach. In this approach a reagent would be introduced to the coals to cleave only a certain well-defined set of bonds and carefully cut out the molecular structures of interest. The highly selective removal of these structures could lead to monomers or precursors to the monomers for some of the high-performance polymer materials. An analogy proposed for direct production of chemicals from coal would be the use of selective oxidation to generate high yields of benzene carboxylic acids from low-rank coals [Song and Schobert, 1993].

On-going Research on Catalytic Synthesis of Chemicals in This Laboratory

In this section, specific examples will be provided from work in progress in our laboratory, including conversion of aromatic compounds in coal liquids to value-added chemicals, specialty chemicals, and monomers for polymer materials. We are exploring the catalysts, reactions, and processes for developing value-added chemicals and materials from coal-derived, carbon-based compounds.

Production of Phenol and Aromatics from Coals via Liquefaction. We are studying coal liquefaction in conjunction with the production of aromatic chemicals. Analysis of various coal-derived oils indicates that there are many 1- to 4-ring aromatic and polar compounds in coal-derived liquids that can be converted into valuable chemicals [Lai et al., 1992; Song and Schobert, 1993; Burgess et al., 1993; Huang et al., 1994; Saini and Song, 1994; Song and Saini, 1994; Lai and Song, 1995]. For example, phenol, naphthalene, and phenanthrene are rich in coal liquids from primary liquefaction of some coals. Phenol is one of the top twenty organic chemicals [CEN, 1994] and is commercially synthesized through multi-step process (benzene isopropylation, oxidation of isopropyl benzene, separation of phenol). However, phenol is rich in the oils from coal liquefaction, particularly when the liquefaction is promoted by dispersed catalysts and water [Song and Saini, 1994; Saini and Song, 1994]. Phenol can be separated directly from the coal liquids, and it can be used as or converted into monomer for many aromatic polymers and engineering plastics, including those shown in Scheme I. Naphthalene and its derivatives are rich in the oils from some bituminous coals. Naphthalene and 2-alkylnaphthalene are important aromatic chemicals. It should be noted that the use of aromatic compounds, that are in coal liquids and heavy oils, for making value-added chemicals requires the starting material to be reasonably pure. Our recent catalytic studies include the shape-selective conversion of two- to three-ring aromatic compounds (naphthalene, phenanthrene, and their derivatives) into value-added chemicals, as described below.

Shape-selective Alkylation of Naphthalene. This catalytic reaction can produce 2,6-dialkyl substituted naphthalene (2,6-DAN). 2,6-DAN is needed now as the feedstock of monomer for making the advanced polyester materials such as polyethylene naphthalate (PEN, Scheme I), polybutylene naphthalate (PBN, Scheme I), and liquid crystalline polymers (LCP, Scheme II). By using some shape-selective catalysts, we have achieved selective alkylation of naphthalene, with over 65% selectivity to 2,6-DAN by using isopropanol [Song and Kirby, 1993, 1994] or propylene as the alkylating agent [Schmitz and Song, 1994]. We also found some simple and effective methods for

enhancing the selectivity, which are not available in the prior arts [Schmitz and Song, 1994, unpublished data].

Ring-shift Isomerization of Phenanthrene Derivatives. This reaction leads to anthracene derivatives, particularly sym-octahydroanthracene (sym-OHAn). We have found that some catalysts selectively promotes the transformation of sym-octahydrophenanthrene into sym-OHAn, which we call ring-shift isomerization [Song and Moffat, 1993, 1994]. Some catalysts can afford over 90% selectivity with high conversion [Lai and Song, 1994, unpublished data]. This work could provide a cheap route to making anthracene and its derivatives, which are valuable chemicals in demand, from phenanthrene, which is rich in coal tar from coal carbonization, pyrolysis, and liquefaction. Examples of the possible applications of sym-OHAn may include the manufacturing of anthracene (which is in demand for making dyestuffs), anthraquinone (which is an effective pulping agent), and pyromellitic dianhydride (which is the monomer for making polyimides such as Du Pont's Kapton).

Conformational Isomerization of cis-Decalin to trans-Decalin. The commercial decalin solvents are almost equimolar mixtures of cis-decalin and trans-decalin. In an earlier work using decalin as a solvent, we found accidentally that cis-decalin isomerize into trans-decalin at low temperatures (250°C) over some catalysts [Song and Moffat, 1993, 1994], which would otherwise requires a high temperature such as 450°C [Song et al., 1992]. This work is a continuation of our earlier observation that trans-decalin has substantially higher thermal stability at high temperatures [Song et al., 1992]. Our recent experimental results indicate that it is possible to achieve over 90% conversion with 95% selectivity with some catalysts at low temperatures such as 200°C [Lai and Song, 1994, unpublished]. Possible application of this work is the manufacture of high-temperature heat-transfer fluids. Another application lies in the production of advanced thermally stable jet fuels, which can be used both as heat sinks and as fuels that are required for high-Mach aircraft [Schobert et al., 1994].

Shape-selective Naphthalene Hydrogenation. Complete hydrogenation of naphthalene in conventional process produce mixtures of cis- and trans-decalin, and . In recent studies on naphthalene hydrogenation, we have found that certain catalysts selectively promote the formation of cis-decalin or trans-decalin [Song and Grainne, 1993, unpublished data; Schmitz and Song, 1994, unpublished data]. Now we can selectively produce cis-decalin, with over 80% selectivity at 100% conversion [Schmitz and Song, 1994, unpublished data]. cis-Decalin may have potential industrial application as the starting material for making sebacic acid, which can be used for manufacturing Nylon 6,10 and softeners.

PRODUCTION OF CARBON MATERIALS FROM COALS

Carbon materials represent an important market for non-fuel applications of coal and coal-derived pitch materials. We have discussed the possibilities of developing various coal-based carbon materials recently [Song and Schobert, 1993] based on the materials listed in several reviews by Walker [1986, 1990] and by Marsh [1989, 1991]:

- | | |
|---|-------------------------------|
| • Metallurgical cokes | • Activated carbons |
| • Molecular sieving carbons (MSC) | • Activated carbon fibers |
| • Pitch-based carbon fibers | • Carbon electrodes |
| • Mesocarbon microbeads (MCMB) | • Carbon blacks |
| • Mesophase-based carbon fibers | • Intercalation Materials |
| • Carbon fiber reinforced plastic | • Elastic carbons |
| • Carbon whiskers or filament | • Composite materials |
| • Graphite and graphite-based materials | • Fullerenes or "bucky-balls" |
| • Diamond-like films | |

Carbon-based Materials Made Directly from Coals. Currently the production of metallurgical coke is the largest non-fuel use of coals, primarily bituminous coals. It is estimated that about 500 million tonnes (metric tons) of coke are produced annually in the world [Mochida and Sakanishi, 1993]. China is one of the largest producers and consumers of coals and coke. In 1992, China produced 1204 million short tons of coals [EIA IEO, 1994]. About 10% of coals mined in China are used for making metallurgical coke [Guo, 1994].

Figure 2 shows the profile of the U.S. metallurgical coal consumption and coke production over the period 1950-1992. Coal consumption by the U.S. coke industry (and some other industrial sectors) trended downward since early 1970s. The reasons have been discussed in our previous review [Song and Schobert, 1993]. In 1993, the metallurgical coal consumption and coke production in the U.S. were 31.3 and 23.2 million short tons, respectively. The annual demand for coke in the U.S. is expected to further decrease to 18.7 million short tons by 2002 [Gilbert, 1993]. The decrease in coke production also means a decline in coal tar production, which could lead to the shortage of both aromatic chemicals, particularly 2- to 4-ring chemicals, and the pitch feedstocks for making carbon fibers and other needed carbon materials. This also gives rise to the need for developing alternate coal-based feedstocks for making various aromatic chemicals and carbon materials.

Activated carbons are used mainly as adsorbents for liquid-phase and gas-phase applications. In 1992, the world total annual production of activated carbons from various feedstocks was estimated

to be about 450,000 tonnes; among which 70,000 tonnes were produced in China, with about 30,000 tonnes made from coal and 40,000 tonnes from the other feedstocks [Gao, 1994]. The amount of coals used worldwide for producing activated carbons are estimated to be 200,000 tonnes/year [Golden, 1992]. Significant growth potential exists for this application, primarily for environmental protection, e.g., purification of water and air. Jagtoyen and Derbyshire have carried out a series of studies on the production of activated carbons from bituminous coals by chemical activation [Jagtoyen et al., 1992, 1993]. The liquid phase applications include water purification, decolorizing, food processing, and gold recovery, etc.; the gas phase applications cover air purification, gas treatment, and solvent recovery. More information on activated carbons may be found in a recent review by Derbyshire and co-workers [Derbyshire et al., 1994].

The amount of coals used worldwide for producing molecular sieving carbons are estimated to be 3,000 tonnes/year [Golden, 1992]. The application of molecular sieving carbons (MSC) for gas separation by pressure-swing adsorption (PSA) is now commercially viable. For example, MSC is used for air separation by Air Products and Chemicals Inc. It is expected that more companies will be engaged in producing MSC in the 1990's and into the next century.

The other industrial non-fuel uses of coals are included in those by industries and manufacturing plants, especially those who make chemicals, cement, paper, ceramics, and various metal products. Table 4 shows the U.S. coal consumption at manufacturing plants in 1992 by standard industrial classification (SIC) code [EIA QCR, 1994]. Use of coal for gasification can be partly classified as non-fuel use when the products are used as chemical feedstocks. Gasification is currently used for making synthesis gas ($\text{CO} + \text{H}_2$) and for producing H_2 for various hydrogenation and hydroprocessing in petrochemical and petroleum refining industries. The use of coal for gasification is included in Table 4 at the manufacturing plant with SIC code 29.

The details of the non-fuel uses at manufacturing plants are not available. However, direct coal injection into blast furnace is already in industrial practice. This use may have been included in SIC Code 33 in Table 4. There are some other interesting uses [Bonskowski, 1994]. Some lignite can be used as additive in drilling mud (drilling for oil and gas) as a lubricant and sealant. Young [1993] reviewed some other non-fuel applications of coals, particularly low-rank coals. They are 1) form coke from non-coking coals for use as a reductant in the metallurgical industries; 2) agricultural use of low-rank coals for production of coal-based fertilizers, soil conditioners, and humic acids; 3) special adsorbent carbons for storage of gases such as methane; and 4) production of carbon black and carbon support for making catalysts.

Carbon-based Materials Made from Coal-derived Liquids. The heavy fractions of coal tars, widely called coal tar pitches, are the raw materials for making carbon fibers and other carbon materials such as mesocarbon microbeads [Matsumura, 1989; Song and Schobert, 1993; Derbyshire et al., 1994].

The liquids and semi-liquids derived from coal extraction and liquefaction can also be used for making various carbon-based materials such as carbon fibers and graphitic materials. Kimber et al. [1981] and Zondlo et al. [1993] reported on the production of graphitic materials from carbonization of coal extracts. Kimber and Gray [1976] also noted that there are potential advantages in using coal-based coke for making carbon electrodes. Fei et al. [1994] reported on the production and properties of carbon fibers from coal-derived liquids as well as shale oils. Some lignite in California is used in an extraction process to make Montan wax, which may be used in shoe polishes, elastics, and electrical insulating [Bonskowski, 1994].

On-going Research on Production of Carbon Materials from Coal and Coal Liquids in This Laboratory

In the following section, specific examples will be provided from work in progress on carbon materials in our laboratory, including conversion of coal and pitch materials into various carbon materials.

Conversion of anthracite into graphite. Our interest in the possibility of converting anthracite into graphite was stimulated by two considerations: anthracites already contain well over 90% carbon, with aromaticities of essentially 1; and while anthracite currently sells in the range of \$80 per ton, the best quality graphite materials sell for about \$80 per pound. Our initial research was motivated by two hypotheses. First, the alignment of the large aromatic sheets presumed to exist in anthracite into the ideal graphitic structure could be facilitated by removing any residual heteroatom or aliphatic carbon atoms that might serve as covalent crosslinks "locking" the aromatic sheets into disordered structures. This, it was hypothesized, could be accomplished by reaction of anthracite with powerful hydrogen donors, such as 9,10-dihydrophenanthrene or 1,2,3,4-tetrahydro-fluoranthene prior to graphitization. Second, this process would be facilitated further if the spent donor (e.g., phenanthrene arising from 9,10-dihydrophenanthrene) was itself a graphitizable material and could therefore provide sites around which the graphitic structure could grow.

We have investigated the reactions of several Pennsylvania anthracites with hydrogen donors [Atria et al., 1993, 1994; Atria, 1995]. Co-carbonization of anthracite with a hydrogen donor, followed by high-temperature graphitization, produces a material having crystalline d-spacings in the range 0.3357–0.3361 nm, values which are quite close to the ideal value for graphite, 0.3354 nm. However, the crystalline height, L_c , of the best materials are in the range 54.7–58.8 nm, about half the value

(104.0 nm) observed in commercial graphite. As part of this work we have obtained unequivocal evidence that hydrogenation of anthracite does occur by direct reaction with hydrogen donors.

To further improve the quality of the graphitic product, we have begun an investigation of the catalytic graphitization of anthracites [Zeng et al., 1995a]. In this work, six Pennsylvania anthracites are being evaluated as feedstocks. The catalysts currently under investigation are La_2O_3 , Ce_2O_3 , and Gd_2O_3 , mixed with anthracites in amounts up to 5%. A second aim of this present project is to reduce substantially the temperature of graphitization. We are investigating graphitization temperatures as low as 1800°C, whereas in our earlier work much of the graphitization was done at 2900°C. A very large reduction in graphitization temperature translates to a significant energy saving in the graphitization process.

Conversion of Coals into Activated Carbons. At present, the main thrust of our work is again devoted to Pennsylvania anthracites. A small collateral effort is underway on activation of Turkish low-rank coals, in conjunction with various agricultural products indigenous to Turkey.

Steam and air activation have been investigated for production of carbons from anthracites [Gergova et al., 1993a, 1993b]. The highest BET surface area obtained was 720 m^2/g [Gergova et al., 1993b]. The particle size of the anthracite is a critical parameter; the best carbon (in terms of apparent surface area) was obtained from anthracite of <1 mm particle size. Subsequent work [Gergova et al., 1995] has used an environmental scanning electron microscope (ESEM) to observe development of a porous structure in real time, even though the ESEM operates at 2 Torr, whereas normally activation is done at atmospheric pressure. In this work we also investigated air treatment of the anthracite (e.g., 3 h at 300°C) prior to steam activation. The activated anthracites produced in the latter study have a microporous structure with a significant fraction of the pores having molecular dimensions. This suggests that molecular sieve materials could be produced from Pennsylvania anthracites.

Related Studies on Anthracites. Anthracite has long been an "orphan" in coal science research. Only a tiny fraction of the coal literature is devoted to reports of work on anthracites; in consequence, little fundamental information is available on anthracite properties and structure. Recently we have begun a collaborative effort with Carbone-Lorraine North America to investigate the basic physical properties of anthracites [Zeng et al., 1995b]. Major physical properties, including density, mechanical strength, hardness, coefficient of thermal expansion, and microstructure, are being measured and correlated with chemical properties such as proximate and ultimate analyses, porosity, apparent surface area, and aromaticity. The aim is to evaluate further the potentialities of using anthracites as raw materials for the production of various carbon products.

Very limited testing of the electrical properties of Pennsylvania anthracites has shown that they are not substantially below mesocarbon microbeads in some properties affecting use in lithium batteries or other dry cells [Zeng, 1994]. We infer, from this encouraging preliminary work, that limited, but controlled, structural modification of anthracites could make them attractive candidates for electrodes in batteries.

CONCLUDING REMARKS

Despite the relatively small amount of their non-fuel use, research into efficient use of the valuable hydrocarbon resources such as coal for non-fuel applications is becoming important.

We must always bear in mind that coal is an important source of hydrocarbons. There are many ways of using the hydrocarbon resources. Burning is only one of them. Expansion of the non-fuel uses is desirable, because coal will also become more important as source of both energy and chemical feedstocks in the next century. From the viewpoints of the resource conservation and effective utilization, many of the components in coals as well as in petroleum should be converted to, or used as value-added chemicals, polymers, and carbon materials.

George A. Olah, the 1994 Nobel Prize winner, pointed out recently [1991] that "oil and gas resources under the most optimistic scenarios won't last much longer than through the next century. Coal reserves are more abundant, but are also limited. ... I suggest we should worry much more about our limited and diminishing fossil resources." James L. Adams indicated in his recent book [1991] that "oil and coal used as fuel have allowed us to work wonders, but they are too valuable as complex hydrocarbons that can be converted into all sorts of the forms (such as plastics) to be so rapidly burned in automobiles, power plants, and furnaces."

ACKNOWLEDGMENTS

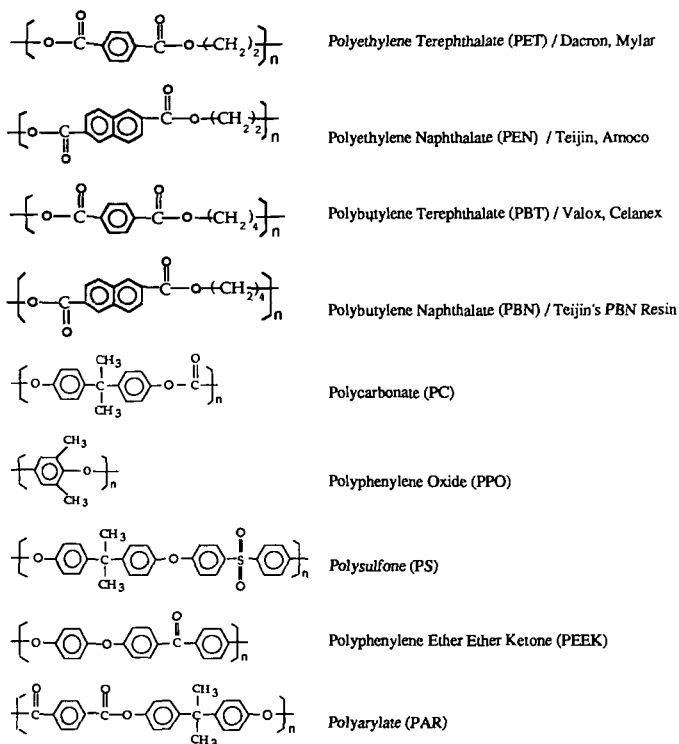
Various portions of our research were supported through funding or donations of special samples from the U.S. Department of Energy, Pittsburgh Energy Technology Center, Pennsylvania Energy Development Authority, Air Products and Chemicals Inc., PQ Co., and Duracell Co. Helpful discussions with Professor H. Marsh of Southern Illinois University, Dr. T. Golden of Air Products and Chemicals Inc., Dr. G.M. Kimber of British Coal Co., Dr. K.C. Krupinski of Aristech Chemical Co., Dr. R. F. Bonskowski of DOE/EIA, Dr. J. Broadhead of Duracell Worldwide Technology Center, and Drs. F. Rusinko, S. Eser, S. Zeng, W.-C. Lai, and A. Schmitz of PSU are gratefully acknowledged.

REFERENCES

- Adams, J. L. *Flying Buttresses, Entropy, and O-Rings. The World of an Engineer.* Harvard University Press, 1991, p.241.
- Atria, J. S.M. Zeng, H.H. Schobert, and F. Rusinko, Jr. A novel approach to the production of graphite from anthracite, *Proceedings 21st Biennial Conference on Carbon*, pp. 342-343, 1993.
- Atria, J.V., S. Zeng, F. Rusinko, Jr., and H.H. Schobert. Novel approach to the production of graphite from anthracite. *Am. Chem. Soc. Div. Fuel Chem. Prepr.*, 1994, 39, 884-888.
- Atria, J.V. Production of anthracite from graphite, M.S. Thesis, The Pennsylvania State University, University Park, PA, 1995.
- Bonskowski, R. F. Energy Information Administration, U.S. DOE. personal communication. November 9, 1994.
- Burgess, C. E., K. Wenzel, C. Song, P. G. Hatcher, and H. H. Schobert. Structural Correlation of Coal Liquefaction Oils with Flash Pyrolysis Products. *Proc. 7th Internat. Conf. Coal Sci., Banff Canada*, Sept. 12-17, 1993, Vol. I, pp.311-314.
- CEN *Chem. Eng. News*, July 4, 1994
- Collin, G. Erdol und Kohle - Erdgas Petrochem. 1985, 38 (11), 489-496
- Derbyshire, F. J., M. Jagtoyen, Y. Q. Fei, and G. Kimber. *Am. Chem. Soc. Div. Fuel Chem. Prepr.*, 1994, 39 (1), 113-120.
- Energy Information Administration (EIA). *Annual Energy Review (AER) 1992*, U.S. DOE, Report No. DOE/EIA-0384(92), June 1993.
- EIA AEO *Annual Energy Outlook 1994*, DOE/EIA-0383(94), January 1994.
- EIA IEO *International Energy Outlook (IEO)*, DOE/EIA-0484(94), July 1994.
- EIA IPSR *International Petroleum Statistics Report (IPSR)*, DOE/EIA-0520(94/04), April 1994.
- EIA MER *Monthly Energy Review (MER)*, DOE/EIA-0035(93/08), August 1993.
- EIA QCR *Quarterly Coal Report (QCR)*, July-September 1993, DOE/EIA-0121(93/3Q), February 1994.
- EIA QCR *Quarterly Coal Report (QCR)*, January-March 1994, DOE/EIA-0121(94/1Q), August 1994.
- Fei, Y.Q., F. Derbyshire, M. Jagtoyen, and I. Mochida. Advantages of Producing Carbon Fibers and Activated Carbon Fibers from Shale Oils. *Proc. of 1993 Eastern Oil Shale Sym.*, May 1994.
- Gao, S. Activated Carbon Industry in China. *Tanso (Japanese)*, 1994, No. 163, 145-149.
- Gergova, K., S. Eser, and H.H. Schobert. Pyrolysis/activation of anthracite for production of activated carbons, *Proceedings, 21st Biennial Conference on Carbon*, pp. 412-413, 1993.
- Gergova, K., S. Eser, and H.H. Schobert. Preparation and characterization of activated carbons from anthracite. *Energy and Fuels*, 1993, 7, 661-668.
- Gergova, K., S. Eser, H.H. Schobert, M. Klimkiewicz, and P.W. Brown. Environmental scanning electron microscopy of producing activated carbons from anthracite using one-step pyrolysis/activation. *Fuel*, 1995, in press.
- Gilbert, B.R. Co-production of Iron and Methanol. *Proc. 10th Ann. Internat. Pittsburgh Coal Conf., University of Pittsburgh, Pittsburgh*, Sept. 20-24, pp.410-415, 1993.
- Golden, T.C. *Air Products Co.*, personal communication, April 24, 1992.
- Guo, S. Present State and Overview of Coal Utilization Technology in China. *Energy & Resources (Japanese)*, 1994, 15 (2), 161-165.
- Hirota, T., M. Nomura, and C. Song. A Method for Manufacture of Aromatic Chemicals from Coals. *Japan Patent*, 1-279990 (Assigned to Osaka Gas Company, Japan), November 10, 1989 (in Japanese).
- Huang, L., C. Song, and H. H. Schobert. Liquefaction of Low-Rank Coals as a Potential Source of Specialty Chemicals. *Am. Chem. Soc. Div. Fuel Chem. Prepr.*, 1994, 39 (2), 591-595.
- Jagtoyen, M., M. Thwaites, J. Stencel, B. McEnaney, and F. Derbyshire. Adsorbent Carbon Synthesis from Coals by Phosphoric Acid Activation. *Carbon*, 1992, 30 (7), 1089-1096.
- Jagtoyen, J. Groppo, and F. Derbyshire. Activated Carbons from Bituminous Coals by Reaction with H₃PO₄: The Influence of Coal Cleaning. *Fuel Process. Technol.*, 1993, 34, 85-96.
- Kimber, G. M., and M. D. Gray. Comparison of Evolution of Heteroatoms from Coal and Petroleum Based Electrode Cokes. *Am. Chem. Soc. Sym. Ser.*, 1976, 21, 445-450.
- Kimber, G. M., A. Brown, and J. N. Kirk. Arc-steel Electrodes from Coal via Solvent Extraction. *High Temp. - High Press.*, 1981, 13, 133-137.
- Lai, W.-C., C. Song, H. H. Schobert, and R. Arumugam. Pyrolytic Degradation of Coal- and Petroleum-Derived Aviation Jet Fuels and Middle Distillates. *Am. Chem. Soc. Div. Fuel Chem. Prepr.*, 1992, 37 (4), 1671-1680.
- Lai W.-C. and C. Song, 1994, unpublished data, The Pennsylvania State University.
- Lai, W.-C. and C. Song. Temperature-Programmed Retention Indices for GC and GC-MS Analysis of Coal- and Petroleum-derived Liquid Fuels. *Fuel*, to be published, 1995.
- Marsh, H. 1991. "New and Traditional Carbon Materials from Petroleum and Coal Sources". Paper presented at *Information Transfer Session, Cooperative Program in Coal Research*, November 18-19, Pennsylvania State University, University Park, PA.
- Marsh, H. (Ed.), 1989. "Introduction to Carbon Science", Butterworths, London, 321 pp.
- Matsumura, Y. Current Status and Prospectives of Coal Pitch-Based Carbon Fibers. *Kagaku Keizai (Japanese)*, 1989a, No.9, 33-41
- Matsumura, Y. Expanding Applications of Pitch-Based Carbon Materials. *JETI (Japanese)*, 1989b, 37 (No.9), 223-226.
- Mochida, I. and K. Sakanishi. Tasks and Scopes of Coal Science. *J. Japan Inst. Energy (Japanese)*, 1993, 72 (5), 312-320.
- Murakami, H. *Nenryo Kyokai-Shi (Japanese)*, 1987, 66 (6), 448-458.
- NCA *Facts about Coal.* National Coal Association, July 1993.

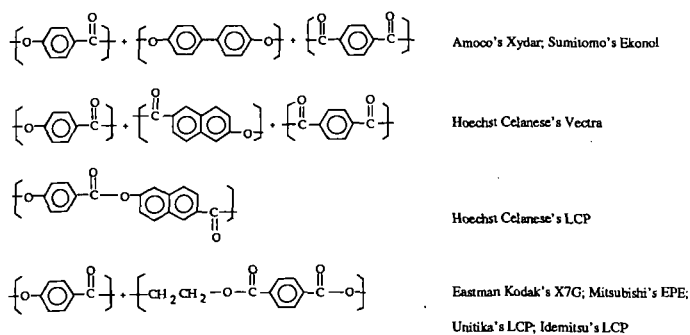
- Olah, G. A. Nonrenewable Fossil Fuels. Chem. Eng. News, February 11, 1991.
- Saini, A. K., and C. Song. Two-Dimensional HPLC and GC-MS of Oils from Catalytic Coal Liquefaction. Am. Chem. Soc. Div. Fuel Chem. Prepr., 1994, 39 (3), 796-800.
- Schmidt, E., and C. Song. Model Hydrocracking Reactions over Monometallic and Bimetallic Dispersed Catalysts. Am. Chem. Soc. Div. Fuel Chem. Prepr., 1994, 39 (3), 733-737.
- Schmitz, A., and C. Song. Shape-Selective Isopropylation of Naphthalene over Dealuminated Mordenite. Am. Chem. Soc. Div. Fuel Chem. Prepr., 1994, 39 (4), 986-991.
- Schmitz and Song, 1994, unpublished data, The Pennsylvania State University.
- Schobert, H.H., 1984. In: W.R. Kube, E.A. Sondreal, and C.D. Rao (Eds.), Technology and Utilization of Low-rank Coals. U.S. Dept. of Energy Report DOE/METC/84-13; pp. 83-103.
- Schobert, H.H., S. Eser, C. Song, P. G. Hatcher, P. M. Walsh, and M. M. Coleman. Advanced Thermally Stable Jet Fuels. Technical Report, U.S. Department of Energy, DE-FG22-92PC92104-TPR-8, July 1994, 96 pp.
- Sheldon, R.A. Chemicals from Synthesis Gas. Reidel Pub. Co., Boston, 1983.
- Song, C., K. Hanaoka, and M. Nomura. Short-Contact-Time Pyrolytic Liquefaction of Wandoan Subbituminous Coal and Catalytic Upgrading of SCT-SRC. Fuel, 1989, 68 (3), 287-292.
- Song, C. and H. H. Schobert. Specialty Chemicals and Advanced Materials from Coals: Research Needs and Opportunities. Am. Chem. Soc. Div. Fuel Chem. Prepr., 1992, 37 (2), 524-532.
- Song, C. and S. Kirby. Shape-Selective Alkylation of Naphthalene over Molecular Sieve Catalysts. Am. Chem. Soc. Div. Petrol. Chem. Prepr., 1993, 38 (4), 784-787.
- Song, C. and K. Moffatt. Zeolite-Catalyzed Ring-Shift and Conformational Isomerization Reactions of Polycyclic Hydrocarbons. Am. Chem. Soc. Div. Petrol. Chem. Prepr., 1993, 38 (4), 779-783.
- Song, C. and H. H. Schobert. Opportunities for Developing Specialty Chemicals and Advanced Materials from Coals. Fuel Processing Technol., 1993, 34 (2), 157-196.
- Song, C. and H. H. Schobert. Aromatic Polymer Precursors from Coals: A New Direction in Coal Chemistry. Proc. 10th Ann. Internat. Pittsburgh Coal Conf., University of Pittsburgh, Pittsburgh, Sept. 20-24, pp.384-389, 1993.
- Song, C. and S. Kirby. Shape-Selective Alkylation of Naphthalene with Isopropanol over Mordenite Catalysts. Microporous Materials, Elsevier, 1994, 2 (5), 467-476.
- Song, C. and K. Moffatt. Zeolite-Catalyzed Ring-Shift Isomerization of sym-Octahydrophenanthrene and Conformational Isomerization of cis-Decahydronaphthalene. Microporous Materials, Elsevier, 1994, 2 (5), 459-466.
- Song, C., H.H. Schobert, and A.W. Scaroni. Current Status of U.S. Coal Utilization Technologies and Prospects. Energy & Resources (Japanese), 1994, 15 (2), 142-153.
- Song, C., and A. K. Saini. Using Water and Dispersed MoS₂ Catalyst for Coal Conversion into Fuels and Chemicals. Am. Chem. Soc. Div. Fuel Chem. Prepr., 1994, 39 (4), 1103-1107.
- Speight, J.G. (Ed.), Fuel Science and Technology Handbook. Marcel Dekker: New York, 1990, 1193 pp.
- Speight, J.G., The Chemistry and Technology of Petroleum. Marcel Dekker: New York, 1991, Chapter 21 (Petrochemicals), p.717.
- Swain, E.J. U.S. Crude Slate Gets Heavier, Higher in Sulfur. Oil Gas J., 1991, September issue, 59-61.
- Walker, P.L., Jr. 1986. Review Article: Coal Derived Carbons. Carbon, 24 (4): 379-386.
- Walker, P.L., Jr. 1990. Carbon: An Old but New Material Revisited. Carbon, 28: 261-279.
- Young, B.C. Meeting the Value-Added Challenge with Coal Briquetting and Pelleting. Proc. 10th Ann. Internat. Pittsburgh Coal Conf., University of Pittsburgh, Pittsburgh, Sept. 20-24, pp.402-407, 1993.
- Zeng, S. Unpublished data, The Pennsylvania State University, University Park, PA, 1994.
- Zeng, S., F. Rusinko, Jr., H.H. Schobert, D.P. Struble, and W.A. Nystrom. Graphitization of anthracites with the addition of rare earth compounds. Proceedings, 22d Biennial Conference on Carbon, (submitted, 1995).
- Zeng, S., F. Rusinko, Jr., H.H. Schobert, D.P. Struble, and W.A. Nystrom. Investigation of the physical properties of Pennsylvania anthracites. Proceedings, 22d Biennial Conference on Carbon, (submitted, 1995).
- Zhou, P.-Z., Marano, J.J. and Winschel, R.A., 1992. Prepr. Pap.-Am. Chem. Soc., Div. Fuel Chem., 37 (4), 1847-1854.
- Zondlo, J.W., P.G. Stansberry, and A.H. Stiller. Pitch and Coke Production via Solvent Extraction of Coal. Proc. 10th Ann. Internat. Pittsburgh Coal Conf., University of Pittsburgh, Pittsburgh, Sept. 20-24, pp.379-383, 1993.

Scheme I. Structures of Some Important Aromatic Plastics Materials



Scheme II. Structures of Some Important Liquid Crystalline Polymers (LCPs)

Thermotropic Polyester LCPs



Lyotropic LCP



Table 1. World and U.S. Energy Supply and Demand

Year	Total	Petroleum	N. Gas	Coal	Nuclear	Hydropower	Other
World Total Energy Consumption / Quadrillion Btu (10^{15} Btu)							
1992	347.5	136.3	74.3	88.9	21.5	22.3	4.4
U.S. Energy Consumption / Quadrillion Btu							
1992	82.42	33.51	20.34	18.89	6.65	2.81	0.22
U.S. Energy Production / Quadrillion Btu							
1992	66.93	15.22	20.67	21.68	6.65	2.81	0.22
U.S. Energy Input at Electric Utilities / Quadrillion Btu							
1992	29.56	0.95	2.83	16.19	6.65	2.76	0.19

Note: According to DOE EIA, 1 quadrillion Btu is equivalent to 45 million short tons of coal, 170 million barrels of crude oil, and 1 trillion cubic feet of dry natural gas.

Table 2. Non-fuel Use of Fossil Fuels in the U.S. in 1992

Coal		Petroleum							N. Gas
Coke	Other	Petro-chemical feedstocks	Asphalt and Road Oil	Liquefied Petroleum Gases	Lubricant Petroleum	Petroleum Coke	Special naphtha	Wax, etc.	Chemical feedstocks
Physical Unit / million short tons for coal; million barrels for oil; billion cubic feet for natural gas									
32.37	1.8	202	166	386	54	42	19	27	611
Energy Unit / Quadrillion Btu (10^{15} Btu)									
0.73	0.05	1.14	1.10	1.35	0.33	0.25	0.10	0.16	0.63

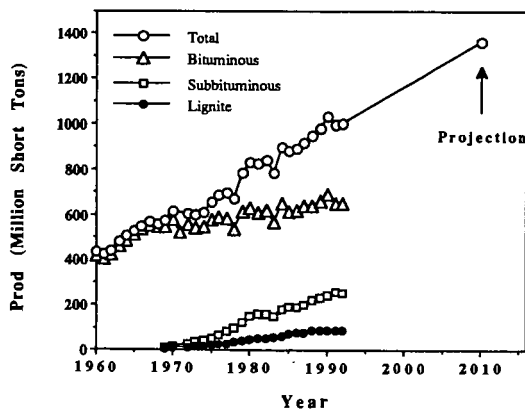


Figure 1. Production of coal by type in the U.S. during 1960-1992 (1 short ton = 0.907 metric ton).

Table 3. U.S. Coal Production and Consumption

Coal Supply and Demand / million short tons					
Year	Production	Consumption	Export	Import	Others and losses
1992	997.545	892.421	102.516	3.803	9.407
Coal Consumption by Sectors / million short tons					
Year	Electric Utilities	Coke Plants	Other Industrial	Residential and Commercial	Total consum.
1992	779.860	32.366	74.042	6.153	892.421

Note: 1 short ton = 907.184 kg = 2000 pounds = 0.907 metric ton

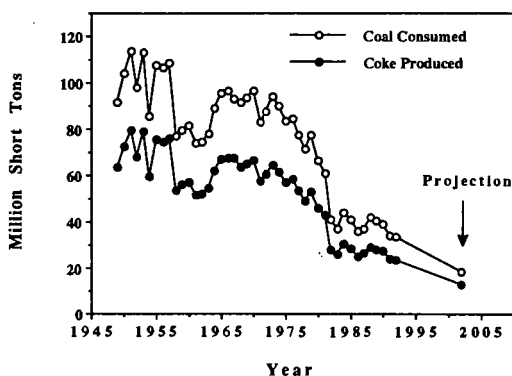


Figure 2. U.S. metallurgical coke production during 1949-1992

Table 4. U.S. Coal Consumption at Manufacturing Plants by Standard Industrial Classification Code (Thousand Short Tons)

SIC Code	Jan-March 1993	Apr-June 1993	July-Sept 1993	Oct-Dec 1993	U.S. Total
20 Food and kindred products	2264	1568	1491	2479	7802
21 Tobacco products	184	156	154	154	648
22 Textile mill products	370	313	258	334	1275
24 Lumber and wood products	27	29	23	30	109
25 Furniture and fixtures	35	18	16	32	101
26 Paper and allied products	3302	2918	2946	3270	12436
28 Chemicals, allied products	3490	3079	3044	3338	12951
29 Petroleum and coal products ¹	1760	1832	1695	1963	7250
30 Rubber, misc. plastics products	78	67	56	64	265
32 Stone, clay, glass products	2781	3170	3329	3478	12758
33 Primary metal industries ²	1623	1833	1700	1872	7028
34 Fabricated metal products	113	59	33	80	285
35 Machinery, except electric	180	84	48	121	433
36 Electric, electronic equipment	89	59	29	68	245
XX Other manufacturing industries (SIC: 23, 27, 31, 37, 38, 39)	w	w	w	w	w
U.S. Total	17175	15705	15268	17931	66079

1) Includes coal gasification projects.

2) Excluding coke plants. w Withheld by DOE to avoid disclosure of individual company data.

PROCESSING, STRUCTURE AND PROPERTIES OF PITCH-BASED CARBON-CARBON COMPOSITES

S. P. Appleyard, B. Rand and C. E. Ahearn
School of Materials, University of Leeds,
Leeds, LS2 9JT, U.K.

Keywords: Carbon-carbon composite, pitch, fibre-matrix interface

INTRODUCTION

The potential of carbon-carbon (CC) composites as materials for high temperature applications was recognised at a very early stage, leading to their development in the 1960's as materials for thermal protection during space vehicle re-entry. By the early 1970's, two basic approaches to the formation of the carbon matrix were established, namely through chemical vapour deposition from a hydrocarbon gas (CVD) (1) and through carbonisation of a carbon-bearing resin or pitch (2). Fundamentally, little has changed since those early years with respect to these basic methods of CC composite fabrication. Further developments have, however, involved the introduction of multidirectional fibre architectures in order to reduce the mechanical anisotropy present in unidirectionally and bidirectionally reinforced composites caused by poor mechanical properties in the unreinforced directions. The strategic importance of several aerospace applications of CC composites, including military rocket nozzles and nose cones, the NASA space shuttle nose cone and leading edge protection surfaces, aircraft brake discs and gas diverter fins, ensured their continued development during the 1970's and 1980's.

The technique of liquid impregnation is now a major procedure for the densification of CC composites (3). Despite nearly 30 years of development, however, the utilisation of fibre strength in densified CC composites is still only around 65 % (3). There is, therefore, a need for a comprehensive understanding of the factors giving rise to this lost potential so that improvements in properties may be achieved. Furthermore, new applications of CC composites are currently emerging which exploit some of the thermal characteristics of the composite structure as manifest in the graphite crystal structure. There is thus a need to further understand the ways in which the composite microstructure may be controlled during the fabrication process. This paper reviews the principal microstructural features of interest in CC composites produced with pitch precursors to the carbon matrix and illustrates the influence of fibre-matrix interactions on the microstructure and properties.

MICROSTRUCTURE OF CC COMPOSITES

The microstructures of CC composites may be very complex, involving various degrees of crystallinity and texture on differing scales of magnitude, and several types of interfaces, pores and microcracks, conceivably all in the same specimen (4). Both fibre and matrix undergo significant microstructural changes during fabrication; the fibre and matrix may interact, thus producing unique microstructural features that cannot be obtained by identical processing of the separate constituents (5).

The orientation of the outer turbostratic sheath of carbon fibres has been observed to increase on graphitisation compared with that of a fibre graphitised independently of a composite (6). This increased alignment is thought to arise from an interfacial stress effect. Fibres may thus undergo a substantial increase in modulus of elasticity during thermal processing of a CC composite (7). Such stresses, caused by strong fibre-matrix coupling and matrix shrinkage during carbonisation of the composite, have also been claimed to damage the fibre (8).

Although the overall texture of CC composites is dominated by the structure and architecture of the fibre reinforcement, the existence of preferred orientation (texture) in the microstructure of the matrix is significant. Texture in the matrix is established primarily from two sources, namely the chemistry of the organic matrix precursor and fibre-matrix interfacial effects. Matrix carbons derived from pitches tend to be structurally anisotropic, a product of the development of layers during the growth and coalescence of mesophase spheres in the initial stages of pyrolysis. If unhindered and mechanically undisturbed, the coalesced mesophase produces a coarse microstructure (9). Plastic deformation during this stage, due to externally applied stresses or the formation of gaseous by-products of pyrolysis, may disrupt long range ordering of the mesophase resulting in a finer microstructure. Similar effects are caused either by the application of pressure during carbonisation or by

chemical cross-linking of the structure (10, 11). Controlled alteration of the matrix microstructure may be achieved by the blending of various fractions of pitches (12).

Texture has been observed to initiate in previously structurally isotropic matrices on heat treatment to graphitising temperatures (13). This effect has been ascribed to a concentration of stress developing along the fibre-matrix interface, arising from the combined actions of matrix densification (volume shrinkage) and thermal expansion mismatch between the fibre and the matrix. A second form of fibre-matrix interfacial effect, characteristic of structurally anisotropic matrices, involves the development of carbon atoms arranged in planar layers oriented parallel to the fibre surface (14). A full understanding of this effect has not been reached. The "matrix sheath" may result from fluid flow rather than from wetting (15), though forces acting on the disc-like molecules by the surface do produce a strong anchoring effect, as detected by the resistance to orientation induced by a magnetic field (16). Disruption of the sheath can be produced by the application of pressure during carbonisation and the effects of chemical cross-linking of the structure (10, 11). Given the potential anisotropy in properties conferred by the structure of graphite, the ability to control the texture of the matrix is clearly important in order to allow complete control over the properties of the composite.

Graphitisation of anisotropic matrix carbons causes further structural changes to occur. These changes include "fold-sharpening" and "polygonisation". The former appearing to constitute the first point at which the process of graphitisation becomes microscopically evident (17); shrinkage cracking tends to break a sheet or fold into segments at fairly regular intervals, and these segments sharpen to decreasing radii of curvature. Polygonisation is evidenced by the formation of mosaic block type structures, and has the effect of relaxing the compressive stresses generated by the tendency to shear the layers into graphitic registry (17).

Few studies have been reported concerning the characterisation of porosity in CC composites. Jortner (18) distinguishes between "pores" and "cracks". Pores primarily arise from processing problems. Examples of these include pores formed by incomplete filling by the matrix (perhaps due to poor wetting of the fibres, or incomplete compaction of prepregs resulting in dry zones within the composite) and by the entrapment of gases produced during solvent removal, curing or pyrolysis while a matrix precursor is still liquid or plastic (18). Cracks, comprising "shrinkage", "cooldown" and "thermal stress heating" cracks, arise from stresses due to structural rearrangements during heat treatment or thermomechanical effects.

The geometry of the fibre architecture and nature of fabrication of CC composites generate a number of interfaces present on both the "mini-mechanical" and "micro-mechanical" scales (18). Interfaces that occur on the mini-mechanical scale include fibre tow-fibre tow, bundle-bundle, bundle-matrix and layer-layer interfaces. On the micro-mechanical scale exist fibre-matrix and matrix-matrix interfaces (18). The strength of the fibre-matrix interface is critical to the behaviour of CC composites under mechanical loading. A good fibre-matrix coupling is required to maximise energy transfer from the matrix to the fibre, though it must not be so strong as to cause brittle failure of the composite (19). Matrix-matrix interfaces also have importance as they may limit the ability of the matrix to distribute the load equally between fibre-matrix units or to redistribute the load around individual unit failures (20). In pitch-based carbon matrix composites, the structure of the interfacial zone is monopolised by the presence of matrix sheath, described above. This sheath may actually be a source of debonding of the interface due to the actions of fold-sharpening and polygonisation during graphitisation (11).

The exact nature of "bonding" at the interfaces in CC composites, and hence what controls the bond strength, is not fully understood. Various types of interaction across the interface may exist, including strong and weak chemical bonds, mechanical interlocking and friction (4). Full characterisation and control of interfaces remains one of the most elusive aspects of the technology of CC composites.

EXPERIMENTAL

Model unidirectional CC composites comprising continuous PAN-based fibres and petroleum pitch-based matrices were fabricated by wet-winding and moulding in a heated press, followed by heat treatment. Several types of PAN fibre were used. These included a surface treated standard modulus fibre (SMS) and an untreated high modulus fibre (HMU). Two main temperatures were chosen for the routine

heat treatment of composites. These were a "carbonisation" temperature of 900 °C and a "graphitisation" temperature of 2250 °C. The porous composites so formed were densified by means of pitch-melt impregnation. Composites were studied by optical and scanning electron microscopy and X-ray diffraction. Various properties were studied including electrical resistivity and mechanical behaviour.

STRUCTURAL AND PHYSICAL CHARACTERISATION

A major characteristic of the initial establishment of CC composite structures during carbonisation and graphitisation was the creation of a large number of voids due to matrix shrinkage. After initial carbonisation of the HMU-pitch composites, point counting revealed only ~ 20 % of the fibre surface to be contiguous with matrix. Cracks had developed which were mainly located at the fibre-matrix interface. These cracks, however, were extensively interconnected and enabled very efficient densification of the structure by pitch-melt impregnation. Cracks in the SMS composite, conversely, were generally located within the matrix and tended to have a thin lath-like morphology. This reflected the greater strength of the fibre-matrix interface due to the surface treatment of the fibre, and also revealed the matrix to be prone to failure due to cleavage of the anisotropic structure along planes of weakness. Densification of the SMS composites was not very efficient due to the "bottle-shape" nature of the voids. The location of shrinkage cracks was thus strongly influenced by the combination of the fibre-matrix interface strength and the strength and texture of the matrix (Figure 1). In turn, the void shapes and their degree of interconnectivity governed the efficiency of densification by liquid impregnation.

X-ray diffraction (002) profiles of the green and carbonised composites were largely dominated by the fibre (002) profiles. On graphitisation, marked changes in the composite (002) profiles occurred as they became matrix dominated. Deconvolution of the (002) intensity profiles into separate fibre and matrix profiles enabled $d_{(002)}$ and L_c to be determined for each constituent (Figure 2). The matrix L_c values were greater with respect to similarly heat treated bulk raw materials, indicating the effects on structure of fibre-matrix interactions during graphitisation.

Measurements of electrical resistivity were made both parallel and perpendicular to the fibre axes. Of the densified composites, the carbonised SMS composites exhibited the lowest electrical anisotropy (~ 6). This reflected both the lower structural anisotropy of the SMS fibre and matrix structures (cf. graphitised fibres / matrices) and the high degree of fibre-matrix contiguity present in the composite. Departures from one or more of these conditions resulted in greater anisotropy. Matrix resistivity in the axial direction was calculated by considering the composite as a sequence of parallel resistors, together with knowledge of the longitudinal fibre resistivities, V_f , V_m and V_v . The carbonised matrix resistivity averaged $1.64 \times 10^{-6} \Omega m$, reducing to $4.02 \times 10^{-6} \Omega m$ on graphitisation. The axial resistivity of the graphitised pitch matrix thus approximately matched that of highly oriented Amoco P-100 pitch-based fibres after individual heat treatment to 2500 °C (21). These measurements clearly illustrate the potential of the matrix sheath regarding control of composite properties; alignment of matrix carbon basal planes parallel to the fibre axis greatly enhanced composite electrical conductivity in the longitudinal direction.

MECHANICAL PROPERTIES

Flexural strengths were measured at span-to-depth ratios of 80:1. The strength of the fibre-matrix interface strongly influenced the mode of fracture during flexural testing. A range of fracture behaviour was observed, from "brittle-catastrophic" to "pseudo-ductile", depending on the fibre-matrix combination and fabrication history. The carbonised SMS composites failed by a brittle failure mechanism; only 25 % of the fibre strength was utilised. Failure of the carbonised, densified HMU composite was evidently by means of multiple matrix cracking followed by fibre failure and fibre pull-out. In this case 60 % utilisation of fibre strength was achieved (assuming the contribution of the matrix to strength to be negligible). Graphitisation may give rise to changes in the mode-of-failure due to changes in the nature of the interface and matrix texture. Similarly, low temperature oxidation, in which the oxidation reaction clearly takes place preferentially at the fibre-matrix interface may weaken the fibre-matrix interface enabling debonding and fibre sliding. Increases in utilisation of fibre strength may thus occur as a result of the greater strains at which maximum load occurs.

CONCLUSION

Successful control of fibre-matrix interactions at each stage of fabrication is key to the control of properties of CC composites. The void network established during the initial heat carbonisation has a large effect on the efficiency and effectiveness of subsequent densification processing. The influence of matrix texture on the electrical properties of CC has been illustrated; as the lattice properties of anisotropic carbons are similarly reflected in the properties of modulus of elasticity, thermal expansivity and thermal conductivity, an ability to control matrix texture is clearly of great importance. These properties are of especial importance regarding an emerging application of CC composites, namely the packaging of electronic systems. Finally, if improvements in utilisation of fibre properties are to be achieved, it is imperative to advance understanding of the various structural features influencing modes-of-failure.

REFERENCES

1. H. M. Stoller and E. R. Frye, Symposium of the 73rd Annual Meeting of the American Ceramic Society, *Advanced Materials: Composites and Carbon*, American Ceramic Society (1973) p163.
2. A. R. Taverna and L. E. McAllister, *ibid.* p199.
3. R. A. Meyer, *Materially Speaking* (Publication of The Materials Technology Centre, Southern Illinois University at Carbondale) **9**, Summer (1994) p1.
4. L. H. Peebles Jr., R. A. Meyer and J. Jortner, Proc. of 2nd Int. Conf. on Composite Interfaces, American Society of Metals, Ohio, Published as *Interfaces in Polymer, Ceramic and Metal Matrix Composites*, Ed. H. Ishida, Pub. Elsevier, New York (1988) p1.
5. R. J. Diefendorf, Extended Abstracts of the 13th Biennial Conference on Carbon, American Carbon Society, Irvine (1977) p381.
6. W. Kowbel, E. Hippo and N. Murdie, *Carbon* **27** (1989) p219.
7. R. Bacon, L. C. Nelson, S. L. Strong, E. F. Valla and G. Wagoner, Extended Abstracts of the 19th Biennial Conference on Carbon, American Carbon Society, Penn State (1989) p342.
8. E. Fitzer and A. Bürger, Proc. 1st Int. Conf. on Carbon Fibres, The Plastics Institute, London (1971) p134.
9. J. E. Zimmer and J. L. White, Disclination Structures in the Carbonaceous Mesophase in *Advances in Liquid Crystals* **5**, Pub. Academic Press, New York (1982) p157.
10. E. Fitzer, W. Hüttner and L. M. Manocha, *Carbon* **18** (1980) p291.
11. J. L. White and P. M. Sheaffer, *Carbon* **27** (1989) p697.
12. S. Kimura, E. Yasuda, K. Yasuda, Y. Tanabe, K. Kawamura and M. Inagaki, *Tanso* **125** (1986) p62.
13. Y. Hishiyama, M. Inagaki, S. Kimura and S. Yamada, *Carbon* **12** (1974) p249.
14. J. E. Zimmer and J. L. White, *Carbon* **21** (1983) p323.
15. J. H. Cranmer, I. G. Plotzker, L. H. Peebles Jr. and D. R. Uhlmann, *Carbon* **21** (1983) p201.
16. J. E. Zimmer and R. L. Weitz, *Carbon* **26** (1988) p579.
17. J. Dubois, C. Agache and J. L. White, *Metallography* **3** (1970) p337.
18. J. Jortner, *Carbon* **24** (1986) p603.
19. L. Boyne, D. Cook, J. Hill and K. Turner, Proc. 4th London Int. Carbon and Graphite Conf., Soc. of Chemical Industry, London (1974) p215.
20. B. L. Butler, D. A. Northrup and T. R. Guess, *J. Adhesion* **5** (1973) p161.
21. Y. Tanabe and E. Yasuda, Report of the Research Laboratory of Engineering Materials, Tokyo Institute of Technology **17** (1992) p137.

ACKNOWLEDGEMENTS

S. P. Appleyard would like to acknowledge the financial support of the Science and Engineering Research Council (SERC), Swindon, Wiltshire, UK. and ICI Advanced Materials, ICI Wilton Research Centre, Middlesbrough, Cleveland, UK.

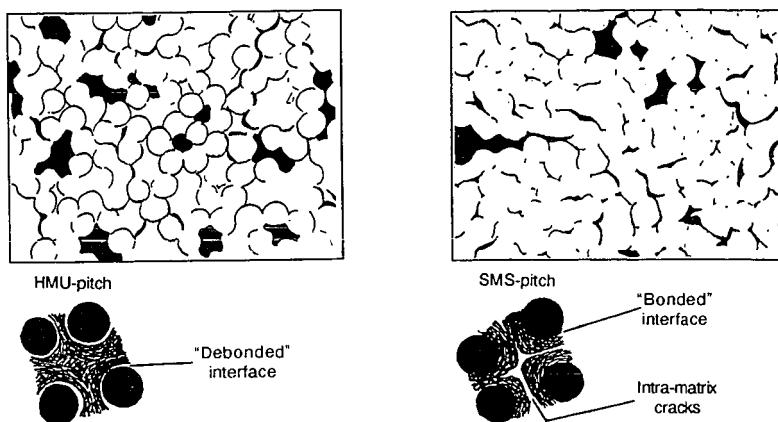


Figure 1
Schematic illustrations of the different void network structures arising from the different fibre-matrix interactions that occurred in HMU-pitch and SMS-pitch composites on carbonisation.

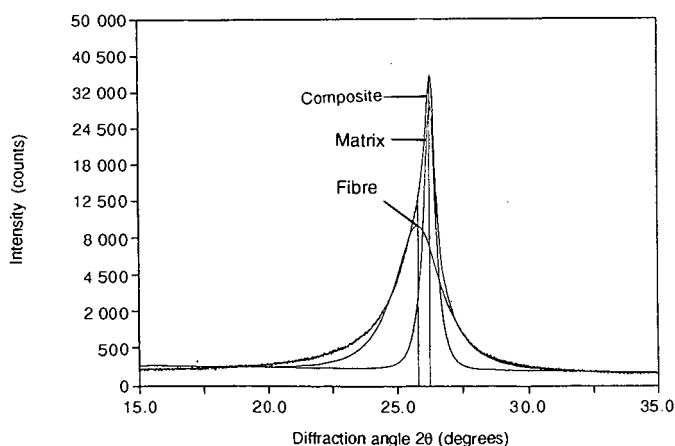


Figure 2
X-ray diffraction profile given by HMU-pitch composite (carbonised, re-impregnated with pitch and then graphitised) with component fibre and matrix profiles obtained by computational deconvolution of the intensity profile.

EVALUATION OF RESIDUAL SHALE OILS AS FEEDSTOCKS FOR VALUABLE CARBON MATERIALS

You Qing Fei and Frank Derbyshire
Center for Applied Energy Research, University of Kentucky,
3572 Iron Works Pike, Lexington, KY 40511-8433

Keywords: Shale oil, carbonization, solvent extraction

INTRODUCTION

Oil shale represents one of the largest fossil fuel resources in the US and in other parts of the world. Beginning in the 1970s until recently, there was considerable research and development activity directed primarily to technologies for the production of transportation fuels from oil shale. Due to the low cost of petroleum, as with other alternate fuel strategies, oil shale processing is not economically viable at present. However, future scenarios can be envisaged in which non-petroleum resources may be expected to contribute to the demand for hydrocarbon fuels and chemicals, with the expectation that process technologies can be rendered economically attractive.

There is potential to improve the economics of oil shale utilization through broadening the spectrum of products that can be derived from this resource, and producing added-value materials that are either unavailable or more difficult to produce from other sources. This concept is by no means original. The history of oil shale development shows that most attempts to commercialize oil shale technology have relied upon the marketing of by-products [1]. These have included asphalts, construction bricks, cement, soil additives, town gas, lamp oil, rock wool insulation, ammonia, sulphur, paraffin, olefins and other chemicals, and power generation.

In this context, we have conducted investigations to assess the potential for producing premium carbon materials from shale oil residues. Retorted shale oils generally contain more high-boiling fractions than petroleum crudes [2,3]. This is especially true for eastern US shale oils. These properties make shale oils very attractive as carbon sources because the heavy fractions have high carbon contents. Another characteristic of shale oils is their high nitrogen content, which presents difficulties also in upgrading these liquids to clean fuels because extensive and deep hydrogenation is required. The nitrogen-containing species are more concentrated in the higher boiling fractions and accentuate the problem [4,5]. On the other hand, the nitrogen-containing compounds can become highly valuable feedstocks or chemicals if they are separated collectively or individually from shale oils.

We have already reported the successful production of isotropic carbon fibers and activated carbon fibers from the asphaltene fraction of residual shale oil produced from eastern US shale by the Kentort process [6, 7]. While the mechanical properties of the carbon fibers have yet to be assessed, the presence of nitrogen has been shown to enhance the catalytic properties of activated carbon fibers for reactions such as the ambient-temperature oxidation of SO_2 [8], and the nitrogen content is believed to contribute to the wide pore structure that is formed in the activated fibers [7,9].

As the maltene fraction of the shale oil residue has a much lower nitrogen content than the asphaltene fraction, it may be more suitable for the synthesis of other forms of carbon. In this paper, we present the results of studies to investigate the carbonization properties of this material, and to determine the potential for generating a pitch with high mesophase (a carbonaceous liquid crystal) content that could serve as a precursor for the production of materials such as needle cokes (a highly-oriented and graphitizable carbon) for the manufacture of graphite electrodes, and high-performance carbon fibers.

EXPERIMENTAL

A shale oil residue (SOR), produced in the Kentort II process from eastern oil shale [10,11], was used in the study. This residual oil was collected in an electrostatic precipitator and comprised 70-80 wt% of the total oil products from the retort. The sample was further fractionated by extraction with boiling hexane in a Soxhlet apparatus to obtain fractions with different heteroatom contents or polarity [12], namely, hexane-soluble (HS) and hexane-insoluble fractions. The parent shale oil sample and the extracted fractions were subjected to elemental and ^1H and ^{13}C -NMR analyses.

Carbonization reactions were conducted both at atmospheric pressure and elevated pressure. Atmospheric pressure carbonization was performed in a Pyrex tube. Samples were heated in the tube reactor under nitrogen flow at 440 °C for 4h, in a vertical electric furnace. Pressurized

carbonization was conducted using a stainless steel tubing bomb ($\phi 1'' \times 4''$) [13, 14]. The bomb was charged with 15-20g of sample and placed in a sand bath preheated at 440-500 °C for a reaction time of 4- 6 h. The reaction pressure was maintained at 700 kPa by pressurizing the bomb with nitrogen before the carbonization reaction and automatically releasing excess pressure through a relief nozzle over the course of the experiment. The carbonized products were weighed and further characterized by elemental analysis and optical microscopy (Leitz, MVP2), using polarized light, after mounting and polishing.

RESULTS AND DISCUSSIONS

Almost the same yields of hexane-soluble (SOR-HS) and hexane-insoluble (SOR-HI) fractions were obtained upon extraction. This means that the eastern crude shale oil contains 30-40 wt% of asphaltenes, in comparison with western shale oils which have less than 5 wt% [2,3]. Table 1 shows some analytical data for the parent shale oil and the extracted fractions. In the order of SOR-HS, parent SOR and SOR-HI, the aromaticity increased and the H/C atomic ratio decreased. Aliphatic components are concentrated in the maltene (SOR-HS) fraction which has correspondingly low aromaticity. Sulfur is distributed evenly in both extracted fractions although it is to be noted that the sulfur concentration is much higher than found in other shale oils [2,3]. About 85% of the total nitrogen in the parent shale oil is concentrated in the SOR-HI fraction, where nitrogen content is about six times higher than that of SOR-HS.

Figure 1 shows the optical texture of products obtained by atmospheric pressure carbonization of the parent shale oil and the hexane soluble fraction. Both feeds produced mosaic texture cokes. The product from the parent shale oil has a fine mosaic texture (about 5 μm in size), while larger isochromatic units ($\sim 20 \mu\text{m}$ size) were observed in the SOR-HS coke. The hexane insoluble fraction (SOR-HI) also gave a fine mosaic texture very similar to that of the parent shale oil, possibly because the presence of the HI fraction dominates the carbonization progress, as indicated by carbonization yield in Table 2. The hexane soluble fraction alone gave a yield of only 8 wt %, whereas it was 46 wt% for the hexane-insoluble fraction. The yield for the parent shale oil was 26 wt%, essentially following the additive rule.

The optical micrographs of products obtained by pressurized carbonization of the shale oil and the hexane-soluble fraction are shown in Figure 2. Under these conditions, excellent flow domain textures were formed from the SOR-HS fraction. The full-range shale oil gave a mosaic texture, $\sim 20 \mu\text{m}$, larger than that obtained under atmospheric pressure. The effects of using elevated carbonization pressure have been reported to be favorable for anisotropy development for many other heavy oils, and it has been employed commercially to produce needle cokes [14]. It has been reported that a western shale oil and its maltene fraction also produce mosaic texture cokes upon the atmospheric carbonization, even after various preheat treatments [15, 16]. These results are consistent with the experiment results described above, although there may be differences in composition, structure and reactivity between the eastern and western shale oils. The experiment results indicates the importance of both solvent fractionation and overpressure to the carbonization of shale oil products. The results of the present study further suggest that the maltene fraction of eastern shale oil may be used to produce mesophase pitches for the synthesis of high-performance carbon fibers, or for premium coke production if sulfur and nitrogen contents are acceptable. Elemental analyses of green cokes shows that much lower nitrogen cokes are produced by using the maltene fractions rather than the full-range shale oil, Table 3.

The influence of carbonization conditions on coke yield can also be seen in Table 2. Pressurized carbonization can substantially increase the yield. Notably, the yield from the maltene fraction was increased by a factor of about four at 700 kPa. The effects of high pressure and a closed system will be to prevent the escape of volatile components and cracked products and retain a higher proportion of the precursor in the liquid phase. The coke yield also reflects the high reactivity of the SOR-HI fraction: there was only a 20% increase in yield upon going to pressurized carbonization.

Based upon previous findings [6,7] and the results of the present investigation, at least one scheme can be proposed for the more effective use of residual shale oils, Figure 3. The first step involves solvent separation into maltene and asphaltene fractions. Deasphalting processes have been used to prepare feedstocks for delayed coking in order to produce high grade cokes from petroleum heavy oils and lower the impurity contents (basically metals, such Ni and V) of the coke products. The same step seems necessary to render shale oils suitable for premium coke production, although the reasons appear to be somewhat different.

The asphaltene fraction from shale oil contains a high concentration of nitrogen species and has a high coking reactivity that can inhibit mesophase development [5]. The nitrogen-containing species also tend to be retained in the resultant cokes, and could cause puffing problems at graphitization. Although the sulfurs in the SOR-HS may also result in puffing, desulphurization can be achieved relatively easily by mild hydrogenation [17]. Thus, by removing asphaltenes, a material can be obtained that would be a suitable precursor for the production of needle cokes, or a mesophase pitch for the manufacture of high performance carbon fibers. Alternatively, maltene fractions may be completely refined to produce liquid fuels by conventional catalytic upgrading, since most of problematic nitrogen-containing species are removed.

The asphaltene fractions can be used as a source of specialty carbons with high nitrogen content. The combustion of such high nitrogen-content fuels could result in unacceptable emission of nitrogen oxides [18]. The production of isotropic carbon fibers and activated carbon fibers with unique properties may be an example of their practical utilization. Thus, starting with a heavy shale oil, we may produce a variety of valuable carbon materials in the form of pitch, coke and carbon fibers, with optical texture ranging from isotropic, fine mosaic to flow domain.

REFERENCES

1. C.F. Knutson, B.F. Russel and G.F. Dana, Proc. 20th Oil Shale Symposium, Colorado School of Mine, Golden, CO, USA, 1987, p217.
2. C.S. Scouten, In Fuel Science and Technology Handbook, edited by James G. Speight, published by Marcel Dekker, Inc. New York and Basel, (1990), p1008.
3. Perry Nowacki, In Oil Shale Technical Data Handbook, Published by Noyes Data Co., 1981, p19.
4. J.W. Bunker, P.A.V. Devineni and D.E. Cogswell, Reprint, American Chemical Society, Div. Fuel Chemistry, 37(2), 581(1992).
5. Pinky Udaja, Gregory J. Duffy and Martin D. Chensee, "Coking reactivities of Australian shale oils", Fuel, 69(9), 1150(1990).
6. Y.Q. Fei, F. Derbyshire and T. Robl, "Carbon fibers and activated carbon fibers from shale oil residue", Preprints, Am. Chem. Soc., Div. Fuel Chemistry, 38(2) 427(1993).
7. Y.Q. Fei, F. Derbyshire, M. Jagtoyen and I. Mochida, "Advantages of producing carbon fibers and activated carbon fibers from shale oils", Proc., Eastern Oil Shale Symposium, Lexington, KY, USA, Nov.16-19, 1993, p38.
8. F. Derbyshire, Y.Q. Fei, M. Jagtoyen and I. Mochida, Abstracts, International Workshop: Novel Technology for DeSOx and NOx, Fukuoka, Japan, Jan., 1994.
9. Y.Q. Fei, M. Jagtoyen, F. Derbyshire and I. Mochida, "Activated carbon fibers from petroleum, shale oil and coal liquids", Ext. Abstracts and Program, International Conference on Carbon, Granada, Spain, June 3-8, p.666, 1994.
10. S.D. Carter, T. Robl, A.M. Rubel and D.N. Taulbee, "Processing of Eastern US Oil Shale in a Mutistaged Fluidized Bed System", Fuel, 69(9), 1124(1990):
11. S.D. Carter, A.M. Rubel, T. Robl and D.N. Taulbee, "The development of the Kentort II process for Eastern Oil Shale", Final Report to DoE, Contract No. DE-FC21-86LC11086, May 1990.
12. Y.Q. Fei, K. Sakanishi, Y.N. Sun, R. Yamashita and I. Mochida, Fuel, 69(2), 261 (1990).
13. I. Mochida, Y.Q. Fei and Y. Korai, "A study of the carbonization of ethylene tar pitch and needle coke formation", Fuel, 69(6), 667(1990)
14. I. Mochida, K. Fujimoto and T. Oyama, In Chemistry and Physics of Carbon, Vol.24, edited by P. Thrower, published by Marcel Dekker, Inc., 1994, p111
15. M.A. Sadeghi, V.L. Weinberg and T.F. Yen, "Alternative precursors for mesophase formation", Extended Abstracts and Program, American Conf. Carbon, 1983, p116.
16. M.A. Sadeghi, V.L. Weinberg and T.F. Yen, "Shale oil delayed coking products utilization for manufacturing graphites" Preprints, Am. Chem. Soc., Div. Fuel Chemistry, 29(3), 224(1984)
17. See Ref. 2, p199.
18. R.K. Lyon and J.E. Hardy, "Combustion of spent shale and other nitrogenous chars", Combustion and Flame, 51,105(1983).

Table 1 Analytical data for the parent shale oil and fractions

Sample ID	Yield (wt%)	Elemental Analysis(wt%)				Atomic Ratio		fa
		C	H	N	S	H/C	N/C(x100)	
SOR	—	82.02	8.58	1.38	1.84	1.26	1.47	0.57
SOR-HS	52	82.55	10.21	0.41	1.85	1.48	0.43	0.45
SOR-HI	48	81.39	6.88	2.49	1.81	1.01	2.62	0.71

* SOR, parent shale oil; HS, hexane-soluble fraction;
HI, hexane-insoluble fraction; fa, fraction of aromatic carbon

Table 2 Carbonization yield (wt%) of parent shale oil and fractions

Feedstock	Atmospheric pressure	Pressurized (700 kPa)
SOR	26	40
SOR-HS	8	31
SOR-HI	46	57

* SOR, parent shale oil; HS, hexane-soluble fraction;
HI, hexane-insoluble fraction

Table 3 Properties of green cokes obtained from parent residual shale oil and HS fraction

Feedstock	SOR	SOR-HS
Carbonization condition	440 °C-700 kPa	440 °C-700 kPa
Optical texture	Mosaic	Flow
N content (wt%)	3.22	1.08

* SOR, parent shale oil; HS, hexane-soluble fraction.

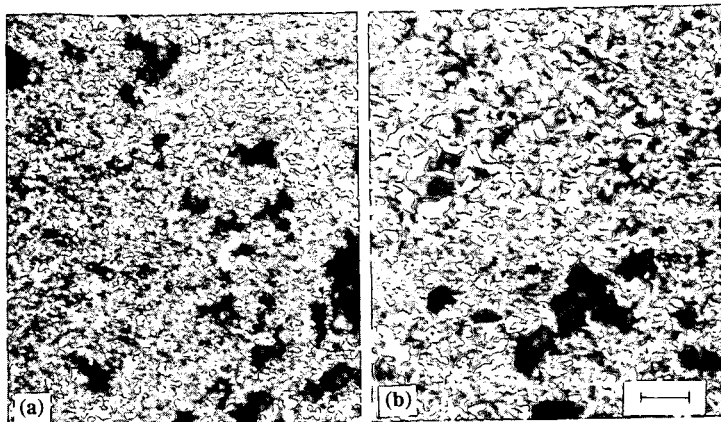


Figure 1 Optical texture of products carbonized at atmospheric pressure from: (a) Parent SOR, (b) Hexane-soluble fraction of SOR

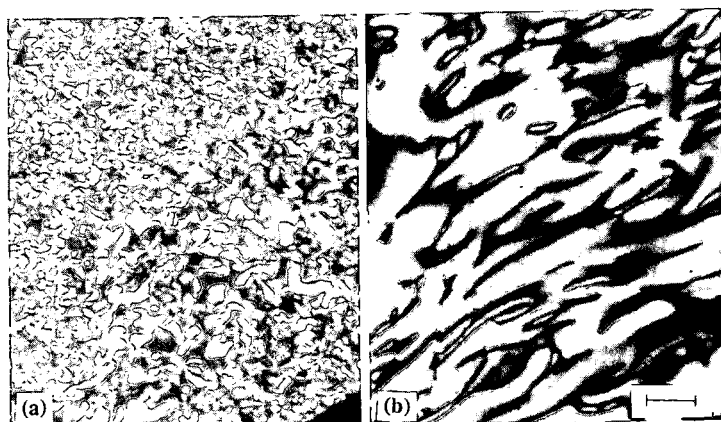


Figure 2 Optical texture of products carbonized under pressure (700 kPa) from: (a) Parent SOR, (b) Hexane-soluble fraction of SOR

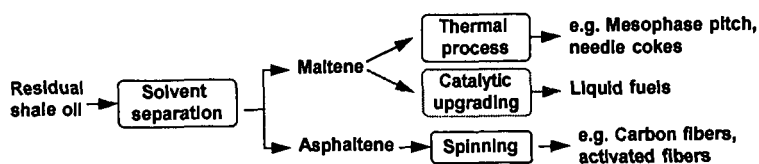


Figure 3 Illustration of a value-adding route for utilization of residual shale oils and resultant intermediate and final products

PRODUCING VAPOR GROWN CARBON FIBERS WITH HIGH SULFUR COAL WITHOUT SO₂ EMISSIONS

R. Alig, M. Lake, J. Guth, and D. Burton
Applied Sciences, Inc.
P.O. Box 579
Cedarville, OH 45314

Keywords: SO₂ Control Technologies, Coal Pyrolysis, Organic Sulfur Removal

ABSTRACT

This paper describes the development of a unique process that produces a highly graphitic, vapor grown carbon fiber (VGCF) from the gas phase in pound quantities. Past vapor grown carbon fiber progress has stagnated because the iron catalyst did not grow filaments profusely enough to make a practical continuous reactor. It has been found that adding H₂S at an equimolar level with the iron catalyst, the filament formation vastly increases. Coal is desirable as a sulfur source, for it eliminates the need for handling toxic H₂S, and it is a very low cost hydrocarbon supply for the process. We show that Ohio, high-sulfur coal containing 2.5 to 4.6% sulfur accomplishes both tasks. There is also evidence that sulfur from the coal remains with the carbon fiber catalyst during the reaction and does not exhaust as SO₂ into the atmosphere.

INTRODUCTION

Carbon fibers have been of practical interest within the industrial community for over a century; Thomas Edison tried them as filaments for light bulbs. The Air Force started carbon fiber development for aerospace in the 1950's because of their mechanical and electrical shielding properties. These fibers were found to be stronger than steel, stiffer than titanium, and yet lighter than aluminum. Today, golf clubs, fishing poles, and tennis rackets are typical uses in the commercial sector.

A. Commercial fibers

Commercial carbon fiber uses are limited because they are more expensive than competing metals for engineering applications. Furthermore, their diameter is 8 μ , which is larger than normal fillers, such as carbon black, for reinforcement. This imposes expensive and limited processing techniques into composite applications. Hand lay-ups and slow pultrusion techniques are the norm; straight injection molding is out of the question. The total U.S. market for carbon fibers in 1990 was 6 million lb, of which 0.8 million lb were for the recreational market at an average cost of 23 \$/lb for the carbon fiber¹. For comparison: 3 billion lb of carbon black were shipped to rubber manufacturers in 1992² at an average cost of 0.25 \$/lb.

Commercial carbon fibers are formed from polymer precursors such as polyacrylonitrile (PAN) or petroleum pitch. The precursor is extruded or spun similar to textiles into a continuous filament or thread, oxidized under tension to 200^o C, and followed by slow heating in the absence of air to 1000^o C to carbonize the fiber. Sometimes, the carbon fiber is given additional heating up to 3000^o C to develop higher degrees of graphitization, which is needed for expensive ultra-high strength (2000 \$/lb range) applications.

B. Vapor grown carbon fiber

This paper is based upon a unique form of carbon fiber requiring no precursor filament. It is called vapor grown carbon fiber (VGCF), known as PYROGRAF IIITM. From initial inventions at General Motors, the patents were licensed to Applied Sciences, Inc. in 1992 for further development and manufacture. The process began by early workers, exposing vapor phase metals, generally iron, supported on inert substrates while exposed to hydrocarbons and hydrogen³ at a temperature in the 1000 - 1150^o C. range. This catalyzed the growth of long, slender, partially graphitic filaments⁴ as

shown in Figure 1. Although these methods remained essentially batch processes and too inefficient for mass production, this VGCF when subsequently heat-treated has a thermal conductivity of 1950 W/m-K (highest value found in nature except for diamond) and is sold as a carbon/carbon composite for aerospace thermal management materials. This was followed by attempts at a continuous process by injecting and dispersing the iron catalyst particles directly into the gas stream, and eliminating the use of a substrate for growth^{5,6,7}. This was still non-productive; the iron catalyst did not grow filaments profusely enough to make a practical continuous reactor. A breakthrough occurred when it was found and confirmed from early work in the 1950's by Kauffman and Griffiths⁸ that sulfur was vital to fiber formation. Adding hydrogen sulfide (H_2S) at an equimolar level with the iron catalyst, vastly increase^{9,10} the filament formation making a continuous reactor practical (Figure 2). We believe that the sulfur is incorporated in the fiber by being adsorbed onto the catalyst, and subsequently overcoated with graphite.

Figure 3 shows scanning electron micrographs of vapor grown carbon fibers grown by a gas phase process in comparison with typical continuous commercial carbon fibers. The diameter of PYROGRAF III generally averages 0.2μ as produced, while commercial fibers are 8μ in diameter. Due to the nature of the gas phase generation, the fibers become entangled during growth and are not continuous like commercial fibers. The length/diameter ratio for PYROGRAF III ranges from 40 to 200. Due to the process and purity with which carbon is formed into the fiber, VGCF is highly graphitized (Table 2) and the stress/strain properties for 7.5μ VGCF (Figure 4) results in similar or higher property ranges than commercial carbon fibers. The smaller diameter and entanglements of the PYROGRAF III defy measurement.

C. Coal

Most of the VGCF made to date used laboratory grade methane, benzene, acetylene, etc. as a hydrocarbon source as a step toward reproducible results. Since we have developed one product line that can produce almost a pound per hour, natural gas is frequently used for high volume trials. Although the addition of H_2S was instrumental in achieving this improvement, it is used with great reluctance. Hydrogen sulfide is expensive, highly corrosive to rubber seals and metal fittings, flammable, and its toxicity is on a par with hydrogen cyanide.

This suggests that a fossil fuel such as Ohio high sulfur coal may be especially apropos for this problem since Ohio coal production has gone from 55 million tons in 1970 to 33 million tons in 1990. Ohio coal's high sulfur content is most responsible for this decline, which is projected to go lower due to the 1990 Clean Air Act Amendment. Furthermore, coal would have a tremendous effect on the eventual price of the fiber. The hydrocarbon is the most expensive cost item, followed by the electric oven energy and the catalyst. Although the energy consumption and output capabilities are not yet optimized for a total cost picture, the formulations that will be discussed later show that coal at 30 \$/ton not only drastically reduces the cost of the carbon source, but totally eliminates the price of the sulfur:

PYROGRAF III MATERIAL COST COMPARISON

	Control Methane Only (\$/lb)	Control Natural gas only (\$/lb)	Trial 1 94% N.G. 6% Coal (\$/lb)	Trial 2 100% Coal (\$/lb)
Sulfur Source	0.189	0.194	0	0
Carbon Source	69.83	0.44	0.419	0.067

EXPERIMENTAL

In this experiment, a reactor that normally uses a feedstock mixture of 99.9% pure methane was converted to enable use of coal as the hydrocarbon feedstock (Figure 3). Helium is bubbled through liquid iron pentacarbonyl to provide Fe catalyst particles, and 99.3% pure H_2S gas is simultaneously injected into the 1100° C reactor. A typical control formulation that produces a 25% yield is shown in Table I. A screw type apparatus was assembled to feed the coal and driven by a variable speed motor. It is similar to commercial equipment except the feed box is sealed from the air; otherwise, it may cause combustion as the coal enters the reactor. A carrier gas is used to transport the coal dust from the screw feed into the reactor hot zone.

Two trials using coal are shown in Table 1. In Trial 1, the hypothesis is that sulfur-bearing coal can replace H_2S as the source of sulfur in the reaction. Coal and methane were used as the hydrocarbon feedstock. The formulation was developed so that the sulfur content in the coal was equivalent (1.6 $H_2S/Fe(CO)_5$ molar ratio) to the sulfur in the "control" formulation using methane and hydrogen sulfide. Ohio #8 Coal from CONSOL Inc., at 4.71% total sulfur and 46.6% total carbon, was pulverized to less than 63 μ . Methane was the carrier gas at a rate calculated to maintain a similar 1.6 molar sulfur/carbon ratio as the "control". It was assumed that all the sulfur in the coal was converted to hydrogen sulfide.

Trial 2 was to test the hypothesis that coal could serve as the only supply of the hydrocarbon and sulfur, and produce vapor grown carbon fiber. The pulverized coal was carried into the reactor with a non-hydrocarbon carrier (hydrogen). Upper Freeport Seam coal was obtained from Kaiser Engrs. with 2.5 % total sulfur and an estimated 65% carbon content. In this case without methane dilution, the molar sulfur/catalyst ratio is 4.5, which is considerably higher than the minimum 1/1 ratio for good filament formation.

RESULTS AND DISCUSSION

Carbon yield is here defined as the fraction of fiber harvested to the total carbon introduced into the reaction from all hydrocarbon sources. In the "control", vapor grown carbon is routinely produced with a yield of 25% with a 2% standard deviation. In Trial 1, with coal, methane, and no H_2S , the carbon yield is 19%. The photomicrograph in Figure 6 shows very good growth and confirms that the sulfur contained in the coal plays an active role in the catalytic process, and can potentially replace the need for using H_2S in the reaction.

The sulfur content in coal is well beyond the optimum amount for the formation of carbon fibers. Figure 6, reproduced from one of our prior papers¹⁰, shows SEM photomicrographs of carbon fiber produced with $H_2S/Fe(CO)_5$ ratios of 0, 1.4/1 and 17/1. The sparse fiber in the photo without sulfur clearly illustrates the need for sulfur. However, the photo at the very high 17/1 ratio still produces very good carbon fiber; the fiber length is shorter, and tends to be more jagged and the soot content increases. Nevertheless, this leads to the possibility that high sulfur coal in spite of its problems for other uses may be a unique asset for the production of acceptable vapor grown carbon fiber.

In Trial 2, coal is the only source of both hydrocarbon and sulfur; a yield of 47% was obtained and a SEM photomicrograph is shown in Figure 5. There is good, but shorter fiber formation with a fair amount of soot and perhaps some ash. From past experience, the high carbon yield is anticipated, for we know that at extremely high sulfur levels, only soot will be formed. Nevertheless, these results support the conclusion that the inherent carbon in coal is actively pyrolyzed to products which participate in the catalytic fiber nucleation and growth process.

Photomicrographs are the basic estimate of fiber formation. However, X-ray diffraction can estimate the graphitic ordering and is the crucial property for assuring the quality of the fiber's strength and conductivity. Samples from the trials were analyzed by X-ray diffraction; Table 2 shows that the fiber samples from coal Trials 1 and 2 have a graphitization index that is typical for low modulus commercial fiber.

In earlier trials that rely on introducing H_2S into a pure methane feedstock at equivalent ratios with the catalyst, periodic analysis has been made of the exhaust. To date, sulfur has not been detected in the exhaust. This could be explained by the proposal¹⁰ that the sulfur dissolves in such large amounts that it melts the iron catalyst and thus stays with the catalyst at the base of the fiber. How much sulfur can be dissolved as the sulfur increases is unknown; there is a limit where fiber is no longer formed. A packed column gas chromatograph (GC) with thermal conductivity detector was used to estimate the composition of the exhaust gases of a series of coal trials when the sulfur was running at 4.5 times the usual amount (Trial 2) and the presence of sulfur was not detected. This instrument does not have the sensitivity to measure nitrogen or sulfur compounds below about 0.1-1 percent. Gastec detection tubes capable of detecting sulfur dioxide concentrations of 0.25 ppm and above were also used and no SO_2 was detected. Future work is needed with a capillary column GC with dedicated nitrogen and sulfur detectors.

Nevertheless, the data does support the theory that the sulfur does unite with the catalyst during fiber formation and would eliminate or reduce the release of harmful sulfur compounds into the atmosphere. Future work should also address the sulfur content, if any, in the residual ash over a wide range of sulfur/catalyst ratios. Although further work is needed to assess the effects of the organic and ash content variation in coal, their presence does not prevent the growth of a carbon fiber with graphitic ordering. For some applications such as rubber reinforcement, it is possible that the sulfur content in the fiber may be uniquely desirable and enhance the bonding during the rubber vulcanization process.

While these studies indicate the viability of using high sulfur coal as the hydrocarbon feedstock in production of VGCF, in practice, the high percentage of sulfur in various coals, as well as the variability of the percentage of sulfur in coal, will most likely mandate a combination of hydrocarbon feedstocks in order to maintain the process balance needed for optimum production. The role of coal in contributing to the hydrocarbon balance, as well as the sulfur balance, has significant implications.

CONCLUSIONS

It has been demonstrated that high sulfur coal can be used to make VGCF, contributing both carbon and sulfur to the reaction. This work suggests an ecologically safe process for utilization of high sulfur coal. If future trials continue to confirm these conclusions, the economic impact of coal on the price of carbon fiber will open new applications for carbon fiber in rubber reinforcements, cement, composites for automobiles, electronics, and aerospace components.

ACKNOWLEDGEMENT

This research was supported in part by the Ohio Coal Development Office/Ohio Department of Development under Grant Number CDO/R-922-8. The authors also gratefully acknowledge the contribution of Dr. Gary Tibbetts, General Motors NAO Research & Development, for his assistance and pioneering work that has made vapor grown carbon fibers a commercial reality, Dr. David Anderson from the University of Dayton Research Institute in providing X-ray analysis, and much assistance from the OCDO staff in performance of this work.

REFERENCES

1. C. Petersen, **ADVANCED COMPOSITES**, March/April 1994, pp 20.
2. **CARBON LINES** Vol. 4, No. 1, March 1993, Newsletter by Huber engineered Carbons Division.
3. G.G. Tibbetts, *Carbon* 30, 399 (1992).
4. J.L. Kaas, *Carbon* 23, 665 (1985).
5. M. Endo and T. Koyama, Japanese patent 1983-180615, Oct 22 (1983).
6. Y. Komatsu and J. Endo, Japanese patent 60-32818, Feb 22 (1985).
7. K. Arakawa, U.S. Patent 4,572,813, Feb. 25 (1986).
8. H.F. Kauffman and D.J. Griffiths, U. S. patent 2,796,331, June 18 (1957).
9. G.G. Tibbetts, D.W. Gorkiewicz, and R.L. Alig, **CARBON** 31, 809 (1993).
10. G. G. Tibbetts, C. A. Bernardo, D. W. Gorkiewicz, and R. L. Alig, "Effect of Sulfur on the Production of Carbon Fibers in the Vapor Phase" **CARBON**, 32, no. 4, pp. 569-576, (1994).

TABLE 1. TRIAL FORMULATIONS*

	CONTROL	TRIAL 1	TRIAL 2
METHANE	96.90	87.58	NONE
COAL	NONE	9.33	80.68
SULFUR	0.47	0.44	2.02
HYDROGEN	NONE	NONE	13.30
HELIUM	0.96	0.96	1.45
Fe(CO) ₅	1.68	1.69	2.55

* Formulations are in per cent by weight

TABLE 2. X-RAY DIFFRACTION ANALYSIS

HEAT TREAT (°C)	FIBER TYPE	D-Spacing (nm)	g _D * (%)
AS-GROWN	VGCF	.34490	--
1300	ex-PAN	.354	--
AS-GROWN	COAL & METHANE	.3459	--
AS-GROWN	COAL ONLY	.3451	--
2500	ex-PAN	.342	23
2500	VGCF	.3377	73
as-grown	PYROGRAF III	.3385	64
--	P-120	.3378	72

$$*g_D = (0.3340 - D\text{-Spacing}) / (0.3440 - 0.3354)$$

Fiber Nucleation and Growth Model

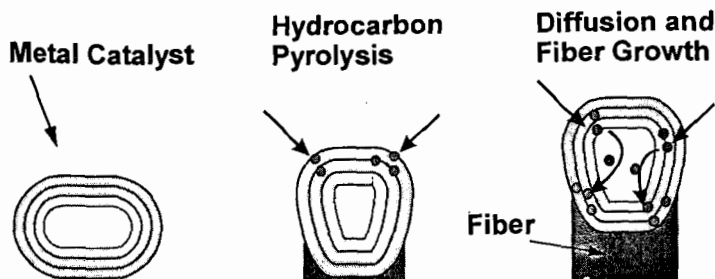


Figure 1. Fiber Nucleation and Growth Model

Carbon Fiber Process

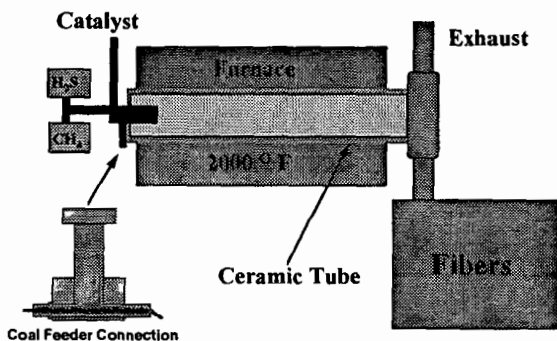


Figure 2. Carbon Fiber Processing

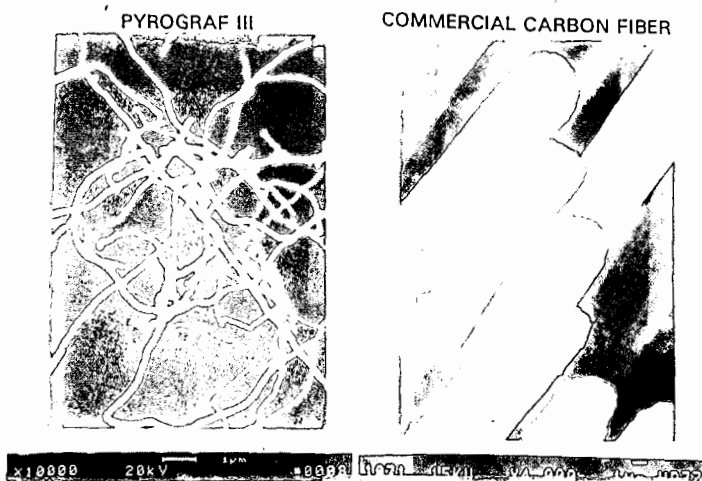


Figure 3. Scanning Electron Micrographs Comparing Vapor Grown Carbon Fiber with Commercial Carbon Fiber

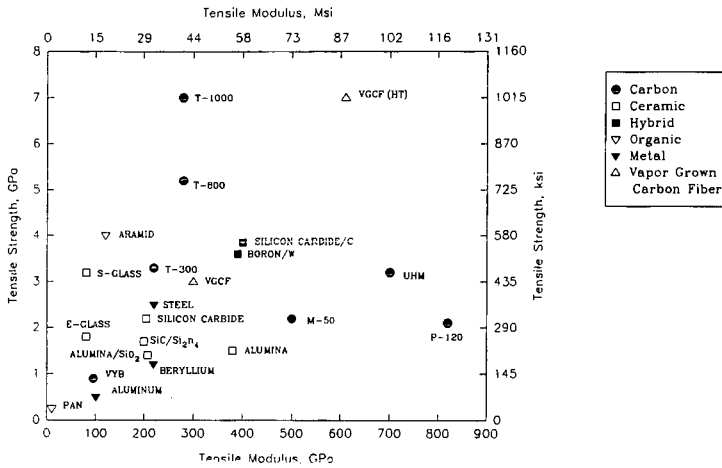


Figure 4. Tensile-Modulus Properties

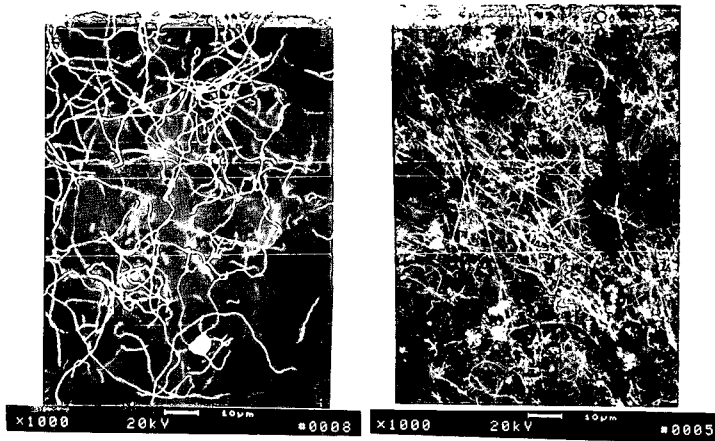


Figure 5. Coal Derived Fiber

Effect of H₂S on Fiber Growth

SEM Photomicrographs

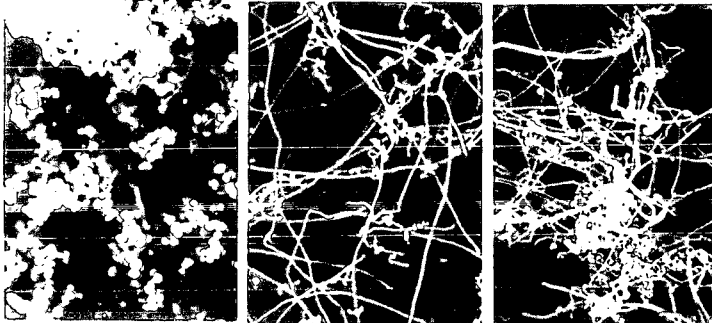


Figure 6.

No H₂S Flow

H₂S/Fe.(CO)₅=1.4/1

H₂S/Fe (CO)₅=17/1

THE PREPARATION OF FINE CARBIDE POWDERS FROM COAL SOLUTIONS

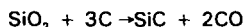
David. L. Morgan, Vladimir Cukan and Sara N. Prins
Division of Materials Science and Technology, CSIR
P O Box 395, 0001 Pretoria, South Africa.

Keywords: silicon carbide, coal solution, sol-gel.

INTRODUCTION

Non-oxide ceramics, such as silicon carbide [1], find use in applications requiring extreme hardness, chemical inertness and high-temperature strength. Transition metal carbides, such as tungsten carbides cemented with cobalt or nickel, are used extensively as wear components. Articles are generally fabricated by sintering pressed powder bodies at high temperatures. To maximise strength and hardness of the ceramic bodies, fine powders below 1 micron in size are needed together with small additions of sintering aids. Boron carbide plus carbon are used as sintering aids for silicon carbide. Very uniform dispersion of the sinter aid or binder metal with the carbide powder is necessary. This is achieved by milling the components together, often for many hours. The carbides are generally prepared by reacting the metal or oxide together with carbon. The low reactivity of particulate carbon means that high temperatures have to be used with extensive milling being required to reduce the particles to a suitable size. The end result of these requirements is that sinterable powders are expensive.

Fine oxide ceramic powders with very uniformly dispersed additives are prepared by the sol-gel process where the components are mixed as solutions or sols and the mixture then gelled [2]. The solvent is removed and the ceramic converted at relatively low temperature to fine, easily-sinterable powder. It would be very desirable to be able to extend those ideas to the preparation of fine carbide powders by bringing a carbon source into very intimate contact with an oxide followed by carbothermal reaction to the carbide e.g.:



However no low-cost carbon source has been readily available. Carbohydrates have been used in solution with colloidal silica sols but non-uniform drying could be expected [3]. Polycarbosilanes and silanes may be converted to silicon carbide but are very expensive [4]. Most organic polymers pyrolyse to carbon, but generally in low yield.

Coal solutions may be used as an effective and inexpensive source of carbon for the sol-gel preparation of silicon carbide. The coal molecules may also be brought into very intimate contact with the oxide by co-precipitating coal from solution together with an oxide gel under conditions of high shear. This approach is more general as maintaining both coal and metal oxide sol in solution together prior to gelling is not a simple matter. Absorbing coal molecules into a high surface area oxide is also effective. The coal is immobilised by gelling prior to solvent recovery.

We have prepared silicon carbide from coal solution by each of these three approaches [5]. The products from the co-gel and co-precipitation routes were both fine powders, with a very small content of fibrous whiskers whilst that prepared by the mixing route was predominantly fibrous in nature.

X-ray diffraction measurements showed that in all cases the silicon carbide was in the β -form, as would be expected from the low conversion temperature.

COAL SOLUTION

The coal solution was prepared by alkali-induced solubilisation of a medium-volatile bituminous coal in dimethylformamide (DMF) [6,7]. Over 90% of the organic part of suitable coals dissolve in DMF on addition of 10% (based on coal) of sodium or potassium hydroxide. The conditions for extraction are mild-atmospheric pressure,

temperature of 90°C but strict exclusion of oxygen. The mineral components are removed by centrifugation and filtration giving a purified solution of "refcoal". The refcoal solutions used for carbide preparation had typically a concentration of 8% coal-derived material.

Refcoal solution gels on addition of 5% water or sufficient acid to neutralise the alkali present, giving a soft gel strong enough for a cylinder 2cm x 6cm high to be self-supporting.

The refcoal after removal of solvent contained less than 0,2% ash and gave 75% yield of carbon on pyrolysis at 1000°C.

EXPERIMENTAL

The coal used was a flotation concentrate, with essentially all particles being smaller than 0,85 mm. The analysis is given in the Table.

PREPARATION OF COAL SOLUTION

Coal (5,0 kg), DMF (50 kg) and sodium hydroxide pearls (0,5 kg) were stirred together under nitrogen at 90°C for 5 hours. The minerals and undissolved coal were removed by settling followed by filtration through polypropylene filter cloth. The clarified solution contained 8,0% dissolved coal material. The viscosity was 2,9 cP at 30°C.

PREPARATION OF SILICON CARBIDE BY SOL-GEL ROUTE

A silica sol was prepared by mixing ethyl silicate (40% SiO₂, 7,5 kg) in DMF (3,5 kg) with 1% HCl solution in water (1,33 kg). The mixture warmed and became homogeneous over 60 minutes.

The silica sol was cooled to below 5°C and rapidly mixed (within 5 seconds) with coal solution (50 kg), also cooled to below 5°C. The mixture thickened and then gelled. The gel was broken up and the solvent removed under reduced pressure at 95°C to give a coarse powder which was pressed into briquettes (~ 8 g mass) under high pressure. The briquettes were pyrolysed at 900°C for 3 hours and then converted to silicon carbide by heating to 1500°C for 7 hours in a stream of argon (15 l/min). After cooling under argon the briquettes were crushed to smaller than 1 mm and excess carbon burned off at 700°C for 5 hours in a muffle furnace. Measurement of free silica showed 99,5% conversion although this may represent some re-oxidation during carbon burnoff. Sodium salts arising from the alkali present in the coal solution were removed with a dilute acid wash and the product was dried.

The silicon carbide was a fine grey powder. Size analysis gave a median particle size of 1,5 micron. SEM examination showed that the particles were made up of agglomerates of sub-micron particles. Whisker-like particles were virtually absent - a few could be found on active searching.

PREPARATION OF SILICON CARBIDE BY CO-PRECIPITATION ROUTE

Sodium silicate solution (300 ml, containing 18,0 g SiO₂ and 5,45 g Na₂O), sulphuric acid (48 ml, containing 8,5 g H₂SO₄) and coal solution (300 ml) were pumped separately but simultaneously over 5 minutes using peristaltic pumps into a reactor (30 ml) fitted with a high-shear mixer. The overflow of gelatinous co-precipitate was collected and recirculated through the high-shear mixer for 30 minutes at 100 ml/min.

The co-precipitate was dried and sodium sulphate removed by washing with water. The precursor powder was briquetted under pressure and converted to silicon carbide by heating to 1450°C for 6 hours under flowing argon. Conversion of silica was complete. Excess carbon was burned off at 700°C for 5 hours.

The silicon carbide was a fine grey powder with a median particle size of 3,5-5 micron. SEM examination showed that the particles were made up of agglomerates of sub-micron particles. Few whiskers were seen but there were

more than were present in the co-gelled product.

PREPARATION OF SILICON CARBIDE BY MIXING ROUTE

The precipitated silica used was Crosfield Neosyl GP, containing 88% SiO₂ and with a typical BET surface area of 200 m²/g. Precipitated silica (20,5 g, containing 18 g SiO₂) was mixed with coal solution (300 ml). Water (15 ml) was added to gel the coal solution. The solvent was removed to give a precursor which was converted to silicon carbide as above. The conversion of silica was total.

The silicon carbide after excess carbon burnoff formed a felt of fibrous material. SEM examination showed that the great bulk of the product was fibrous with some interspersed amorphous material.

DISCUSSION

The fineness and freedom from fibrous material of the silicon carbide prepared by the three different approaches from coal solution is clearly affected by the degree of inter-dispersion of the refoal with the silica. The sol-gel route would be expected to give the highest inter-dispersion of carbon and silica as the components had been mixed together in solution prior to gelling. The mixed precursor might be expected to have the poorest inter-dispersion with the co-precipitated precursor in between. The properties of the silicon carbide prepared from co-precipitated precursor were very similar to that prepared from the co-gel material which suggests that the inter-dispersion was also similar. This augurs well for successfully extending the co-precipitation route to the preparation of other carbides, because control of this method is simpler than that of co-gelling coal solutions with oxide sols. Clearly the properties of the silicon carbide prepared by the co-gel route are better than those of co-precipitate material. However the cost of silica from sodium silicate is very much less than that from ethyl silicate so that our further efforts are being concentrated on optimising the co-precipitation route, and on the introduction of homogeneously dispersed sintering aids.

ACKNOWLEDGEMENTS

The authors wish to thank the CSIR and the South African Department of Mineral and Energy Affairs, through the National Energy Council, for funding this work. Patents arising from the Project are held by Enerkom (Pty Ltd).

Technical assistance by Alpheus Bokaba, Tom Hardenberg and Samuel Sibanda is gratefully acknowledged.

REFERENCES

1. Y. Somiya and S. Inomata (eds.): Silicon Carbide Ceramics vols 1 and 2. Elsevier Science Publishers Ltd., London (1991).
2. L.L. Hench and J.K. West Chem. Rev. 1990 **90** 33.
3. A. Jubbe, A. Larbot, C. Guizard, L. Lot, J. Charpin and P. Bergez, Mat. Res. Bull. 1990 **25** 601.
4. R.M. Laine and F. Babonneau Chem. Mater. 1993 **5** 260.
5. D.L. Morgan and V. Cukan S.A. Patent No. 93/5725.
6. D.L. Morgan Preprints ACS Div. Fuel. Chem. 1992 **37(4)** 1996.
7. D.L. Morgan US Patent No. 5 120 430.

TABLE: COAL ANALYSIS

Moisture	0,7%
Ash	10,8
Vol. Mat.	22,6
Fixed carbon	65,9
DAF carbon	90,5
hydrogen	5,4
nitrogen	1,9

ACTIVATED CARBONS FROM NORTH DAKOTA LIGNITE AND LEONARDITE

Brian C. Young, Edwin S. Olson, Curtis L. Knudson, and Ronald C. Timpe
University of North Dakota Energy & Environmental Research Center (EERC)
Grand Forks, ND 58202

KEYWORDS: Leonardite activated carbons

INTRODUCTION

The EERC is undertaking a research and development program on carbon development, part of which is directed towards investigating the key parameters in the preparation of activated carbons from low-rank coals indigenous to North Dakota. Carbons have been prepared and characterized for potential sorption applications in flue gas and waste liquid streams.

Lignite, owing to its wide occurrence and variability in properties, has received significant attention as a precursor of active carbon manufacture. Mineral matter content and its alkaline nature are two highly variable properties that can have important consequences on the production of suitable activated carbons. Other factors affecting the production include carbonizing conditions, the activation agents, activation temperature, and activation time (1, 2). However, as previously noted, the relationship between the above factors and the sorption activity is particularly complex (2). Part of the difficulty is that sorption activity encompasses at least three parameters, namely, surface area, pore distribution, and surface acidity/basicity. The presence of mineral matter in the coal can affect not only carbonization but also the activation and subsequent sorption and desorption processes.

Lignite-based activated carbons typically have a low micropore volume, some 17% of the pores being micropores versus 35%–50% macropores (3). The macropores contribute little to the surface area and hence have a small impact on the adsorption process. Samaras, Diamadopoulos, and Sakellariopoulos (4) have recently shown that the removal of mineral matter improves the micropore volume of activated carbons since the mineral matter catalyzes the pyrolysis and carbonization reactions, leading to an enlargement of the pores. Several inorganic species, such as Fe, K, Mg, Ca, and Na are likely gasification catalysts, but the mechanism is not well understood. Removal of mineral matter from lignites decreases the reactivity of the chars towards carbon dioxide and oxygen (5) and produces random changes in the surface area as a result of structural changes (6).

As well as surface area and surface heterogeneity, the presence and structure of particular oxygen surface groups are also important for the adsorption of specific gases or vapors (7, 8). Basic oxygen groups with a pyronic structure, for instance, favor the adsorption of sulfur dioxide (9). Furthermore, Davini (10) has recently demonstrated that carbons containing a significant mineral matter content, particularly if an appreciable amount of iron is present, and an enhanced content of acidic oxygen groups have reduced capacity for SO_2 sorption.

This paper reports recent results of an investigation of demineralization, carbonization temperature, activation temperature, and activation time for one lignite and one leonardite from North Dakota. The majority of the work has been carried out with leonardite. This work is developing further data and understanding on leonardite char adsorbents reported earlier in a patent by Knudson (11).

EXPERIMENTAL

The feedstocks included a Beulah-Zap lignite and a Georesources leonardite. The coals were crushed, ground, and sieved in the usual manner to recover the -10×30 - or -12×30 -mesh fraction for testing. The coal analyses (thermogravimetric [TGA] and proximate) are shown in Table 1. The composition of the mineral matter of the leonardite by x-ray fluorescence was also determined.

Two reactors were used to produce the chars, a large capacity (100 grams) TGA unit and a nominally 12-kg capacity Cress kiln (model X31TC). The latter has a bottom distributor plate through which gas, preheated by the kiln, enters to permeate the bed. The chars were activated in the TGA unit or a Lindbergh Type 59344 furnace (TF) incorporating a 19-inch-long by 1-inch-diameter Vycor tube.

A representative sample of the leonardite containing a high mineral matter content was physically and chemically cleaned. Physical cleaning involved float-sink with Certi-grav and using the 1.4 and 1.6 float fractions. Both hydrochloric and hydrofluoric acids were used for chemical cleaning.

The initial carbonization conditions were as follows:

1. TGA unit — Approximately 50 g of feed was carbonized at 700°C to 850°C under N_2 for up to 1 hour followed by steam activation at the same temperature for up to 1 hour.
2. Kiln vessel — Approximately 12 kg of feed was at 480°C under N_2 for 1 hour. Subsequently, the leonardite was carbonized at different temperatures (see below).

Table 2 lists the conditions for activating the leonardite carbonized at 480°C in the kiln. Once the optimum activation temperature was established, the optimum activation time was determined by repeating the test conditions. Table 3 shows the variables used in optimizing the conditions for sorbent preparation from the leonardite. Beulah lignite was activated at 750°C for 20 minutes under 20% steam in nitrogen.

TABLE 1
Coal and Char Proximate Analyses

Coal	Carbonization Temp., °C	Activation Temp., °C	wt%, ar* Moisture	wt%, mf** Volatiles	wt%, mf Fixed C	wt%, mf Ash
Geo*	NA**	NA	32.6	44.1	27.6	28.3
Geo-1.6 Float	NA	NA	22.3	38.4	51.7	9.9
Geo-1.4 Float	NA	NA	42.9	51.2	41.8	7.0
Beulah	NA	NA	31.8	43.9	49.9	6.2
Geo	480	NA	5.3	32.8	47.2	20.0
Geo	480	700	1.1	8.7	52.6	38.6
Geo	480	750	1.1	8.4	53.6	38.0
Geo	480	800	0.9	7.0	57.6	35.5
Beulah	750	750	1.6	6.6	79.7	13.7

* As-received.
 ** Moisture-free.
 * Georesources leonardite.
 ** Not applicable.

TABLE 2
Test Conditions for Activating Georesources Leonardite Char Carbonized at 480°C in the Kiln Reactor*

Test No.	Sample Size, g	Reactor	Temperature, °C
1	10	TGA	700
2	10	TGA	750
3	10	TGA	800
4	10	TGA	850
5	50	TF	800
6	50	TF	850
7	50	TF	900
8	50	TF	950
9	50	TF	1000

* All samples were activated in 20% steam in nitrogen for 10 minutes.

TABLE 3
Test Conditions for Optimizing Char Sorbent Preparation

Variable	Condition
Activation Time under Steam	0, 10, 20, 40, 60 minutes
Coal Cleaning Prior to Charring	1.4, 1.6 Float; HCl, HCl/HF leach
Carbonization Temp.	350, 480, 550°C
Carbonization Temp.	350, 480, 550°C
Activation Temp.	750°C
Activation Gas	Steam, steam/O ₂
Gas-Char Contact Time	10, 20, 20 (steam)/5 (O ₂) minutes

The activating agent was steam in nitrogen, with an approximate concentration range of 20% v/v. In one case, the leonardite char was activated with steam for 20 minutes followed by 3.5% v/v oxygen in nitrogen for an additional 5 minutes.

The activated carbons were characterized by TGA proximate analysis, SO₂ sorption in argon at ambient temperature and at 100°C, iodine number, surface area, and pore volume analysis.

RESULTS AND DISCUSSION

Demineralization of the leonardite reduced the mineral matter to 6.8 wt% on a moisture-free basis with HCl and to 0.4 wt% moisture-free with HF. The proximate analyses of the raw, cleaned, and carbonized leonardite, as a function of carbonization and activation temperatures, are shown in Table 1 along with proximate analysis data for the carbonized lignite. Overall ash levels remain approximately constant with activation temperature for the uncleared leonardite carbonized at 480°C and steam activated at temperatures of 700°C and above. As expected, volatile matter decreases with increasing activation temperature.

X-ray fluorescence analysis of the leonardite ash revealed that silicon, aluminum, and calcium are the major components, making up around 72 wt% on an oxygen-free basis, but the total weight of these four elements in the leonardite is 10.6 wt% as a consequence of the significantly high mineral matter

content (28.3 wt%) of the feedstock. The presence of calcium may be detrimental in the activation process for achieving microporosity but could be beneficial for assisting in the capture of SO₂.

A limited set of experiments was carried out on the lignite sample. Sorption tests with SO₂ at 100°C and 5000 ppm resulted in a small uptake, 2.4 wt% (g SO₂/100 g char) with fine carbon and 1.9 wt% with carbon pellets containing a binder, the carbons being produced in the TGA unit. Desorption at 100°C yielded a 0.2 and 0.4 wt% change, respectively, for the different samples, whereas desorption between 100° and 400°C yielded 1.0 and 0.9 wt% respectively.

Differences in sorption activity of products from the TGA and tube furnace reactor were seen in the case of the Georesources leonardite. Here the sorption activity was examined as a function of steam activation temperature for leonardite char carbonized at 480°C. Figures 1 and 2 show the SO₂ sorption data for ambient and 100°C conditions, respectively. The dependence of sorption activity on reactor type is less marked at the higher sorption temperature where the sorption capacity of the tube furnace product approached that of the TGA product. Reactor conditions would seem to affect significantly the resultant sorption activity where mass flow fields are appreciably different. The maximum sorption activity at ambient temperature and 100°C appears to occur for char activated between 750° and 800°C (6.1 and 6.8 wt% SO₂, respectively, at ambient temperature). However, the sorption activity is about one-third lower at 100°C (2.3 and 2.4 wt% SO₂, respectively,) than that at ambient temperature.

Owing to the similarity between the trends in Figures 1 and 2, it is feasible to plot the ratio of the two sorption values at the two sorption temperatures against activation temperature, as illustrated in Figure 3. The observed linear relationship leads to the following expression:

$$\%_{\text{Amb}}\text{SO}_2 = 2.79 \times \%_{100^\circ\text{C}}\text{SO}_2$$

Differences between the sorption activity at the two temperatures can be explained by the weakness of the physisorption bonding (Van der Waals) and the decline in relative strength between the Van der Waal's bond and the increasing vibrational component of the bond energy with increasing thermal energy.

The iodine number provides an alternative measure of sorption activity, the results of which are depicted in Figure 4 for the range of activation temperatures examined. Here it is seen more sharply that the optimum activation temperature for uncleaned leonardite char produced at 480°C is 750° to 800°C, corresponding to the SO₂ sorption results at 100°C (see Figure 2). However, the maximum iodine number of 460 mg I₂/g char (590 mg I₂/g C) is at the lower end of the range of that reported (600 to 1450 mg I₂/g C) for a commercial carbon.

Preliminary investigations on optimizing the carbonization and activation of leonardite (uncleaned) show that the maximum sorption activity as measured by SO₂ (5000 and 10,000 ppm in argon at 100°C) to be as follows: carbonizing temperature: 350°C, activation temperature: 750°C, activation time: 20 minutes. The results are shown in Figure 5. Subsequent activation with 3.5% v/v oxygen in nitrogen for an additional 5 minutes reduced the sorption by approximately 17%. This result is presumably due to a lowering of the microporosity as a result of increased burnoff.

Improvements in sorption activity of leonardite were found through physical cleaning. Carbonizing the 1.4 and 1.6 Certi-grav float-sink fractions (10.9 and 7.8 wt% ash, respectively) at 480°C, activation temperature of 750°C, and activation time of 20 minutes yielded 10.9 and 10.1 wt% SO₂, respectively, at 10,000 ppm SO₂ in argon at ambient temperature. The uncleaned leonardite yielded about 20% less SO₂ sorption (8.4 wt%).

Chemical cleaning of leonardite did not lead to successful sorption of SO₂ since both the HCl and HF severely modified the carbon matrix by removing the bridging divalent ions. The remaining gel-like carbonaceous material after carbonizing and activation yielded sorption data that were comparable to that determined for the carbons derived from the uncleaned leonardite. The behavior of acid-washed leonardite is significantly different from that of acid-washed lignite, as determined from our study of chemically cleaned lignite.

The surface areas, determined by N₂ multipoint BET, for the uncleaned and physically cleaned (1.6 float-sink) leonardite char, both steam-activated at 750°C for 20 minutes, were 81.6 m²/g and 90.0 m²/g, respectively. Although physical cleaning enhances the surface area slightly, nonetheless, gasification of leonardite char appears to affect the development of the surface area significantly.

CONCLUSIONS

Enhanced sorption activity towards SO₂ was obtained with physically cleaned leonardite (< 7 wt% ash) activated carbon. The conditions for its production were as follows: carbonization temperature: 480°C, activation temperature: 750°C, activation time with steam: 20 minutes. The best sorption activity determined was 10.9 wt% SO₂ with 10,000 ppm SO₂ in an argon stream. The surface area of the physically cleaned leonardite was 90.0 m²/g. Optimization of these conditions is expected to enhance the adsorptivity of the char significantly.

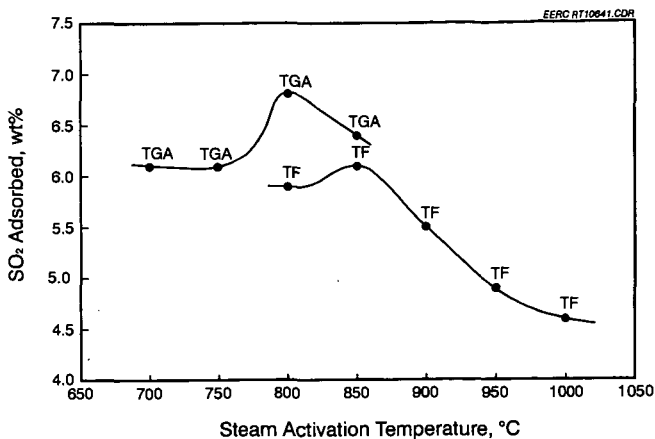


Figure 1. Dependence on activation temperature of SO_2 adsorption from flowing gas containing 5000 ppm SO_2 in argon at ambient temperature for Georesources leonardite (480 $^{\circ}\text{C}$) char.

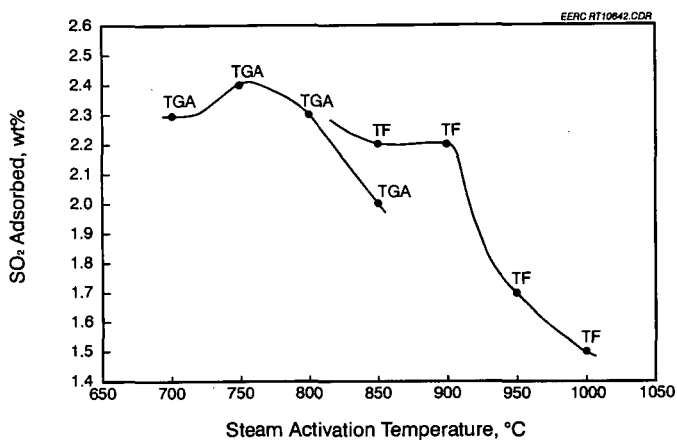


Figure 2. Dependence on activation temperature of leonardite SO_2 adsorption from 5000 ppm SO_2 in argon at 100 $^{\circ}\text{C}$ for leonardite (480 $^{\circ}\text{C}$) char.

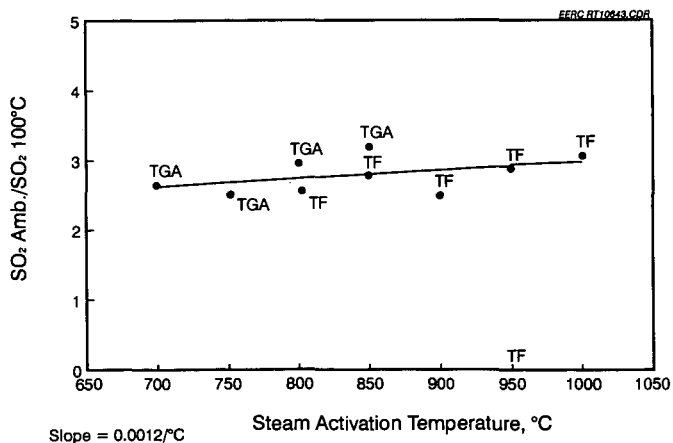


Figure 3. Ratio of SO_2 sorption capacity at ambient temperature to sorption capacity at 100 $^{\circ}\text{C}$ for leonardite (480 $^{\circ}\text{C}$) char versus steam activation temperature.

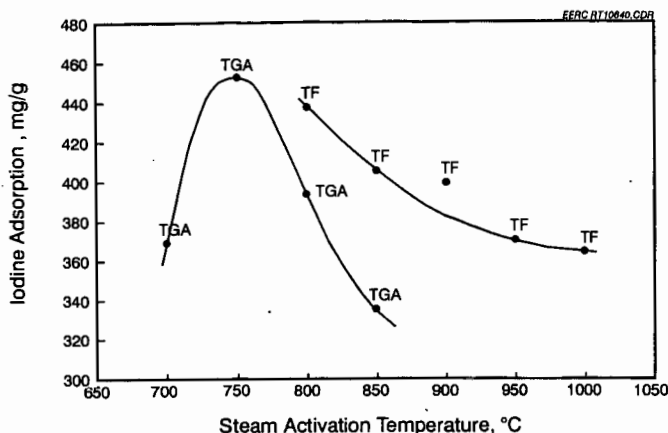


Figure 4. Sorptive capacity for I_2 of uncleaned leonardite (480°C) char steam activated at increasing temperatures.

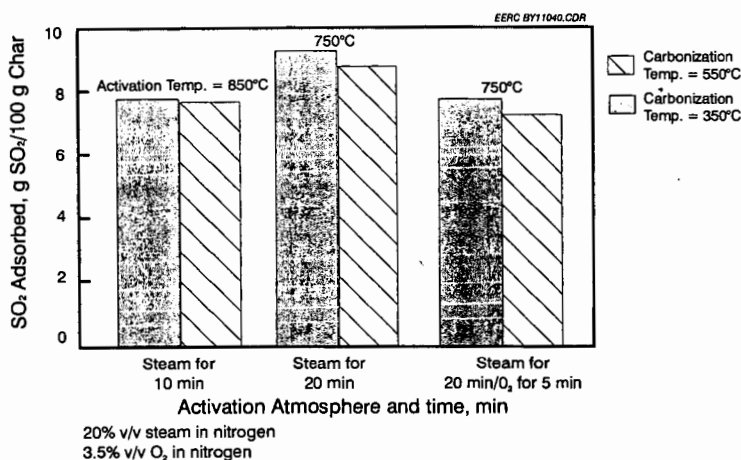


Figure 5. Effect of carbonization temperature and activation gas on SO_2 (10,000 ppm) adsorption at ambient temperature for leonardite chars.

REFERENCES

1. Wilson, J. *Fuel* **1981**, *60*, 823.
2. Samaras, P.; Diamadopoulos, E.; Sakellaropoulos, G.P. *Carbon* **1981**, *29*, 1181.
3. Bansal, R.C.; Donnet, J.-B.; Stoeckli, F. *Active Carbon*; Marcel Dekker: New York, 1988; p ix.
4. Samaras, P.; Diamadopoulos, E.; Sakellaropoulos, G.P. *Carbon* **1994**, *32*, 771.
5. Fernandez-Morales, I.; Lopez-Garzon, F.J.; Lopez-Peinado, A.; Moreno-Castilla, C.; Rivera-Utrilla, J. *Fuel* **1985**, *64*, 666.
6. Serio, M.A.; Solomon, P.R.; Basilakis, R. In *Proceedings of the International Conference on Coal Science*; Tokyo, Oct. 1989, pp 341-344.
7. King, A.J. *Chemical Society* **1937**, 1489.
8. Boehm, H.P.; Heck, W.; Sappok, R. *Angewandte Chemie* **1984**, *76*, 742.
9. Voll, M.; Boehm, H.P. *Carbon* **1971**, *9*, 481.
10. Davini, P. *Carbon* **1983**, *31*, 47.
11. Knudson, C.L. "Leonardite Char Adsorbents," U.S. Patent No. 5 254 521, Oct. 19, 1993.

ACKNOWLEDGMENTS

The authors express their thanks to Mark Musich and Ron Kulas, both at the EERC, for their assistance in preparing the coals and chars and testing the carbons and to Georesources Inc. for supplying the leonardite. The authors also wish to extend gratitude to the U.S. Department of Energy Morgantown Energy Technology Center (METC) for financial support for this project.

PRODUCTION OF CHARCOAL AND ACTIVATED CARBON AT ELEVATED PRESSURE

Xiangfeng Dai, Niclas Norberg and Michael J. Antal, Jr.,
Hawaii Natural Energy Institute and the Department of Mechanical Engineering,
University of Hawaii at Manoa, Honolulu, HI 96822

Keywords: Biomass, Charcoal, Activated carbon

INTRODUCTION

With its wide range of properties, charcoal finds many commercial applications for domestic cooking, refining of metals (steel, copper, bronze, nickel, aluminum and electro-manganese), production of chemicals (carbon disulfide, calcium carbide, silicon carbide, sodium cyanide, carbon black, fireworks, gaseous chemicals, absorbents, soil conditioners and pharmaceuticals), as well as production of activated carbon and synthesis gas. In 1991, the world production of charcoal was 22.8 million cubic meters (3.8 million metric tons) (FAO, 1992) as shown in Table 1. Brazil is the world's largest charcoal producer---5.9 million cubic meters or one million metric tons was produced in 1991, most of which is used in steel and iron industry (Calle et al, 1992). African countries produced 45% of the world total amount of charcoal, where 86% of the wood-based energy is for domestic use (Khristova et al., 1993), most of which is inefficiently used. Charcoal is produced commercially in kilns with a 25% to 30% yield by mass on a 7 to 12 day operating cycle. Until recently, the highest yield of good quality charcoal reported in the literature was 38%.

Activated carbon has a wide range of applications, mostly as a purifying agent to remove trace quantities of undesirable species from gas or liquid phase, also as an economical media to recover materials. Some of the common applications are listed as follows: food industry, pharmaceutical industry, water purification, gas or air treatment, chemicals, oil refinery processing. Special applications of activated carbon are found in agriculture, as catalyst and catalyst support in chemical industry, for precious metal recovery and making batteries and military clothing, and in nuclear power stations. The consumption of activated carbon in industrialized countries in 1988 was 300,000 tons (Roskill, 1990), which was the majority of the world total. The United States and Japan account for 60% of this consumption---130,000 tons for U.S. and 50,000 tons for Japan. The yield of activated carbon produced commercially is low (typically 10% to 12%) from raw material.

In this paper, an ASME code rated experimental system is presented for producing charcoal and activated carbon from biomass feedstock. Very high yield of high quality charcoal is obtained in short cooking time, while very low yield of tar is found in the process from this system.

EXPERIMENTAL

Six biomass species were employed in this work, namely, Eucalyptus, Kiawe, Leucaena, Coconut husk, Macadamia nut shells and Kukui nut shells. All these feedstocks were air dried, the moisture contents of which are listed in Table 2. Macadamia nut shells and Kukui nut shells retained their original sizes of about 25 mm in diameter in hemispheric shape when being fed into the reactor. The other feedstocks were cut into small pieces (about 60 mm X 25 mm X 25 mm) in order to fit the feeding port of the reactor.

The experimental apparatus is schematically shown in Fig. 1. The reactor is made of 168 mm diameter X 1200 mm long steel pipe welded with flanges on both ends. A 114 mm diameter stainless steel canister is used to load feedstocks and to unload the reaction products. The available volume of the canister is 7.5 liters (2 gallons). The internal heating source consists of two 4 kW electric heaters, which are mounted on the bottom flange of the reactor. The heaters are controlled by a temperature controller. The Watt-hour meter is used to measure the power consumption. A back pressure regulator controls the reactor pressure. Thermocouples are placed in the center line of the reactor for measuring the temperature profile of the biomass bed. The effluents are flared in an exhaust line. For production of activated carbon by a thermal activation process, a steam and air mixture is used. The steam generator is built to provide a maximum steam flow of 3 kg/hr at 5.4 MPa pressure. Air is provided by an air tank with flow rate of 4 kg/hr. The whole system is ASME code rated---a "State Special" unit, which is operated with permission of the Hawaii State Boiler Inspector.

Feedstock is manually fed into the reactor. The experiment terminates when temperature or pressure remains stable or after a second temperature rise is observed. The heating time is about 3 hours from cold start. A tar converter is placed at the exit port. Charcoal and feedstock are analyzed according to ASTM standards by Huffman Laboratory, INC. The heat contents of Kukui nut shells and Kiawe are assumed 22 MJ/kg, which are conservatively estimated according to data of Macadamia nut shells and of Redwood (heartwood), respectively. The heat content of Eucalyptus (Grandis) is obtained using the following equation (Graboski et al., 1981):

$$\text{HHV} = 2.3236[(141C + 615H - 10.2N + 39.95S) - (1-ASH)(17244H/C) + 149] \quad (\text{kJ/kg})$$

where HHV is the higher heating value on a dry basis, and C, H, N, S, ASH are the weight percent of carbon, hydrogen, nitrogen, sulfur and ash in the sample. Gas samples are analyzed using a gas chromatograph equipped with flame ionization and thermal conductivity detectors.

RESULTS AND DISCUSSIONS

The mass yield of charcoal is the ratio of dry charcoal to dry feedstock by mass. In Table 2 are shown the experimental results for mass yields of charcoal. All these species give very high mass yield—from 42% to 65%. The nut shells have higher mass yield than these wood species probably due to their higher fixed carbon content. For example, Macadamia nut shells has 23.7% fixed carbon content, while Eucalyptus (Grandis) 16.9% (Jenkins, 1989). Nevertheless, the mass yields of charcoal from these feedstocks are much higher than that produced from commercial kilns.

The energy yield, the ratio of heat content of dry charcoal to that of dry feed, is another indication of charcoal conversion. In Table 2 are also listed the energy yields of these charcoals. All of these give very high energy yield ranging from at least 64% to more than 88%.

The results of charcoal analysis are shown in Table 3. Samples for analysis are obtained from two extreme positions inside the reactor. Therefore, two sets of data are listed in the table. Generally speaking, charcoal closer to the heaters has higher fixed carbon (FC) content and higher heat content. Most of the charcoals have FC content and heating value lower than or close to British standard. However, after looking at the data from the previous work (Dai, 1993) which have higher FC content and heating value as well as very high mass yield, we conclude that the quality of these charcoals can be improved by a somewhat higher temperature cook. (This work is now in progress.) Moreover, Macadamia nut shell charcoal has FC content close to and heating value higher than British standard. Nevertheless, all these charcoals have higher FC content and higher heat content than commercial briquette charcoal, which implies that they are suitable for domestic cooking and their precursors are suitable raw materials for charcoal production.

Charcoal density is low due to its high porosity, which implies that charcoal is reactive and good for further pore development by activation process to make activated carbon. The bulk densities of charcoal are in the range of 45% to 65% of their raw materials. The bulk densities of Macadamia nut shells and Kukui nut shells are about 470 kg/m³ and 510 kg/m³, respectively. The shells sink in water.

From the temperature profiles in these experiments, it is found that under the reaction conditions, hemicellulose exothermicity occurs at about 275°C and cellulose exothermicity at about 350°C.

The result of gas analysis shows that the main gas species are H₂O, CO, CO₂, H₂ and CH₄. Other hydrocarbons are negligible. The typical molar ratio of CH₄, CO and CO₂ to H₂ is 1.7, 1.7 and 4.9.

Tar yield is very low, which reflects success of the reactor design and the tar converter. This also contributes to the high yield of charcoal.

Unfortunately, activated carbon production is now in process, and no information is available at this time.

CONCLUSION

Charcoal with very high yields of 42% to 65% has been produced from six biomass species in the newly built ASME code rated charcoal reactor. The nature of the feedstocks affect the yield and quality of charcoal significantly—the nut shells give higher yield and heat content of charcoal than wood species. Very low yield of tar is obtained in the process. Further work is now in progress to improve the uniformity of charcoal throughout the bed and to improve the quality of charcoal in terms of FC content and heating value while keeping mass yield still high.

REFERENCES

- Calle, F. R., Furtado, P., Hall, D. O. "Brazil charcoal: a case study for sustainable production and use". *Biomass Users Network*. July-Aug., 1992.
- Dai, X. "Charcoal production and gasification under pressure". MS thesis, May, 1993.
- Food and Agriculture Organization of the United Nation, *FAO Quarterly Bulletin of Statistics*, Vol. 5, No. 4 1992.
- Jenkins, B. M. "Physical properties of biomass". *Biomass handbook*. 1989.
- Khristova, P., Vergnet, L. "Evaluation of usher wood and karkadeh stem for charcoal in Sudan". *Biomass and Bioenergy*. Vol. 4, No. 6, 455-459, 1993.
- Paddon, A. "Review of the available data concerning the amount of charcoal and fuelwood in Sudan". Field Project Document No. 22. FAO, Khartoum, 1987.
- Graboski, M., Bain, R. "Properties of biomass relevant to gasification". *Biomass gasification principle and technology*. Ed.: Reed, T. B., 1981.
- Roskill Information Services, Ltd. "The economics of activated carbon 1900". *PTS Research Studies*. 1-180. Aug. 9, 1990.

Table 1: The world annual production of charcoal for 1980 and 1991 (1000 cubic meter)

region	1980	1991
world	17117	22784
Africa	6883	10453
N. & C. America	821	904
S. America	6170	7480
Brazil	4779	5924

Table 2. Charcoal yields

Species	Mass yield (%)	Energy yield (%)	Feed moisture content (%)
Eucalyptus	46	67	15.7
Kiawe	53	>64	10.0
Leucaena	42*	66*	1.5*
Macadamia nut shells	51; 42*	76; 65*	13.5; 7.20*
Kukui nut shells	65; 62*	>84; >88*	12.1; 12.5*
Coconut husk	50	66	88.1

*data from the previous work (Dai, 1993).

Table 3. Charcoal evaluation

Species	Fixed carbon (%)	Volatile matter (%)	Ash (%)	HHV (MJ/kg)
Eucalyptus	53.1; 67.5	42.2; 30.9	4.66; 1.59	22.60; 28.62
Kiawe	57.4; 60.1	41.6; 30.9	0.95; 0.94	27.11; 26.08
Leucaena	67.6*	30.0*	2.34*	28.51*
Macadamia nut shells	68.9; 72.0	30.4; 27.1	0.74; 0.87	31.11; 31.74
Kukui nut shells	89.4*	9.37*	1.22*	32.43*
Coconut husk	52.3; 67.3	44.1; 29.2	3.55; 3.42	26.88; 29.71
Commercial	78.8*	18.4*	2.26*	31.13*
Commercial briquette	56.7; 62.8	39.7; 26.7	3.63; 10.6	24.37; 26.18
Commercial Kiawe	46.5	36.4	17.2	22.8
Commercial Mesquite	69.8	28.3	1.96	29.7
Commercial	86.8	9.04	4.17	31.8
British Standard (Paddon, 1987)	>75	<20	<7.0	>30.0

a *data from the previous work (Dai, 1993);

b The two numbers indicate samples from top and bottom of the reactor, respectively.

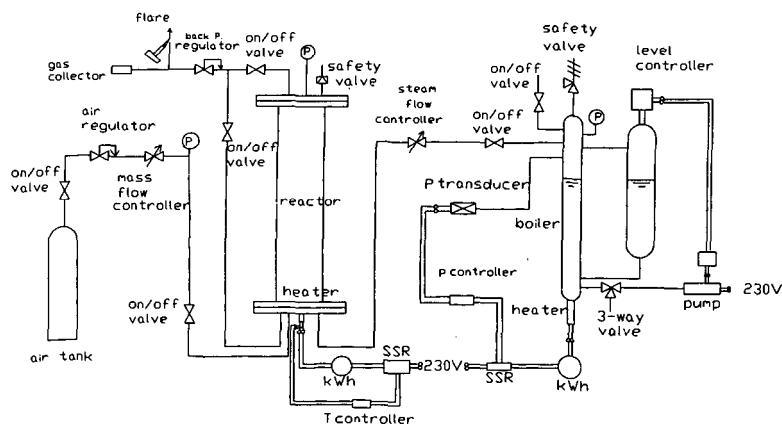


Fig. 1. Schematic diagram of the charcoal reactor

ACTIVATED CARBONS FROM STEAM EXPLODED WOOD.

Marit Jagtoyen, Frank Derbyshire, Robert S. Wright* and Wolfgang Glasser*
University of Kentucky, Center for Applied Energy Research,
Lexington, KY 40511-8433

*Biobased Materials Center, Virginia Polytechnical Institute,
Blacksburg, Virginia 24061-0323

Keywords: Activated carbon, Steam explosion, Porosity

INTRODUCTION

In a continuing experimental program, we are investigating the conversion of hardwoods, such as white oak (*Quercus alba*) to activated carbons by chemical activation with phosphoric acid¹⁻³. The aims of the research are to establish the relationships between chemical and morphological change and porosity development, with the long term goal of developing new adsorbents with controlled porosity and surface chemistry, through the selection of the precursor, reagent, and reaction parameters. The research is further directed to enhancing the use of wood materials, some of which are not appropriate feedstocks for conventional industrial applications, and to providing potential solutions to the problem of the economic utilization of wood wastes from primary and secondary wood industries.

Our previous work on phosphoric acid activation has demonstrated that there is a direct correspondence between porosity development and a dilation of the altered wood structure that takes place at heat treatment temperatures above about 200-250°C¹. While the mechanisms that lead to this structural expansion are unclear, it is clearly related to the effects of the reaction of phosphoric acid with the biopolymers in the wood, primarily lignin and cellulose. For example, compared to reaction in the absence of this reagent, phosphoric acid produces an increase in carbon yield that is attributed primarily to the retention of cellulose, albeit in altered form, through the promotion of crosslinking reactions. However, lignin and other biopolymers, also contribute to the pore structure. The most significant chemical changes seem to occur at low temperatures: ¹³C NMR spectra show that by 50°C there is a loss of carboxyl and methyl groups from the lignin structure, and the carbohydrate (cellulose and hemicellulose) signature disappears by 100°C⁴. These findings correspond with observations that lignin appears to undergo partial digestion or depolymerization at low temperatures¹. It has been reported in other work that wood transforms into a "plastic" state on heat treatment to low temperatures⁵.

For these reasons, current studies focus on elucidating the roles of wood biopolymers upon activation with H₃PO₄, and how they influence the porosity of the carbon product. In this context, wood and wood fractions have been produced by a technique known as steam explosion, that has been combined with extraction methods to provide materials with a range of different compositional characteristics for the synthesis of activated carbons. Steam explosion of lignocellulosic biomass from agricultural and forest resources is a technology that was developed for converting woody resources not qualified for the production of paper pulp into constitutive biopolymers⁶. The results presented here will consider how the pore size distribution of the activated carbons is influenced by the severity of the steam explosion treatment and fractionation protocol.

EXPERIMENTAL

Materials and Materials Preparation

Quantities of white oak were supplied in the form of wood chips (3 x 2 x 0.5 cm) by Westvaco Corporation. The chips were subjected to steam explosion treatment at four severity levels in a pilot scale unit at the Virginia Polytechnic Institute (VPI). Samples of the products were then subjected to solvent extraction to provide a total of 17 starting materials with different compositional characteristics: the parent wood; the complete steam exploded product at four severities, and extracted fractions from each of these - insoluble fractions from water and alkali extraction and recovered lignin from alkali extraction. A schematic of the steam explosion process and product separation scheme is shown in Figure 1.

The conditions used for steam explosion influence the chemical and molecular characteristics of the product and product fractions. A calculated severity parameter, log R₀, is used to denote the combined effects of time, temperature and steam pressure that are used in any particular treatment⁷. Differences in cell structure and in chemical structure are caused by varying the severity of steam explosion thus providing material of altered composition and microstructure.

Water extraction of the steam exploded wood fiber removes most of the hemicellulose. Alkali extraction creates a cellulose-rich fibrous fraction from which most of the lignin has been removed.

Extraction is accomplished using a liquor to wood ratio of 8:1, at a caustic charge of 15-20% of dry fiber, at 80 to 90°C for 30 minutes. Samples are then filtered, washed in a counter current mode and the solubles and insolubles are recovered. A lignin-rich fraction can be produced as a precipitate upon neutralization of the alkaline filtrate (approx. 90% lignin). By these procedures, the component biopolymers are isolated as xylose-rich water soluble solids; as cellulose-rich fiber solids; and as lignin-rich fraction by acid precipitation.

Chemical Activation

Activated carbons are synthesized by mixing an aqueous solution of phosphoric acid with the starting material, after first grinding the sample to produce a -100 mesh powder (to ensure good contact). The acid is added as an 85% solution in a volume such that the weight ratio of acid to as-received sample is 1.45 : 1.0. The mixture is then heat treated in two stages. First, low temperature heat treatment to 170°C for 30 min. under nitrogen flow to allow time for penetration of the reagent and to complete the initial reactions. This is followed by heating (again in flowing nitrogen) to a final temperature in the range 300-650°C, with a hold time of 1 hr. at maximum temperature. The product, after cooling, is then leached extensively with distilled water to pH 6-7 to recover the reagent, before drying and further characterization.

Characterization

Information on the carbon pore structure was derived from nitrogen adsorption isotherms obtained at 77K on a Coulter Omnisorb 100CX apparatus. Surface areas were determined by the BET method. Micropore volumes (pores less than 2 nm diameter), W_0 , were determined using the Dubinin-Raduskevich equation ⁸, and mesopore volumes (pores of diameter 2 to 50 nm diameter) were determined by the BJH method ⁹.

RESULTS AND DISCUSSION

One of the apparent effects of modifying the wood structure by steam explosion is that, compared to the parent wood, there is more visible evidence of reaction commencing at room temperature upon addition of the acid solution. This observation could be considered to be due to the opening of the wood structure by the steam explosion treatment, permitting increased access by the phosphoric acid. However, thermogravimetric analyses of samples of the parent wood and product from pretreatment at $\log R_0 = 4.0$ have failed so far to show any significant differences in behavior on H_3PO_4 activation.

The micropore and mesopore volumes of activated carbons produced from the parent wood and from samples subjected to steam explosion treatment at different severities (without subsequent fractionation) are shown in Figure 2, together with the totals of these volumes. It can be seen that, even at the lowest severity, steam explosion causes an appreciable increase in total pore volume (excluding macropores, defined as > 50 nm diameter). Compared to the parent wood, steam explosion at $\log R_0 = 4.0$ increases the total pore volume by about 30%. Most of this change is due to an increase in micropore volume, with an associated change in BET surface area from 1300 to 1950 $m^2 g^{-1}$, Figure 3. The result demonstrates that wood pretreatment by steam explosion can be very effective for producing structural changes that strongly influence the pore characteristics of the derived carbons.

As can be seen, with further increase in $\log R_0$ there is a progressive reduction in total pore volume, due to decreases in both micropore volume, as reflected by the changes in BET surface area shown in Figure 3, and in mesopore volume. The fact that the volumes in both pore ranges decrease together suggests that the effect of steam explosion severity on porosity is more complex than simply shifting the overall pore size distribution to larger or smaller pore sizes. It appears that, at high treatment severities, the wood structure is so extensively disrupted that the normal mechanisms by which phosphoric acid activation generates porosity begin to become appreciably impaired.

Further modifications to the steam exploded wood samples were effected by the solvent extraction scheme described earlier to produce: water-insoluble fractions; alkali-insoluble fractions; and lignin-rich fractions recovered from the alkali-solubles by precipitation. The pore structural parameters of activated carbons produced from these precursors, at the different levels of steam explosion severity, are summarized in Table 1: micropore volume, mesopore volume, and BET surface area - note that macroporosity is not included.

Although the reproducibility of these preliminary experiments has yet to be confirmed, certain trends can be tentatively identified. For the series of carbons produced from the water-insoluble fractions, the micropore volumes appear to be insensitive to $\log R_0$, over the range studied, while there is a reduction in mesopore volume with increasing severity. The alkali-insolubles produce carbons with lower microporosity, but here the mesopore volume increases with severity. The data indicate that mesoporosity passes through a maximum, but in any case very high mesopore

volumes have been measured at high severities. Carbons with these characteristics would be suitable for liquid phase applications, where wider pores are desirable from the standpoint of being able to accommodate large molecules, and to facilitate diffusion of the adsorbate through the liquid in the pores.

The lignin-rich fractions produced carbons with micropore volumes similar to those in the carbons from the alkali-insolubles, and again were unaffected by severity. However, the mesoporosity was reduced to low values at steam explosion severities greater than 4.0.

SYNOPSIS

The principal outcome of this research to date is that it has demonstrated that the techniques of steam explosion and solvent extraction allow the production of substantially different materials from a single wood type, and that these materials can function as precursors for the synthesis of powdered activated carbons possessing a range of pore structural characteristics. For example, low severity steam explosion can be used to increase the micropore volume and surface area and produce a carbon that would be more suitable for the adsorption of small molecules, typical requirements for gas phase adsorption. In contrast, high severity steam explosion followed by isolation of the alkali-insolubles can produce a carbon with high mesopore volume, suitable for liquid phase applications. The differences between these materials are clearly illustrated by the nitrogen adsorption isotherms in Figure 4: whereas adsorption on the predominantly microporous carbon approaches a plateau at a relative pressure above about 0.3, adsorption on the mesoporous carbon continues to rise due to the filling of wider pores.

In future work, further studies will be made to establish links between precursor composition and the properties of the powdered activated carbons, and investigations will be made of the feasibility of producing extruded activated carbons from these same precursors.

REFERENCES

1. M. Jagtoyen and F. Derbyshire, *Carbon*, **31** [7], 1993, 1185-1192.
2. M. Jagtoyen, F. Derbyshire, *Proceedings CARBON'94*, Granada, Spain, July 3-8, 1994, pp 232-233.
3. M. Jagtoyen, F. Derbyshire, W. Glasser, *Proceedings CARBON'94*, Granada, Spain, July 3-8, 1994, pp 228-229.
4. M. Solum, M. Jagtoyen, F. Derbyshire and R. Pugmire, accepted for publication, *Carbon*, 1995.
5. US Patent 5,238,470, 1993.
6. W. G. Glasser, B. K. Avellar, *Symposium on Lignocellulosic Reactions-II*, AIChE 1990 Spring National Meeting, March 11-12, Orlando, Florida, 1990.
7. R. P. Overend, E. Chornet, *Phil. Trans. R. Soc. Lond., A* **321**, 1987, 523-536.
8. Dubinin, M. M. Zaverina, E. D. and Raduskevich, L. V. *Zh. Fiz. Khimii*, 1351-1362, 1947.
9. E.P. Barrett, L. G. Joyner and P. H. Halenda, *J. Amer. Chem. Soc.*, **73**, 1951, 373.

ACKNOWLEDGEMENT

The authors would like to thank the US Department of Agriculture, Contract #93-02345, Program Director: Dr. Charles Cleland, and University of Kentucky, Center for Applied Energy Research for financial support.

Table 1: Micro- and mesopore volumes and BET surface areas of activated carbons from fractions of steam exploded wood.

Severity	Steam Exploded	Water Extracted	Alkali Extracted	Lignin
Micropore volume(cc/g) [*Parent wood 0.51 cc/g]				
4.01	0.77	0.76	0.60	0.56
4.26	0.67	0.73	0.42	0.58
4.35	0.7	0.75	0.44	0.59
4.43	0.59	0.77	0.60	0.57
Mesopore volume(cc/g) [*Parent wood 0.34 cc/g]				
4.01	0.36	0.41	0.21	0.56
4.26	0.44	0.26	0.45	0.13
4.35	0.26	0.22	1.07	0.14
4.43	0.25	0.18	0.69	0.17
BET surface area(m²/g) [*Parent wood 1300 m²/g]				
4.01	1945	1920	1408	1697
4.26	1589	1746	1166	1327
4.35	1691	1789	1314	1369
4.43	1413	1792	1734	1328

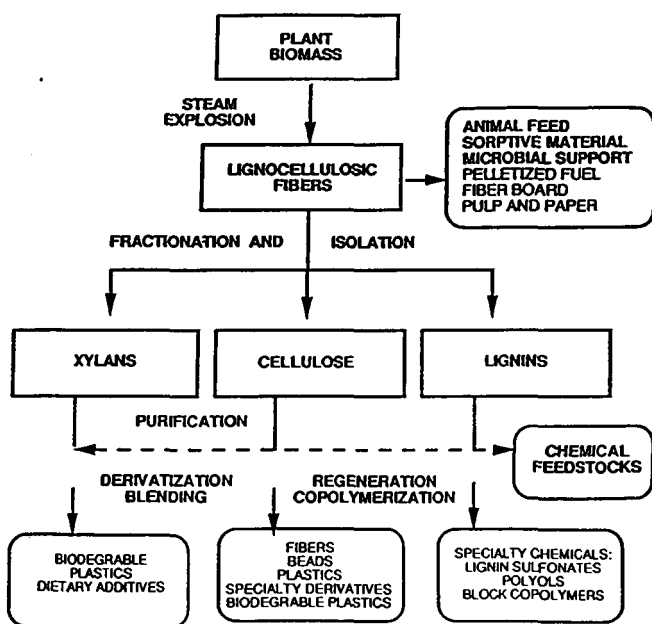


Figure 1: Schematic for separation of biomass into constituent polymers (Biobased Materials Center, Virginia Polytechnic Institute)

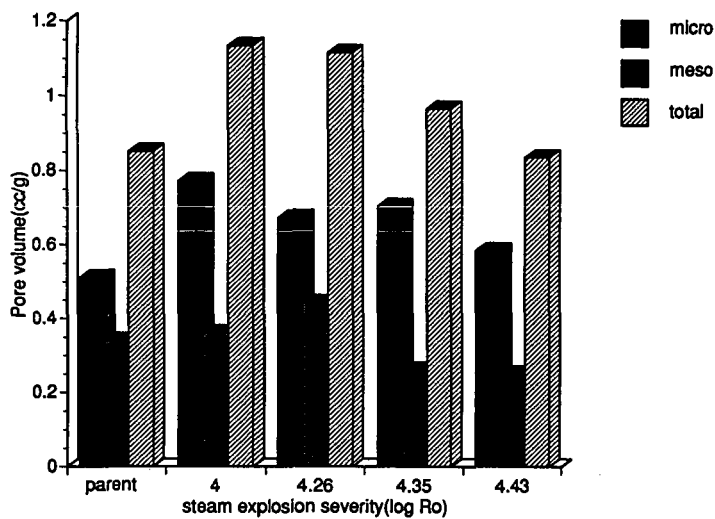


Figure 2: Influence of steam explosion severity on porosity of activated carbons (H_3PO_4 activation).

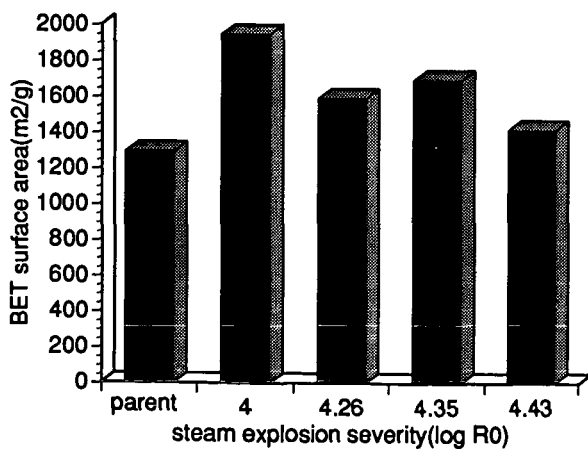


Figure 3: Influence of steam explosion severity on BET surface area of activated carbon (H_3PO_4 activation).

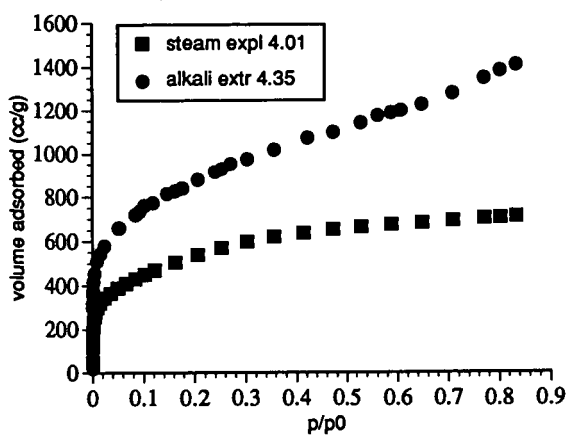


Figure 4. Nitrogen adsorption isotherms (77K) of activated carbons. (precursor materials derived from white oak)

X-RAY CHARACTERIZATION OF SOME ACTIVATED CARBON PREPARED FROM ILLINOIS BITUMINOUS COAL 106 AT THE CAER

David L. Wertz, Shuhua Jin, and Charles B. Smithhart*

Department of Chemistry & Biochemistry
and

Center for Coal Product Research
University of Southern Mississippi
Hattiesburg, MS 39406-5043 USA

Key Phrases: Activated carbon, x-ray spectroscopy, x-ray diffraction, phosphorus retention.

INTRODUCTION

X-ray fluorescence spectroscopy (XRS) has been an established research tool for at least seventy-five years for the elemental analysis of condensed phases. Because of recent advances in materials development for the transmission and collection of soft x-rays ($\lambda > 10 \text{ \AA}$), XRS offers new advantages in the study of fossil fuels and their processed products. Wavelength dispersive x-ray fluorescence spectroscopy offers the added advantages of a very low background and excellent peak length/width ratio. Taken together, these features allow WDXRS to be used for the detection of elements in condensed phases at the parts per million abundance level, and in some cases significantly lower.¹

With WDXRS, as well as many other types of radiation experiments, attenuation of the incident and secondary radiation beams by the sample occurs. The result is that the measured intensity I_{meas} cannot be related to sample abundance.²

The absorption-corrected intensity of a WDXRS peak, $I^0(\lambda_Q)$, is directly proportional to the abundance of analyte Q at λ_Q . $I^0(\lambda_Q)$ is related to the intensity measured at λ_Q by:

$$I^0(\lambda_Q) = [\alpha \cdot \sum w_A \cdot \mu_A(\lambda_p) + \delta \cdot \sum w_A \cdot \mu_A(\lambda_Q)] \cdot I_{\text{meas}}(\lambda_Q) \cdot [1 - \exp\{-\{\alpha \cdot \sum w_A \cdot \mu_A(\lambda_p) + \delta \cdot \sum w_A \cdot \mu_A(\lambda_Q)\}\}]. \quad (1)$$

In eq. 1, w_A represents the abundance of element A in the condensed phase sample, $I_{\text{meas}}(\lambda_Q)$ is the intensity measured at wavelength λ_Q due to the presence of analyte Q in the sample. The mass absorption coefficients, $\mu_A(\lambda_p)$ and $\mu_A(\lambda_Q)$, are for the attenuation (absorption) of the primary radiation (chromium in these experiments) and for the secondary radiation emitted by the analyte Q, respectively. Constants related to the mass of the sample are represented by α and δ . The terms containing the absorption coefficients are designated the "matrix absorption" due to the sample and have a pronounced effect on the relationship between the measured intensity and the absorption-corrected intensity for analyte Q.

The condition of "infinite thinness" may be achieved when the matrix absorption effect $\rightarrow 0$ and is relatively constant. When this condition is satisfied, $w_Q = I_{\text{meas}}(\lambda_Q)/K'$; and the intensity of the peak at λ_Q provides a useful measure of the abundance of analyte Q. The condition of "infinite thinness" is achieved in cleaned coal and biomass samples, where the presence of metal atoms is quite small and the structural units are predominantly either hydrocarbons and/or carbohydrates.

EXPERIMENTAL

Samples were obtained from Jagtoyen as fine powders and were examined as received using conventional x-ray diffraction and x-ray spectral methods.

RESULTS AND DISCUSSION

As seen in Figure 1, the FeS_2 , Fe_2O_3 , SiO_2 and/or CaCO_3 (which are strong absorbers of Cu K_α X rays) had been successfully removed from the IBC 106 prior to its use.

Jagtoyen and Derbyshire have discussed the processes by which bituminous coals and hardwood have been treated by their high temperature (HTT) phosphoric acid process.^{3,4}

Shown in Figure 2 are the WDXRS spectra obtained from several samples of demineralized IBC 106 coal treated by the CAER hot phosphoric acid process used over the temperature range from ambient temperature (labeled DM coal) to 650°C. At ambient temperature a

large sulfur peak ($\lambda = 5.372 \text{ \AA}$) is noted, corresponding to an organo-sulfur abundance of ca. 2.1% in the cleaned coal. Comparison of the sulfur peak intensities indicates that as the process temperature is increased, the percentage of sulfur retained in the carbon fibers reduced. When processed at 650°C , the fibers retain ca. 0.4%. Accompanying the increase in process temperature is a retention of phosphorus ($\lambda = 6.155 \text{ \AA}$).

A similar increase in phosphorus retention is found in the white oak samples treated by Jagtoyen.^{3,4}

WDXRS cannot be extended to provide detailed information about the structural role(s) of the phosphoric acid species involved in the CAER process because the technique only provides elemental (and not molecular) information.

We have previously shown⁵ that the full-width at half maximum (FWHM) for the graphene stacking peak, found at $3.5\text{--}4.0 \text{ \AA}$ in bituminous coals, measures the regularity of the stacking of the graphene layers in coals. Shown in Figure 4 are the x-ray diffractograms (XRD's) obtained from the unprocessed IBM 106 coal and the coal processed at the several temperatures noted above. Comparison of the XRD's indicates that the FWHM of the graphene stacking are affected significantly by the process temperature, with the higher process temperatures causing improved regularity of the graphene peaks.

Shown in Figure 5 is evidence that the reduction in FWHM is not due to thermal effects.

Jagtoyen⁶ has measured the BET surface area of the activated carbon produced from the IBC 106 as a function of process temperature. In addition, the CAER team reports a significant reduction in the hydrogen component of the activated carbon produced by their HTT process.³ The increase in surface area and the reduction in hydrogen content parallel, at least crudely, with phosphorus uptake (measured by WDXRS) and the re-alignment of the graphene layers in the activated carbon (measured by XRD).

CONCLUSIONS

The two x-ray characterization methods, wavelength dispersive x-ray spectroscopy and x-ray diffraction, each provide limited information about carbon fibers prepared by Jagtoyen and Derbyshire. Unfortunately, neither method provides definitive information about the structural and/or bonding roles of the phosphorus moieties in the activated carbon.

REFERENCES

* Support via a DOE-EPSCoR Graduate Fellowship is gratefully acknowledged.

1. Jenkins, R., "X-Ray Spectrometry", John Wiley & Sons, NY, 1988.
2. Klug, H. and Alexander, L. E., "X-Ray Diffraction Procedures", Wiley-Interscience, NY, p. 360.
3. Toles, C., Rimmer, S. M., Derbyshire, F., and Jagtoyen, M., *Am. Chem. Soc., Div. Fuel Chem.*, 1994 (39) 596.
4. Jagtoyen, M. and Derbyshire, F. J., *Carbon*, 1993 (31) 1185.
5. Wertz, D. L. and Bissell, M., *Energy & Fuel*, 1994 (8) 613.
6. Jagtoyen, M., private correspondence.

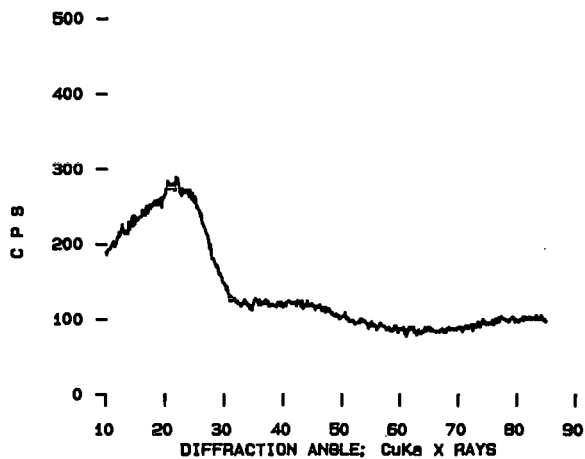


FIGURE 1. XRD OF THE CLEANED IBC 106.

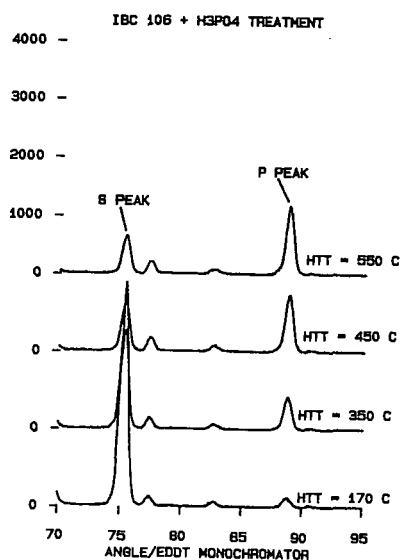


FIGURE 2. WAVELENGTH DISPERSIVE X-RAY SPECTRA OF THE IBC SAMPLES TREATED WITH THE KCAER HTT TREATMENT OVER THE RANGE FROM AMBIENT TO 550°C. SULFUR AND PHOSPHORUS PEAKS ARE LABELED.

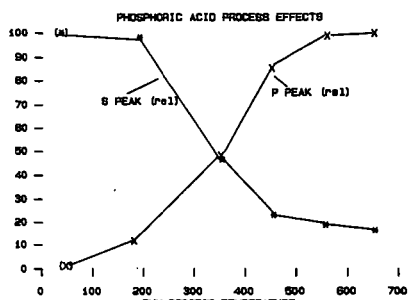


FIGURE 3. HTT EFFECTS ON ORGANO-SULFUR AND PHOSPHORUS UPTAKE.

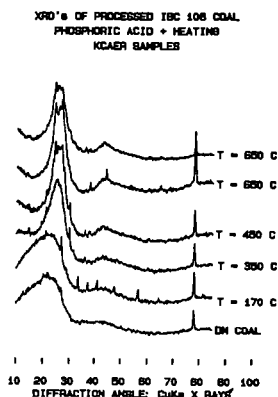


FIGURE 4. HTT EFFECTS ON THE XRD's OF THE ACTIVATED CARBONS.

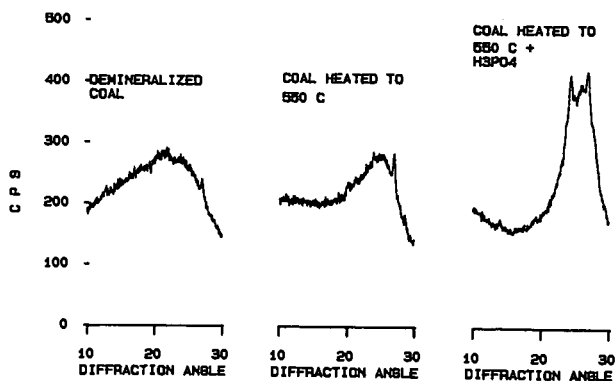


FIGURE 5. CORRELATION OF PHOSPHORUS RETENTION WITH BET SURFACE AREA⁶ MEASURED FOR THE ACTIVATED CARBONS.

PYROLYSIS AND HYDROLYSIS OF BIOMASS AND LIGNINS - ACTIVITIES AT THE INSTITUTE OF WOOD CHEMISTRY IN HAMBURG, GERMANY

Dietrich Meier, Jochem Berns and Oskar Faix
Federal Research Centre for Forestry and Forest Products
Institute of Wood Chemistry and Chemical Technology of Wood
21027 Hamburg, Germany

Keywords: biomass, lignin, hydrocracking, pyrolysis, liquefaction

INTRODUCTION

After the first oil price crisis in 1973 research activities were initiated throughout the world to produce oil from renewable feedstocks like lignocellulosic biomass. Countries with huge biomass resources and strong dependence on imported petroleum such as Canada and the United States of America were leading in research at that time. At the Pittsburgh Energy Research Center (PERC) high pressure liquefaction of cellulosic wastes was studied using carbon monoxide and sodium carbonate as a catalyst (1), and a pilot plant in Albany, Oregon was constructed. At the same time, another high pressure conversion process for woody biomass was investigated at the Lawrence Berkeley Laboratories (2). The scaled-up version of this process was also tested in Albany. After several years of operation, the pilot plant was shut down due to economical and technical reasons. It was felt that high pressure technology is too sophisticated for the thermal conversion of biomass into liquid fuels and that simpler technologies should be developed. Therefore, in 1980 the Solar Energy Research Institute (today NREL) in Golden, Colorado, organized a specialists' workshop on fast pyrolysis of biomass. This process promised to give high yields of liquid products. During the workshop, researchers working on coal and biomass presented papers on both fundamental aspects - such as heat transfer mechanisms - and practical work regarding process parameters such as feedstock, particle size, heating rate, residence time, pressure etc. Since the early eighties a lot of progress has been made in the development of conversion technologies for biomass. The most important processes with their characteristics are compiled in Table 1.

In 1982 the German government also recognized the need for using renewable feedstocks and funded a research project dealing with the direct conversion of wood into a liquid fuel and/or chemical feedstocks. Based on the large tradition and experiences in coal conversion by the high pressure Bergius-Pier process in Germany (14 plants produced all transportation fuels during World War II) the Institute of Wood Chemistry (IWC) adopted the process principles to woody feedstocks. During several years of experimental work at IWC, various process alternatives were studied covering

- slurry phase hydrocracking in batch and semi-continuous reactors
- hydrolysis in batch and semi-continuous reactors
- flash pyrolysis in a bench-scale fluidized bed reactor.

In the present paper the research activities and main results on thermochemical conversion of biomass and lignins are summarized.

HIGH PRESSURE EXPERIMENTS

Initial hydrocracking experiments were conducted in 25 ml autoclaves to compare conversion rates of different lignocellulosic feedstocks and to develop methods for separation and chemical characterization of the liquids (3, 4). Palladium on active charcoal (Pd/C) was initially used as a catalyst. Temperature was 475°C and initial hydrogen pressure 6 Mpa. Surprisingly, very small amounts of solid residue ranging from 0.5 to 6.8 % were observed for all kinds of biomass such as softwood, hardwood, straw, sugar cane bagasse, lignins and cellulose. The oil

yields of the lignocelluloses were in the range of 41 %. Cellulose and hemicelluloses gave rise to around 30 % and lignins to ca. 62 % of an oil. The average molecular weight of the oil was around 500 Dalton indicating severe depolymerization of the feedstocks during hydrocracking. The mass balance of these studies demonstrated that lignin is a more suitable feedstock with respect to oil yields than cellulose and hemicelluloses which have a tendency to give more char, water and gas.

After these orienting studies with the micro-autoclaves, experimental work was continued including a 1-L autoclave system (see Figure 1).

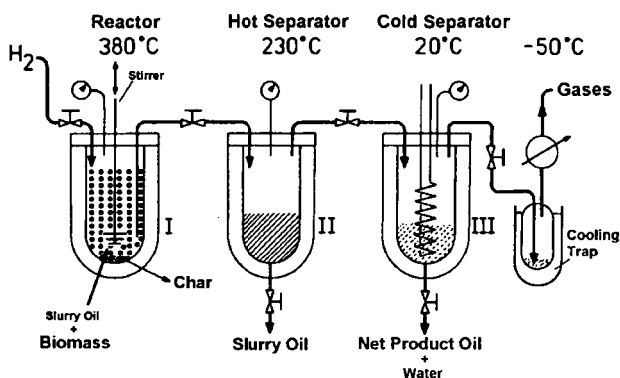


Fig. 1-L autoclave system for hydrocracking of biomass

It consists of a high pressure stirred reactor, a high pressure hot separator and a high pressure cold separator (5). A slurry phase catalytic hydrocracking process was developed with Pd/C as catalyst. In general, spruce wood particles were mixed with the high boiling recycle oil fraction which was condensed in the hot separator at 230 °C. The light and middle distillate fraction was collected in the cold separator and yielded around 37 % of a net product oil (NPO). Several consecutive runs were made in which always the hot separator fraction of the previous run was used as a slurry oil. In this way, the stability of the recycled oil was proved and the conditions of a continuous process could be simulated. The experiments revealed that the NPO yields and the amount of recovered recycle oil were almost constant in all runs. Therefore, a mass balance was established which reflects the overall yields of each product fraction from hydrocracking of biomass (Figure 2).

Beside palladium, other catalysts were included in the hydrocracking experiments such as Co, Mo, Cr, Ni, Fe, and red mud. However, none of these catalysts reached the NPO yields of palladium. The slurry oil could be completely recycled only in the presence of the iron catalyst and a NPO yield of 28 % was found. In general, the NPO's had a heating value of around 37 MJ/kg. An energy balance for the hydrocracking conversion process is presented in Figure 3, taking into account a hydrogen consumption of 4 % and the individual proportions and heating values of the biomass constituents. The balance demonstrates that 59 % of the input energy can be recovered and concentrated in the NPO. Its light fraction amounted to 50 % having a boiling point range < 220°C. The rest could be completely distilled between 220-360°C. In

comparison to oils obtained in the Albany plant, the NPO had a very low viscosity of 3.88 cSt at 20°C, a low pour point of -24°C, and a low density of 0.92 g/l (6).

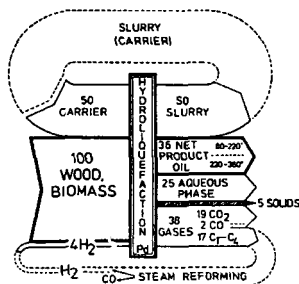


Figure 2 Mass balance for hydrocracking of biomass

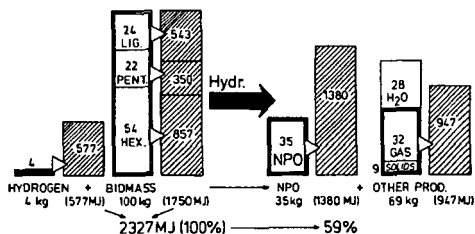


Figure 3 Energy Balance for hydrocracking of biomass

The variation of process parameters was also studied and is documented in various publications (7-9). There is a positive correlation between the pressure and the yield of liquids and a negative correlation between the pressure and the amount of char. At 3 MP initial hydrogen pressure the char yield is as high as 40 % but between 10 and 13 MPa, char formation is very low and amounts to ca. 5 % (8) (see Figure 4). The chemical characterization of the NPO's was mainly done by capillary gas chromatography and mass spectrometry with special emphasis on the qualitative and quantitative determination of phenolics which industry is mostly interested in. However, the unambiguous assignments of reaction products was difficult for the slurry oil phase reactions because the recycling oil was also degraded to a certain extent.

Therefore, we carried out hydropyrolysis experiments without a co-solvent using the same conditions as before in the hydrocracking experiments. Beside spruce wood and china grass, we also included technical lignins from various pulping processes as feedstocks in our experimental designs. Conversion of the feedstocks was excellent (10-12). In some cases, at suitable conditions, no char was formed. In general, lignins gave very high liquid yields of up to 80 %. VEBA OEL, the largest German refinery company, showed interest in lignin

hydrocracking for phenol production as methyl-aryl-ethers can be used as octane enhancers in gasoline. For this reason, we concentrated our work on lignin. A lot of experiments were performed at IWC including the application of slurry oils derived from petroleum and lignin. Despite of the high conversion rates, the amount of mono-phenols did not come up to our expectations. In the best case the yield of monomeric phenols was around 13 wt% (13,14).

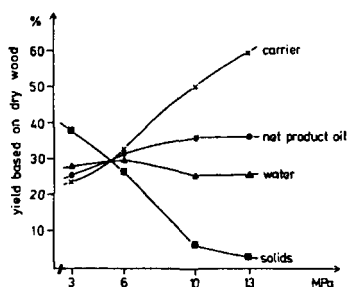


Figure 4 Yield of hydrocracking products at different initial hydrogen pressures

FLASH PYROLYSIS OF BIOMASS IN A FLUIDIZED-BED REACTOR

Since the aforementioned workshop on flash pyrolysis, several technologies have been developed mainly in Canada and the United States. At the moment, the most advanced flash pyrolysis technologies available are from ENSYSN, Gloucester, Ontario, Canada, (circulating fluidized bed), the University of Waterloo, Waterloo, Canada, (stationary fluidized bed) and NREL, Golden, Colorado, USA (vortex reactor). The Canadian know-how is now being exported to Europe. Especially the Waterloo Fast Pyrolysis Process (WFPP) is applied in research laboratories in Spain, Great Britain, Finland, and Germany. The first pilot plant of the WFPP process, with a capacity of 200 kg/h, was installed in Spain funded by the EU and UNION FENOSA, a Spanish energy producer. Another pilot plant from ENSYN, Canada, will be erected in Italy in 1995. A typical mass balance of the flash pyrolysis process is shown in Figure 5. The elemental composition of the liquids is very similar to wood. Their quality is quite different from high pressure oils. They contain water (10 to 35 %) and are rich in oxygenated compounds. Pyrolysis liquids are corrosive due to their low pH-value and thermally unstable because they tend to condensate at elevated temperatures. Therefore, the direct use is difficult and upgrading is necessary depending on the application.

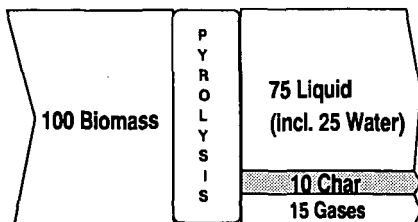


Figure 5 Mass balance of flash pyrolysis

Recently, the investigations on thermochemical conversion at IWC were also extended to flash pyrolysis using a continuously operating bench scale fluidized-bed reactor from the University

of Waterloo with a capacity of 100 g/h. A reactor description is given elsewhere (15). There are several reasons why fast pyrolysis is now so attractive:

1. There is an increased interest in the EU to produce biofuels by flash pyrolysis for the production of power, transportation fuels, and chemicals.
2. ICW is involved in a EU research project on "Integrated Chemicals and Fuels Recovery from Pyrolysis Liquids Generated by Ablative Pyrolysis". Within this project we can use our expertise in analysis, fractionation, and upgrading of bio-oils.
3. IWC got funds from the German Foundation for Environment to investigate the possibilities of using the flash pyrolysis technology for the disposal of contaminated wood waste.

For this purpose a 1 kg/h pilot plant with a fluidized bed reactor and gas recycling will be erected at IWC in 1995. Flash pyrolysis in fluidized beds has some advantages over conventional incineration of waste wood which actually in Germany is very limited due to legislative restrictions. (1) the gas volume in the process is drastically reduced. Thus, gas cleaning is more easier, (2) the formation of dioxins is unlikely to occur due to the absence of oxygen, (3) the plant capacity can be very small.

REFERENCES

1. Appell, H.R., Y.C. Fu, E. G. Illig, F.W. Steffgen and R.D. Miller (1975) Bureau of Mines, Report of Investigation 8013, Pittsburg.
2. Elliott, D.C., Biotech.&Bioeng. Symp. No. 11 (1981), 187-198.
3. Meier, D., D.R. Larimer and O. Faix (1986) Fuel, 65, 910-915.
4. Meier, D., D.R. Larimer and O. Faix (1986) Fuel, 65, 916-921.
5. Meier, D. K. Fuch and O. Faix (1987) "Energy Biomass & Wastes X", 785-800.
6. Meier, D. and O. Faix (1988) "Research in Thermochemical Biomass Conversion" (eds.: Bridgwater, A.V, J.L.Kuester) Elsevier, 804-815.
7. Meier, D., L. Jakobi and O. Faix (1988) J. Wood Chem. Techn., 8, 523-542.
8. Meier, D. and O. Faix (1989) "Energy from Biomass 4" (eds.: G. Grassi, D. Pirwitz, H. Zibetta) Elsevier, 584-592.
9. Meier, D. and M. Rupp (1991) "Biomass Pyrolysis Liquids Upgrading and Utilization" (eds.: A.V. Bridgwater, G. Grassi) Elsevier, 93-102.
10. Meier, D. and O. Faix (1990) "Biomass for Energy and Industry 5", Vol. 2, (eds.: G. Grassi, G. Gosse, G. dos Santos) Elsevier, 2646-2650.
11. Meier, D. R. Ante and O. Faix (1992) Bioresource Technol., 40, 171-177.
12. Oasmaa, A. R. Alén and D. Meier (1993) Bioresource Technol., 45, 189-194.
13. Meier, D. J. Berns and O. Faix (1994) "Advances in Thermochemical Biomass Conversion (ed.: A.V. Bridgwater) Blackie, Vol.2, 1016-1031.
14. D. Meier, J. Berns, O. Faix, U. Balfanz and W. Baldauf (1994) Biomass & Bioenergy (in press)
15. Scott, D.S. and J. Piskorz (1984) Can. J. Chem. Eng., 62, 404-412.

Table 1 Main processes and characteristics for the thermal conversion of biomass

Technology	Main characteristic	Catalyst	Temperature (°C)	Pressure (bar)	Residence time	Main primary products, application, comments
Combustion	O ₂ /air in access	N	ca. 1000	N	short	heat
Gasification	O ₂ /air limited (also with steam)	Y/N	1000-1500	Y/N	short	synthesis gas, fuel gas, ethene, ethin, ... "1 C chemistry" ... "indirect liquefaction"
Pyrolysis	inert gas atmosph.	N	> 450	Y/N	very long (hrs, days)	charcoal (carbonisation)
Pyrolysis	inert gas	N	>450	N	short (> min)	fuel gas, liquid tar (low yield), solid char
Pyrolysis	inert gas	N	>450	N	very short (< sec)	(flash pyrolysis) aqueous, acidic liquid tar for fuel (high O content) and chemicals
Pyrolysis	inert gas	Y	various	reaction conditions		catalytic pyrolysis under development
Liquefaction	CO (H ₂) in H ₂ O/alkali	Y	350-400	300	>15min	sometimes in combination with pretreatments, O content of liquids is still high
Hydro-pyrolysis	H ₂ atmosph. (gas/solid phase)	Y	350-600	50-200	>15 min	low viscous oil in high yield, low O content
Hydro-cracking	H ₂ atmosph. (gas/liquid phase)	Y	350-450	50-200	>15 min	low viscous oil in high yield, low O content
Hydro-treating	H ₂ atmosph. (gas phase)	Y	various	reaction conditions		used for upgrading of pyrolysis oils, O content below 1 %

CATALYTIC GASIFICATION OF WET BIOMASS IN SUPERCRITICAL WATER

Michael J. Antal, Jr., Yukihiko Matsumura, Xiaodong Xu, Jonny Stenberg, and Peter Lipnik
Hawaii Natural Energy Institute and the Department of Mechanical Engineering,
University of Hawaii at Manoa, Honolulu, HI 96822

Keywords: Wet biomass, Catalytic gasification, Supercritical water

INTRODUCTION

Wet biomass (water hyacinth, banana trees, cattails, green algae, kelp, etc.) grows rapidly and abundantly around the world. As a biomass crop, aquatic species are particularly attractive because their cultivation does not compete with land-based agricultural activities designed to produce food for consumption or export. However, wet biomass is not regarded as a promising feed for conventional thermochemical conversion processes because the cost associated with drying it is too high. This research seeks to address this problem by employing water as the gasification medium. Prior work has shown that low concentrations of glucose (a model compound for whole biomass) can be completely gasified in supercritical water at 600°C and 34.5 MPa after a 30 s reaction time (Dehui et al., 1993). Higher concentrations of glucose (up to 22% by weight in water) resulted in incomplete conversion under these conditions. The gas contained hydrogen, carbon dioxide, carbon monoxide, methane, ethane, propane, and traces of other hydrocarbons. The carbon monoxide and hydrocarbons are easily converted to hydrogen by commercial technology available in most refineries. This prior work utilized capillary tube reactors with no catalyst. A larger reactor system was fabricated and the heterogeneous catalytic gasification of glucose and wet biomass slurry of higher concentration was studied to attain higher conversions.

EXPERIMENTAL

A schematic drawing of the reactor system is presented in Figure 1. The reactor was constructed of Inconel 625 tubing with a 0.375" OD and 0.187" ID. The temperature of the reactant flow was abruptly raised to a desired value using an entry heater/cooling water jacket combination. The reactor was maintained at isothermal conditions using a furnace and downstream heater/cooling water jacket combination. To improve the heat transfer from the heaters to the fluids inside the reactor, the heaters were coiled on stainless steel rods in direct contact with the Inconel reactor. Different amounts of solid catalyst could be packed inside the reactor, giving the desired weight hourly space velocity (WHSV), which is defined as the ratio of the mass flow rate of the reactant to the mass of a proprietary "catalyst X" used in the heated zone. The axial temperature profile along the reactor's functional length of approximately 0.48 m was measured with 15 fixed, type K thermocouples. Pressure in the reactor system was measured using a pressure transducer. A back pressure regulator reduced the working pressure from 34.5 MPa to atmospheric pressure. After passing through the back pressure regulator, the reactor effluent then passed through an in-house fabricated glass gas-liquid separator. The gas flow rate was measured using a wet test meter.

The aqueous solution of glucose was fed into the reactor by an HPLC pump. A balloon feeding system was employed to feed the wet biomass slurry. Wet biomass was first ground with a blender and then with a homogenizer. The heterogeneous biomass slurry filled the 500 ml high pressure/temperature vessel, which was equipped with a magnetic drive. A meteorological balloon was placed in the vessel together with the biomass slurry. Water was pumped into the balloon, and as the balloon expanded the biomass slurry was forced into the reactor.

The analysis of the gaseous products was accomplished on a gas chromatograph equipped with flame ionization and thermal conductivity detectors. A 800/100 mesh carboxosphere molecular sieve packed column was used, operating at 35°C for 4.2 min, followed by a 15°C/min ramp to 227°C, a 70°C/min ramp to 350°C, and a 5.3 min hold at 350°C. The following gases were detected as the products of glucose gasification: H₂, CO, CO₂, CH₄, C₂H₄, C₂H₆, C₃H₆, and C₃H₈. Gas yields were calculated as the ratio of mole of detected gas to the mole of reactant. Carbon gasification efficiency was calculated as the ratio of carbon converted into gas.

Ten cubic centimeters of the liquid effluent from the experiments were dried in small beakers in an oven and the weight gain measured. A dark tar deposit remained on the bottom of the beaker after the drying for lower temperature or higher concentration. Tar yield was calculated as the ratio of the weight of tar to the weight of the reactant.

RESULTS AND DISCUSSIONS

1. Temperature effect

The effect of temperature on the gasification of glucose in the presence of catalyst X is shown in Table 1. Complete carbon conversion was observed at 600°C; however, as temperature dropped, carbon gasification efficiency decreased drastically. When the reaction temperature was

below 580°C, resulting in incomplete gasification conversion, the liquid effluent became yellowish and there was a thin layer of a dark brown, oil-like tar. Figure 2 illustrates the amount of tar present in the liquid sample as a function of reaction temperature. It is obvious that the tar yield in the liquid sample increases as temperature decreases. The tar yield at 600°C is significantly small.

2. Reactant concentration effect

When 0.2 M glucose was gasified without the solid catalyst X at about 30 s residence time in supercritical water at 600°C, 34.5 MPa, complete carbon conversion was observed. The liquid sample was clear. As the reactant glucose concentration increased, the carbon conversion decreased. With 0.8 M glucose reactant, the conversion dropped to 88%, and a dark brownish oil layer was present in the liquid sample.

The presence of solid catalyst X resulted in complete conversion of glucose feed with concentration as high as 1.2 M at a WHSV of 22.2 (g/h)/g (see Table 2). The liquid effluent was clear. Gas yields of H₂, CO, CH₄, and CO₂ increased significantly with the addition of catalyst X.

3. Pressure effect

When the pressure increased from 25.6 MPa to 34.5 MPa, the overall carbon gasification efficiency remained almost the same. However, as pressure increased, the yield of methane increased. This finding confirms the results of Elliott et al. (Elliott et al., 1993a, 1993b; Baker et al., 1989; Sealock et al., 1993).

4. Deactivation of catalyst

Deactivation of catalyst was observed in an 8-hour experiment using 1.2 M glucose as a reactant. As shown in Table 3, the carbon gasification efficiency decreased, while the solid residual and carbon content in the liquid sample increased with time.

The liquid samples were collected for total organic carbon (TOC) analysis. TOC yield was calculated as the weight ratio of carbon in the liquid effluent to that in the reactant. Because of the lower carbon gasification efficiency, more carbon remained in the liquid effluent at the later stage of the experiment, as indicated in Table 3. Notice that the tar yield (which is a measurement of the non-volatile residual in the liquid effluent) also increased with time.

5. Whole biomass gasification

Various whole biomass feeds, including water hyacinth, depithed bagasse liquid extract, sewage sludge, and paper sludge, were studied in the packed bed reactor. The gasification of the above feeds with catalyst X at 600°C, 34.5 MPa, resulted in a complete conversion to gas. The gas contained H₂, CO₂, CH₄, and trace amounts of high hydrocarbons. The amount of carbon monoxide in the gaseous product mixture was very small. Virtually no tar or char products were detected by the evaporation of the liquid effluent. The TOC analysis confirmed this result. Typical results are illustrated in Table 4, which presents data for the gasification of sewage sludge.

CONCLUSION

Glucose as high as 22% by weight in water can be completely gasified to a hydrogen-rich gas with catalyst X at a WHSV as high as 22.2 (g/h)/g in supercritical water at 600°C, 34.5 MPa. Complete conversions of low concentrations of whole biomass feeds, including water hyacinth, depithed bagasse liquid extract, and sewage sludge, have also been achieved.

REFERENCES

- Baker, E. G., L. J. Sealock, Jr., R. S. Butner, D. C. Elliot, and G. G. Newenschwander (1989), "Catalytic destruction of hazardous organics in aqueous wastes: Continuous reactor system experiments," *Hazardous Waste & Hazardous Mat.*, 6, 87-94.
- Dehui, Y., M. Aihara, and M. J. Antal, Jr. (1993), "Hydrogen production by steam reforming glucose in supercritical water," *Energy and Fuels*, 7(5), 574-577.
- Elliott, D. C., E. G. Baker, R. S. Butner, and L. J. Sealock, Jr. (1993a), "Bench-scale reactor tests of low temperature, catalytic gasification of wet industrial wastes," *J. Sol. Energy Eng.*, 115, 52-56.
- Elliott, D. C., L. J. Sealock, Jr., and E. G. Baker (1993b), "Chemical processing in high-pressure aqueous environments. 2. Development of catalysts for gasification," *Ind. Eng. Chem. Res.*, 32, 1542-1548.
- Sealock, L. J. Jr., D. C. Elliott, E. G. Baker, and R. S. Butner (1993), "Chemical processing in high-pressure aqueous environments. 1. Historical perspective and continuing developments," *Ind. Eng. Chem. Res.*, 32, 1535-1541.

Table 1. Temperature effect on the gasification of glucose in supercritical water with catalyst X (1.0 M glucose reactant, WHSV = 13.5 (g/h)/g, 34.5 MPa)

Temperature	600°C	550°C	500°C
Gas yields			
H ₂	1.97	0.62	0.46
CO	2.57	1.67	1.57
CO ₂	1.54	0.73	0.85
CH ₄	0.90	0.37	0.25
C ₂ H ₄	0.01	0.01	0.02
C ₂ H ₆	0.25	0.10	0.07
C ₃ H ₆	0.01	0.03	0.04
C ₃ H ₈	0.11	0.05	0.04
Carbon gasification efficiency	0.98	0.54	0.51
Tar yield	0.1%	0.9%	1.3%

Table 2. Glucose reactant concentration effect on the gasification efficiency in supercritical water at 600°C, 34.5 MPa, with catalyst X. (Flow rate: 1.0 cm³/min)

	1.2 M glucose with 0.6 g catalyst (WHSV = 22.2 (g/h)/g)	0.8 M glucose with no catalyst (Res. time = 28 s)
Gas yield		
H ₂	2.24	0.70
CO	0.79	1.63
CO ₂	3.09	2.01
CH ₄	1.23	0.75
C ₂ H ₄	0.00	0.04
C ₂ H ₆	0.35	0.22
C ₃ H ₆	0.00	0.04
C ₃ H ₈	0.13	0.09
Carbon gasification efficiency	1.03	0.88
Tar yield	0.008%	Not available

Table 3. Stability of catalyst X in a continuous run of glucose gasification in supercritical water at 600°C, 34.5 MPa (1.2 M glucose, WHSV = 19.9 (g/h)/g, catalyst X 2.55 g)

Time on stream	0.7 h	1.77 h	3.92 h	5.2 h
Gas yield				
H ₂	3.83	3.85	1.97	1.53
CO	0.79	0.63	2.41	2.71
CO ₂	3.32	3.49	1.84	1.18
CH ₄	0.95	0.94	0.93	0.83
C ₂ H ₄	0.00	0.00	0.01	0.01
C ₂ H ₆	0.26	0.26	0.25	0.21
C ₃ H ₆	0.00	0.01	0.01	0.02
C ₃ H ₈	0.15	0.13	0.11	0.09
Carbon gasification efficiency	1.00	1.00	1.01	0.91
Tar yield	0.02%	0.03%	0.07%	0.16%
TOC yield	1.4%	2.5%	5.4%	5.8%

Table 4. Sewage sludge gasification in supercritical water at 600°C, 34.5 MPa, with catalyst X (28 g/dm³ sewage sludge with 2.96 g catalyst X, WHSV = 0.50 (g/h)/g)

Gas product	Yield ^a	Mole fraction ^b
H ₂	2.7%	33%
CO	3.5%	2.9%
CO ₂	66.2%	36%
CH ₄	16.3%	24%
C ₂ H ₄	0.05%	0.04%
C ₂ H ₆	7.7%	5.7%
C ₃ H ₆	0.3%	0.15%
C ₃ H ₈	1.7%	0.89%
total	98.4%	
Liquid yield ^c	0.99%	
TOC analysis	0.28 g-carbon / dm ³	
Mass balanced ^d	99.4%	

a Gas yield = weight of gas / weight of reactant

b Mole fraction = mole of gas / total mole of gas in the effluent

c Liquid yield = weight of solid residue in liquid / gram of reactant

d Mass balance = total gas yield + liquid yield

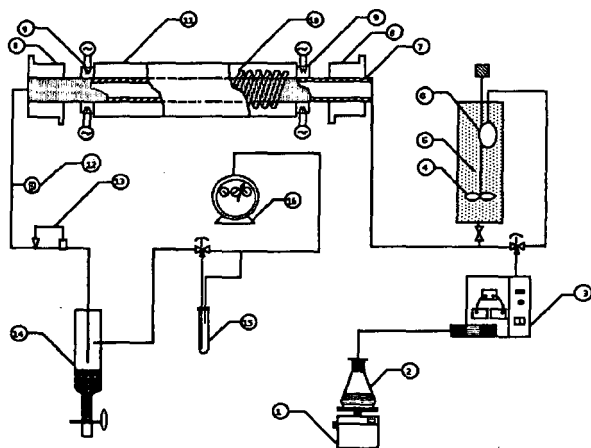


Fig. 1. Reactor system scheme. 1) Balance; 2) Flask with reactant; 3) HPLC pump; 4) Feeding vessel with agitator; 5) Wet-biomass slurry; 6) Balloon; 7) Inconel 625 tube; 8) Cooling jacket; 9) Heater; 10) Furnace; 11) Furnace shell; 12) Pressure transducer; 13) Back pressure regulator; 14) Gas sample output; 15) Liquid-gas separator; 16) Wet test meter

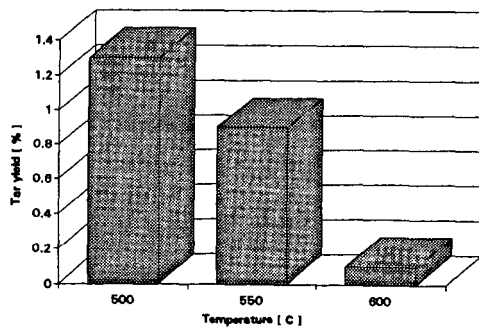


Fig. 2. Tar yield vs. reaction temperature (1.0M glucose reactant, WHSV = 13.5 (g/h)/g)

COMMERCIAL DEVELOPMENT OF ADVANCED PFBC TECHNOLOGY

James D. McClung
Foster Wheeler Development Corporation
12 Peach Tree Hill Road
Livingston, New Jersey 07039

Keywords: Pressurized fluidized bed combustion, coal-fired, combined cycle

INTRODUCTION

In the 1970s, the coal-fired power generation industry recognized that the declining price of electricity over the previous five decades was coming to an end. Maximum use had been made of existing cycle efficiencies and scale-up. As researchers looked for a new approach, the focus shifted from the fully developed Rankine cycle to a new array of coal-fired plants using combined-cycle technology. Now, coal-fired combined-cycle plants are being introduced that shift power production to the Brayton cycle. Integrated Gasification Combined Cycle (IGCC) and Pressurized Fluidized Bed Combustion (PFBC) are two technologies at the forefront of this approach.

The PFBC approach burns coal in a fluidized bed combustor at elevated pressure. The plant generates electricity from a gas turbine (expanding the hot, pressurized products of combustion) in addition to the conventional steam (bottoming) cycle. Such a plant can achieve thermal efficiencies of about 40 percent and have a leveled busbar cost below any competing coal-based technology. In addition to the economic benefits, the "built-in" feature of environmental control (SO_2 and NO_x) in the combustion process eliminates the need for external gas cleanup such as scrubbers. A PFBC can burn a wider range of coals than a pulverized-coal-fired (PCF) boiler and is simpler to operate and maintain than an IGCC power plant.

By combining the salient features of PFBC and IGCC, a new generation of PFBC plants promises increased efficiency and lower cost, while avoiding the increased complexity and higher cost of the IGCC systems. Foster Wheeler's (Second-Generation) "Advanced" Pressurized Fluidized Bed Combustion concept achieves this goal. The partial conversion of coal to syngas and subsequent firing in a gas turbine at 1288°C (2350°F) increases the thermal efficiency of a PFBC plant to about 45 percent (HHV basis). Studies have further shown that 49 percent (HHV) efficiency can be achieved with high-pressure steam systems and advanced gas turbine technology under development.

The path to successful commercialization of APFBC technology involves conceptual design, pilot-scale component testing, integrated system testing, and demonstration. The developmental programs designed to achieve commercial status of the technology are described in the following sections.

ADVANCED PFBC CONCEPT

In Foster Wheeler's Second-Generation PFBC concept (Figure 1), coal is fed to a pressurized pyrolyzer (carbonizer), where it is converted to a low-Btu fuel gas and char. The relatively low carbon conversion that takes place in the carbonizer results in a simpler sulfur-removal process than is typically required in coal gasification processes. The char (unreacted coal, coal ash, and unreacted/reacted sorbent) that is produced in the carbonizer is transferred to a circulating pressurized fluidized bed combustor (CPFBC), where it is subsequently burned. The fuel gas produced in the carbonizer is cleaned of particulates and alkali and is fired in a specially designed combustor outside a high-temperature gas turbine using the CPFBC flue gas (vitiating air) as the oxidant. Steam is raised and superheated in the CPFBC.

The shaded components in Figure 1 represent the additional elements required to increase the efficiency of first-generation PFBC plants. The redistribution of electric power produced in first-generation PFBC plants (20 percent in the gas turbine/80 percent in the steam turbine) to that produced in second-generation PFBC plants (50 percent in the gas turbine/50 percent in the steam turbine) is shown in the figure.

COMPONENT TESTING—FWDC PILOT PLANT/UTSI

In Phase 1 of a three-phase, U.S. Department of Energy sponsored program, a nominal 500-MW plant was designed, and the costs, operational and environmental performance were compared with a conventional PCF plant with wet scrubbers. The plant is modular, with two parallel power island trains consisting of a carbonizer, CPFBC, and associated hot-gas cleanup systems feeding a gas turbine fired at 1288°C (2350°F) and a heat recovery steam generator

(HRSG). A single reheat steam turbine is powered by the combined steam flows of the two power island trains. About 45 percent of the combined-cycle power is produced by the two gas turbines and 55 percent by the steam turbine. Plant auxiliary power is very low (about 3 percent); the net thermal efficiency is 44.9 percent. The estimated heat rate of the plant is about 18 percent lower than the PCF plant. The results of the conceptual design study confirmed the objectives of the program—to design an APFBC plant with a 45-percent thermal efficiency and a cost-of-electricity (COE) 20 percent lower than a conventional PCF plant with flue gas desulfurization (FGD).

In Phase 2, a 254-mm (10-in.) carbonizer was tested at Foster Wheeler's Research Center in Livingston, New Jersey. Tests were conducted with operating temperatures ranging from 816 to 982°C (1500 to 1800°F) and pressures from 1.01 to 1.42 MPa (10 to 14 atm). Pittsburgh No. 8 coal and Ohio Plum Run dolomite were the predominant feedstocks, although Illinois No. 6 and Eagle Butte (a Wyoming subbituminous) were also tested, along with an Alabama limestone. Carbonizer fuel gas was predominantly carbon monoxide, carbon dioxide, hydrogen, and methane. No hydrocarbon vapors were produced throughout the entire test program—an important finding, since one of the major technology-related issues for this type of plant is the concern that hydrocarbon vapors, if present, could foul the barrier-type filters required to protect the high-temperature gas turbine from particulate erosion and deposition.

The pilot plant carbonizer test results, compared to the carbonizer performance assumptions used in the Phase 1 study, produced a higher fuel gas heating value, a higher sulfur-capture efficiency, and a lower yield of ammonia in the fuel gas. The better sulfur capture and lower ammonia yield (when converted to NO_x) result in lower plant emissions than predicted in the design study. The higher-quality fuel gas translates to a higher topping combustor firing temperature, a further increase in plant efficiency (44.9 to 46.2 percent), and an increase in power production in the gas turbine from 45 to 50 percent.

The carbonizer was subsequently converted to a 203-mm (8-in.) diameter x 11-m (34 ft-6 in.) tall CPFBC, and the CPFBC was tested using petroleum coke, four coals (Pittsburgh No. 8, Illinois No. 6, Kentucky, and Eagle Butte), char (produced in the earlier carbonizer tests), dolomite, and two limestone sorbents. Combustion efficiency was very high (greater than 99.5 percent) for all the fuels tested, including char. Sulfur capture efficiencies were generally high (greater than 96 percent) using Ca/S ratios ranging from 1:1 to 2:1. As a result of the "short" CPFBC height (the carbonizer was converted to the CPFBC), the NO_x and calcium sulfide conversions were not optimized.

Parallel to the pilot plant testing, Westinghouse has conducted topping combustor tests at the University of Tennessee Space Institute (UTSI). The topping combustor must burn low heating value fuel gas delivered from the carbonizer at approximately 870°C (1600°F) and 1.17 MPa (170 psi). The fuel gas entering the topping combustor has been previously cleaned of particulate and alkali, but contains fuel-bound nitrogen present as ammonia. The ammonia is significant because it will selectively oxidize to NO_x if the fuel is burned under the highly oxidizing conditions of standard turbine combustors. The fuel gas must be burned with the hot vitiated air from the CPFBC. The vitiated air has also been cleaned of particulates and alkali, but is partially depleted in oxygen. The 870°C (1600°F) vitiated air must be utilized to cool the topping combustor.

Tests completed with 305-, 356-, and 457-mm (12-, 14-, and 18-in.) diameter multiannular swirl burners (MASBs) using synthetically produced carbonizer fuel gas doped with ammonia confirmed that the MASB can be successfully cooled with 870°C (1600°F) vitiated air (supplemented with additional cooling air at the hottest locations). Good temperature distribution patterns were obtained and stable, complete combustion was achieved. To reduce ammonia conversion, the MASB was redesigned to improve backmixing and increase residence time in the rich zone.

In Phase 3, scheduled to begin in late 1994, a 254-mm (10-in.) I.D. carbonizer and 356-mm (14-in.) I.D. CPFBC—each with gas cleanup and solids feeding systems—will be tested in an integrated mode at the Foster Wheeler Research Center.

INTEGRATED TESTING—WILSONVILLE POWER SYSTEMS DEVELOPMENT FACILITY

In parallel with the pilot plant testing, work is under way to design and build a larger, integrated test facility. The test facility is part of the Power Systems Development Facility (PSDF) to be operated by Southern Company Services at Wilsonville, Alabama. The \$145 million PSDF consists of several "modules" for long-term testing of APFBC, advanced gasification, hot-gas cleanup systems, and fuel cells. The PSDF is a joint, cost-shared effort between the DOE, the EPRI, and industry.

Most of the second-generation PFBC components will be tested in the Wilsonville configuration. The exception is a steam turbine is not incorporated in the design. The APFBC plant will

provide the first full integration of the gas side of the power island—that is, operation of a gas turbine topping combustor with hot pressurized fuel gas from the carbonizer and hot pressurized flue gas from the CPFBC. A key element of the program is long-term testing and assessment of particulate control devices (PCDs) that directly supports DOE's Clean Coal program. The nominal 7-MW APFBC plant is scheduled to begin operation in late 1995.

The design coal and sorbent are Illinois No. 6 and Longview limestone. Eagle Butte subbituminous coal is an alternative fuel. The plant is designed for a coal feed rate of 0.69 kg/s (5500 lb/h) and a sorbent feed rate of 0.13 kg/s (1050 lb/h). Provision has been made in the design to test the CPFBC under low excess-air conditions, feeding coal and sorbent directly to the CPFBC.

The carbonizer, like the Livingston pilot plant unit, is a "jetting" fluidized bed pyrolyzer without heat-transfer surface. The refractory-lined vessel has a bed section (lower part) [approximately 914 mm (3 ft) diameter], 14.6 m (48 ft) high and a disengagement section (upper part) [approximately 1.22 m (4 ft) diameter]. The carbonizer is designed to feed coal pneumatically in the bottom of the vessel; alternate feed points are located radially at two different elevations. The feed system has been designed to accommodate both dry and paste feed.

The CPFBC, shown in Figure 2, is a refractory-lined vessel with an 838-mm (33-in.) diameter upper section. The integrated heat exchanger is a refractory-lined vessel that contains four cells—an inlet, an outlet, and two heat transfer cells. Heat is removed in the integrated heat exchanger by a once-through condensate system. The unit has been designed so that it can operate between 20- and 300-percent excess air to test both first-generation and advanced PFBC concepts. An oxidizer/cooler cools the CPFBC bed material from 871 to about 260°C (1600 to about 500°F) and transports the bed (ash) to a lockhopper for discharge from the unit.

High-temperature gas cleaning (HTGC) systems control particulates and alkalis. Two independent HTGC systems handle the carbonizer fuel gas stream and the CPFBC flue gas stream. Each HTGC system consists of a cyclone, PCD, and alkali getter.

An Industrial Filter & Pump Mfg. Co. low-density fiber ceramic candle filter design is being used as the carbonizer PCD. The refractory-lined filter vessel (Figure 3) has a 1.5-m (60-in.) diameter and contains candles arranged in six groups for back-pulse cleaning. The candles are of aluminosilicate fiber construction, with binders of silica and alumina. The monolithic flared flange and end cap of the candle are of densified ceramic fiber construction, as are the tubesheet and the candle retainer.

PCD service for the CPFBC will be provided by a Westinghouse ceramic candle filter consisting of a refractory-lined pressure vessel containing six arrays, or "clusters," of 60-mm (2.36-in.) diameter x 1.5-m long (59-in.) diameter candle elements. The individual clusters are supported from a high-alloy tubesheet and expansion assembly that spans the 3.1-m (10.2-ft) pressure vessel and separates the "clean" and "dirty" gas. The Westinghouse cluster concept is illustrated in Figure 4.

The alkali getters are sorbent packed beds contained in vertical, refractory-lined pressure vessels. The sorbent material reacts irreversibly with sodium and potassium vapor-phase compounds at high temperature.

The topping combustor is designed to operate with a vitiated air temperature of 1600°F, however, there is provision to introduce compressor air upstream of the topping combustor to cool the vitiated air to about 1400°F before it enters the topping combustor. The topping combustor is fired at an exhaust gas temperature of 1288°C (2350°F), the firing temperature for a commercial plant, using 899°C (1650°F) carbonizer fuel gas. While the advanced PFBC commercial plant uses an advanced industrial turbine with a turbine inlet temperature of 1288°C (2350°F), Wilsonville uses a turbine which operates at a maximum temperature of 1080°C (1975°F). Wilsonville will demonstrate that a firing temperature of 1288°C (2350°F) is viable with respect to emissions and burner design. However, because of the lower turbine operating temperature required, part of the compressor air will be used to cool the exhaust gas downstream of the topping combustor.

The gas turbine generator set is a modified Allison Model 501-KB5 gas turbine, which drives a synchronous generator through a speed-reducing gearbox. The hot exhaust gas from the topping combustor is expanded through the gas turbine, powering both the electric generator and the air compressor. Air from the compressor supplies all APFBC plant process air requirements.

DEMONSTRATION

A 95-MW plant utilizing Foster Wheeler's Advanced PFBC technology will be demonstrated

under the U.S. Department of Energy's Clean Coal Technology V (CCT V) program. The proposed plant will operate in a cogeneration mode, providing electric power and extraction steam for manufacturing. Following a 30-month demonstration period, the plant will continue to operate on a commercial basis. The plant is scheduled to start up in 1998.

Coal paste and limestone are fed to the carbonizer, and the char from the carbonizer, additional coal paste, and limestone are burned in the CPFBC. The carbonizer is a refractory-lined vessel approximately 14 m (46 ft) high. The lower (bed) section of the carbonizer is 2.6-m (8-ft) diameter while the upper section of the vessel expands to 3.3-m (10-ft) diameter. The gas in-bed residence time is about 5 seconds, equivalent to the pilot plant and Wilsonville designs. The CPFBC is a Foster Wheeler single-vessel design incorporating membrane wall construction, cyclone, "J" valve, integrated heat exchanger (INTREX™), and ash stripper/cooler—all housed in a pressure vessel.

The CPFBC generates steam from the waterwalls and INTREX™, and additional steam is generated in the HRSG to drive the steam turbine generator. At full load, Four Rivers will generate about 70 MW of electricity and provide 39.1 kg/s (310,000 lb/h) steam at 1.31 MPa absolute (190 psia) and 215°C (420°F). The gas turbine generates 38 MW, and the extraction/condensing steam turbine generates 32 MW.

The particulate matter in the carbonizer fuel gas is removed using multiple ceramic candle filter systems supplied by Westinghouse. The CPFBC flue gas particulate matter is removed using a proprietary ceramic candle filter design supplied by Lurgi-Lentjes-Babcock (LLB), formerly Deutsche Babcock Energie. Seven 457-mm (18-in.) MASBs fire the carbonizer fuel gas in the topping combustor. The hot exhaust gas from the topping combustor drives a Westinghouse Model 251 gas turbine.

BEYOND DEMONSTRATION

Following demonstration, the APFBC technology will be ready for rapid world-wide commercialization. When proved successful, the technology will allow the effective use of high-sulfur coal, lower power generation costs, reduce emissions, extend fuel supplies, and provide utilities and industry with a reliable option for repowering and new generation capacity. As coal continues to play an important role in power generation, Advanced Pressurized Fluidized Bed Combustion will provide one of the most cost-effective and environmentally friendly technologies in the next century. Foster Wheeler is committed to the successful commercialization of this technology.

REFERENCES

- McClung, J., et al., 1994, "Design and Operating Considerations for the Advanced PFBC Facility at Wilsonville, Alabama, ASME International Joint Power Generation Conference, Phoenix, Arizona.
- Domeracki, W. F., et al., 1993, "Topping Combustor Development for Second-Generation Pressurized Fluidized Bed Combined Cycles," Westinghouse PGBU. ASME Turbo Expo '94 Conference, The Hague.
- Hyre, M., et al., 1991, "PFBC Performance and Cost Improvements Using State-of-the-Art and Advanced Topping/Bottoming Cycles," *Proceedings, 1991 International Conference on Fluidized Bed Combustion*, Vol. 1. The American Society of Mechanical Engineers, New York, NY.
- Robertson, A., et al., 1989, "Second-Generation Pressurized Fluidized Bed Combustion Plant—Conceptual Design and Optimization of a Second-Generation PFBC Combustion Plant," Foster Wheeler Development Corporation, FWC/FWDC/TR-89/11 (Phase 1—Task 1 Report), prepared for U.S. Department of Energy.

ADVANCES IN THE SHELL COAL GASIFICATION PROCESS

E. L. Doering
Shell Oil Company
and
G. A. Cremer
Shell Synthetic Fuels Inc.
P. O. Box 2099
Houston, Texas 77252-2099

Keyword: Shell Coal Gasification Process; Demkolec Project; Integrated Coal Gasification Combined Cycle Power Generation

Process Summary

The Shell Coal Gasification Process (SCGP) is a dry-feed, oxygen-blown, entrained flow coal gasification process which has the capability to convert virtually any coal or petroleum coke into a clean medium Btu synthesis gas, or syngas, consisting predominantly of carbon monoxide and hydrogen.

In SCGP, high pressure nitrogen or recycled syngas is used to pneumatically convey dried, pulverized coal to the gasifier. The coal enters the gasifier through diametrically opposed burners where it reacts with oxygen at temperatures in excess of 2500°F. The gasification temperature is maintained to ensure that the mineral matter in the coal is molten and will flow smoothly down the gasifier wall and out the slag tap. Gasification conditions are optimized, depending on coal properties, to achieve the highest coal to gas conversion efficiency, with minimum formation of undesirable byproducts.

The hot syngas exiting the gasifier is quenched to below the softening point of the slag and then cooled further in the syngas cooler. Entrained flyash is removed to less than 1 ppm using ceramic candle filters. Downstream syngas treating includes low level heat recovery and conventional cold gas cleanup to minimize trace metal emissions and to remove chlorides, and sulfur and nitrogen compounds. Essentially all of the nitrogen is ultimately converted to molecular nitrogen, and essentially all of the sulfur is recovered as salable, elemental sulfur. Slag and flyash are also recovered as marketable by-products. A simplified SCGP flow scheme is shown in Figure 1.

Technology Development

Research on the Shell Coal Gasification Process began in 1972, based on Shell's extensive experience with oil gasification. In 1976, a 6 TPD process development unit was placed in operation at Shell International's Amsterdam laboratory, and in 1978, a 150 TPD pilot plant was started up near Harburg, Germany. The Harburg unit, which operated until 1983, demonstrated the key technical features of the SCGP technology.

A very important element in the SCGP development program was the construction and operation of SCGP-I, the 250 TPD demonstration unit which operated between 1987 and 1991 at Shell Oil's Deer Park Manufacturing Complex near Houston, Texas. SCGP-I was based on a scaled down version of commercial unit. During its 15,000 hours of operation, SCGP-I clearly demonstrated the reliability, flexibility, efficiency, and environmental superiority of SCGP. Coal to clean gas efficiencies were typically above 80% and sulfur removal efficiencies were consistently above 99% for the 18 diverse feedstocks gasified at SCGP-I. The SCGP-I feedstocks included domestic coals ranging from lignite to high sulfur bituminous coals, three widely traded foreign coals, and petroleum coke.

The extensive environmental, engineering and operating data collected during the SCGP-I operating program provide the basic information necessary to permit, design, construct, and operate future SCGP plants. Moreover, the SCGP-I program yielded a number of process improvements and innovations which have since been incorporated into commercial designs.

The Demkolec Project

The first commercial application of SCGP is the Demkolec Project, a 253 MW integrated gasification combined cycle (IGCC) power plant located in the Netherlands. Demkolec B.V., a wholly owned subsidiary of the Dutch Electricity Generating Board, selected SCGP as the coal gasification technology for their project in 1989 and executed an SCGP license agreement with Shell International later that year. Environmental permits based on NO_x emissions of 0.17 lb/MM Btu and SO₂ emissions based on 0.06 lb/MM Btu of design coal were obtained in April 1990. Construction began in July 1990, commissioning was completed in 1993 and startup was initiated in late 1993. An extensive, three-year demonstration program has been identified and is underway.

The Demkolec Project employs a single SCGP gasifier to fuel a Siemens V94.2 combustion turbine coupled with steam turbine and generator. The SCGP plant is fully integrated with the combined cycle plant, including the boiler feed water and steam systems; additionally, the compressed air for the high pressure air separation unit is supplied by extraction air from the combustion turbine air compressor.

The Demkolec Project features a multiple burner gasifier scaled up from the SCGP-I gasifier to 2000 TPD coal. Also, the Demkolec Project includes a number of process improvements which were successfully demonstrated during SCGP-I operation. Among these are:

- increased slagging efficiency and a reduction in slag entrainment;
- dry solids removal which offers higher flyash removal efficiency and lower cost;
- dry flyash recycle to improve carbon conversion and slagging efficiency;
- flux addition to promote slag flow and optimize gasification conditions, depending on coal properties;
- catalytic hydrolysis of hydrogen cyanide (HCN) and carbonyl sulfide (COS) to reduce corrosion, reduce emissions and simplify gas treating;
- zero aqueous process discharge for environmental considerations; and
- a turbine lead/gasifier follow control system for load following.

Additional SCGP improvements and innovations have been developed since the Demkolec design was completed with the aim of further reducing costs and improving performance. In the last several years, a number of design and optimization studies and capital cost estimates have been carried out for Shell-based IGCC systems with different engineering firms and equipment suppliers, including General Electric, Westinghouse, Air Products, Fluor/Daniel, Black & Veatch, and Bechtel, and with support from the Electric Power Research Institute. Developments in SCGP, improvements in gas turbine performance, and the ongoing experience of equipment manufacturers have all contributed to the Shell Synthetic Fuels' commercial design for SCGP.

Shell Synthetic Fuels' SCGP Commercial Design

The SCGP commercial design is the latest effort by Shell Synthetic Fuels Inc. to combine SCGP technology developments subsequent to the SCGP-I program and the Demkolec Project design with other related IGCC improvements. The SCGP commercial design is based on a single train SCGP plant coupled with a high pressure air separation unit (ASU) to fuel a single combustion turbine operating in combined cycle service. If the GE frame 7FA combustion turbine is used, IGCC net power output is estimated to be approximately 265 MW. With a high sulfur Illinois coal, heat rate is estimated at slightly less than 8150 Btu/kWh. Even lower heat rates can be expected with most other bituminous coals.

The principal objective of the SCGP commercial design is to deliver competitive capital and maintenance costs with superior efficiency and environmental performance. Each of the main systems associated with a Shell-based IGCC plant is reviewed below.

Coal Pulverizing and Drying

Roller or bowl mill pulverizers have been demonstrated in higher capacity service in the last several years. The SCGP commercial design includes two large commercial scale pulverizers for a single gasifier/gas turbine train. (Three pulverizers would be premised for a two

gasifier/gas turbine system.) Each pulverizer has excess capacity so that sufficient availability is provided without the need for an additional pulverizer. Heat and nitrogen savings have also been designed into the drying system for higher moisture content coals.

SCGP Gasifier

The SCGP-I unit was shutdown in March 1991. Considerable analyses of the later stages of the SCGP-I operation showed that the cold gas efficiency could be further increased and that the scaleup/severity parameters were less restrictive than anticipated. These less conservative scaleup rules allow reduced gasifier physical dimensions for a design coal/syngas rate. Further engineering studies into the results of the gasifier scaleup tests at SCGP-I have led to a more compact gasifier design, while at the same time leading to increased syngas production. Gasifier materials' life is extended by operating the gasifier cooling medium at lower pressure.

Syngas Cooling and Dry Solids Removal

The SCGP dry coal feed system leads to very high coal to gas conversion efficiencies as well as gasifier exit temperatures which are higher than those from coal slurry feed systems. The high gasifier exit temperature and low moisture content of the raw syngas allow most of the waste heat to be recovered at high levels through syngas cooling, at a relatively modest cost. Extensive low level heat utilization is not required to achieve high thermal efficiencies. Consequently, for SCGP, the cost of syngas cooling will almost always be justified by the value of the high level steam produced. Clearly, however, the benefits of syngas cooling can be enhanced by reducing equipment capital and maintenance costs.

The syngas cooling equipment demonstrated at SCGP-I and employed in the Demkolec Project is a series of water wall exchangers including superheat, evaporation and boiler feed water economizers. Cost/benefit studies led to the conclusion that, where SCGP can be closely heat integrated with the combined cycle plant, the SCGP steam should be superheated in the combined cycle heat recovery steam generator (HRSG) rather than in the syngas cooler. In the Demkolec IGCC Project, the SCGP syngas cooler steam will be mildly superheated, then sent to the HRSG for further superheating.

Second, early plant performance at SCGP-I and subsequent engineering studies identified that dry solids removal with ceramic candle filters at an intermediate temperature offered SCGP the opportunity to change the economizers from water wall to shell and tube exchangers. Further equipment developments in hot gas particulate removal identified that the evaporator of the syngas cooler could be located downstream of the filter and utilize relatively dust free firetube exchange. Each study led progressively to a better understanding of the tradeoffs between the costs of the filter system and the high temperature exchange surfaces.

The SCGP commercial design uses a dust laden, raw gas firetube exchanger downstream of the conventional recycle gas quench section, followed by dry flyash removal. Further cost reductions were achieved in the lockhopper system used for flyash recycle through scaleup studies on the continuous ash pressure letdown system demonstrated at SCGP-I. Additional low level heat recovery sources have been identified downstream of dry solids removal and may be included in the integrated boiler feed water/steam cycle if the capital costs are justified by the efficiency gains.

Dry Chloride Removal

Chloride in the coal vaporizes in the reducing atmosphere of the gasifier and most of it appears in the form of hydrogen chloride. Past practice has been to wash out the chloride and neutralize the acid in a wet gas cleanup section downstream of the syngas cooler/dry solid removal sections. Depending on the level of chloride in the coal, it can be more cost effective to utilize a dry chloride removal technique with a sorbent. Dry chloride removal offers the additional advantages of reducing catalyst poisons for downstream catalyst beds and of allowing more low level heat recovery from the raw gas.

Cold Gas Cleanup

Very high sulfur removal efficiencies are achievable with the SCGP cold gas cleanup system. Either of two Shell solvents can be used to hydrolyze trace amounts of carbonyl sulfide in the syngas to hydrogen sulfide and then remove the hydrogen sulfide through absorption. Recent studies have premised a total sulfur level of 20 ppm or less in the clean syngas, which allows additional low level heat recovery in the HRSG. In the SCGP commercial design a proprietary system for removing volatile metals such as mercury and arsenic has been combined with the SCGP cold gas cleanup system to further reduce emissions of hazardous air pollutants (HAPs).

Integration of SCGP with Combined Cycle and Air Separation Units

The General Electric 7F and the Westinghouse 501F gas turbines provide high fuel gas to electricity generating efficiency and improved combined cycle performance. The increased gas turbine performance has served to increase net IGCC power output which has in turn helped to reduce the IGCC \$/kW cost. Additional IGCC cost and performance benefits can be realized through careful integration of the three basic technologies: SCGP, air separation, and combined cycle power generation. Figure 2 illustrates a highly integrated Shell-based IGCC power plant.

Turbine simulation studies have shown that the clean SCGP coal gas can be diluted with either nitrogen or water to reduce NO_x formation and at the same time provide low CO emissions over a wide range of performance conditions. Recent studies have concluded that return of the excess nitrogen from the air separation unit to the combustion turbine is most advantageous for a Shell-based IGCC plant and that saturation of the return nitrogen to the degree desired for gas turbine operation is more attractive than fuel gas saturation and can assure a more reliable fuel gas composition for combustor design and control. Since there is little low level heat for fuel gas saturation in SCGP, the lowest overall IGCC heat rate is obtained with 100% air extraction from the gas turbine for a pressurized air separation unit (ASU), as will be practiced in the Demkolec Project. However, higher net IGCC power output can be achieved by providing the ASU with its own air compressor. The optimum level of air extraction will in fact depend on the specific situation and must be determined as part of an optimized Shell-based IGCC plant design.

Another recent development in Shell-based IGCC plant design derives from the fact that the SCGP syngas composition is very constant over a wide operating range. Combined with new gas turbine control systems, this has led to reductions in turbine fuel gas control valve pressure, which in turn leads to similar reductions in gasifier design pressure and cost.

Environmental Attributes

Environmental emissions of Shell-based IGCC are estimated to be extremely low. Total SO₂ emissions of 0.05 lb/MM Btu or less are achievable, corresponding to greater than 99.5% sulfur removal efficiency. NO_x emissions can be controlled to 0.09 lb/MM Btu (corresponding to 25 ppmv in the HRSG flue gas) or less, and hazardous air pollutant emissions as defined in the 1990 Clean Air Act Amendments are expected to be less than 0.5 tons/year for a nominal 265 MW Shell-based IGCC plant.

As shown in Figure 3, the estimated air emissions from a Shell-based IGCC power plant are well below the regulatory limits and in fact are much closer to those from a natural gas-fired power plant than from a typical coal-based facility. Moreover, long term, on-site storage of solid byproducts is not required since slag, flyash and elemental sulfur are all marketable products.

Conclusions

The first commercial application of the Shell Coal Gasification Process and the world's first fully commercial IGCC facility is Demkolec's 253 MW IGCC power plant in the Netherlands. Experience from the Demkolec Project has provided the foundation for other Shell-based IGCC commercial projects.

The Shell Synthetic Fuels' SCGP commercial design, which includes a number of technology improvements contributing to lower costs, higher efficiency and reduced emissions compared to earlier designs, is now available. Improvements include:

- a more compact gasifier design, aimed at reducing capital cost and increasing coal to gas conversion efficiency;
- revised syngas cooler design to reduce capital costs and maintenance requirements;
- continuous flyash letdown to improve reliability and reduce maintenance requirements;
- dry chloride removal to further simplify downstream gas treating;
- techniques to increase efficiency and reduce formation of undesirable byproducts in the gasifier;
- methods for improved removal and recovery of volatile metals such as mercury and arsenic to reduce HAP emissions; and
- integration of SCGP with the combined cycle and air separation units to minimize \$/kW cost, while maintaining performance and operability requirements.

FIGURE 1
SHELL COAL GASIFICATION PROCESS
PROCESS FLOW SCHEME

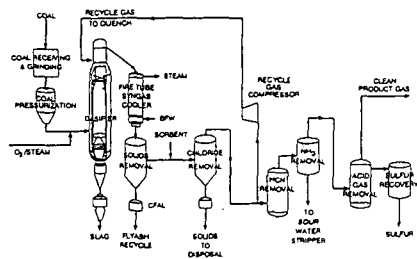


FIGURE 2
HIGHLY INTEGRATED SHELL COAL GASIFICATION
COMBINED CYCLE POWER PLANT CONFIGURATION

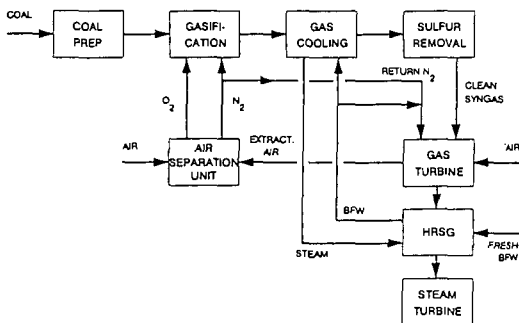
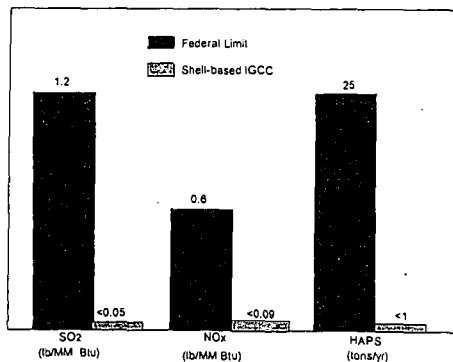


FIGURE 3
SHELL-BASED IGCC AIR EMISSIONS



AMERICAN ELECTRIC POWER
PRESSURIZED FLUIDIZED BED COMBINED CYCLE
TECHNOLOGY STATUS

M.Marrocco
American Electric Power Service Corporation
One Riverside Plaza
Columbus, Ohio 43215

Keywords: Clean Coal Technology, Pressurized Bubbling Bed, Combined Cycle

INTRODUCTION

The Ohio Power Company's Tidd Pressurized Fluidized Bed Combined Cycle (PFBC) program continues to be the only operating PFBC demonstration program in the nation. The 70 MWe Tidd Demonstration Plant is a Round 1 Clean Coal Technology Project constructed to demonstrate the viability of PFBC combined cycle technology. The plant is now in its fourth year of operation. The technology has clearly demonstrated its ability to achieve sulfur capture of greater than 95%. The calcium to sulfur molar ratios have been demonstrated to exceed original projections. Unit availability has steadily increased and has been demonstrated to be competitive with other technologies. The operating experience of the first forty-four months of testing has moved the PFBC process from a "promising technology" to a viable, proven option for efficient, environmentally acceptable base load generation.

Funding for the \$210 million program is provided by Ohio Power Company, The U.S. Department of Energy, The Ohio Coal Development Office, and the PFBC process vendors - Asea Brown Boveri Carbon (ABBC) and Babcock and Wilcox (B&W).

PLANT DESCRIPTION

The project involves the repowering of a 1940's vintage pulverized coal plant with PFBC components. The original Tidd plant consisted of two 110 MWe steam turbine generators supplied with steam by conventional coal fired boilers. The unit 1 steam turbine was repowered at approximately 50% capacity by the addition of a PFBC combustor steam generator and a gas turbine exhaust economizer. Other additions included in the AB scope of supply were the gas turbine and generator, the coal preparation system, the coal and sorbent feed systems, the gas cleaning system, and the cyclone and bed ash removal systems. The major balance of plant improvements included the addition of an electrostatic precipitator, combustor building, bed ash and cyclone ash silos, and sorbent preparation facilities. Modification of the coal and sorbent storage areas and a revamped control room completed the needed improvements for the conversion. The remainder of the balance of plant utilized the original Tidd balance of plant components and systems.

The PFBC Power Island (Figure 1), which was incorporated into the existing plant, was designed to provide 440,000 pounds per hour of steam flow at 1300 psia and 925°F. Plant generation output was expected to be 72.5 MWe gross (57.1 MWe from the steam turbine generator and 15.4 MWe from the gas turbine generator).

Air, at approximately 175 psia, is provided to the combustor by the gas turbine compressor through the outer annulus of a coaxial air/ gas pipe. Inside the combustor vessel, the air is ducted into the boiler where it fluidizes the bed materials and provides oxygen for combustion. The bed design temperature is 1580°F, which was established by the maximum acceptable gas turbine inlet temperature. This temperature is well above the minimum coal combustion temperature and provides sufficient margin to preclude melting of the coal ash constituents. In addition, this temperature is conducive to a relatively high reaction rate for SO₂ capture by direct sulfation of the calcium carbonate in the sorbent, while being well below the temperature at which alkalis vaporize and present a corrosion problem for the gas turbine. Formation of thermal NO_x is essentially nil due to the low combustion temperature and the reduction of much of the NO_x formed from nitrogen in the coal to N₂ and O₂ at char sites in the bed. Seven parallel strings of gas cleaning cyclones remove 99% of the ash elutriated by the gas leaving the bed. Six of the strings consist of a primary and a secondary cyclone, the seventh is comprised of a primary cyclone in series with an experimental ceramic Advanced Particle Filter (APF).

All of the cyclones are located in the combustor vessel. The APF is located outside the combustor in a separate pressure vessel. The gas from all seven strings is combined inside the pressure vessel and routed to the gas turbine via the coaxial air/gas pipe. The gases are expanded through an ABB Stal GT-35P gas turbine, which produces shaft power to run the gas turbine compressor (approximately 2/3 of the power at full load) and to drive the gas turbine generator (remaining 1/3 of the power). The turbine exhaust gases then pass through the economizer where excess heat is transferred to the feedwater and then through the electrostatic precipitator for further particulate collection. The gases then are ducted to Cardinal Unit No. 1 where they are combined with that unit's exhaust stream and exit to atmosphere via the Cardinal stack.

The steam cycle is a Rankine cycle with a subcritical once-through boiler. Condensate is heated by two stages of low pressure heaters and a gas turbine intercooler as it is pumped to the deaerator. A single high pressure heater and the turbine exhaust gas economizer raised the final feedwater temperature to approximately 480°F. The feedwater then passes through the boiler bottom hopper and furnace wall enclosures where additional subcooled preheating occurs. The feedwater then enters the in-bed evaporator tubes where the steam is generated and attains a slight degree of superheat. The steam then passes through the in-bed primary superheater, is attemperated and attains final steam temperature in the in-bed secondary superheater. At steam flows below 40% capacity, a circulation pump maintains sufficient flow rate through the evaporator circuits for cooling protection. The resultant moisture in the evaporator outlet steam is separated by centrifugal action in a vertical separator.

Coal is injected into the fluidized bed as a paste nominally containing 25 percent water by weight. Raw coal of 3/4 inch top size is fed to a double roll crusher which reduces the material to minus 1/4 inch. The crushed coal is conveyed to a screen to collect oversized material then to a mixer where water is added to make the paste. A recycle line, which is located upstream of the screen, returns a portion of the material to the crusher. Recycle is regulated to attain a sufficient quantity of coal fines, which are necessary to make a cohesive and pumpable coal paste. The paste is fed from the mixer into two interconnected surge tanks which supply six hydraulically driven piston pumps. These pumps feed the paste to individual fuel nozzles which deliver the paste into the fluidized bed just below the tube bundle.

The sorbent, which is generally dolomite, is crushed to minus 1/8 inch size and dried in a hot air swept hammermill crusher. This material is then injected into the fluidized bed via alternating dual lockhoppers that feed a dilute phase pneumatic transport system. The original transport system design splits the flow into two feed nozzles, however, the system has recently been modified to provide a total of four feed nozzles.

Material is drained from the bed to maintain the bed level. This "bed ash" accounts for approximately 40% of the total ash and is generally 99% larger than 60 mesh (250 microns). The ash is drained in a controlled manner by gravity via two parallel lockhoppers. Material elutriated from the bed and collected in the cyclones, approximately 60% of the ash, is generally 99% smaller than 60 mesh. This "cyclone ash" is removed by means of a pneumatic transport system which depressurizes and cools it.

BED PROCESS FINDINGS

Post-Bed Combustion

Initial operation of the unit revealed that combustion was occurring beyond the bed resulting in excessively high temperatures of the gas in selective cyclone strings and in the primary cyclone dip legs. The dip leg combustion was attributed to excessive unburned carbon carryover; whereas, the gas stream combustion was attributed to carryover of unburned volatiles. Both of these phenomena were attributed to high localized fuel release combined with rapid fuel breakup and devolatilization. Insufficient oxygen in these localized regions resulted in plumes of low O₂ gas with unburned volatiles and fine char. This was documented through oxygen measurements taken in the freeboard above the fuel nozzle discharge points. This problem was minimized through improved fuel splitting, installation of a steam induced freeboard gas mixing system, and

improvements in the coal paste quality. The latter factor proved to have the greatest impact on reducing the degree of post bed combustion.

Recently, the unit has operated for extended periods with no signs of post bed combustion. However, upsets in coal paste preparation still result in upward swings in freeboard gas temperature. Such swings pose a potential trip risk at full bed height due to excessive gas turbine temperatures. At lower bed heights, these swings are not a problem, since the freeboard temperature runs well below the bed temperature due to the convective cooling action of the tubes above the top of the bed. The post bed combustion phenomenon is understood to the extent that operations personnel are able to monitor plant conditions and take early action to prevent or mitigate such occurrences.

Sinter Formation

The formation of small quantities of hollow egg shaped agglomerates, in the range of 1 - 2 inches in size (Sintering), has been observed throughout the operation of the unit. However, these did not pose a major operating problem at low bed levels, since the formation rate was slow and sinters drained from the bed at a rate which prevented any significant buildup. In late 1993 and early 1994, sintering became a significant operating problem. The rate of sinter formation increased greatly when the unit was operated at higher bed levels. At these higher formation rates, sinters accumulated in the bed causing bed conditions to deteriorate. Uneven bed temperatures, decaying bed density, and a reduction in heat absorption are common symptoms of bed sintering.

Initial speculation as to the cause of high load sintering focused on the higher local heat release associated with higher loads and insufficient fuel splitting. Modifications were made to both the fuel nozzles and the fuel distribution baffles to improve mixing. However, no significant improvements were observed. The hypothesis that poor bed mixing and less than ideal fluidization were key contributors was subsequently developed. A series of performance tests were proposed to demonstrate that better mixing would significantly reduce sintering. Improvements in fluidization were achieved by reducing the size consist of the dolomite feed, thereby reducing bed size consist, while maintaining fluidizing velocity constant. The introduction of finely crushed dolomite (-12 mesh) versus the normal coarse crush (-6 mesh) significantly reduced sintering to the extent that full bed temperature of 1580°F could be maintained with no evidence of sintering.

The most severe incidents of sintering all occurred when feeding limestone. It is postulated that the reduced amount of MgO in the limestone may contribute to the uncontrolled sintering. The mechanism for this sintering is likely fluxing of the potassium-alumina-silicate clays in the coal ash by calcium from the sorbent. The nuclei of the sinters appear to be coal paste lumps which become sticky and collect bed ash on their surface. The coal then burns away, leaving the coal ash to react with the bed material. The less aggressive sintering with dolomite is explained by the fact that increased quantities of MgO tend to raise the melting temperatures of CaO-MgO-Al₂O₃ mixtures. In evaluating the sintering problem, it must be recognized that the extremely low ash fusion temperature of the Pittsburgh No. 8 coal burned at Tidd is likely a major contributing factor to sintering.

UNIT PERFORMANCE

Testing has progressed significantly since completion of the first three years of operation. The improved unit availability has provided the opportunity to conduct a greater number of varied performance tests than was previously possible. The most recent series of tests, were devised to address sintering issues by reducing the size consist of the bed. The finer sorbents, which were specified and purchased with a narrow size consist range, proved to be successful in addressing sintering while at the same time demonstrating exceptional improvement in the Ca/ S molar ratios.

The data clearly shows a significant improvement in sulfur capture resulting from the injection of finer dolomitic material as a the sorbent. The improvement in performance is significantly greater than can be explained solely by the larger sorbent exposed area due to the finer material. The noted improvement in performance must also be the result of significant improvements in bed fluidization and mixing. Especially when a number of

other recorded system parameters such as steam generation and bed/evaporator temperature profiles also point to enhanced bed dynamics.

Performance testing has been limited to approximately 115 inches due to summer limitations on the gas turbine. However, overall testing has provided a sufficient basis to confirm the correlations, previously developed at Grimethorpe, thereby permitting extrapolation of the data to varied temperatures, bed heights, and sulfur captures. Figures 2 and 3 show sorbent utilization (Ca/S) versus bed height for 90 and 95 percent sulfur capture.

The affect of sorbent feed size consist on sorbent utilization is clearly seen. Reducing sorbent size consist from coarse sorbent (-6 mesh) to finer sorbent (-12 to -20 mesh) results in significant increases in sorbent sulfation and therefore reduced sorbent feeds to achieve a predetermined level of sulfur capture. In addition to sorbent size consist effect on sorbent utilization, Figures 3 and 4 show the impact of sorbent reactivity. National Lime Carey dolomite (NL) has generally been demonstrated to be less reactive than the Plum Run Greenfield dolomite (PRG).

CONCLUSION

The Tidd PFBC Demonstration Plant has now achieved over 9921 hours of coal fired operation. Approximately 3865 hours, including the longest continuous run of 1070 hours, were achieved during the last ten months of operation. Unit availability during this period was approximately 52%.

A total of 62 performance tests have been conducted to date. Eleven tests were completed during the latest run. Test objectives during the run were aimed at reducing bed sintering and improving sorbent utilization. The tests were conducted using -12 to -20 mesh sorbent. The finer sorbent was expected to improve bed mixing and fluidization, thereby mitigating sintering and improving sorbent utilization. Bed conditions improved significantly and operation at 1580°F bed temperature was achieved with little, if any, bed sintering. Performance testing was completed at 1580°F, 115 inch bed level and 90% sulfur capture. The results showed a marked improvement in sorbent utilization, Ca/S molar ratios around 1.3 were indicated. This data extrapolates to Ca/S molar ratios, at full bed heights, of 1.2 and 1.5 for 90% and 95% sulfur capture respectively.

In addition to improved sorbent utilization, the unit demonstrated better heat transfer than had previously been achieved as well as a more homogeneous bed temperature distribution.

The reliability of PFBC has and continues to be demonstrated. The process, which was initially demonstrated in early operation, has been refined and optimized to the point where PFBC is competitive with all other technologies for both low and high sulfur coals. Expected enhancements of both systems and process are expected to further improve sorbent utilization and system performance beyond the levels already achieved while continuing to demonstrate the service life of both the gas turbine and the boiler tube bundle. The process has been demonstrated to be environmentally sound, cost effective, and capable of achieving the reliability and availability required in a power generating unit. Commercial deployment remains the only hurdle left to PFBC technology.

REFERENCES

1. D.A.Bauer, W.P.Reinhart, M.E.Zando, W.L.Irons. " Update on the Operation and Performance Testing of the Tidd PFBC Demonstration Plant", EPRI Fluidized Bed Combustion for Power Generation Conference, Atlanta (May,1994).
2. D.R.Haffer, et al " Test Results from the 70Mw Tidd PFBC Demonstration Plant," 12th Internl. Conference on Fluidized Bed Combustion, San Diego (May,1993).

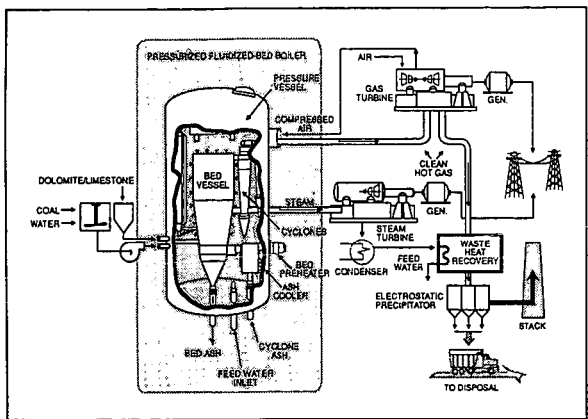


FIGURE 1 - TIDD PFBC COMBINED CYCLE

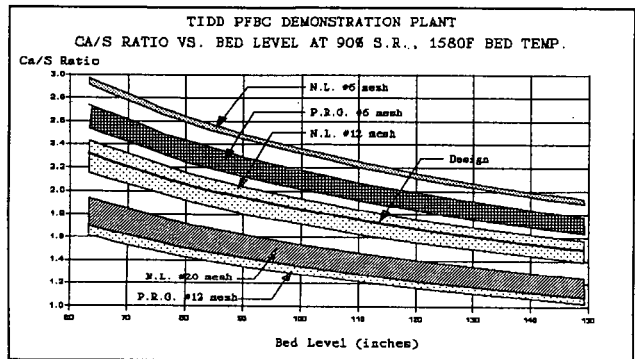


FIGURE 2

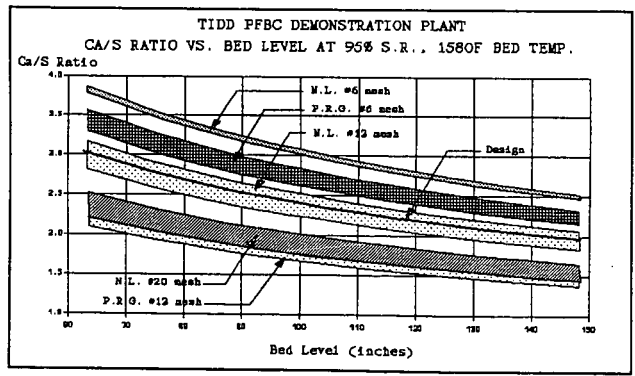


FIGURE 3

THE POWER SYSTEMS DEVELOPMENT FACILITY AT WILSONVILLE, ALABAMA

James R. Longanbach
U.S. Department of Energy
Morgantown, WV 26507-0800

Timothy E. Pinkston
Southern Company Services, Inc.
Birmingham, Alabama 35202

Keywords: Power, IGCC, PFBC, Filters, Fuel Cells

INTRODUCTION

One of the Morgantown Energy Technology Center's (METC's) goals is to: "Commercialize Advanced Power Systems with improved environmental performance, higher efficiency, and lower cost." Advanced coal-based power generation systems include Integrated Gasification Combined Cycle (IGCC), Pressurized Fluidized-Bed Combustion (PFBC), and Integrated Gasification/Fuel Cell systems. The strategy for achieving this goal includes: (1) Show the improved performance and lower cost of Advanced Power Systems through successful Clean Coal Technology demonstration projects, (2) Build and operate Technology Integration Sites in partnership with U.S. Industry (these sites will resolve key technology issues and effect continuous product improvement, and these partnerships result in leveraging of research and development (R&D) funds), and (3) Set up partnerships with other agencies and organizations such as Electric Power Research Institute (EPRI) to leverage R&D funds and skills.¹

Demonstration of practical high-temperature particulate control devices (PCD's) is crucial to the evolution of advanced, high-efficiency coal-based power generation systems. There are stringent particulate requirements for the fuel gas for both turbines and fuel cells. In turbines, the particulates cause erosion and chemical attack of the blade surfaces. In fuel cells, the particulates cause blinding of the electrodes. Filtration of the incoming, hot, pressurized gas is required to protect these units. Although filtration can presently be performed by first cooling the gas, the system efficiency is reduced. Development of high temperature, high pressure, is necessary to achieve high efficiency and extend the lifetime of downstream components to acceptable levels.

THE POWER SYSTEMS DEVELOPMENT FACILITY - A TECHNOLOGY INTEGRATION SITE

The Power Systems Development Facility (PSDF) combines a number of pilot-scale test facilities at a single site to reduce the overall capital and operating cost compared to individual stand-alone facilities. Combining all of these pilot-scale facilities in a new 60x100 foot structure and sharing resources common to different modules, such as coal preparation, are estimated to save nominally \$32 million over the cost of separate facilities. The PSDF will be located 40 miles southeast of Birmingham, Alabama, at Southern Company's Clean Coal Research Center in Wilsonville, Alabama.

The objective is to establish a flexible test facility that can be used to develop advanced power system components such as high-temperature, high-pressure particle control devices, evaluate advanced power system configurations, and assess the integration and control issues of these advanced power systems. The facility will also support the Department of Energy (DOE) Clean Coal Program.

The PSDF will consist of five modules. Two of the modules will produce particulate-laden gas, an Advanced Pressurized Fluidized-Bed Combustion (APFBC) module and an Advanced Gasifier module. The PCD's will be in a Hot-Gas Cleanup module, and there will also be a Compressor/Turbine module, and a Fuel Cell module. Four separate PCD technologies will be tested at the facility using the gas from the two gas-producing modules.

The PSDF project team is led by Southern Company Services (SCS) and is comprised of M. W. Kellogg, Foster Wheeler, Westinghouse, Allison, Southern Research Institute (SRI), and several developers of PCD's. The facility design reflects the Power System's R&D needs as identified by DOE and EPRI. The involvement of these diverse private sector organizations will ensure that the duration, scale, and results

of the PSDF test program will be sufficient to gain private sector acceptance.

THE ADVANCED GASIFIER

The advanced gasifier module uses M. W. Kellogg's transport reactor technology (Figure 1). The transport reactor was selected for the gas generator due to its flexibility to produce gas and particulates under either pressurized combustion (oxidizing) or gasification (reducing) conditions for parametric testing of PCD's over a wide range of operating temperatures, gas velocities, and particulate loadings.² The transport reactor is sized to process 1814 kg/hr (2 tons/hr) of coal to deliver .472 actual m³/s (1,000 acfm) of particulate laden gas to the PCD inlet over the temperature range of 538 to 982°C (1,000-1,800°F) at 1269-1951 kPa (184-283 psia). Two PCD's will be tested on the transport reactor, at alternate times. Short term (500 hour) parametric tests will be conducted using the transport reactor.

THE ADVANCED PRESSURIZED FLUIDIZED-BED COMBUSTION SYSTEM (PFBC)

The PFBC uses Foster Wheeler's second-generation PFBC technology (Figure 2).³ The advanced PFBC system consists of a pressurized 1172 kPa (170 psia) carbonizer at 871-982°C (1600-1800°F) to generate .708-.802 actual m³/s (1500-1700 acfm) of low-Btu fuel gas and a circulating pressurized fluidized-bed combustor (CPFBC), operating at 1034 kPa (150 psia) and 871°C (1600°F), which generates 2.93 actual m³/s (6,200 acfm) of combustion gas. The coal feed rate to the carbonizer will be 2495 kg/hr (2.75 tons/hr). A Ca/S molar ratio of 1.75 is required to capture 90 percent of the sulfur in the carbonizer/CPFBC. Char which is not converted to gas in the carbonizer is transferred hot to the CPFBC. The gases exiting from the carbonizer and the CPFBC will each be filtered hot in separate PCD's to remove particulates prior to entering the topping combustor.

THE TOPPING COMBUSTOR/GAS TURBINE

A topping combustor will be used to raise the inlet temperature of the gas turbine to 1288°C (2350°F) (Figure 3). The higher turbine inlet temperature will raise the net plant efficiency of advanced PFBC systems to 45 percent, while maintaining low levels of NOx. To withstand the expected severe conditions in the topping combustor application, a Multi-Annular Swirl Burner developed by Westinghouse has been chosen to combust the gases from the carbonizer and increase the temperature of the CPFBC flue gases, consistent with turbine inlet temperatures offered on advanced commercial high-efficiency turbines.⁴ At the PSDF, however, the topping combustor flue gas must then be cooled to 1077°C (1970°F) in order to meet the temperature limitation of the small, standard gas turbine (Allison Model 501-KM) which will be used to power both the air compressor and an electric generator to produce about 4 MW of electric power.

PARTICLE FILTERS

At the PSDF, PCD's will be tested at temperatures, pressures, and other gas conditions characteristic of a number of gasifiers and PFBC's.⁵ The critical issues include integration of the PCD's into the advanced power systems, on-line cleaning, chemical and thermal degradation of components, fatigue and other modes of physical failure, blinding, collection efficiency as a function of particle size, and scale-up issues.

The hot gases coming off the transport reactor, carbonizer, and CPFBC will be cleaned by different PCD's. The particulate control devices to clean gases from both the Foster Wheeler Carbonizer and Kellogg's transport reactor are the same size, to allow for the possibility of interchanging these three PCD's. One larger PCD will be tested on the combustion gases from the CPFBC.

A total of four PCD's from three developers have been selected for initial testing at the PSDF. Each of the PCD's is expected to maintain outlet particulate loadings of less than 20 ppmw with no more than 1 percent of the particles larger than 10 microns and no more than 10 percent of the particles larger than 5 microns to protect the gas turbine from erosion. The baseline pressure drop of the PCD's is expected to be less than 24.9 kPa (100 inches of water) with the maximum pressure drop less than 49.8 kPa (200 inches of water). The

commercial version of the PCD's should have a temperature drop of less than 5.6°C (10°F) but in the PSDF a target of 33°C (60°F) has been set because of the smaller size of the PCD's.

The two PCD's which will be tested initially on the transport reactor are described below. They will operate at .472 actual m³/s (1000 acfm) gas flow rates at 538-982°C (1000-1800°F), 1379-2068 kPa (200-300 psia), and 4000-16000 ppmw particle loading under both oxidizing and reducing conditions.

For one of the transport reactor/carbonizer filters, Westinghouse will use a vessel which can be fitted with ceramic candles, cross flow filters, CeraMem ceramic filters, or 3M ceramic bag filters in a tiered arrangement (Figure 4). The filter vessel will be a refractory-lined, coded, pressure vessel. The filters will be individual filter elements attached to a common plenum and discharge pipe to form clusters. Clusters of filters will be supported from a common high-alloy, uncooled, tubesheet. Each plenum of the filter will be cleaned from a single pulse nozzle. The number and size of the filters required will vary. For instance, 20 CeraMem filters or 80 candle filters would be needed.

The other filter on the transport reactor will be the Combustion Power Company granular-bed filter (Figure 5). The gas is introduced into the center of a downward moving-bed of granules, 6 mm spheres mostly made of aluminum oxide and mullite, which serve as the filter media to remove the particles from the gas. The gas reverses direction and moves counter current to the direction of the filter media to leave the pressure vessel. Clean media is constantly introduced from the top of the vessel. The particulate-containing media is removed from the bottom of the filter vessel and pneumatically conveyed and cleaned in a lift pipe. At the top of the lift pipe the particulate and clean media are separated in a disengagement vessel and the clean media is returned to the filter vessel. The transport gas and dust are cooled in a regenerative heat exchanger and the dust is removed in a baghouse. The transport gas is cooled in a water cooled heat exchanger and a mist eliminator, and then a boost blower is used to overcome the pressure drop in the system and the gas is reheated in the regenerative heat exchanger and recycled to the lift pipe.

Initial testing of a filter manufactured by Industrial Filter and Pump (IF&P) will be done on the PFBC carbonizer. The IF&P PCD will operate at .708-.802 actual m³/s (1500 - 1700 acfm) gas flow rates at 871-982°C (1600 - 1800°F), 1172 kPa (170 psia), and 11,000 ppmw particle loading. The IF&P filters are ceramic candles made of low density aluminosilicate fiber and silica with an alumina binder and have densified monolithic end caps and flanges. The tubesheet is made of the same densified material. The 152.4 cm (60 inch) diameter, refractory-lined filter vessel will contain 78 candles arranged in 6 groups of 13 each for pulse cleaning. Individual jet pulse nozzles are provided to each candle. An EnhancerTM consisting of an orifice-type device at the outlet of the candle increases the pulse intensity and also serves as a fail-safe plug in case of a candle failure.⁶

A larger Westinghouse filter will be tested on the PFBC combustor. The Westinghouse PCD will operate at 2.93 actual m³/s (6200 acfm) gas flow rate at 871°C (1600°F), 1034 kPa (150 psia), and 15,000 ppmw particle loading. This filter will contain six clusters of ceramic candles in a 3.11 m (10.2 foot) outside diameter, refractory-lined pressure vessel. Two clusters of filters are attached to a common plenum and discharge pipe and each cluster is cleaned from a single pulse nozzle source. The three plenums of filter clusters are arranged vertically in the filter vessel. The cluster concept allows replacement of individual filters and provides a modular approach to scale-up.

THE FUEL CELL

Plans are being made to eventually integrate a Fuel Cell module with the transport gasifier. Molten carbonate fuel cell and solid-oxide fuel cell concepts are under consideration for use at the PSDF. The capacity of the fuel cell to be tested initially is 100 kW. This will be accomplished by utilizing EPRI's 100 kW Fuel Cell Test Skid at the facility. Provision has been made in the site layout of the PSDF to phase in a multi-MW fuel cell module with commercial stacks utilizing more than 80 percent of gases from the transport gasifier. At a

multi-MW scale, testing can begin to address integration issues and overall plant performance for integrated gasification/fuel cell systems.

CURRENT STATUS OF THE PSDF

Environmental approvals for the PSDF were received in August 1993. Site preparation was completed in December 1993. All of the technologies have been selected and contracts have been signed. Detailed design is nearing completion and equipment fabrication is underway. Construction of the process tower began in mid November 1994.

SCHEDULE

The project will be completed in four Phases. Phase I, Conceptual Design, was completed in June 1992. Phase 2, Detailed Design, will be completed in the first quarter of 1995. Phase 3, Construction, began with site clearing in September 1993 after National Environmental Policy Act (NEPA) approval was obtained for the site. Construction of the transport reactor is scheduled for completion in September 1995 and for the APFBC in March of 1996. Phase 4, Operation, will begin as soon as shutdown and commissioning of each part of the facility is completed and will extend until December 1997 under the present agreement. A detailed test plan is being developed for the first operating phase. It is expected that additional operating phases will be funded, with the addition and/or substitution of other equipment and processes.

SUMMARY

The PSDF design incorporates advanced power system technology modules into integrated process paths. The size of the PSDF allows key component and system integration issues to be addressed at a reasonable engineering scale. Besides individual components testing, this design scheme allows testing and demonstration of integrated, advanced coal-based power generating systems. PCD's and components may be tested under long-term, realistic IGCC and advanced PFBC conditions.

Testing and development of components and systems under long-term, realistic conditions, are critical to the development of cleaner, more efficient, coal-fired power generating systems. The Power Systems Development Facility will play an important role in achieving these tests to support scale-up to demonstration plant sizes. This should have a significant impact on the design and cost of demonstration plants for the development of new technology in the future.

The result of this project will be a reduction or stabilization in the cost-of-electricity and a reduction in environmental emissions for new coal-based power plants.

REFERENCES

1. "METC Strategic Plan 1994," Morgantown Energy Technology Center, August 24, 1994.
2. Gbordzoe, E.A., Henningsen, G. B., and Campbell, W. M., "Development of a Pressurized Transport Gasifier by the M. W. Kellogg Company," Presented at the Ninth Annual Pittsburgh Coal Conference, Pittsburgh, PA, October 12-16, 1992.
3. McClung, James D., Froehlich, Robert E., Quandt, Michael T., "Design Update for an Advanced PFBC Facility at Wilsonville," Presented at the 1993 International Joint Power Generation Conference and Exposition, Kansas City, MO, October 17-22, 1993.
4. McClung, J. D., Kastner, C., Dellefield, R., and Sears, R., "Design and Operating Philosophy for an Advanced PFBC Facility at Wilsonville," Presented at the 12th International Conference on Fluidized-Bed Combustion, San Diego, CA, May 9-13, 1993.
5. Haq, Z. U., Pinkston, T. E., Sears, R. E., and Vimalchand, P., "The DOE/SCS Power Systems Development Facility," Presented at the Twelfth Electric Power Research Institute Annual Conference

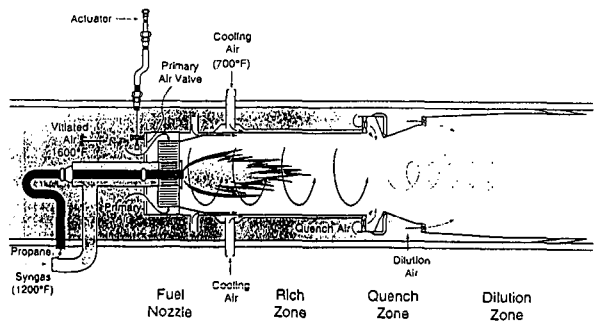
6. Moore, D. L., Vimalchand, R., Haq, Z. U., McClung, J. D., and Quandt, M. T., "PFBC Perspectives at the Power Systems Development Facility," Presented at the Electric Power Research Institute's Conference on Fluidized-Bed Combustion for Power Generation, Atlanta, GA, May 17-19, 1994.

The diagram illustrates a PFBC system with a gas turbine and a separate gas turbine cycle. The main components and their connections are as follows:

- Transport Reactor:** Receives **Feed Gas** and **Coal**. It is equipped with a **Start-up Heater** and **Air** input. The reactor output goes to a **Screw Cooler**.
- Screw Cooler:** Cools the reactor output, which then enters a **Gas Turbine** (labeled '1').
- Gas Turbine (1):** Produces **Exhaust Gas**, which is directed to a **Cyclone**.
- Cyclone:** Separates the exhaust gas into **Spilling Gas** (which returns to the reactor) and **Quench** (which goes to a **Gas Cooler**).
- Gas Cooler:** Cools the quench gas, which then enters a **Thermal Oxidizer**.
- Thermal Oxidizer:** Treats the quench gas, with **Air** input. The output goes to a **Pressure Letdown** valve.
- Pressure Letdown:** Reduces the pressure of the gas before it enters a **Stack**.
- Stack:** Releases the **Exhaust Gas** from the thermal oxidizer.
- Separate Gas Turbine Cycle:**
 - Nitrogen Quench:** Provides **Quench** to a **Gas Cooler**.
 - Gas Cooler:** Cools the nitrogen quench gas, which then enters a **Gas Turbine** (labeled '2').
 - Gas Turbine (2):** Produces **Exhaust Gas**, which is directed to a **Cyclone**.
 - Cyclone:** Separates the exhaust gas into **Spilling Gas** (which returns to the reactor) and **Quench** (which goes to a **Gas Cooler**).
 - Gas Cooler:** Cools the quench gas, which then enters a **Thermal Oxidizer**.
 - Thermal Oxidizer:** Treats the quench gas, with **Air** input. The output goes to a **Pressure Letdown** valve.
 - Pressure Letdown:** Reduces the pressure of the gas before it enters a **Stack**.
 - Stack:** Releases the **Exhaust Gas** from the thermal oxidizer.

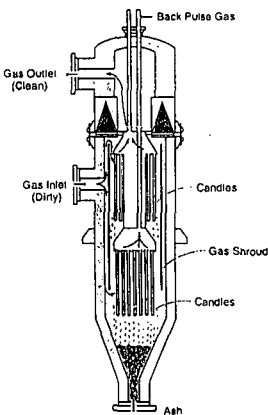
[illegible]

FIGURE 3. TOPPING COMBUSTOR



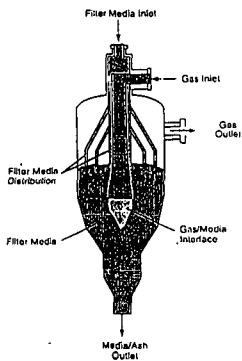
MS5000630W

FIGURE 4. CANDLE FILTER



MS5000627W

FIGURE 5. GRANULAR BED FILTER



MS5000631W

Preparation and Modification of Recoverable Particle Catalysts for Coal Liquefaction

Isao Mochida, Kinya Sakanishi, Hideki Taniguchi, Haru-umi Hasuo,
and Osamu Okuma^{*)}

Institute of Advanced Material Study, Kyushu University,
Kasuga, Fukuoka 816, Japan

^{*)}Polymer & Chemical Technology Lab., Kobe Steel, Ltd.,
Kobe, Hyogo 651-22, Japan

INTRODUCTION

Highly active catalyst of higher activity is still a key to design the more efficient coal liquefaction process, which will increase the oil yield, minimize its cost, and environmental impact due to catalyst disposal.

The authors assumed that the recovery and recycle of the catalyst from the residue are an approach to improve the economy of coal liquefaction and to reduce the solid waste.^{1,2} The organic residue has been recycled with the catalyst and minerals to the primary liquefaction stage as the bottom recycle. Its favorable results have been reported, although the accumulation of the inorganic solid requires a fixed rate of purging the catalyst as well as minerals.

The authors have examined Fe_3Al , strong ferromagnetic particles, as one of the potentially recoverable catalysts^{1,2}, in order to prepare an active catalyst with the recovery function through magnetic separation.

Ketjen Black(KB) particles have hollow spheric structure which carries their extremely high surface area and for high dispersion of catalytic species and low specific gravity for catalyst recovery through the gravimetric separation. The activity of carbon particles and their supporting NiMo catalysts have been reported,^{3,5} to exhibit the high activity for the hydrogen transferring cracking, hydrosulfurization and hydrocracking. KB-supported NiMo catalyst is expected to be one of the most promising catalysts to exhibit a large activity for hydrogenation and liquefaction at its least catalyst amount. To achieve the successful reuse of recovered catalyst, the deactivation, contamination, and adhesion of the catalyst should be avoided by designing the liquefaction and distillation schemes. The pretreatment and hydrogen transferring liquefaction prior to the catalytic steps are responsible to define the forms of minerals and to reduce the coke precursors^{6,8}. Separation of the catalyst should assure its dispersed state.

In the present study, two types of recoverable catalysts were examined in terms of catalytic activities for the liquefactions of Wyoming coal (USA) and Tanitohalm coal (Indonesia). Optimization of reaction conditions and design of recovery procedures were studied in order to practice recovery and recycle of the catalysts in the liquefaction of both coals as well as to increase the oil yield with the least yield of organic residue.

EXPERIMENTAL

Some properties of Ketjen Black(KB) EC and JD, and Fe₃Al examined in the present study are summarized in Table 1. Ni, Mo-supported KB catalysts (NiMo/KB) were prepared by impregnation method from Ni(NO₃)₂ or Ni(OAc)₂ and (NH₄)₆Mo₇O₂₄ or Mo dioxyacetylacetonate (MoO₂-AA) in their water or methanol solutions, respectively. The catalyst precursors were dried at 120°C for 12 h in vacuo and presulfided in 5% H₂S/H₂ flow at 360°C for 2 or 3 h prior to the reactions. KB was pretreated in conc. nitric acid at 80°C for 1 h followed by filtration, repeated washing with water, and drying at 120°C in vacuo. The nitric acid-treated KB JD was abbreviated as KB JD-O.

Synthetic pyrite powder and KF842 (NiMo/Al₂O₃, pellet or its powder (<60 mesh)) provided by NEDO and Nippon Ketjen Co., respectively were also used as the reference catalysts for the comparison. These catalysts and Fe₃Al particles were also presulfided under the same conditions as KB-based catalysts.

The elemental analyses of Wyoming and Tanitohalm coals are summarized in Table 2. Tetralin (TL) of commercial guaranteed grade was used as a liquefaction (hydrogen donating) solvent. The liquefaction was carried out in an autoclave of 50 ml capacity (11 or 20°C/min) at the prescribed temperatures(380 - 460°C). The coal (3.0 g), the solvent (4.5 g) and catalyst (0.09 - 0.10 g) were charged into the autoclave, which was then pressurized with hydrogen to 6~9.3 MPa at room temperature after replacing the air with nitrogen gas. After the reaction, the product remaining in the autoclave was recovered with THF, and extracted in sequence with hexane, acetone and THF after evaporating THF. The hexane soluble (HS), hexane insoluble-acetone soluble (HI-AS), acetone insoluble-THF soluble (AcI-THFS), and THF insoluble (THFI) substances were defined as oil(O), asphaltene(A), preasphaltene(PA), and residue(R), respectively. The gas yield was calculated by the difference between weights of the initial coal and recovered product.

RESULTS AND DISCUSSIONS

Liquefaction of Wyoming Coal with KB-supported NiMo Catalyst

Figure 1 illustrates the effects of reaction temperatures on the liquefaction of Wyoming coal with KB-ED-supported NiMo catalyst under initial H₂ pressure of 6.6 MPa at 380 - 460°C. The oil yield increased with reaction temperature in the range of 380 - 440°C, reaching the maximum oil yield of 40 % at 440°C, and then decreased at 460°C with a significant increase of gas yield.

Figure 2 shows the comparative activity of the KB JD-O-supported NiMo catalyst prepared by the successive impregnation method with the commercial NiMo/Al₂O₃ catalyst and synthesized pyrite for the liquefaction of Wyoming coal at 440°C for 20 min. The KB-supported NiMo catalyst gave the higher oil and asphaltene yields with less yields of preasphaltene and residue. The commercial NiMo and pyrite catalysts provided the lower oil plus asphaltene yields with higher gas and preasphaltene yields and higher asphaltene yield, respectively.

Liquefaction of Tanitohalm Coal with Recoverable Catalysts

Figures 3 and 4 compare liquefaction results of Tanitohalm coal without and with sulfided Fe_3Al ($\text{Fe}_3\text{Al-S}$), NiMo/KB-JD , and synthetic pyrite at 450°C for 60 min under the initial H_2 pressures of 6.0 and 9.3 MPa, respectively. The sulfided NiMo/KB-JD catalyst exhibited the highest activity for the much higher oil yield over 60 % under the higher hydrogen pressure. It is noted that the much lower yields of preasphaltene and residue were obtained in the liquefaction of Tanitohalm coal compared to those of Wyoming coal. The pyrite showed the similar activity as NiMo/KB-JD under the lower hydrogen pressure, although it failed in increasing the oil yield under the higher hydrogen pressure. Sulfided Fe_3Al particles do not essentially show any activity even after the grinding to smaller particle size under the present reaction conditions.

Figures 5 and 6 illustrate the liquefaction of Tanitohalm coal with NiMo/KB-JD catalyst at $380 - 450^\circ\text{C}$ under the initial H_2 pressures of 6.0 and 9.3 MPa, respectively. The oil yield increased very much with reaction temperatures under the higher hydrogen pressure, reaching the maximum yield of 62% with least yields of preasphaltene and residue. In contrast, the oil yield appeared to be saturated around 45% in the temperature range of $420 - 450^\circ\text{C}$, while the yields of asphaltene, preasphaltene and residue decreased and the gas yield increased sharply.

Recovery and repeated use of recoverable catalysts

The magnetically recoverable Fe_3Al particles were found to be more easily recovered from the whole liquefaction product than from the THFI residue, because the mineral matters and organic residue in THFI were strongly adhered together to include the catalyst in the grains, making it difficult to recover the catalyst separately.

Ketjen black supporting catalysts were found to be recovered from the whole product by gravimetric floatation technique using methanol, hexane and water in this order, although the weight of recovered catalyst was gained to some extent probably due to the inclusion of organic materials on the catalyst.

The KB-supported catalyst and Fe_3Al were found recoverable after the liquefaction, although some carbon adhesion took place. The KB-supported catalyst exhibited an excellent activity for the coal liquefaction. Addition of acidic properties may provide higher activity for the asphaltene conversion. Fe_3Al is found to have very small activity. Its application as the catalyst support can be examined.

The multi-stage approach consisting of coal pretreatment, solvent-mediated dissolution, and catalytic hydrocracking steps should be further developed to suppress the catalyst deactivation.

References

- 1) Mochida, I., Sakanishi, K., Kishino, M., Honda, K., Umezawa, T., Yoon, S.H., ACS Div. Fuel Chem., 1993, 38(1), 93.
- 2) Mochida, I., Sakanishi, K., Sakata, R., Honda, K., Umezawa, T., Energy & Fuels, 1994, 8, 25.
- 3) Derbyshire, F.J., DeBeer, V.H.J., Abotsi, G.M.K., Scaroni, A.W., Solar, J.M., Skrovanok, D.J., Appl. Catal., 1986, 27, 117.
- 4) Farcasiu, M., Smith, C., Energy & Fuels, 1991, 5, 83.
- 5) Duchet, J.C., van Oers, E.M., de Beer, V.H.J., Prins, R., J. Catal., 1983, 80, 386-402.
- 6) Mochida, I., Yufu, A., Sakanishi, K., Korai, Y., Fuel, 1988, 67, 114.
- 7) Mochida, I., Kishino, M., Korai, Y., Sakanishi, K., J. Fuel Soc. Jpn., 1986, 65, 828.
- 8) Mochida, I., Sakata, R., Sakanishi, K., Fuel 1989, 68, 306.

Table 1 Some properties of KB carbon blacks and Fe₃Al particles

Samples	Particle size (μm)	Surface area (m^2/g)	Specific gravity (-, $\text{H}_2\text{O}=1$)
Fe ₃ Al	7.2(<500 mesh)	0.5	6.5 - 7.9
KB-EC	30×10^{-3}	800	0.145
KB-JD	30×10^{-3}	1270	0.115

Table 2 Elemental analyses of coals

	wt%, daf basis				H/C	Ash
	C	H	N	(O+S)	(-)	(wt%)
Wyoming	68.9	5.4	1.0	24.7	0.94	3.7
Tanitohalm	75.9	5.6	1.5	17.1	0.87	4.8

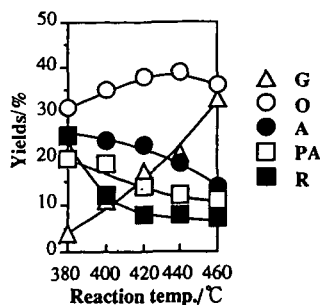


Fig.1 Effect of reaction temperature on the liquefaction of Wyoming coal.

solvent(Tetralin)/coal=1.5

reaction time : 40min

H₂ initial pressure : 6.6MPa

catalyst : Ni-Mo/KB EC(Ni2wt%,Mo10wt%/simultaneous impregnation from Ni(NO₃)₂ and (NH₄)₆Mo₇O₂₄)

3%addition based on coal presulfided at 360°C for 3h

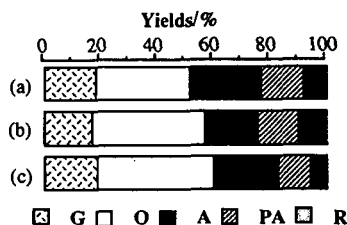


Fig.2 Effect of catalysts species on the liquefaction of Wyoming coal at 440°C

(a) Synthesized FeS₂

(b) Commercial Ni-Mo/Al₂O₃

(Ni:3wt%,Mo:15wt%)

(c)Ni-Mo/KB JD-O(MoO₂-AA, Ni(OAc)₂

successive impregnation)

reaction temperature : 440°C

reaction time : 20min

(Other conditions are same as Fig.1)

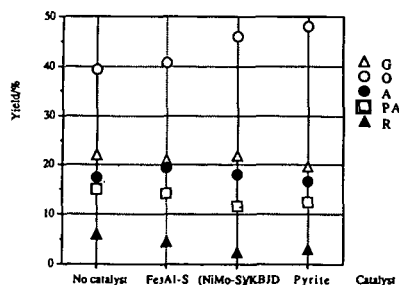


Fig. 3 Activity of catalysts for the liquefaction of Tanitohalm coal under lower H₂ pressure

solvent(Tetralin)/coal(Tanitohalm)=1.5

Reaction time 60min, Reaction temp. 450°C

Heating rate 20°C/min, H₂ initial press. 6.0MPa

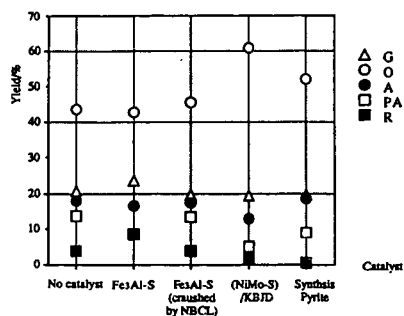


Fig. 4 Activity of catalysts for the liquefaction of Tanitohalm coal under higher H₂ pressure
 solvent(Tetralin)/coal(Tanitohalm)=1.5
 Reaction time 60min, Reaction temp. 450°C
 Heating rate 20°C/min, H₂ initial press. 9.3MPa

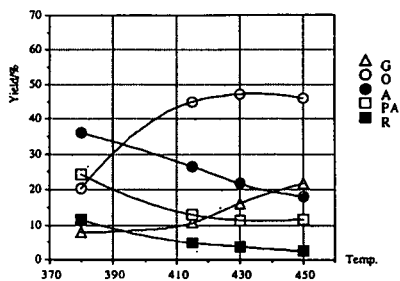


Fig. 5 Effect of reaction temperature on the liquefaction of Tanitohalm coal under lower H₂ pressure
 solvent(Tetralin)/coal(Tanitohalm)=1.5
 Reaction time 60min, Heating rate 20°C/min
 H₂ initial press. 6.0MPa
 catalyst:NiMo/KB JD(Ni:2wt%, Mo10wt%)
 3wt% addition based on coal presulfided at 360°C for 2h

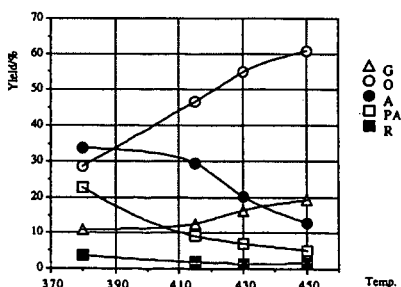


Fig. 6 Effect of reaction temperatures on the liquefaction of Tanitohalm coal under higher H₂ pressure
 solvent/coal=1.5
 Reaction time 60min, Heating rate 20°C/min
 H₂ initial press. 9.3MPa
 catalyst:NiMo/KB JD(Ni:2wt%, Mo10wt%)
 3wt% addition based on coal presulfided at 360°C for 2h

COMPARISON OF THE ACTIVITIES OF FINE-PARTICLE SIZE CATALYSTS*

Frances V. Stohl, Kathleen V. Diegert, David C. Goodnow
Process Research Department 6212
Sandia National Laboratories
P.O. Box 5800
Albuquerque, NM 87185-0709

ABSTRACT

The objectives of Sandia's fine-particle size catalyst testing project are to evaluate and compare the activities of the fine-particle size catalysts being developed in DOE/PETC's Advanced Research Coal Liquefaction Program by using standard coal liquefaction test procedures. The standard procedures use Blind Canyon coal, phenanthrene as the reaction solvent, and a factorial experimental design with temperatures from 350°C to 400°C, reaction times from 20 to 60 minutes, and catalyst loadings up to 1 wt%. Catalytic activity is measured in terms of tetrahydrofuran conversion, heptane conversion, the amount of 9,10-dihydrophenanthrene in the product, and the gas yield. Several catalysts have been evaluated including a commercially available pyrite, a sulfated iron oxide from the University of Pittsburgh, and several preparations of 6-line ferrihydrites from Pacific Northwest Laboratories. Results have demonstrated that significant differences in activity can be detected among these catalysts.

INTRODUCTION

There are several potential advantages of using cheap, unsupported, fine-particle size (<40 nm) catalysts in direct coal liquefaction. These include improved coal/catalyst contact due to good dispersion⁽¹⁾ of the catalyst, and the potential for using low quantities of catalyst (<0.5% based on the weight of coal) because of their very high surface areas. These catalysts could be combined with the coal as either active catalysts or catalyst precursors that would be activated in situ. Research efforts that have been performed to develop fine-particle size, unsupported catalysts for direct coal liquefaction⁽²⁾ indicate that the use of these catalysts could result in significant process improvements, such as enhanced yields of desired products, less usage of supported catalyst, and possibly lower reaction severities. These improvements would result in decreased costs for coal liquefaction products.

The Advanced Research (AR) Coal Liquefaction Program, which is managed by the United States Department of Energy's Pittsburgh Energy Technology Center (PETC), is funding numerous research efforts aimed at developing these types of catalysts for direct liquefaction. Although most catalyst developers have the capability of testing the performances of the catalysts they develop, it is difficult if not impossible to compare results among researchers because of the different testing procedures used. Therefore, to guide the research and development efforts for these fine-particle size, unsupported catalysts, it is necessary to evaluate each catalyst's performance under standard test conditions so that the effects of catalyst formulations from different laboratories can be compared.

The objectives of this project are to develop standard coal liquefaction test procedures, to perform the testing of the novel fine-particle size liquefaction catalysts being developed in the PETC AR Coal Liquefaction program, and to evaluate reaction mechanisms. Previously reported work^(3,4) described the reaction procedures, product workups, and the factorial experimental design to be used in this project as well as results obtained by testing a commercially available pyrite and the University of Pittsburgh's sulfated iron oxide catalyst. This paper will describe the recent results obtained from evaluating a Pacific Northwest Laboratories' (PNL) catalyst.

EXPERIMENTAL SECTION

Materials. The coal being used in this project is the DECS-17 Blind Canyon Coal obtained from The Penn State Coal Sample Bank. It is a high volatile A bituminous coal with 0.36% iron, 0.02% pyritic sulfur, and 7.34% mineral matter (on a dry basis). The particle size is -60 mesh. Phenanthrene is used as the reaction solvent. Elemental sulfur was added to the reactors to sulfide the catalyst precursors.

Microautoclave Reactors. The testing is performed using batch microautoclaves made of type 316 stainless steel components. The total volume of a reactor is 43 cm³ with a liquid capacity of 8 cm³. The reactors are loaded with 1.67g coal and 3.34g reaction solvent. If the reaction is catalytic, the catalyst loading will be either 0.5 wt% or 1.0 wt% on an as-received coal basis. The amount of sulfur addition is specified by the catalyst developer. The reactors are charged to 800 psig H₂ (cold charge) and heated to reaction temperatures in fluidized-sand baths. Temperatures, pressures and times are recorded with a digital data acquisition system every 30 seconds during the course of the reactions. Following the heating period, the reactors are rapidly cooled to ambient temperature in a water bath and a gas sample is collected. The reaction data is analyzed to determine the actual reaction time and the averages and standard deviations for reaction temperature and pressure. Heat-up times and cooling times are also determined.

Product Workup Procedures. The reaction products are rinsed out of the reactors with tetrahydrofuran (THF). THF and heptane solvent solubilities are measured using a Millipore 142 mm diameter pressure filtration device with air pressurization and Duropore (0.45 micron) filter paper. The filter cakes are rinsed twice with THF or heptane as appropriate. After the filtrations are complete, the filter papers are dried under vacuum at 70°C, cooled to room temperature and weighed to determine the insoluble portions. The THF soluble material is quantitatively sampled for gas chromatographic (GC) analysis, which is used to determine the reaction solvent recovery and composition. The THF is removed from the solubles by rotary evaporation prior to determining the heptane conversion. The quantity of gases (CO, CO₂, CH₄, C₂H₆) produced in a reaction is calculated using the postreaction vessel temperature and pressure with the ideal gas law and the mole percents in the gas sample as determined using a Carle GC and standard gas mixtures.

Factorial Experimental Design and Analysis. The factorial experimental design (Figure 1) evaluates the effects of three variables at two levels: temperature (350 and 400°C), time (20 and 60 minutes), and catalyst loading (0 and 1 wt% based on as-received coal). With this full factorial experimental design, the experimental results are evaluated for all combinations of levels of the three variables so that 2³ evaluations are required. Additional reactions are also performed at the center point of this cubic design. An Analysis of Variance (ANOVA) is performed to estimate the effects of the experimental variables and to statistically test their significance. Replication of the experiments is used to estimate measurement error and to reduce its effect on the estimated effects of the variables. Models are constructed using the estimates of the effects of the variables to calculate the expected experimental results for specified sets of reaction conditions⁹. The controlled factors used in the ANOVA are the measured average reaction temperature, measured reaction time, and the actual weight of catalyst used.

Catalyst. J. Linehan (PNL) supplied Sandia with the -325 mesh fraction of a 6-line ferrihydrite catalyst precursor for evaluation using the full factorial experimental design. No pretreatment was required. Linehan recommended testing this material with a 1:1 sulfur to catalyst precursor ratio on a weight basis. All reactions including thermal reactions had the same amount of added sulfur, so the impact of sulfur could be determined.

RESULTS and DISCUSSION

Experimental Results of Testing PNL's 6-Line Ferrihydrite Catalyst

The testing of PNL's 6-line ferrihydrite catalyst precursor plus sulfur was performed by two operators: operator 1 (a previous operator) and operator 2 (the current operator). The measured experimental results obtained by operator 2 using the full factorial experimental design are given in Table 1. The reproducibility of the measured THF conversions is good for most of the data. However, results at 350°C for 60 minutes show high variability. These reaction products were significantly more difficult to filter than those from other conditions; the reason for this is unknown. Negative values for heptane conversion occur because the values are very close to zero, and the variability is high.

Modeling of Experimental Results

Results of the statistical analyses of the data in Table 1 are given in Tables 2 and 3. These tables show calculated estimates of the effects of the variables and the interactions among variables over the region bounded by the cubic design, calculated estimates of the mean values of the reaction results at the nine sets of reaction conditions, standard errors of the estimates, the means of the measured values in Table 1, and R² values for the fit of the model to the data. The constant represents the estimate of the reaction results when all variables are at their low levels: temperature=350°C, time=20 minutes, and catalyst loading=0%. The variables with statistically significant effects are listed under the constant; the larger the estimated value, the greater the effect. The estimate of experimental error, which is presented as a standard deviation, accounts for all variability in the data not accounted for by the fixed and random effects of the model. Included in this estimate are variabilities due to measurement, process and material inconsistencies, and modeling inadequacies. The estimates of reaction results at the nine sets of reaction conditions are calculated from the model and can be compared to the means of the measured values. The standard errors of the estimated results at cube corners are derived from the experimental error, which pertains to a single measurement.

The results of the modeling show that temperature has the largest effect on both the THF (33.6%) and heptane (17.5%) conversions. The catalyst has the second largest effect on THF conversion (16.6%) but no significant effect on heptane conversion. The lack of catalytic effect on heptane conversion was also observed when pyrite and the University of Pittsburgh's catalyst were evaluated.^{3,4} The other significant parameters for THF conversion are time (11.5%) and the temperature-catalyst interaction (9.3%). For heptane conversion the other significant parameters are the time-temperature interaction (7.5%) and time (2.8%). The significant effects for gas yield are temperature (0.91%), the time-temperature interaction (0.43%) and time (0.23%). The 9,10-dihydrophenanthrene (DHP), which was formed by hydrogenation of phenanthrene, in the reaction product has the most complicated model with six parameters having significant effects: temperature-catalyst interaction (2.83%), time-catalyst interaction (2.39%), temperature (1.03%), catalyst (0.85%), time-temperature interaction (0.52%), and time (0.40%). The R-square values for the fit of the models were 0.94 for THF conversion and 0.96 for the other three models.

Procedure for Estimating Experimental Results from the Linear Model. To use one of the linear models in Tables 2 or 3 to determine an estimate for an experimental result within the cube, first calculate proportional levels for each variable that has a significant effect. For example, to calculate THF conversion for a reaction at 375°C for 40 minutes with 0.5% catalyst:

$$PTIME = (40 \text{ min} - 20 \text{ min}) / (60 \text{ min} - 20 \text{ min}) = 0.5$$

$$PTEMP = (375^\circ\text{C} - 350^\circ\text{C}) / (400^\circ\text{C} - 350^\circ\text{C}) = 0.5$$

$$PCAT = (0.5 \text{ wt}\% - 0 \text{ wt}\%) / (1.0 \text{ wt}\% - 0 \text{ wt}\%) = 0.5$$

These calculated p's are used in the following equation (see Table 2):

$$K + PTIME^a + PTEMP^b + PCAT^c + PTEMP^d PCAT^d$$

where K is the estimated constant (18.5%), a is the estimated time effect (11.5%), b is the estimated temperature effect (33.6%), c is the estimated catalytic effect (16.6%) and d is the estimated temperature-catalyst interaction (9.3%). The calculated THF conversion is 51.7, which agrees within round off errors with the value in Table 2. For calculating a result for any point within the region

bounded by the cube, the p values will range from 0 to 1. Extrapolation beyond the limits of the cube is usually not recommended.

Evaluation of Operator Effects

To compare results from the University of Pittsburgh's catalyst and PNL's catalyst, it is necessary to evaluate operator effects. The testing of PNL's catalyst using the full experimental design (Table 1) was performed by operator 2, whereas operator 1 performed the evaluation of the University of Pittsburgh's catalyst as well as a limited number of reactions on PNL's catalyst. The experiments performed by each operator on PNL's catalyst are shown in Table 4. A statistical analysis of the THF conversion results for operator 2 (Table 1) showed that a model (Table 2) with significant effects for temperature, catalyst, time and the temperature-catalyst interaction fit the data well ($R^2=0.94$). To compare the results from the two operators, operator 2's data for reactions at 350°C for 20 minutes were not used because operator 1 had not performed these reactions. Results of the comparison are shown in Table 5. The values in Table 5 for the model of THF conversion obtained by operator 2 are slightly different from those in Table 2 because Table 2's results included reactions performed at 350°C for 20 minutes.

Comparison of the constants for the two operators shows that there are significant differences in THF conversions at 350°C for 20 minutes without catalyst. Using these two models to calculate THF conversion at 375°C for 40 minutes with 0.5% catalyst (the center point of the experimental design) gave 56.7% for operator 1 and 49.9% for operator 2. Calculating results at 400°C for 60 minutes with 1wt% catalyst gave a THF conversion of 88.4% for operator 1 and a similar value of 87.5% for operator 2. Comparison of these three sets of calculated results shows that the biggest differences between the two operators were at the lowest severity conditions. Because of these differences, only the high severity results are compared in Table 6. The estimates of error variability (within their respective data sets) were comparable for the two operators. Similar conclusions were obtained for comparison of heptane conversion results between the two operators. Operator 1 had higher conversions than operator 2, particularly at low temperature. Unfortunately, a model for heptane conversion could not be fit for operator 1 results, because the time-temperature interaction is important for heptane conversion, and operator 1 did not perform tests at 350°C for 20 minutes.

Comparison of Catalysts

A comparison of results (Table 6) from PNL's catalyst with results from the University of Pittsburgh's catalyst and pyrite at the higher severity conditions indicates that PNL's catalyst is the most active. THF results show that PNL's catalyst increases conversion by 25.8% over its thermal baseline with 1% sulfur addition. The University of Pittsburgh's catalyst and pyrite increase conversion above their respective baseline values by 19.3% and 18.5% respectively. Comparison of the three baseline results shows that sulfur addition has an effect on THF conversion. Therefore, the best comparison among these three catalysts is obtained by using the thermal baseline without sulfur addition (54.9%). Using this baseline gives 34.5% total conversion for PNL's catalyst, 27.4% conversion for the University of Pittsburgh's catalyst and 18.5% for pyrite.

The model for the amount of DHP (Table 3) in the recovered reaction solvent from experiments performed with PNL's catalyst involved the three main effects (time, temperature, catalyst) as well as the three two-way interactions (time-temperature, time-catalyst, temperature-catalyst). This model is somewhat simpler than those obtained for pyrite and the University of Pittsburgh's catalyst, because it doesn't have the three-way interaction. The amount of DHP present in the product from the 400°C reaction for 60 minutes with PNL's catalyst was 8.41%. The University of Pittsburgh's catalyst yielded 5.35% DHP and pyrite yielded 3.88%. These results indicate that PNL's catalyst has the highest hydrogenation activity.

CONCLUSIONS

Results of the evaluation of PNL's 6-line ferrihydrite with 1 wt% sulfur addition have shown that it is more active than either the University of Pittsburgh's sulfated iron oxide with 2 wt% sulfur addition or pyrite. At 400°C for 60 minutes, THF conversion obtained with PNL's catalyst was 89.4% versus 82.3% with the University of Pittsburgh's catalyst, and 73.4% with pyrite. Analyses of DHP in the reaction products show that PNL's catalyst has the highest hydrogenation activity. PNL's catalyst gave 8.41% DHP, versus 5.35% for the University of Pittsburgh's catalyst, and 3.88% for pyrite. There were no catalytic effects for either heptane conversion or gas yield. Future work will involve testing additional catalysts being developed in DOE/PETC's program and evaluating better analytical methods for determining product quality.

ACKNOWLEDGEMENT: This work was supported by the U.S. Department of Energy at Sandia National Laboratories under contract DE-AC04-94-AL85000.

REFERENCES

1. Huffman, G. P.; Ganguly, B.; Zhao, J.; Rao, K. R. P. M.; Shah, N.; Feng, Z.; Huggins, F. E.; Taghiei, M. M.; Lu, F.; Wender, I.; Pradhan, V. R.; Tierney, J. W.; Seehra, M. S.; Ibrahim, M. M.; Shabtai, J.; Eyring, E. M.; *Energy Fuels* 1993, 7, 285-296.
2. Pradhan, V. R.; Tierney, J. W.; Wender, I.; *Energy & Fuels* 1991, 5, 497-507.
3. Stohl, F. V.; Diegert, K. V.; *Energy & Fuels* 1994, 8, 117-123.
4. Stohl, F. V.; Diegert, K. V.; Gugliotta, T. P.; *Proc. Coal Liquefaction and Gas Conversion Contractors' Review Conf.*, September 27-29, 1993, Pittsburgh, PA. p. 123-135.
5. John, P. W. M.; *Statistical Design and Analyses of Experiments*; MacMillan Co., New York, 1971.

Figure 1. Factorial experimental design (temperature = °C, time = minutes, catalyst loading = wt% of as-received coal).

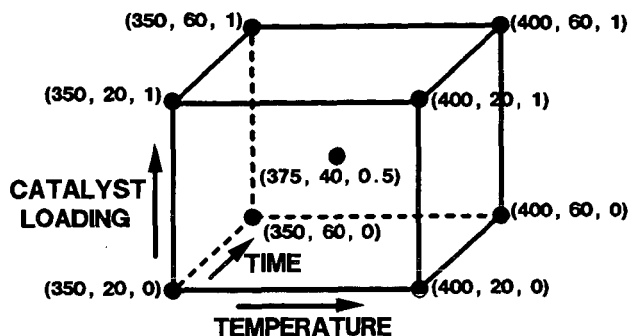


Table 1. Measured experimental results from operator 2.

TEMP. (°C)	TIME (min)	CAT. (mg)	THF Conv. (%)	Heptane Conv. (%)	Gas (%dmmf)	DHP (%)*
350.9	20.5	0	21.86	-2.63	0.34	0.33
349.4	20.5	0	17.28	-4.92	0.30	NA**
350.4	20.5	0	21.14	-1.56	0.25	NA
350.2	60.5	0	26.39	2.47	0.60	0.63
350.2	60.7	0	31.49	1.69	0.52	0.72
350.5	60.5	0	23.31	-2.15	0.44	0.60
349.9	59.0	0	26.98	1.43	NA	0.54
400.0	20.5	0	50.06	14.05	1.23	1.09
399.8	20.5	0	47.33	13.00	1.16	1.05
400.1	60.5	0	63.86	23.40	1.98	2.27
399.7	60.5	0	61.69	NA	1.82	2.36
375.1	40.5	8.4	63.52	7.90	0.83	3.97
374.8	40.5	8.6	56.89	8.59	0.78	4.00
374.8	40.5	8.1	62.12	5.19	0.76	3.78
375.1	41.0	8.3	57.11	8.02	0.75	2.96
375.4	40.5	8.4	54.24	8.48	0.78	3.67
350.5	20.5	16.6	35.01	0.56	0.31	1.04
351.2	20.5	17.2	32.04	-3.15	0.29	0.95
350.0	61.5	17.4	53.57	-1.09	0.54	4.10
350.2	61.0	16.8	52.96	3.22	0.56	4.30
351.2	60.5	17.3	38.82	0.10	0.48	4.03
350.0	61.0	17.0	42.26	-3.34	0.49	4.46
399.7	20.5	16.7	72.80	16.92	1.11	5.04
400.2	20.5	17.0	75.90	16.63	1.33	5.27
399.9	60.5	16.5	88.85	26.04	2.06	8.03
400.2	61.0	16.6	90.38	27.65	1.65	8.16

* Percent in recovered reaction solvent.

** NA= Not available.

Table 2. Results of the statistical analyses of operator 2's measured THF and heptane conversion data.

Parameter	THF Conversion (%)			HEPTANE Conversion (%)		
	Model Estimate	Meas'd Average	Std. Error	Model Estimate	Meas'd Average	Std. Error
Constant*	18.5		2.5	-2.9		1.0
Time	11.5		2.5	2.8		1.2
Temperature	33.6		3.5	17.5		1.5
Catalyst	16.6		3.1			
Time-Temp. Int.				7.5		2.0
Temp.-Cat. Int.	9.3		5.0			
Experimental Error	5.6			2.1		
350°C, 20min, 0%	18.5	20.1	2.5	-2.9	-3.0	1.0
350°C, 60min, 0%	30.0	27.0	2.4	-0.1	0.9	0.7
400°C, 20min, 0%	52.1	48.7	3.0	14.6	13.5	1.1
400°C, 60min, 0%	63.6	62.8	3.0	24.8	23.4	1.2
375°C, 40min, 0.5%	51.6	58.8	1.1	9.1	7.6	0.4
350°C, 20min, 1%	35.1	33.5	1.8	-2.9	-1.3	1.0
350°C, 60min, 1%	46.6	46.9	2.3	-0.1	-0.3	0.7
400°C, 20min, 1%	77.9	74.4	3.0	14.6	16.8	1.1
400°C, 60min, 1%	89.4	89.6	3.0	24.8	26.8	1.2
R ²	0.94			0.96		

* Value calculated for a thermal reaction at 350°C for 20 minutes with 1% sulfur addition.

Table 3. Results of the statistical analyses of operator 2's measured gas yields and DHP in the recovered solvent.

Parameter	GAS YIELD (%dmmf coal)			DHP (%)		
	Model Estimate	Meas'd Average	Std. Error	Model Estimate	Meas'd Average	Std. Error
Constant*	0.25		0.05	0.40		0.42
Time	0.23		0.07	0.40		0.46
Temperature	0.91		0.08	1.03		0.49
Catalyst				0.85		0.48
Time-Temp. Int.	0.43		0.11	0.52		0.49
Time-Cat. Int.				2.39		0.49
Temp.-Cat. Int.				2.83		0.48
Experimental Error	0.12			0.49		
350°C, 20min, 0%	0.25	0.30	0.05	0.40	0.33	0.42
350°C, 60min, 0%	0.48	0.52	0.04	0.80	0.62	0.24
400°C, 20min, 0%	1.15	1.20	0.06	1.43	1.07	0.32
400°C, 60min, 0%	1.82	1.90	0.06	2.35	2.31	0.32
375°C, 40min, 0.5%	0.92	0.78	0.02	2.97	3.78	0.11
350°C, 20min, 1%	0.25	0.30	0.05	1.25	0.99	0.32
350°C, 60min, 1%	0.48	0.52	0.04	4.04	4.22	0.23
400°C, 20min, 1%	1.15	1.22	0.06	5.10	5.16	0.32
400°C, 60min, 1%	1.82	1.86	0.06	8.41	8.10	0.31
R ²	0.96			0.96		

* Value calculated for a thermal reaction at 350°C for 20 minutes with 1% sulfur addition.

Table 4. Number of reactions completed by each operator for PNL's catalyst.

TARGET CONDITIONS			NUMBER OF REACTIONS	
TEMP. (°C)	TIME (min)	CATALYST (wt%)*	OPERATOR 1	OPERATOR 2
350	20	0	0	3
350	60	0	1	4
400	20	0	1	2
400	60	0	2	2
375	40	0.5	0	5
350	20	1	0	2
350	60	1	1	4
400	20	1	1	2
400	60	1	3	2

* Precursor based on as-received coal.

Table 5. Models for THF conversion without the 350°C, 20 minute experimental results.

PARAMETER	ESTIMATES (%)	
	OPERATOR 1	OPERATOR 2
Constant*	28.0	17.0
Time	12.0	11.9
Temperature	25.0	32.7
Catalyst	17.2	16.4
Temperature-Catalyst	6.2	9.5
Experimental Error	3.2	4.3

* Value calculated for a thermal reaction at 350°C for 20 minutes with 1% sulfur addition.

Table 6. Calculated results (400°C, 60 minutes).

	THF Conv. (%)	DHP (%)*
1wt%** PNL Cat. Precursor + 1wt%** Sulfur	89.4	8.41
Thermal + 1wt% Sulfur	63.6	2.35
1wt% U. of Pitt. Cat. Precursor + 2wt% Sulfur	82.3	5.35
Thermal + 2wt% Sulfur	63.0	2.43
1wt% Pyrite	73.4	3.88
Thermal	54.9	1.08

* Percent of recovered reaction solvent.

** Weight percents based on as-received coal.

SYNTHESIS AND CHARACTERIZATION OF NANOSCALE TRANSITION METAL NITRIDES AND CARBIDES FROM METALORGANIC AND HALOGENATED PRECURSORS

R.Ochoa¹, ²P. Zhou, ²W.T. Lee, ²A. Rao, ⁴S. Bandow, and ^{1,2}P.C. Eklund

¹Center for Applied Energy Research, ²Department of Physics and Astronomy, ³Department of Materials Science and Engineering, University of Kentucky, Lexington KY 40506, ⁴Instrument Center, Institute for Molecular Science, Myodaiji Okazaki, 444 Japan.

KEYWORDS: Laser Pyrolysis, molybdenum nitride, molybdenum carbide

INTRODUCTION

High surface area ultrafine particle catalysts offer a large number of advantages compared to conventional catalysts: no diffusion resistance, high accessibility of reactants to the active centers of the catalyst, and a large number of active sites per particle. In coal liquefaction, highly dispersed catalysts are especially needed because the catalyst particles are only able to influence reactions within their immediate vicinity.

Laser pyrolysis constitutes a new method for the preparation of ultrafine particle catalysts. This technique is a versatile non-equilibrium thermodynamic process for the production of nanoscale particles involving fast growth and rapid heating/cooling rates (10^3 °/s) which also allows the synthesis of metastable phases. The process involves a gas phase pyrolysis reaction, of two or more molecular species, sustained by the heat generated through the absorption of CO_2 laser energy into vibrational-rotational excitations of at least one of the reactant gas species. Typical reaction temperatures are estimated to be 800-1000°C. A variety of nanoscale particles have been produced using this technique and include MoS_2 , WS_2 , Fe_3C , Fe_2C , [1,2].

We have also prepared high surface area (50-86 m^2/g) Mo_2C and Mo_2N ultrafine particles (UFP) by Laser pyrolysis using $\text{Mo}(\text{CO})_6$ as the metal precursor. Previously, Mo_2N and Mo_2C (100-200 m^2/g) have been produced by Temperature Programmed Reduction. This method consists in the reduction of MoO_3 by NH_3 [3,4] or a mixture of H_2/N_2 [5] or CH_4/H_2 [3] for Mo_2N and Mo_2C , respectively. It has been reported that these materials exhibit high activity for heteroatom removal in the hydrotreatment of naphtha and upgrading of coal liquids [6].

Mo_2C and Mo_2N are interstitial alloys formed by the incorporation of carbon, nitrogen and oxygen into the lattice of Mo metal. In these materials, the non-metallic elements (C, N, O) enter into the interstitial sites between metal atoms. Since the bonding among those light elements is very similar, carbonitrides, oxynitrides and oxycarbide phases are possible, depending on the conditions of synthesis [7].

The ability of these materials to incorporate oxygen into their structure is particularly important with respect to their catalytic properties since it has been demonstrated that oxygen together with carbon deposits seriously decrease and/or modify their activity. Therefore it is important to address the nature of the surface of these catalysts as well as to be able to prepare these materials in an oxygen free (or controlled oxygen content) and amorphous carbon free form. For this reason, the role of the precursor and the conditions of preparation are very important.

Several reports have been presented in the literature regarding the effect of chemisorbed oxygen, surface oxide or even intercalated oxygen on the catalytic properties of these materials [8-11]. In these studies, it has been suggested that a certain amount of oxygen in the catalyst may confer a double functionality: that of a Lewis acid as well as of a noble metal [8,10].

This work contains the results from the structural and chemical characterization of Mo_2N and Mo_2C UFP catalysts by X-ray diffraction (XRD), scanning tunneling microscopy (STM), x-ray photoelectron spectroscopy (XPS) and thermogravimetry-mass spectrometry (TG-MS). The main objectives are to elucidate the real composition and surface state of these nanoparticles, to correlate structure and composition with catalytic properties and to determine methods to synthesize them in an oxygen-free and carbon-free form.

EXPERIMENTAL

Details from the experimental apparatus and procedure have been reported elsewhere [1]. Briefly, nanoscale Mo_2N and Mo_2C were synthesized from the reaction of $\text{Mo}(\text{CO})_6$ in the presence of ammonia or ethylene. The catalysts were passivated in a flow of 5% O_2 / He for several hours before removal from the reaction chamber.

Mo_2C was also synthesized utilizing MoCl_5 as the metal precursor with the same synthesis parameters that were used for the carbonyl precursor. Table 1 summarizes the reaction conditions employed to synthesize these phases. Notice that the yield of Mo_2C synthesized from MoCl_5 is lower than when $\text{Mo}(\text{CO})_6$ is used.

Synthesis Parameters

Laser Intensity
Chamber Pressure (Torr)
Metal Precursor
Reactant Gas
Flow rate (sccm)
Temperature (sublimation cell)
Yield (g product/g precursor)

TABLE 1

Mo ₂ C	Mo ₂ N	Mo ₂ C
95W	95W	95W
200	200	200
Mo(CO) ₆	Mo(CO) ₆	MoCl ₅
C ₂ H ₄	NH ₃	C ₂ H ₄
80	118	80
105°C	105°C	150°C
1.5g/5g	1.5g/5g	50 mg/2 g

CHARACTERIZATION

X-Ray Diffraction

X ray diffraction was used to identify the crystalline phase of the particles as well as to extract average values of the lattice spacing and of the crystallite size of the nanoscale particles. X-ray data were collected using Cu (K α) radiation using a Philips 3100 powder diffractometer. The average particle diameter was estimated from the Debye-Scherrer (DS) equation $D=0.9\lambda/\text{Acos}(\Theta_{111})$ [12]. Figure 1 presents the X-ray diffraction data obtained from a Mo₂C UFP. The phase of this carbide has been identified as fcc Mo₂C. The crystallite size calculated for this materials is 2.1 nm which is in good agreement with the value obtained using HRTEM [12].

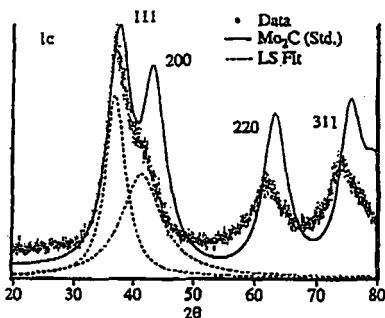


Figure 1
X ray diffractogram of Mo₂C

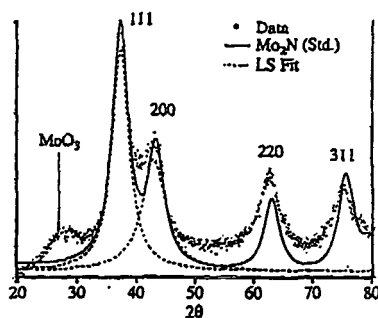


Figure 2
X-Ray diffractogram of Mo₂N

The solid lines in figure 1 correspond to the data generated using a Lorentzian lineshape for the diffraction peaks and an exponential term for the background. The values used for the diffraction peak positions and peak areas were taken from a standard powder diffraction file. The difference in intensities between the standard powder diffraction and the data may be attributed to Mo vacancies in the crystalline structures of the particles or to variations in the metal atom sublattice near the surface. Clear shifts of the diffraction lines toward lower 2Θ angles is seen for Mo₂C. This indicates a lattice expansion, presumably associated with the small crystallite size. Figure 2 presents the X-ray diffraction data for Mo₂N which has been identified as fcc Mo₂N. These particles showed an average crystallite size of 2.5 nm.

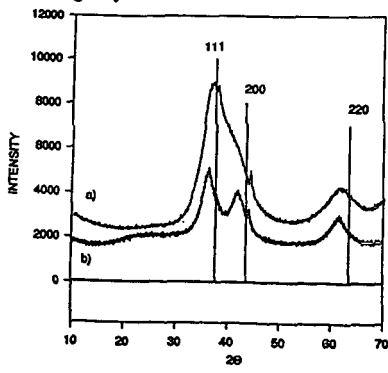


Figure 3
X-ray diffractograms from a) Mo₂C synthesized from Mo(CO)₆ and b) Mo₂C synthesized from MoCl₅.

Figure 3 shows the x-ray diffraction data of Mo_2C synthesized using MoCl_5 . The particle size calculated using the DS equation is 2.4 nm. Notice that now the peaks around $2\theta = 37.7^\circ$ are well resolved and that no sign of MoCl_5 is present. The broad shoulder at $2\theta \sim 25^\circ$ is attributed to the presence of a layer of MoO_3 [2]. High resolution TEM does not show any sign of oxide or carbide coatings. In particular the Mo_2C particles do not appear to have a carbon coating on the surface.

STM

The morphology of atomically flat $\text{Au}(111)$ surfaces coated with mono- and multi-layer nanoscale Mo_2N particles was studied using a vacuum STM ($P < 10^{-8}$ torr). The gold substrates were prepared by melting gold wires (0.5 mm diameter) in an acetylene/oxygen flame. These substrates exhibited large atomically flat areas with dimensions of about $100 \times 100 \text{ \AA}^2$ and terraces with single atomic step of approximately 2.4 Å. The particles were first dispersed in pentane or water solvent. Then they were sonicated for several hours and spin-coated onto the gold substrates. Heat treatment to remove adsorbed water and surface oxide was done in a sample-preparation chamber with a 100 torr of 10% H_2/He mixture. The STM image taken with a Pt/Ir tip is shown in figure 4.

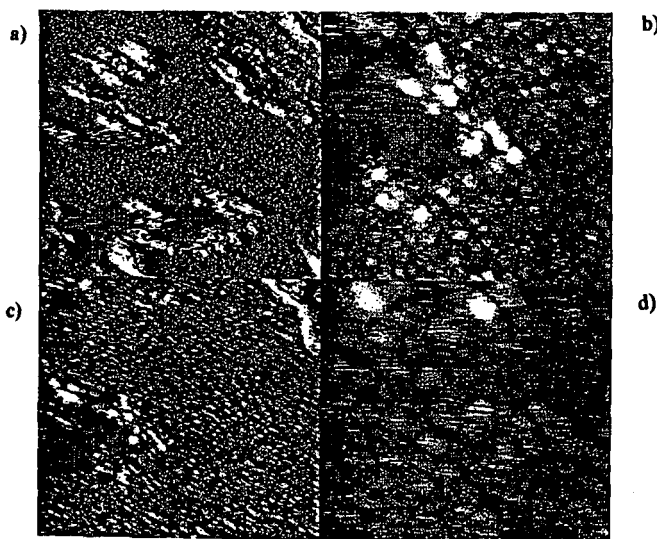


Figure 4

STM images of a layer of Mo_2N UFP deposited on the surface of $\text{Au}(111)$ at different magnifications. Each frame corresponds to an area of a) $8000 \times 8000 \text{ \AA}^2$ b) $2000 \times 2000 \text{ \AA}^2$ c) $4000 \times 4000 \text{ \AA}^2$ d) $1000 \times 1000 \text{ \AA}^2$.

It is observed that a monolayer of nanoparticles has been deposited. The underlying terraces of $\text{Au}(111)$ can still be observed (Figure 4a). The average particle size deduced from these images is ~ 7 nm. This value is higher than the one observed by TEM, probably because these particles correspond to a different batch from the one used to measure the TEM.

X-Ray Photoelectron Spectroscopy (XPS)

The XPS measurements were performed on a Leybold-Heraeus EA-11 spectrometer using Mg K- α (1253.6 eV) radiation at 15 kV and 20 mA. The oxygen/helium-passivated samples were prepared by pressing the powder into 13 mm diameter pellets. Figure 5 shows the XPS spectra from samples of Mo_2C and Mo_2N that were passivated in oxygen prior to their removal from the laser pyrolysis chamber. Figure 5a corresponds to the photoelectron lines of molybdenum $3d_{5/2}$ and $3d_{3/2}$ from Mo_2N , and figure 5b to the carbon 1s line from the same sample. Figures 5c and 5d correspond to the molybdenum and carbon peaks, respectively, from Mo_2C . The peaks at 228.58 eV in figures 5a and 5c have been assigned to the C-Mo and N-Mo bonding energies, whereas the ones at 232.2 eV to the +VI oxidation state of molybdenum, consistent with the presence of MoO_3 [13,14]. Deconvolution of the data gives 90% of surface molybdenum in the form of oxides (mainly MoO_3) for both Mo_2N and Mo_2C .

The carbon 1s peak in figure 5b, located at 284.5 eV is from carbon presumably formed

during synthesis. No evidence was found of the presence of a carbidic surface phase in the molybdenum nitride sample. Deconvolution of the carbon photoelectron line from the molybdenum carbide sample gives two peaks at 283.7 eV and 284.5 eV which correspond to a mixture of carbidic carbon and amorphous carbon [13].

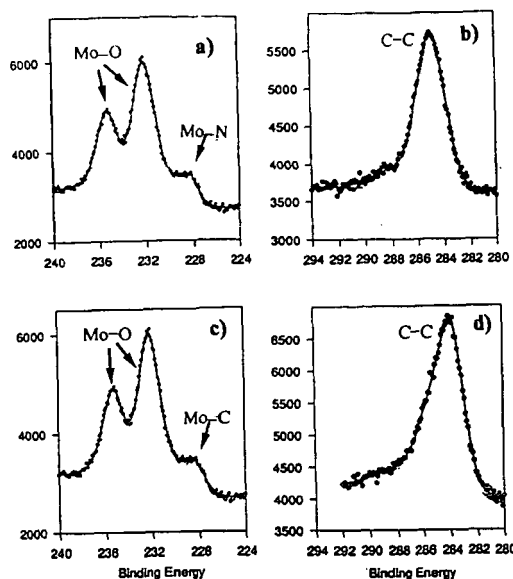


Figure 5
XPS data of Mo_2N and Mo_2C synthesized from the decomposition of $\text{Mo}(\text{CO})_6$

Thermogravimetry-Mass Spectrometry (TG-MS)

Mo_2C and Mo_2N synthesized from the decomposition of $\text{Mo}(\text{CO})_6$ were also studied with TG-MS. This technique provided valuable information about the surface composition and the extent of oxygen present on the catalyst. Between 5 and 7 mg of fresh catalyst (Mo_2N or Mo_2C) were loaded on the TG system and were flushed with He at room temperature for about 30 minutes. Pure He, and He mixed with 50% hydrogen were used as carrier gases in these experiments. The temperature program consisted on heating the samples from room temperature to 100°C. The samples were maintained at this temperature for 5 minutes, then they were heated to 900°C at a constant rate of 1°C/s. During the temperature ramp, the composition of the gas leaving the TG was monitored using a mass spectrometer.

Figure 6 shows the TG trace together with the mass signal from Mo_2C reduced in hydrogen. It is observed that there are three regions of weight loss in this sample. The first region at about 2 minutes (100°C) corresponds to the desorption of adsorbed water on the material. In the second temperature region from 8 to 12 minutes (200-410°C), oxygen is being removed from the sample in the form of water. The desorption of water occurs in the form of a broad peak that starts at about 200°C and which has a maximum at 540°C. There is still some water desorbing simultaneously with CO at a temperature about 620°C. The presence of CO indicates that some oxygen from the sample is reacting with carbon from the material. At about 540°C carbon is being removed from the sample in the form of CH_4 with a maximum removal at 740°C.

Notice also that after 18 minutes (800°C), water continues to desorb indicating that even at this temperature oxygen has not been completely removed from the samples. Oxygen desorbed in the form of water below 500°C has been assigned to surface oxygen and near-surface oxygen [15] whereas that desorbed above that temperature has been assigned to the removal of deeper lying oxygen that has diffused from the particle interior to the surface.

In figure 7 the TG trace from Mo_2N is presented. This catalyst experienced a total weight loss of about 25%. Most of it comes from oxygen removal in the form of water. The water evolved at temperatures below 340°C has been assigned to surface oxygen and near-surface oxygen whereas water evolved above this temperature has been assigned to bulk oxygen. Although no ammonia was detected in the gases evolved, it is observed that at about 800°C the nitride decomposes by losing molecular nitrogen. Since no methane evolved from the heat treatment of Mo_2N , it follows that the methane detected from the carbide corresponds to carbidic carbon that has reacted with hydrogen, and that amorphous carbon was not removed

from the sample. This agrees with reports that this carbon is very difficult to remove [15].

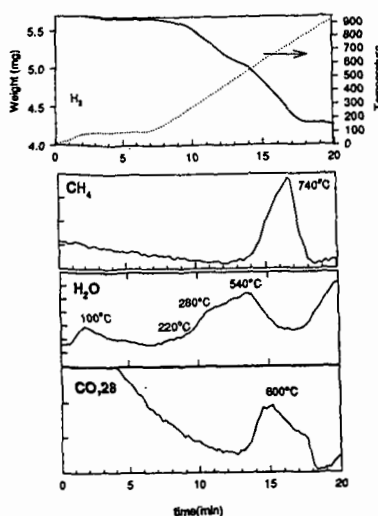


Figure 6
TG-MS trace of Mo_2C treated
hydrogen

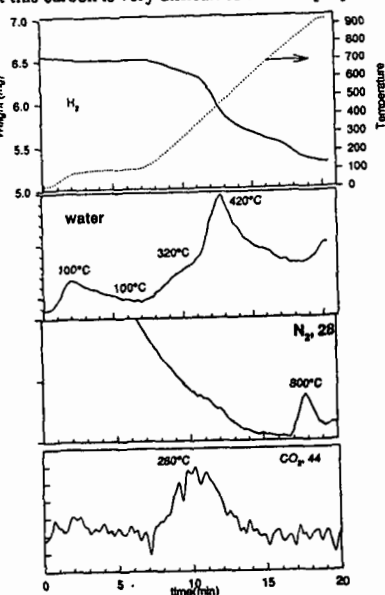


Figure 7
TG-MS trace of Mo_2N treated in
hydrogen.

CONCLUSIONS

Fcc Mo_3N and Mo_2C have been synthesized from the decomposition of $\text{Mo}(\text{CO})_6$ and MoCl_5 using Laser Pyrolysis. From the structural point of view, they appear crystalline with little or no disorder. Even though HR-TEM did not show any sign of oxide or carbide coating on the particle, XPS indicated that a large percentage of Mo atoms on the surface are in the form of an oxide phase produced during surface passivation. In addition, carbon was observed to be present on the surface of both catalysts from the decomposition of the metalorganic precursor. TG-MS shows that oxygen content constitutes a major contaminant on these particles and that polymeric carbon is very difficult to remove.

REFERENCES

- [1] X.X. Bi, B. Ganguly, G.P. Huffman, F.E. Huggins, M. Endo, P.C. Eklund, *J. Mater. Res.* 8(7), (1993) 1666.
- [2] X.X. Bi, Y. Wang, W.T. Lee, K.A. Wang, S. Bandow and P.C. Eklund, *Mat. Res. Soc. Symp. Proc.*, 327, (1994) 47-52.
- [3] S.T. Oyama, J.C. Schlatter, J. Metcalfe, J. Lambert, *Ind. Eng. Chem. Res.* 27, (1988) 1648-1653.
- [4] J.-G. Choi, R. L. Curl, L.T. Thompson, *J. of Catal.* 146, (1994) 218-227.
- [5] R.S. Wise, E.J. Markel, *J. of Catal.* 145, (1994) 344-355.
- [6] S.T. Oyama, R. Kapoor, C. Shudakar, *Prep. of Am. Chem. Soc. Div. Fuel Chemistry*, 37(1), (1992) 233.
- [7] S.T. Oyama, *Catalysis Today*, 15 (1992) 179-200.
- [8] H.S. Kim, G. Bugli, G. Djega-Mariadassou, *Proc. Mater. Res. Soc. Symposium T*, Nov 29-Dec. 1 1994.
- [9] M. Ledoux, *Proc. Mater. Res. Soc. Symposium T*, Nov. 29-Dec 1 1994.
- [10] F. H. Ribeiro, R.A. Dalla Betta, M. Boudart, J. Baumgartner, E. Iglesia, *J. of Catal.* 130, (1991) 86-105.
- [11] G.S. Ranhotra, A.T. Bell, J.A. Reimer, *J. of Catal.* 108, (1987) 40-49.
- [12] X.X. Bi, K.D. Chowdhury, R. Ochoa, W.T. Lee, S. Bandow, M.S. Dresselhaus, P.C. Eklund in *Proc. of Materials Res. Society Symposium T*, Fall 1994, in press.
- [13] M. J. Ledoux, C.P. Huu, J. Guille, H. Dunlop, *J. of Catal.*, 134, (1992) 383.
- [14] C.D. Wagner, W.M. Riggs, L.E. Davis, J.F. Moulder, and G.E. Muilenberg in "Handbook of X-ray Photoelectron Spectroscopy". Perkin-Elmer, Eden Prairie, MN, 1979.
- [15] K.J. Leary, J. N. Michaels, A.M. Stacy, *J. of Catalysis* 101, (1986) 301-313.

PROGRESS IN THE DEVELOPMENT AND PRODUCTION OF NANOSCALE IRON-CONTAINING CATALYSTS

Dean W. Matson, John C. Linehan, John G. Darab, Heather M. Watrob,
Eddie G. Lui, Max R. Phelps, and Michael O. Hogan

Pacific Northwest Laboratory¹
PO Box 999
Richland, WA 99352

Keywords: iron-based catalysts, nanocrystalline catalysts, hydrothermal synthesis, model compounds

INTRODUCTION

The development of effective iron-based powders for use as dispersed catalysts or as precursors to the active catalyst phase in direct coal liquefaction processes is an ongoing area of research.²⁻⁴ Although they are generally catalytically inferior to the more expensive catalyst materials based on molybdenum, cobalt, or nickel, iron-based powders offer the distinct advantages of relative low cost and toxicity. These factors make the prospects for using iron-based powders as one-time "throw away" catalysts attractive for large scale liquefaction operations since the costs associated with catalyst recovery could be avoided. Recent efforts have been aimed at increasing the efficiency of iron-based materials for coal liquefaction applications. Research has been focused on the development of ultrafine powders having very high specific surface areas and high dispersion in liquefaction media,⁴ and on the effect of iron oxyhydroxide phase toward conversion of precursors to the active catalyst phase under liquefaction conditions.⁵

At the Pacific Northwest Laboratory (PNL) we have undertaken a program to investigate nanocrystalline iron-based powders as catalytic precursors in a variety of hydrocracking reactions, including coal liquefaction. One ultrafine powder synthesis method developed at PNL, the Rapid Thermal Decomposition of precursors in Solution (RTDS) process, appears to be particularly promising for use in the large scale production of nanocrystalline powders.^{6,7} Using model compounds we have demonstrated that iron-based RTDS powders can be used to produce highly active carbon-carbon bond scission catalysts under reaction conditions relevant to coal liquefaction processes.^{7,8} In this paper we present recent results of attempts at modifying the activity of RTDS-generated iron-based catalyst powders by doping with other metals and the results of scale-up efforts to produce kilogram quantities of active catalyst precursor by this process.

CATALYST PRECURSOR POWDER SYNTHESIS

When operated with an aqueous solvent, the RTDS powder synthesis method can be described as a continuous flow-through hydrothermal process. It involves the formation of ultrafine solid particles when homogeneous pressurized solutions are rapidly forced through a heated small diameter linear reactor (1-30 sec residence time). Under these conditions, well-known hydrothermal reactions, leading to nucleation of solid oxides or hydroxides, occur between dissolved metal species and the solvent.⁹ Particle growth is quenched at the end of the reactor by passing the RTDS solution through an orifice, abruptly removing it from the hydrothermal environment. RTDS products are collected as aqueous suspensions in a cooled vessel, and typically contain submicrometer-sized aggregates of nanometer-sized crystallites. The solid powders can be separated from the suspension by centrifugation, spray drying, or freeze drying. Details of the RTDS process have been presented elsewhere.⁶⁻⁸

PNL currently has two operational RTDS units. One of these is referred to as a bench-scale unit and is used primarily for quick response feasibility studies and small batch (1-10 liters of precursor solution) sample processing. The reactor tube in this unit consists of a 1 to 2 meter length of 1/8 inch O.D. stainless steel high pressure tubing. Typical feedstock consumption rates and reaction residence times are 50-75 cc/min and 1-5 sec, respectively. The second RTDS system is referred to as an engineering-scale unit and has a larger reactor volume (with residence times of 5-30 sec) and greater throughput capacity (150-250 cc/min). In this system the reactor tube is a 2.25 meter length of 9/16 inch O.D. high pressure stainless steel tubing. The engineering-scale unit is used exclusively for runs involving greater than 10 liters of precursor solution.

While a range of iron-based oxide and oxyhydroxide phases can be produced using the RTDS method, we have targeted one phase, 6-line ferrihydrite,¹⁰ as a candidate for large scale production as a coal liquefaction catalyst precursor. Preliminary tests have shown that this phase is consistently active as a liquefaction catalyst precursor,^{5,8} and that it is particularly amenable to preparation using the RTDS method. Although 6-line ferrihydrite can also be produced using standard laboratory synthesis methods,¹¹ these are batch processes that are not necessarily scalable to larger batch sizes. Furthermore, benchtop 6-line ferrihydrite synthesis requires a time consuming dialysis step that can be eliminated by using the continuous RTDS method. We have investigated enhancing the rate of 6-line ferrihydrite production on the engineering-scale RTDS unit by increasing the iron salt content in the feed solution from 0.1 M to as high as 0.5 M.

In addition to single phase metal oxides and oxyhydroxides, mixed or doped oxide/oxyhydroxide powders are easily produced by the appropriate choice and loadings of dissolved solute in the RTDS feed solution. We evaluated the RTDS method for making 6-line ferrihydrite doped with 10

mole percent or less of an additional metal using the bench-scale RTDS apparatus. All doped 6-line ferrihydrite samples were prepared using a 0.1 M ferric nitrate solution as the iron source, and urea (0.5 M) was added to the feed solution to raise the pH of the solution in the hydrothermal region. RTDS reaction temperatures used were $300 \pm 5^\circ\text{C}$. The source of dopant metal ion and its nominal concentration in the feed solution are summarized in Table 1.

Unless otherwise noted, catalytic activities of all 6-line ferrihydrite powders reported in this work were evaluated using samples that had been separated from suspension by centrifugation, dried under flowing nitrogen, and ground and sieved to -325 mesh. Selected samples were calcined in air at 300°C for one hour. Catalytic evaluation of sample powders was undertaken by monitoring consumption of the model compound naphthylbiphenylmethane (NBBM) under a standard set of conditions. These tests were performed in sealed tubes containing 25 mg of NBBM, 100 mg of 9,10-dihydrophenanthrene, 3 mg catalyst precursor and 3 mg of sulfur. The tubes were suspended for 1 hr in a sand bath at the desired reaction temperature. Phase analyses of RTDS products were performed using powder X-ray diffraction (XRD) and metal contents were analyzed by inductively coupled plasma/mass spectrometry (ICP/MS).

RESULTS AND DISCUSSION

The catalytic activity of RTDS-generated undoped 6-line ferrihydrite toward the consumption of NBBM is shown in Figure 1. The 6-line ferrihydrite catalyst precursor was ground and sieved, and the -325 mesh fraction was calcined at 300°C for 1 hr prior to these tests. This figure clearly illustrates the high catalytic activity of this precursor phase at 400°C , consuming essentially all of the model compound at that temperature. Furthermore, moderate activities were retained to reaction temperatures as low as 300°C , where 30 percent of the model compound was consumed during a one hour reaction time.

ICP/MS analysis of powders produced by co-precipitation of iron and a second metal species in the presence of added urea using the bench-scale RTDS unit confirmed the usefulness of the RTDS technique for generating doped products of well-defined compositions (Table 1). XRD analysis of the doped powder products confirmed that 6-line ferrihydrite was the primary crystalline phase present in the products. A minor hematite component was also detected in the tin-doped powder product.

In general, the greatest discrepancies between the nominal dopant contents in the RTDS feed solutions and the measured dopant contents of the dried powders were found in the samples having the smallest dopant contents (1 mole percent dopant metal). The primary source of these discrepancies most likely resulted from uncertainties in weighing the dopant salts when preparing the RTDS feed solutions. The analytical results on the doped ferrihydrite products indicate that essentially all of the iron and the dopant metal present in the feed solutions are precipitated in the RTDS unit and that doping levels closely follow the feed concentrations. This suggests that the RTDS process could be very valuable for the co-processing of semi-precious or precious metal catalysts on supports or, as in this case, the production of co-catalysts. The fine control over doping levels exhibited by the RTDS process has important prospective applications beyond coal liquefaction catalyst production. Many different catalysts are mixtures of two or more active species where the exact composition is important to promote both increased reactivity and lower costs. In RTDS experiments with zirconia as the major product constituent similar doping results have been obtained.

Catalyst testing results measuring consumption of the NBBM model compound using the doped 6-line ferrihydrite powders as catalyst precursors are presented in Figure 2. The result of catalyst evaluation of an undoped RTDS 6-line ferrihydrite powder produced under comparable conditions is presented for comparison. When using the centrifuged, dried, and sieved powders as catalyst precursors without calcination (Fig. 2), NBBM consumptions approaching 90 percent and above were observed for chromium, zirconium, and molybdenum doped powders. Cobalt and nickel doped 6-line ferrihydrite products exhibited a range of intermediate to poor activities with the 10 percent nickel product consuming less than 20 percent of the model compound. The tin-doped product that was tested exhibited no apparent activity toward consumption of NBBM whatsoever. We speculate that this was due the presence of residual chlorine (a known catalyst poison) from the salt used as the source of tin ions in the RTDS solution.

XRD analysis of the samples calcined at 300°C for 1 hr indicated that ferrihydrite remained the predominant phase after calcination. Those uncalcined samples exhibiting strong catalytic activity all lost less than 15 percent of their weight upon calcination while those with low activity lost up to 30 percent of their weight, most likely due to adsorbed water. The presence of excess adsorbed water may be detrimental to catalytically enhanced C-C bond scission reactions in the test system. An additional point can be made, however, that loadings of catalyst precursor samples containing excess adsorbed water would contain a correspondingly lower metals content, potentially reducing the measured catalytic activity per unit mass of catalyst precursor powder.

Calcination of the doped 6-line ferrihydrite samples produced a significant improvement in the measured catalytic activities of samples having mediocre activities in the uncalcined state (Fig. 2). Upon calcination, two of the cobalt doped powders consumed more than 90 percent of the model compound. The 10 percent nickel doped sample showed significant improvement as a result of calcination, increasing from less than 20 percent to nearly 70 percent consumption of the NBBM. Those powders previously exhibiting high activity retained that activity after calcination and no

improvement was noted in the activity of the tin doped sample. The undoped ferrihydrite sample also showed an increase in activity with calcination even though the weight loss was only 6 percent. The activity toward NBBM consumption increased from 68 percent to over 90 percent.

Undoped 6-line ferrihydrite powders were produced using the engineering-scale RTDS reactor at increasing RTDS reaction temperatures to evaluate the effects of this variable using a constant 0.1 M ferric nitrate/0.5 M urea feed solution. Product suspensions produced at increasing temperatures starting at 255°C and increasing to 315°C were split into two fractions, one centrifuged and dried as summarized above, and the other spray dried in a bench-scale spray drying unit. Both splits were calcined at 300°C before catalyst testing. When evaluated for catalytic activity (Fig. 3) all of the centrifuged samples promoted NBBM consumptions in excess of 90 percent. Spray dried samples of the same products were generally somewhat inferior catalysts, likely resulting from incorporation of water soluble salts into the spray dried powders. This incorporation of salts in the powder could cover some percentage of the otherwise available catalytic sites and would also reduce the effective metal content per gram of catalyst powder. If spray dried RTDS products are to be used for coal liquefaction applications, catalyst loadings may be required to compensate for this effect.

Efforts at increasing the production rate of 6-line ferrihydrite powders with the engineering scale unit were focused on use of higher concentrations of ferric ion in the feed solution. Ferric nitrate concentrations ranging from 0.1 M to 0.5 M with a constant urea-to- Fe^{3+} ratio of 5:1 were used as feedstocks for these experiments. At the flow rates of the RTDS unit the 0.5 M ferric ion concentration corresponded to a 1 lb of dried powder-per-hour rate of production. The catalytic activities of these powders, as a function of the production rate, before and after calcination are shown in Figure 4. Notice that there is little difference in the activity of the calcined and uncalcined powders up to the highest production rate. Powders produced at 0.8 lb/hr showed some of the highest catalytic activities measured for iron oxide powders.

SUMMARY

The RTDS powder synthesis method has been shown suitable for producing nanocrystalline 6-line ferrihydrite powders that are highly active as precursors to catalysts promoting carbon-carbon bond scission reactions in coal model compounds. Activity of the ferrihydrite powder is maximized if it is sieved to fine aggregate size and pretreated at 300°C prior to use as a catalyst precursor. This material has been shown to exhibit catalytic activity at reaction temperatures as low as 300°C. We have demonstrated the capability to generate the ferrihydrite powder product at rates of up to 1 lb/hr using an engineering-scale RTDS unit. The method has also been demonstrated to be capable of producing ferrihydrite powders accurately doped with a second metal component that may modify the catalyst characteristics.

ACKNOWLEDGMENTS

This work was supported by the U.S. Department of Energy, Office of Fossil Energy. Support for EGL and HMW was provided by the Associated Western Universities, Inc., Northwest Division under Grant DE-FG06-89ER-75522 with the U.S. Department of Energy.

REFERENCES

- (1) Pacific Northwest Laboratory is operated for the US Department of Energy by the Battelle Memorial Institute under contract DE-AC06-76RLO 1830.
- (2) Rabo, J.A., in *Advanced Heterogeneous Catalysts for Energy Applications Vol. II*, U.S. DOE report DOE/ER-30201-H1, 1994, p. 1.1.
- (3) Pradhan, V.R.; Tierney, J.W.; Wender, I.; and Huffman, G.P., *Energy and Fuels*, 1991, 5, 497.
- (4) Derbyshire, F., *Energy and Fuels*, 1989, 3, 273.
- (5) Linehan, J.C.; Matson, D.W.; and Darab, J.G., *Energy and Fuels*, 1994, 8, 56.
- (6) Matson, D.W.; Linehan, J.C.; Bean, R.M., *Materials Letters* 1992, 14, 222.
- (7) Darab, J.G.; Buehler, M.F.; Linehan, J.C.; and Matson, D.W., in *Better Ceramics Through Chemistry VI*, Materials Research Society symposium proceedings vol. 346, Cheetham, A.K., Brinker, C.J., McCartney, M.L., and Sanchez, C., eds. Materials Research Society, pp. 499-510.
- (8) Matson, D.W.; Linehan, J.C.; Darab, J.G.; and Buehler, M.F., *Energy and Fuels*, 1994, 8, 10.
- (9) Rabenau, A., *Angew. Chem., Int. Ed. Engl.*, 1985, 24, 1026.
- (10) This weakly crystalline iron oxyhydroxide phase is named for the number of broad lines present in its powder XRD pattern.
- (11) Schwertmann, U. and Cornell, R.M., *Iron Oxides in the Laboratory*, Weinheim; New York, 1991.

Table I. Iron Oxides Doped with Transition Metals Produced by Co-Processing a Second Metal Salt and 0.1 M Ferric Nitrate using RTDS

Dopant Salt	Nominal Mole Percent Dopant Metal in Feed	Measured Mole Percent Dopant Metal in Isolated Powder	Percent Difference Between Feed and Powder	Phases Detected by XRD
Cobalt Acetate	10	9.27	7	6-line Ferrihydrite
Cobalt Acetate	1	1.11	11	6-line Ferrihydrite
Ni(NO ₃) ₂	10	9.82	2	6-line Ferrihydrite
Ni(NO ₃) ₂	1	1.21	21	6-line Ferrihydrite
SnCl ₂	1	1.10	10	6-line Ferrihydrite/ Hematite
Cr(NO ₃) ₃	10	9.89	1	6-line Ferrihydrite
Cr(NO ₃) ₃	1	1.23	23	nd
ZrO(NO ₃) ₂	10	9.36	6	6-line Ferrihydrite
(NH ₄) ₂ MoO ₄	1	0.98	2	6-line Ferrihydrite

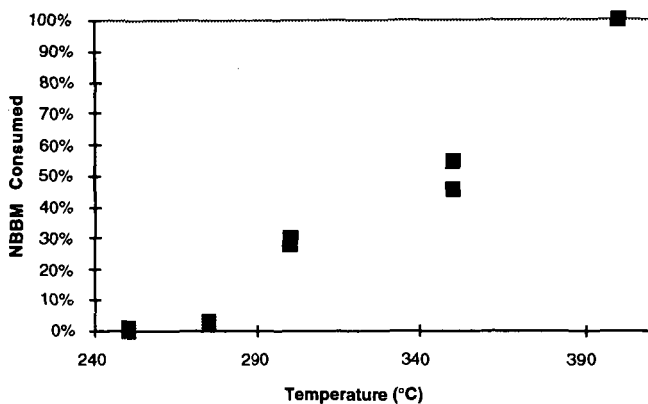


Figure 1. Effect of reaction temperature on catalytic activity of undoped RTDS-generated 6-line ferrihydrite toward consumption of NBBM model compound.

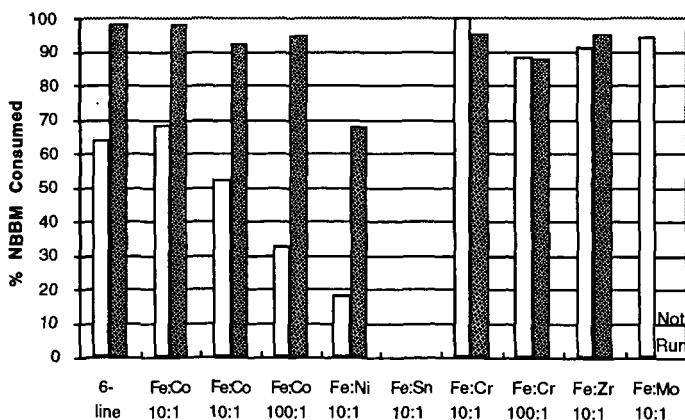


Figure 2. Effect of calcining at 300°C for one hour on activity of RTDS-generated 6-line ferrihydrite and doped 6-line ferrihydrite powders toward consumption of NBBM model compound at 400°C. All samples were sieved to -325 mesh. Unshaded bars represent uncalcined powders, shaded bars represent calcined powders.

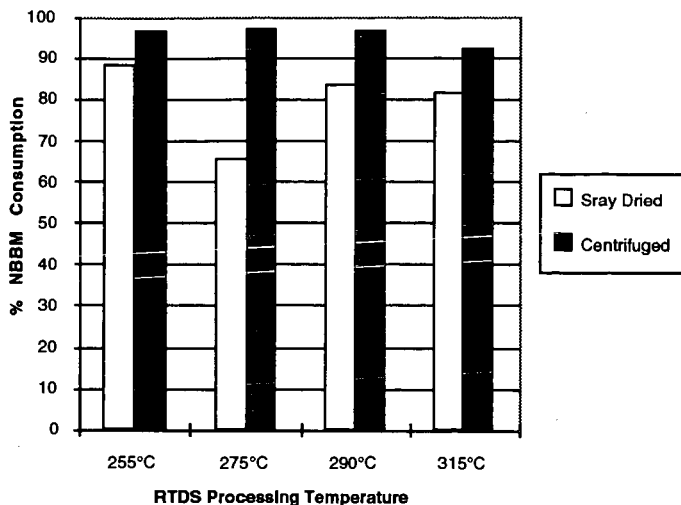


Figure 3. Effect of engineering-scale RTDS temperature and collection method on measured catalytic activity of calcined 6-line ferrihydrite powder toward consumption of NBBM model compound.

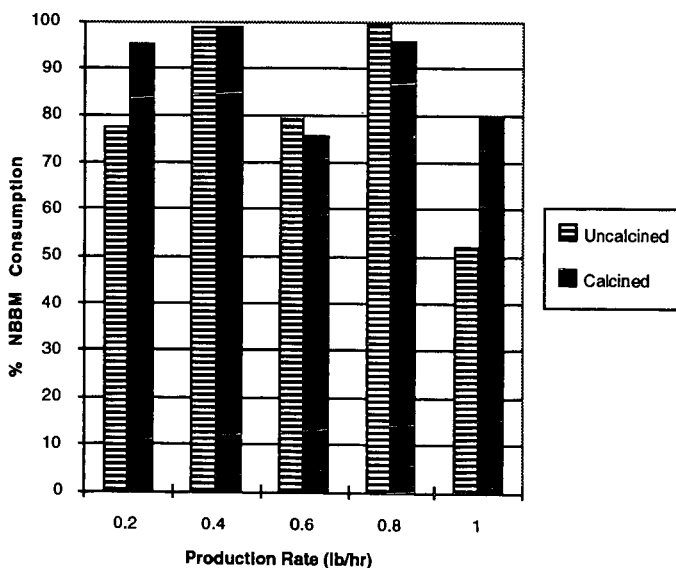


Figure 4. Activities of calcined and uncalcined 6-line ferrihydrite powders produced on the engineering-scale RTDS apparatus at increasing production rates.

CHARACTERIZATION OF Fe_{1-x}S CATALYSTS SYNTHESIZED FROM FERRIHYDRITES UNDER DCL CONDITION

Jianmin Zhao, Zhen Feng, Frank E. Huggins, K. R. P. M. Rao, and Gerald P. Huffman*
The Consortium for Fossil Fuel Liquefaction Science
341 Bowman Hall, University of Kentucky
Lexington, KY 40506

Keywords: Pyrrhotite catalysts; direct coal liquefaction; Mossbauer spectroscopy; XRD; TEM.

INTRODUCTION

Recently, considerable effort has been made to develop low cost, highly dispersed iron-based catalysts for direct coal liquefaction (DCL) [1]. Most iron-based catalysts are in fact the catalyst precursors as the catalysts convert to Fe_{1-x}S (pyrrhotite) under DCL reaction conditions. There has been less work reported on the pyrrhotite phase, in terms of its morphology and structure, and how they influence DCL activity.

In the past, we have extensively investigated the structure and DCL activity of ferrihydrite (FHYD), a highly dispersed iron oxide with surface area $>200 \text{ m}^2/\text{g}$ and average particle size of 30-50 Å. The major drawback of this material as a catalyst is that the small particles quickly agglomerate and transform to a low surface area hematite ($\alpha\text{-Fe}_2\text{O}_3$) at $T > 200^\circ\text{C}$. Moreover, the presence of surface adsorbed water molecules accelerates the agglomeration and phase transformation [2, 3]. This problem has been resolved by chemisorption of small amounts of impurity anions at the surface of ferrihydrite. The impurity anions block the crystal growth sites and thereby effectively inhibit the phase transformation to hematite, allowing the catalyst to maintain its dispersion. A number of binary ferrihydrite catalysts (M/FHYD, M/Fe $\approx 5\%$) with M = Si, Mo, P, and citric acid (CA) have been synthesized in our laboratory [4, 5]. DCL tests using Si/FHYD and CA/FHYD show significant increases of coal-liquid conversion over that obtained from thermal reaction, or with pure ferrihydrite [4, 5].

In this paper, we report the characterization of pyrrhotite catalysts synthesized under simulated DCL conditions using binary ferrihydrites as the catalyst precursors. TEM, XRD, and Mössbauer spectroscopy were used for the characterization.

EXPERIMENTAL

Three ferrihydrites were used: a pure ferrihydrite catalyst (30-Å catalyst) provided by Mach I, Inc., and two binary ferrihydrites Si/FHYD and CA/FHYD synthesized in our laboratory. Details of the synthesis can be found in Ref. 4 and 5.

Sulfidation of the catalysts was performed in a tubing bomb under simulated DCL conditions. The tubing bomb was loaded with 0.25 g of catalyst mixed with tetralin along with dimethyl disulfide (DMDS) as a sulfur donor (S/Fe = 2/1, by weight). The tubing bomb was than pressurized with H_2 to 1000 psi at room temperature and agitated vertically at 400 cycles/min in a fluidized sand bath at 415°C for one hour. After reaction, the samples were subjected to XRD, TEM and Mössbauer investigation.

Mössbauer spectra were recorded using a constant acceleration spectrometer. The radioactive source consists of $\sim 50 \text{ mCi}$ of ^{57}Co in a Pd matrix. Powder X-ray diffraction (XRD) was performed on an automated Rigaku Dmax X-ray diffractometer. Transmission electron micrographs (TEM) were obtained with a Hitachi H800 NA scanning transmission electron microscope (STEM).

RESULTS AND DISCUSSION

TEM For the pure ferrihydrite (30-Å), after sulfidation, TEM shows the formation of well crystallized, hexagonal-shaped Fe_{1-x}S particles with average particle size $> 1000 \text{ Å}$ (Fig. 1). Similar result has been reported previously by Srinivasan et al [6]. Improved dispersion of the Fe_{1-x}S phase is obtained with the binary ferrihydrites as indicated in Fig 1, showing significantly smaller particles of less regular shape.

X-ray diffraction Fe_{1-x}S has the NiAs structure in which each Fe is surrounded by six sulfur atoms, and Fe has 1, 2, or 4 vacancies among its 12 nearest Fe neighbors. The monoclinic (Fe_7S_6) and hexagonal (Fe_9S_{10}) phases are the most common ones. The phase transition of monoclinic to hexagonal occurs at $\sim 300^\circ\text{C}$. The XRD patterns for the three ferrihydrite catalysts after sulfidation are consistent with those for the hexagonal phase (Fig. 2). However, the

pyrrhotite phase formed with Si/FHYD shows diffraction features on the high 2θ sides of the major diffraction peaks, which are also seen in the monoclinic phase (Figure 2a, indicated by arrows). Because of decreased Fe:S ratio, the d spacing for the monoclinic phase is shorter than that for the hexagonal phase, thus the (102) peak for the monoclinic phase is shifted to higher 2θ . Such shifting is also found for the sulfided Si/FHYD and the 350°C sulfided 30-Å catalyst, indicating incomplete mono-hex transition, due to the presence of the surface adsorbed Si and lower sulfiding temperature, respectively. For reasons unclear at the present time, the (102) peak for the sulfided CA/FHYD is shifted to the low 2θ side.

Mössbauer spectra Quantitative analysis for the Fe vacancies in pyrrhotite are obtained using Mössbauer spectroscopy. The Mössbauer spectrum for the hexagonal phase contains three sextets with magnetic hyperfine fields of $H_f = 302, 274,$ and 256 kOe, respectively [7]. These three components are assigned to three Fe positions, which respectively have 0 (position A), 1(B), and 2(C) vacancies among their Fe neighbors. For the monoclinic pyrrhotite, the spectrum also consists of three sextets of $H_f = 300, 256,$ and 225 kOe, corresponding to the Fe atoms with 0 (A), 2(C), and 4(D) vacancies in their Fe neighbors. Figure 3 shows the Mössbauer spectra of the three pyrrhotite catalysts. The spectrum for the sulfided 30-Å catalysts is very similar to that for hexagonal phase, which is dominated by the A, B, and C positions. However, a fourth component (D) is discernable, hence the spectrum is fitted with four sextets. The spectrum for the sulfided Si/FHYD is similar to that for the monoclinic phase, showing splitting of the absorption lines, due to decreased population of the B position and increased population of the C and D positions. The spectrum is fitted with three sextets representing the A, C, and D positions, and a doublet at the center for the unsulfided ferrihydrite. The results are in agreement with the XRD results. The spectrum for the sulfided CA/FHYD also shows increased splitting of the absorption lines as compared with that for Si/FHYD, indicating increased fractions of the C and D components. The spectrum is fitted with four sextets. The Mössbauer parameters are listed in Table 1.

According to the distribution of the four magnetic components (Table 1), a measure of the vacancy content in the nearest Fe shell, V is given by

$$V = \frac{(m*1 + l*2 + k*4)}{(n + m + l + k)} \quad (1)$$

where n, m, l, k represent the normalized fractions of four positions with 0, 1, 2, 4 vacancies, respectively. V values for the three samples are listed in Table 1. Significant increase of the Fe vacancies are found in the sulfided Si/FHYD and CA/FHYD.

In conclusion, we found that in addition to improving the dispersion of the pyrrhotite phases, the presence of impurity anions at the ferrihydrite surface retards the mono-hex phase transition, thus more Fe vacancies are retained in the pyrrhotite phase. The role of these Fe vacancies on catalytic coal liquefaction will be further investigated.

ACKNOWLEDGEMENT This research is supported by the U. S. Department of Energy under contract No. DE-FC22-90PC90029, as part of the research program for the Consortium for Fossil Fuel Liquefaction Science.

REFERENCES

1. Huffman, G. P. et al, *Energy & Fuels* **1993**, 7, 285.
2. Zhao, J.; Huggins, F. E.; Feng, Z.; Lu, F.; Shah, N.; Huffman, G. P. *J. Catal.* **1993**, 143, 143.
3. Feng, Z.; Zhao, J.; Huggins, F. E.; Huffman, G. P. *J. Catal.* **1993**, 143, 510.
4. Zhao, J.; Feng, Z.; Huggins, F. E.; Huffman, G. P. *Energy & Fuels* **1994**, 8, 38.
5. Zhao, J.; Feng, Z.; Huggins, F. E.; Huffman, G. P. *Energy & Fuels* **1994**, 8, 1152.
6. Srinivasan, R.; Keogh, R. A.; Davis, B. H., preprint paper, *ACS Div. Fuel Chem.* **1992**, 37, 1265.
7. Ovanesyan, N. S.; Trukhtanov, V. A.; Ordinetz, G. Yu.; Novikov, G. V., *Soviet Physics JEPT* **1971**, 33, 1193.

Table 1. Mössbauer parameters for the ferrihydrite catalysts after sulfidation without coal. H is for the magnetic hyperfine field; IS the isomer shift; QS the quadruple splitting. A, B, C, and D represent the Fe positions with 0, 1, 2, and 4 Fe vacancies among its Fe neighbors. The average vacancy is determined by Eqn. (1). All spectra were recorded at room temperature.

Sample	H (kOe)	IS (mm/s)	QS (mm/s)	Phase	% Fe	V
30-Å	297	0.69	0.06	A	30.9	1.22
	274	0.72	0.04	B	31.2	
	257	0.69	0.07	C	30.5	
	232	0.60	0.11	D	7.4	
CA/FHYD	296	0.69	0.05	A	32.3	1.35
	273	0.71	0.04	B	23.9	
	255	0.68	0.05	C	32.1	
	227	0.63	0.09	D	11.8	
Si/FHYD	294	0.68	0.05	A	30.0	1.59
	255	0.67	0.05	C	26.6	
	223	0.65	0.09	D	15.3	
		0.45	0.52	FHYD	28.0	

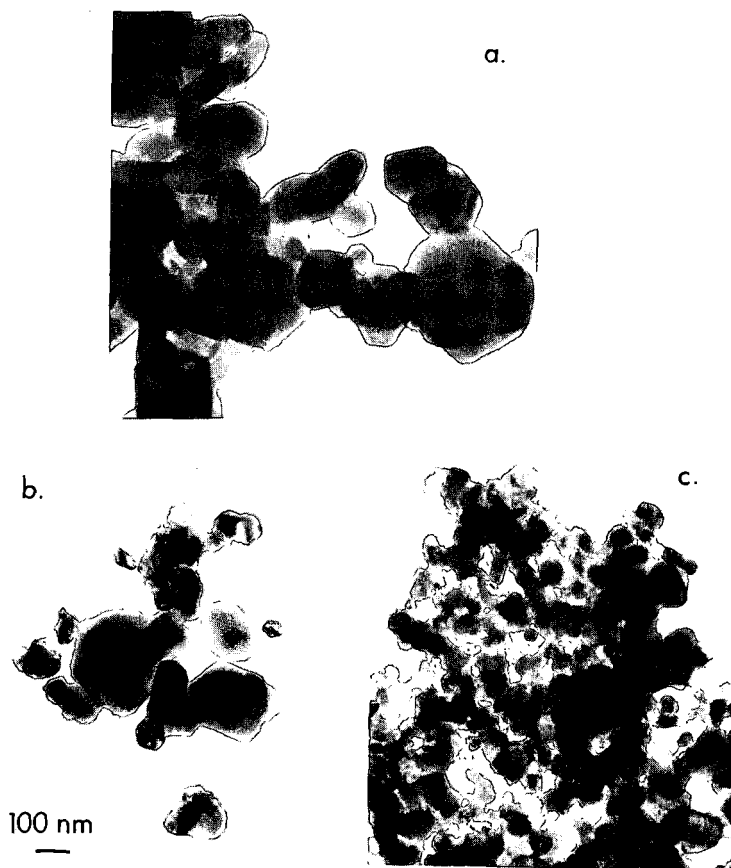


Figure 1 TEM for three sulfided ferrihydrites: a) the 30-A catalyst; b) CA/FHYD; c) Si/FHYD.

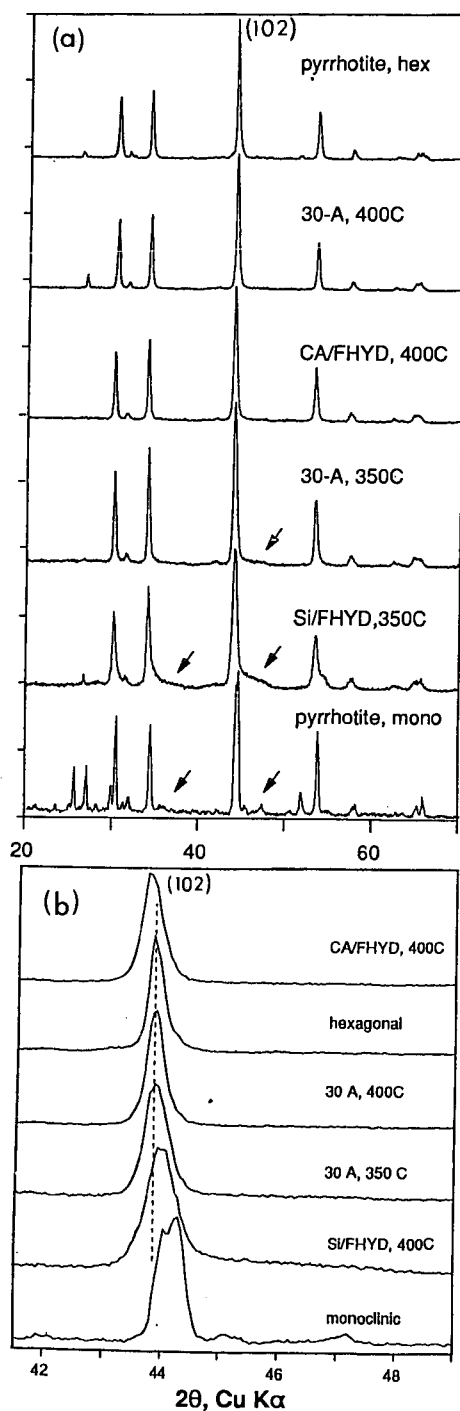


Figure 2. a) XRD patterns for the pyrrhotites and the sulfided ferrihydrite catalysts; b) the (102) peaks for the pyrrhotites and the sulfided ferrihydrite catalysts.

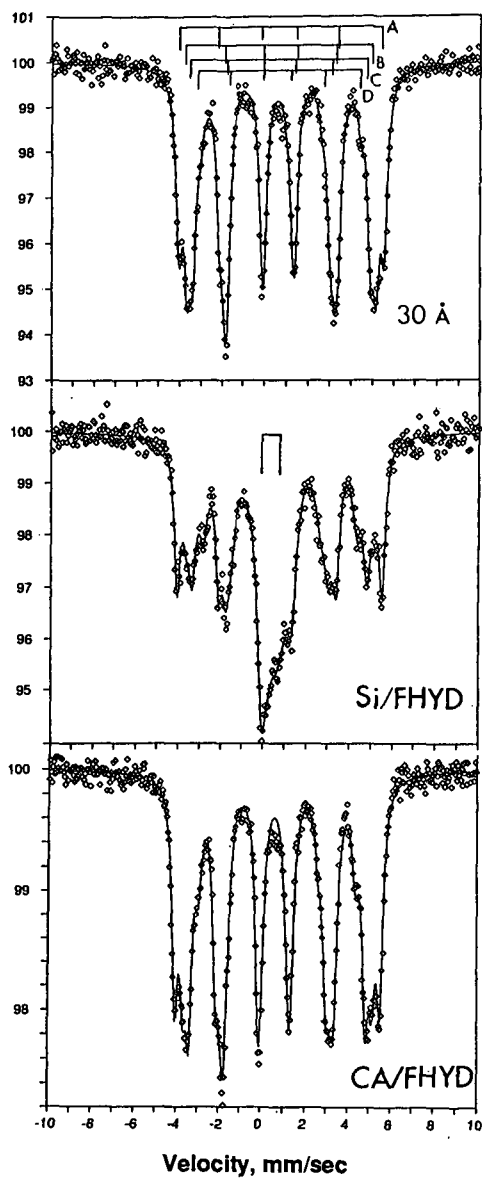


Figure 3. Mossbauer spectra of three sulfided ferrihydrites.

SOL-GEL PREPARATION OF ZIRCONIUM OXIDE

David A. Ward and Edmond I. Ko
Department of Chemical Engineering
Carnegie Mellon University
Pittsburgh, PA 15213-3890

Keywords: sol-gel preparation, aerogel, zirconium oxide (zirconia)

INTRODUCTION

A sol-gel preparation involves first the formation of a sol, which is a suspension of solid particles in a liquid, then of a gel, which is a diphasic material with a solid encapsulating a liquid. The liquid can be removed from a gel by either conventional drying (such as by using an oven) to obtain a product known as a xerogel, or by drying with supercritical extraction (often referred to as supercritical drying for short) to give an aerogel.

Preparing catalytic materials with the sol-gel method has received increasing attention in recent years because of its versatility and excellent control over a product's properties (1). In fact, there are a host of experimental variables, generally referred to as the sol-gel parameters, which can impact on the physical and chemical characteristics of a sample. To date, most studies have focused on sol-gel parameters that are important in the first step which is the formation of a gel. There has been relatively less work on the subsequent processing steps: aging, drying, and heat treatment. Because these steps are often interrelated (2), one should take a broader viewpoint and consider all of them in fine-tuning a sol-gel product.

In this paper we discuss our recent results on the sol-gel preparation of zirconia with an emphasis on three key parameters: the gel time, the starting precursor, and the drying conditions. In our view these parameters, when fully understood and explored, will put us in a better position to develop materials of desirable properties systematically. We are interested in zirconia because of its potential catalytic applications in general (3) and its effectiveness as a support for superacids in particular (4). Furthermore, the phase transformation of zirconia as a ceramic material is of great interest (5).

EXPERIMENTAL

We used two different precursors in our sol-gel preparation. In the first approach (6), zirconium n-propoxide was mixed with n-propanol and nitric acid. This solution was then mixed with another solution containing n-propanol and water and the mixture was vigorously stirred. The gel time was defined as the time required after mixing for the vortex created by the stirring to disappear completely. The resulting gel, known as an alcogel because alcohol was the solvent, was covered and allowed to age for 2 h at room temperature. The alcohol was subsequently removed either by drying in a vacuum oven to form a xerogel, denoted as X-Zr, or by supercritical drying with carbon dioxide to form an aerogel, denoted as A-Zr. The supercritical drying conditions were usually at ca. 343 K and 2.1×10^7 Pa and the resulting aerogel powder was subsequently vacuum dried. Aerogels that were supercritically dried at a higher temperature of 473 K were denoted as A-Zr-473.

In the second approach (7), three different size zirconia sols, provided by Nyacol Products, Inc., were used: 5-10, 50, and 100 nm. These sols were gelled by the addition of ammonium hydroxide to give samples 10-Zr-0.3, 50-Zr-0.3, and 100-Zr-0.3. The first number refers to the initial sol size in nm and 0.3 is the ratio of ammonium hydroxide to nitric acid (which provides the counter ion in the original sol). These gels were allowed to age for 2-3 h at room temperature and then vacuum dried.

The above vacuum drying steps were performed at 383 K and 3.4×10^3 Pa for 3 h. Finally, all the samples were calcined at 773 K for 2 h in flowing oxygen (24 l/h).

An Autosorb-1 gas sorption system (Quantachrome Corp.) was used to obtain nitrogen adsorption/desorption isotherms. Before analysis, all samples were outgassed at 473 K under vacuum for 2-3 h. Pore size distribution data were calculated with the BJH method (8). X-ray diffraction experiments were performed on a Rigaku D/Max Diffractometer with $\text{Cu-K}\alpha$ radiation.

RESULTS AND DISCUSSION

Effect of Gel Time

At its simplest level, sol-gel chemistry involves the hydrolysis of a precursor (which is a metal alkoxide in our aerogel case) and the condensation of partially hydrolyzed species to form a three-dimensional gel network. The gel structure is thus sensitive to the rate of hydrolysis relative to that of condensation (9), and the two rates can be varied by, for example, adjusting the amounts of water and acid used in the preparation.

In our preparation of zirconia alcogels, we found that the gel time increases significantly when we increase the amount of nitric acid used (6). This observation can be understood in terms of an increased concentration of protonated hydroxo ligands with more acid, thus decreasing the condensation rate and increasing the gel time. The amount of water used also affects the gel time

by changing the concentration of the hydrolyzed species. Qualitatively a decrease in water content slows down the hydrolysis and condensation reactions, thus increasing the gel time. As an example of the effects of changing gel times, Figure 1 shows the variation of surface area and pore volume with gel time for zirconia aerogels calcined at 773 K for 2 h. A gel time of zero corresponds to the formation of a precipitate instead of a gel. This happens when no acid is used and a rapid condensation leads to particle growth. The resultant calcined product thus has very little surface area and pore volume. With increasing gel time, we slow down condensation to allow cross-linking to occur concurrent with particle growth. Hence the product has a large surface area and pore volume upon calcination. Under optimal conditions, we could stabilize a tetragonal zirconia that has a surface area of 134 m²/g and a pore volume of 0.37 cm³/g (see Table 1). However, with further lengthening of the gel time, condensation slows down to form a weakly cross-linked network. The collapse of this network during calcination leads to a decrease in surface area and pore volume. The variation of pore size distribution with gel time, as shown in Figure 2, is also consistent with this explanation.

In addition to macroscopic physical properties, gel time affects the microscopic "quality" of the material in terms of defect density. We found that zirconia aerogels prepared at different gel times exhibit different behavior with respect to their tetragonal-to-monoclinic phase transformation. Specifically, at a calcination temperature of 973 K, the ratio of tetragonal to monoclinic phase is a strong function of gel time. Samples with short gel times transform more readily into the monoclinic phase because they have higher defect densities (6). In sum, gel time is an important parameter in controlling the initial gel structure which impacts on all subsequent sol-gel processing steps.

Effect of Starting Precursor

In changing the rates of hydrolysis and condensation of metal alkoxides, one is balancing the growth of particles and the cross-linking of these particles. The particle size in a sol is thus a key parameter in controlling the initial gel structure. To probe this idea, we have used preformed zirconia sols as alternate precursors in order to study the effect of sol size independently. Table 1 summarizes the physical properties of zirconias prepared with three different starting sol sizes.

When solid spherical particles are packed together, the external surface area varies inversely with particle size. This trend is opposite to the data in Table 1, which shows that the sample made with the largest sol also has the highest surface area. This observation is due to the fact that the starting sol particles are not dense, but contain internal micropores which are the primary contributors to the surface area and pore volume of the resulting materials. In fact, we have found that all three zirconia samples have similar pore size distributions and are primarily microporous (7). Recall that zirconia aerogels are mesoporous (see Figure 2) and have pore volumes that are a factor of 3-5 higher (see Table 1).

Table 1 shows that the crystal structure of the 10-Zr-0.3 sample is the same as the zirconia aerogels. On the other hand, both the 50-Zr-0.3 and 100-Zr-0.3 samples contain monoclinic domains. This difference can be explained in terms of a bimodal size distribution in the two larger sols, which contain about half by weight particles in the indicated size and the other half in the 5-10 nm size range (7). Apparently the small particles crystallize into the tetragonal phase upon heat treatment while the large particles are in the monoclinic phase.

These results clearly demonstrate that using a different starting precursor (metal alkoxide versus preformed sols) is a simple and effective way to change the textural and structural properties of a sol-gel product. At the same time they teach us that a careful characterization of preformed sols, in particular their particle size distribution and porosity, is necessary for their applications as precursors.

Effect of Drying Conditions

The basic idea of supercritical drying is to eliminate the liquid-vapor interface in a pore in order to avoid differential capillary pressure in a gel network. Results in Table 1 show that physical properties of a zirconia aerogel (A-Zr) and xerogel (X-Zr) are indeed very different, with the latter having a much lower surface area and pore volume. Furthermore, the xerogel is primarily microporous. However, we note that we intentionally did not take great care in minimizing the capillary pressure in preparing the xerogel to illustrate the effect of drying conditions. There are many effective approaches, such as using a solvent with a low surface tension (10), in obtaining high-surface-area, low-density xerogels that are of catalytic interest.

We have found that varying the temperature while using a single drying agent, carbon dioxide, can also change the properties of a zirconia aerogel (11). We prepared two zirconia aerogels by supercritically drying them at 343 and 473 K. The two samples have similar surface areas, pore volumes, and crystal structures after calcination at 773 K for 2 h, but a more careful examination reveals interesting differences. First, the sample dried at 473 K has a pore size distribution that is shifted towards larger pores. The resulting larger average pore diameter explains why this sample has a larger pore volume but a smaller surface area than the sample dried at 343 K. Second, the sample dried at 473 K crystallizes into the tetragonal phase at a lower heat treatment temperature. Figure 3 shows that after calcination at 673 K for 2 h, the sample dried at 343 K remains X-ray amorphous whereas the one dried at 473 K shows a diffraction peak of tetragonal zirconia.

Our results highlight the fact that a gel is not static during supercritical drying. Indeed, drying should be considered as part of the aging process during which polymerization, coarsening, and phase transformation occur (2). While supercritical drying may be more effective in preserving a gel's network in comparison with evaporative drying, supercritical drying nonetheless accelerates aging because its operating temperature is above ambient. Along this line, we should expect aerogels that are prepared with different supercritical drying agents to have different properties. An example is the finding of Beghi et al. (12), who showed that anatase crystallization in titania-silica is more extensive when the sample is dried in alcohol (which has a higher critical temperature) than in carbon dioxide. Clearly, there are a lot of research opportunities in using supercritical drying conditions to vary the properties of aerogels.

SUMMARY

The sol-gel process has four key steps, gel formation, aging, drying, and heat treatment, each of which consists of a large number of tunable parameters. Furthermore, these steps are interrelated in that what happens in one step usually affects the next step. The initial gel structure will dictate the extent to which it is influenced by drying conditions, differently dried gels will have different structural evolution with heat treatment, and so on. However, it is important to view these complexities as opportunities in using the sol-gel method to prepare catalytic materials with desirable properties. In this paper we have shown the use of three specific parameters in changing the surface area, pore volume, and crystal structure of zirconia. Although these are physical and not chemical properties, results in our laboratory have shown that they have important catalytic implications. We believe more systematic studies are necessary to identify the key parameters in each sol-gel step and to understand the underlying physical and chemical processes. Extension to multi-component systems is of particular interest because of their widespread applications.

ACKNOWLEDGMENT

We thank the National Science Foundation (CTS-9200665) for supporting this work and Nyacol Products, Inc. for providing us with zirconia sols. D.A.W. thanks the Texaco Foundation for the support of a graduate fellowship.

REFERENCES

1. Cauqui, M. A. and Rodríguez-Izquierdo, J. M., *J. Non-Cryst. Solids* **147/148**, 724 (1992).
2. Brinker, C. J. and Scherer, G. W., *Sol-Gel Science: The Physics and Chemistry of Sol-Gel Processing*; Academic: New York, 1990.
3. Tanabe, K., *Mater. Chem. Phys.* **13**, 347 (1985).
4. Hino, M., Kobayashi, S. and Arata, K., *J. Am. Chem. Soc.* **101**, 6439 (1979).
5. Srinivasan, R., Davis, B. H., Cavin, O. B. and Hubbard, C. R., *J. Am. Ceram. Soc.* **75**, 1217 (1992).
6. Ward, D. A. and Ko, E. I., *Chem. Mater.* **5**, 956 (1993).
7. Ward, D. A. and Ko, E. I., *Langmuir*, in press.
8. Barrett, E. P., Joyner, L. G. and Halenda, P. P., *J. Am. Chem. Soc.* **73**, 373 (1951).
9. Livage, J., Henry, M. and Sanchez, C., *Prog. Solid St. Chem.* **18**, 259 (1988).
10. Smith, D. M., Desphande, R. and Brinker, C. J., *Mat. Res. Soc. Symp.* **271**, 567 (1992).
11. Brodsky, C. J. and Ko, E. I., *J. Non-Cryst. Solids*, in press.
12. Beghi, M., Chiurlo, P., Costa, L., Palladino, M. and Pirini, M. F., *J. Non-Cryst. Solids* **145**, 175 (1992).

Table 1. Physical Properties of Zirconium Oxides after Calcination at 773 K for 2 h

Sample notation	BET surface area (m ² /g)	Pore volume (cm ³ /g)	Crystal structure ^a
A-Zr ^b	134	0.37	tetragonal
A-Zr-473 ^c	124	0.43	tetragonal
X-Zr	28	0.029	tetragonal
10-Zr-0.3 ^d	17	0.017	tetragonal
50-Zr-0.3 ^d	131	0.087	tetragonal + monoclinic
100-Zr-0.3 ^d	149	0.124	tetragonal + monoclinic

^a Determined by X-ray diffraction; ^b Taken from (6); ^c Taken from (11);

^d Taken from (7).

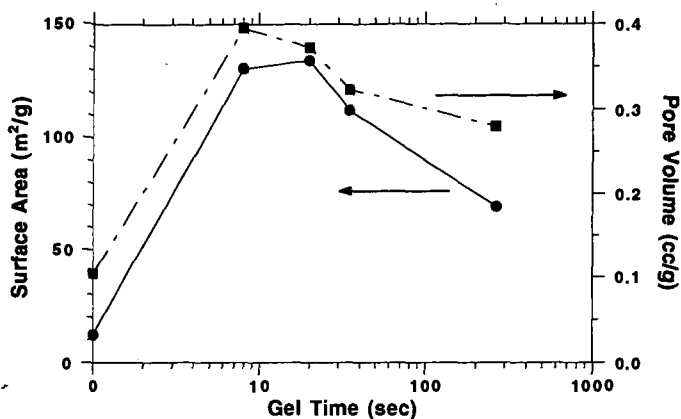


Figure 1. Effect of gel time on the physical properties of zirconia aerogels after calcination at 773 K for 2 h

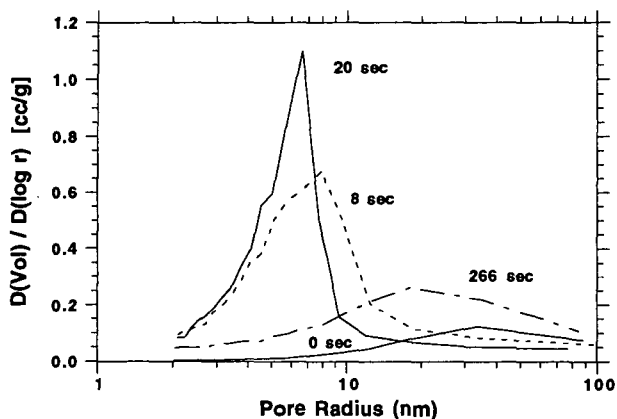


Figure 2. Effect of gel time on the pore size distribution of zirconia aerogels after calcination at 773 K for 2 h

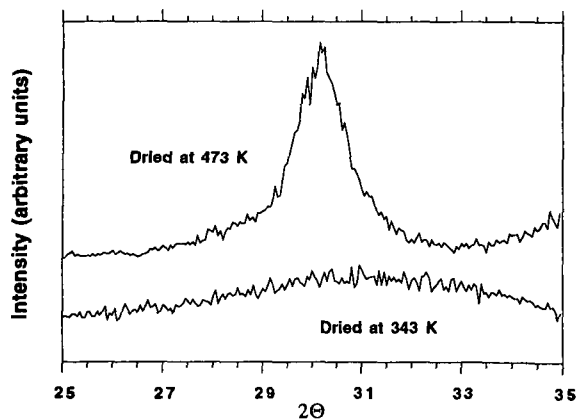


Figure 3. Effect of supercritical drying temperature on the crystallization of zirconia aerogels after calcination at 673 K for 2 h

CATALYTIC HYDRODENITROGENATION OF QUINOLINE WITH NANOSCALE Mo_2N , Mo_2C and MoS_2 SYNTHESIZED BY LASER PYROLYSIS

¹R. Ochoa, ²W.T. Lee, ^{1,2}P.C Eklund,

¹Center for Applied Energy Research

²Department of Physics and Astronomy,

University of Kentucky, Lexington KY 40511.

KEYWORDS: Laser Pyrolysis, hydrodenitrogenation, molybdenum nitride, molybdenum carbide

INTRODUCTION

As the quality of available petroleum feedstocks decreases, the demand for better and more active catalysts for hydrotreatment increases. Nitrogen content in coal, tar sands, shale and petroleum residua is present predominantly in the form of heterocyclic compounds. Quinoline constitutes a molecule representative of these heterocyclic compounds and its catalytic denitrogenation is one of the most studied model compound reactions. Due to the considerable number of stable reaction intermediates with different absorptivities and reactivities, this reaction is a typical example of the complexity of the denitrogenation process.

Nitrogen removal from heterocyclic compounds is a more difficult process than sulfur removal. It has been accepted that it requires hydrogenation of the ring containing the nitrogen atom before hydrogenolysis of the carbon-nitrogen bond occurs [1,2]. This is partly due to the thermodynamics of the aliphatic C-N bond hydrogenolysis reaction.

Figure 1 shows a diagram of the reaction pathway reported by Satterfield et al [3,4] for the denitrogenation of quinoline over a sulfided $\text{NiMo}/\text{Al}_2\text{O}_3$ catalyst. It is seen that the HDN reaction proceeds through the hydrogenation of quinoline (Q) to 1,2,3,4 tetrahydroquinoline (THQ) and 5,6,7,8 tetrahydroquinoline (CHPYD), the first reaction being faster than the second. THQ can either convert into propylaniline (O-PA), through bond cleavage of the C-N bond, or together with CHPYD, it can hydrogenate to form decahydroquinoline (DHQ). The rapid hydrogenation of Q to THQ causes the establishment of a pseudoequilibrium among this hydrogenated derivatives of quinoline [1]. As seen in the figure, this pathway indicates that removal of nitrogen from O-PA requires the hydrogenation of the aromatic ring, consuming more hydrogen in the reaction. Therefore, it is desirable to synthesize hydrodenitrogenation catalysts that will induce nitrogen removal from the molecule without full hydrogenation of the aromatic ring.

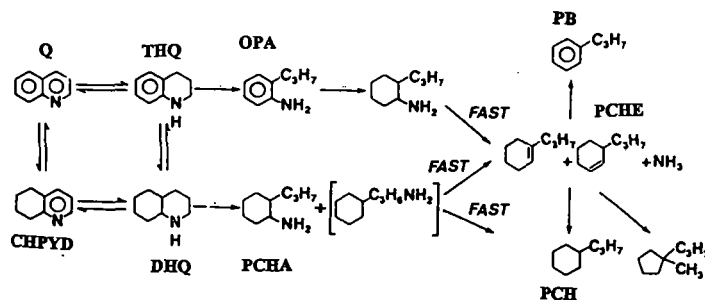


Figure 1
Reaction Pathway for quinoline HDN

It has been reported that nitrides and carbides of transition metals, specially Mo_2C and Mo_2N , synthesized by Temperature Programmed Reduction, possess high activity for heteroatom removal and hydrogenation of coal liquids and model compounds [5-7]. This work presents the results of the evaluation of the catalytic activity of Mo_2N , MoS_2 and Mo_2C ultrafine particle catalysts (UFP), synthesized by laser pyrolysis, for quinoline hydrodenitrogenation (HDN).

EXPERIMENTAL

Mo-based ultrafine particle catalysts (Mo_2C , Mo_2N , MoS_2) were produced by laser pyrolysis from the reaction of $\text{Mo}(\text{CO})_6$ with a gaseous reactant (NH_3 , C_2H_4 , or H_2S) followed by surface passivation in a flow of 5% O_2 balanced He at 300 K. The details of the experimental procedure and apparatus have been reported elsewhere [8,9].

The catalysts structure and morphology have been characterized by X-ray diffraction, high resolution-transmission electron microscopy (HR-TEM) and thermogravimetry-mass spectrometry (TG-MS) [8-11]. The surface area was determined by the nitrogen BET method. The average composition of these particles was obtained by elemental analysis and the chemical state of the surface was characterized by X-ray photoelectron spectroscopy. Irreversible chemisorption of CO was used to measure the number of active sites on the catalyst surface.

Catalytic activity was evaluated using a stainless steel bomb microreactor, 22 cm^3 in volume, which was pressurized at 800 psi of hydrogen. A 5% catalyst loading with respect to a solution of quinoline dissolved in hexadecane was used. The reactor was maintained at 380°C for reaction periods of 15, 30 and 60 min while agitating at 440 rpm in a fluidized sand bath. The effect of the presence of added sulfur in the reaction was studied by adding dimethyl disulfide (DMDS) in 20% excess of the stoichiometric amount required to convert Mo_2N and Mo_2C to MoS_2 . The liquid products were analyzed by gas chromatography with a fused-silica 30 m capillary DB5 column with a Flame Ionizing Detector. In this model compound reaction, the concentration of the liquid phase products is given as a mole percentage of quinoline initially charged to the reactor and normalized to 100%.

RESULTS AND DISCUSSION

Characterization

Table 1 summarizes the structural properties of these materials together with those from the commercial catalyst Shell 324.

TABLE 1

Catalyst	Surface area m^2/g	Crystallite size (nm)	Particle size (nm)	Site Density $\times 10^{15} \text{cm}^{-2}$
fcc Mo_2N	63	3	10	0.92
fcc Mo_2C	75	2	8.5	0.24
hex. MoS_2	86	2	4.3	na
Shell 324*	160	11	7.9	0.27

* From ref [12].

X-ray diffraction and HR-TEM have shown that Mo_2C and Mo_2N exhibit a face centered cubic structure whereas MoS_2 has an hexagonal structure. The crystallite size of the UFP catalysts was calculated from the full width at half maximum of the corresponding x-ray diffraction lines and the particle size from the value of the surface area of the particle using $D_p = 6/\rho S$, where S is the surface area of the particle and ρ is the mass density. The difference observed between particle size and crystallite size indicates that these particles are partially agglomerated. Notice that Mo_2N possesses a density of active sites almost four times higher than that of Mo_2C . However the number of active sites measured is about half of the reported for materials synthesized by Temperature Programmed Reduction [6]. Elemental analysis gave an average composition for Mo_2N of $\text{Mo}_2\text{N}_{0.77}\text{C}_{0.3}$ and Mo_2C of $\text{Mo}_2\text{C}_{0.95}\text{O}_{0.5}$ for the molybdenum carbide. Since this particles are so small, the high oxygen content observed in the results can be accounted for as an oxide monolayer of MoO_3 on the particle surface, as confirmed by XPS analysis [10].

Catalytic Activity

Figure 2 presents the results from the conversion of quinoline with respect to reaction time over Mo_2N , Mo_2C and MoS_2 UFP. It is observed that all three catalysts gave approximately the same high level of conversion. However, because there are numerous nitrogen-containing intermediate products, a high quinoline conversion does not necessarily correlate with high HDN conversion. In this case, quinoline was converted essentially into tetrahydroquinoline (THQ).

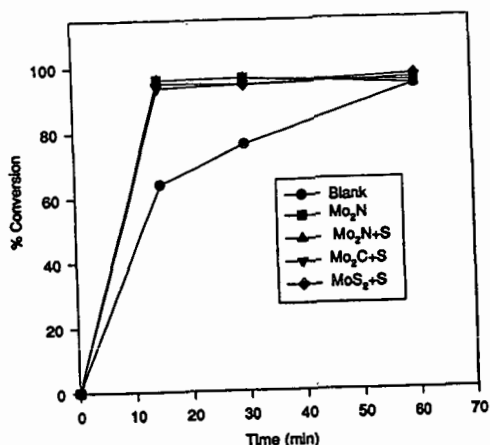


Figure 2

Conversion of quinoline with respect to time over Mo₃N, Mo₃C and MoS₂.

Figure 3 presents the product distribution for quinoline over the molybdenum nanoparticles after 30 minutes of reaction. The results are also compared to those of the commercial catalysts Shell 324 which was sulfided prior to the reaction.

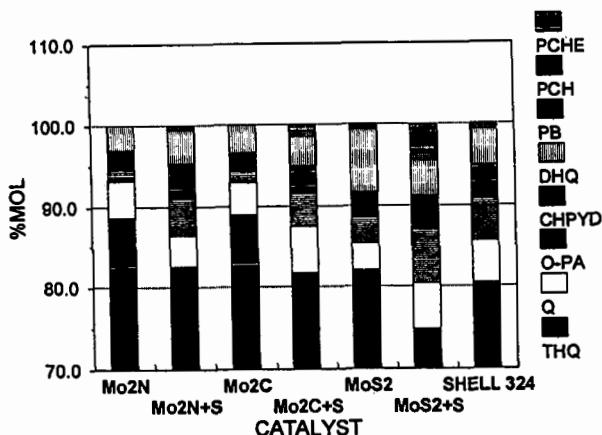


Figure 3. Product distribution after 30 minutes of reaction time

As it was previously mentioned, the main product of the reaction is THQ, in concentrations higher than 70% mol. This high concentration is thermodynamically favored by the elevated hydrogen pressure at which the reaction was carried out [1]. Mo₃C and Mo₃N gave very similar product distribution and concentration. This may be explained in terms of the similarity in surface composition observed from the xps analysis of these two catalysts [10]. Besides THQ, o-propylaniline (O-PA), decahydroquinoline (DHQ) and cyclohexenopyridine (CHPYD) were also produced, while no denitrogenated products were detected. A higher concentration of DHQ (8%) and a small amount of propylbenzene (PB) were produced in the presence of MoS₂. Notice that Shell 324 gave similar conversion as MoS₂.

Longer reaction time periods (Figure 4) induced the conversion of tetrahydroquinoline (THQ) mainly into hydrogenated products, primarily decahydroquinoline (DHQ) with some THQ being dehydrogenated back to quinoline. Only small concentrations of nitrogen-free molecules were detected, less than a total of 1% mol.

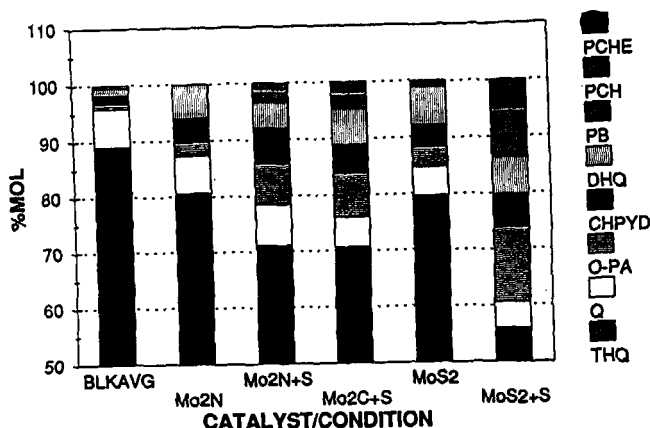


Figure 4. Product Distribution after 60 minutes of reaction time.

When excess sulfur was added to the reaction mixture, the concentration of THQ decreased, especially in the case of MoS_2 , indicating that it was converted into other reaction products. Furthermore, the average concentration of hydrogenated products did not seem to be affected as much as the concentration of propylaniline (O-PA), which increased by more than 200% for the three catalysts. This fact agrees with previous reports that the presence of H_2S enhances hydrogenolysis reactions [1,2]. An increase in the concentration of denitrogenated compounds, mainly propylcyclohexane (PCH) and propylcyclohexene (PCHE) was also observed. Only small concentrations of propylbenzene (PB) (~1-2%) were detected in the product mixture. This result agrees with the reaction pathway shown in figure 1. According to this figure, propylaniline (OPA) is hydrogenated to propylcyclohexylamine, which undergoes rapid denitrogenation to produce propylbenzene (PB), propylcyclohexene (PCHE) and propylbenzene (PB). In addition, decahydroquinoline (DHQ) undergoes hydrogenolysis of the C-N bond to produce propylcyclohexylamine.

Since the concentration of decahydroquinoline (DHQ) does not increase, but in some cases decreases, while the concentration of propylaniline (OPA) increases, it follows that the denitrogenation of decahydroquinoline (DHQ) is favored over the hydrogenation of O-PA. X-ray diffraction of the spent catalysts indicates that there is some transformation of Mo_2N and Mo_2C into MoS_2 after 60 minutes of reaction. This may explain why all three catalysts seem to follow the same reaction pathway.

HDN Activity

The Mo-based ultrafine particles exhibited low activity for HDN even in the presence of added sulfur. This low activity was unexpected, since there are reports of higher conversions and high selectivity for Mo_2C and Mo_2N catalysts, even under sulfur free conditions [6]. This outcome has been attributed in part to the presence of an oxide phase on the surface of these catalysts that may inhibit their activity [13,10].

Figure 5 presents % HDN as a function of time for the Mo-based UFP catalysts in the presence of added sulfur. As it was mentioned above, in the absence of sulfur very little denitrogenation was observed (less than 1%), even if the reaction was carried out for longer time periods or at higher temperatures (up to 2 hours, 400°C).

When H_2S was present, the denitrogenation of quinoline increased from 0.5% to 3% for Mo_2N and to 4% for Mo_2C . Considering that Mo_2C has a lower number of active sites per unit area of catalyst, it follows that it is a more active catalyst than Mo_2N . As shown by figure 5,

MoS₂ was the most active catalyst since it gave the largest percent of denitrogenation (13%).

In terms of product selectivity, all three catalysts favored hydrogenated products over aromatic ones in the form of mixtures of propylcyclohexane and propylcyclohexene.

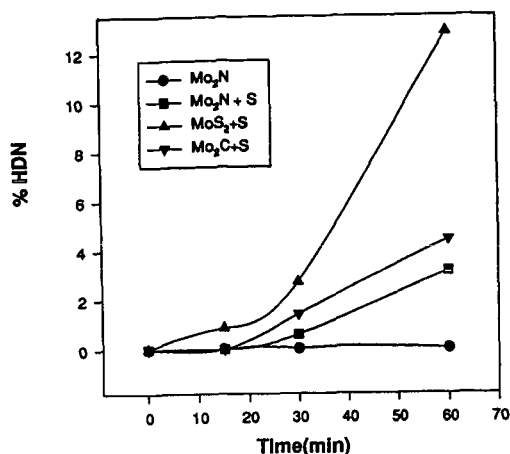


Figure 5
%HDN versus time for Mo₂N, Mo₂C and MoS₂ UFP catalysts.

CONCLUSIONS

Mo₂C, Mo₂N and MoS₂ ultrafine particle catalysts exhibited low activity and selectivity for the hydrogenation of quinoline. MoS₂ appears to be the most active catalyst. In the absence of sulfur, only less than 1% HDN was obtained with these catalysts. The addition of sulfur favored HDN activity by enhancing the hydrogenolysis of decahydroquinoline and tetrahydroquinoline. However, the improvement in activity was not very significant. The lower-than expected activity observed for this reaction, as well as for other model compound reactions tested [13], has been attributed to the presence of oxygen and amorphous carbon on the catalysts surface. In previous studies, it has been shown that surface composition has a large effect on the catalytic behavior of Mo₂C and Mo₂N specially for structure-sensitive reactions like hydrogenolysis and isomerization. Future studies to prevent or remove oxide coatings and to observe the effect on catalytic activity are underway.

REFERENCES

- [1] T.C. Ho, Catal. Rev. -Sci. Eng., 30(1), (1988) 117-160.
- [2] M. J. Girgis, B.C. Gates, Ind. Eng. Chem. Res. 30; (1991)2021-2058.
- [3] C.N. Satterfield, J.F. Cocchetto, Ind. Eng. Chem. Proc. Des. Dev. 17, (1978) 141
- [4] C.N. Satterfield, S.H. Yang, Ind. Eng. Chem. Proc. Des. Dev.23, (1984) 11
- [5] S.T. Oyama, R. Kapoor, C. Shudakar, Prep. of Am. Chem. Soc. Div. Fuel Chemistry, 37(1), (1992), 233.
- [6] S.T. Oyama, J.C. Schlatter, J. Metcalfe, J. Lambert, Ind. Eng. Chem. Res. 27, (1988) 1648-1653.
- [7] S.T. Oyama, J.C. Schlatter, J. Metcalfe, J. Lambert, Ind. Eng. Chem. Res. 27, (1988) 1639.
- [8] X.X. Bi, B. Ganguly, G.P. Huffinan, F.E. Huggins, M. Endo, P.C. Eklund, J. Mater. Res. 8(7), (1993) 1666.
- [9] X.X. Bi, Y. Wang, W.T. Lee, K.A. Wang, S. Bandow and P.C. Eklund, Mat. Res. Soc. Symp. Proc., 327, (1994) 47-52.
- [10] X.X. Bi, K.Das Chowdhury, R. Ochoa, W.T. Lee, S. Bandow, M.S. Dresselhaus and P.C. Eklund, Proc. Mat. Res. Soc. Symp T, Boston, 1994.
- [11] R. Ochoa, P. Zhou, X.X. Bi, W.T. Lee, A. Rao, P.C. Eklund, ACS Prep. Div. Fuel Chem. April 1995.
- [12] C. C Yu, S. Ramanathan, F. Sherif, S.T. Oyama, J. Phys. Chem., 98 (1994) 13038-13041.
- [13] R. Ochoa, G.T. Hager, W.T. Lee, S. Bandow, E. Givens and P.C. Eklund, Proc. Mat. Res. Soc. Symp T, Boston, 1994.

CATALYTIC ACTIVITY OF NANOPHASE METALS PREPARED SONOCHEMICALLY

Taeghwan Hyeon, Mingming Fang, Andrzej A. Cichowlas, and Kenneth S. Suslick*

*School of Chemical Sciences and Materials Research Laboratory,
University of Illinois at Urbana-Champaign, 505 S. Mathews Ave., Urbana, IL 61801
tel, 217-333-2794; fax, 217-333-2685; email, ksuslick@uiuc.edu*

Keywords: ultrasound, sonochemistry, nanophase, nanostructured, heterogeneous catalysis

INTRODUCTION

The chemical effects of high intensity ultrasound arise from acoustic cavitation: the formation, growth, and implosive collapse of bubbles in a liquid, which generates a transient, localized hot spot (1, 2). The local conditions reached have temperatures of ~5000 K, pressures of ~1800 atm, but with cooling rates that exceed 10^{10} K/s (3, 4). We have made use of these extreme conditions to develop a new technique for the synthesis of nanostructured heterogeneous catalysts. When irradiated with high intensity ultrasound in low volatility solvents under argon, volatile organometallic precursors produce high surface area solids that consist of agglomerates of nanometer clusters. These nanostructured solids are active heterogeneous catalysts for hydrocarbon reforming and CO hydrogenation. For Fe and Co, nanostructured alloys can be formed of any composition. Using polymeric ligands or oxide supports, the initially formed nanoscale clusters can be trapped as colloids or supported catalysts, respectively.

A central focus of recent work in materials chemistry has been the preparation of nanostructured materials (5, 6). A variety of chemical and physical preparative methods have been applied to produce materials with nanometer structure; these include metal evaporation (7), decomposition of organometallic compounds (8), and the reduction of metal salts (9, 10). Sonochemical decomposition of transition metal carbonyl compounds has also been proven to be a useful technique to generate nanophase transition metals (11, 12).

One of the advantages of our sonochemical synthesis of nanostructured materials is that various forms of nanophase materials can be generated simply by changing the reaction medium. When precursors are sonicated in high boiling alkane such as decane or hexadecane, nanostructured powders are formed. Using a polymeric ligand (e.g. polyvinylpyrrolidone (PVP)) or inorganic support (silica, alumina, etc.), nanophase metal colloids and nanostructured supported metal catalysts are generated (Scheme 1). A transmission electron micrograph of the nanocolloid Fe/PVP is shown in Figure 1.

EXPERIMENTAL SECTION

All manipulations for the preparation of samples were performed using Schlenk vacuum line and inert atmosphere box (Vacuum Atmospheres, < 1 ppm O₂) techniques. Pentane was distilled over sodium-benzophenone. Decane and hexadecane were distilled over sodium. Ultrasonic irradiation was accomplished with a high intensity ultrasonic probe (Sonic and Materials, model VC-600, 1 cm Ti horn, 20 kHz, 100 Wcm⁻²).

X-ray powder diffraction data were collected on a Rigaku D-max diffractometer using Cu K α radiation (λ = 1.5418 Å). Scanning electron micrographs were taken on a Hitachi S800 electron microscope. Transmission electron micrographs were taken on a Phillips CM-12 electron microscope. Samples for elemental analysis were submitted in sealed vials without exposure to air.

Hydrogen (99.99%, Linde), methane (99.97%, Matheson) and CO (99.0+%, Linde) were further purified through 5 Å molecular sieves and oxy-traps (Alltech). Cyclohexane (99+%, Fischer) was dried over molecular sieves prior to use. In cyclohexane reaction, a MKS mass flow controller maintained the flow of hydrogen at 27.5 cm³ (STP)/min to carry the cyclohexane vapor at a constant partial pressure of 0.1 bar through the catalyst. A quartz reactor was used for both adsorption and gas-solid catalytic studies. The catalysts were transferred from an inert atmosphere box to the catalytic rig without exposure to air. Surface areas were calculated by applying the BET equation to the N₂ adsorption isotherm measured at 77 K. The gas products obtained during the temperature-programmed desorption (TPD) and temperature-programmed reaction (TPR) experiments were analyzed by a quadrupole mass spectrometer (Spectra Instruments). The catalytic reaction products were analyzed by gas chromatography (Hewlett-Packard 5730A) on a n-octane/Porasil C column with flame ionization detector.

RESULTS AND DISCUSSION

Synthesis and catalytic studies of nanostructured silica-supported Fe

Ultrasonic irradiation of decane solutions of iron pentacarbonyl, Fe(CO)₅, in the presence of silica gel produces a silica-supported amorphous nanostructured iron. Silica gel (Universal Scientific Incorporated chemicals, 63-100 mesh) was pretreated at 450°C under vacuum (1×10^{-5} Torr) for 10 hours before use. A solution of Fe(CO)₅ in dry decane was added to this, and the slurry was irradiated at 20°C with a high-intensity ultrasonic probe for 3 hours under argon. After irradiation, the black powder was filtered and washed with dry pentane in an inert atmosphere box. The iron loading on silica can be easily varied by

changing the initial concentration of the $\text{Fe}(\text{CO})_5$ solution. Elemental analysis reveals Fe, Si, O and a trace amount of carbon (<1%) to be present. The origin of carbon most likely arises from the decomposition of CO or the alkane solvent during ultrasonic irradiation. Conventional silica-supported crystalline iron catalysts were prepared using the incipient wetness impregnation method by dissolving $\text{Fe}(\text{NO}_3)_3 \cdot 9\text{H}_2\text{O}$ in an aqueous solution containing silica gel. These samples were dried at 220°C for 12 hours, and calcined at 450°C under an O_2 flow for 1 hour. Reduction of iron supported on silica was carried out in a flow of hydrogen for 1 hour at 200°C, for 1 hour at 300°C, and finally for two hours at 450°C.

Transmission electron microscopy shows that the iron particles produced by sonolysis of $\text{Fe}(\text{CO})_5$ were highly dispersed on the silica surface. The iron particles range in size from 3 to 8 nm. Chemisorption of CO allowed measurement of the dispersion and the average particle size of the iron supported on the silica surface (13). CO chemisorption measurement data at -78°C show the average iron particle size to be ≈ 7.3 nm, which corresponds well with TEM data.

The catalytic activity of the silica supported nanostructured iron was probed in the commercially important Fischer-Tropsch synthesis reaction (i.e., hydrogenation of CO). Figure 2 compares the activity (in terms of turnover frequency of CO molecules converted per catalytic site per second) of silica-supported nanophase iron and conventional silica-supported iron (prepared by the incipient wetness method) as a function of temperature. These catalytic data were obtained at high iron loading and low dispersion to minimize the effects of support and dispersion. The sonochemically produced iron on silica catalyst is an order of magnitude more active than the conventional supported iron. Moreover, the silica-supported nanostructured iron catalyst exhibits high activity at low temperatures (<250°C), whereas the silica supported conventional iron catalyst has no activity. We suggest that the dramatic difference in activity between the two samples below 300°C may be due to the amorphous nature of iron and the inherently highly-defected surface formed during sonolysis of $\text{Fe}(\text{CO})_5$ when the amorphous state of iron is preserved. Above that temperature the activity of our sonochemically prepared catalyst declines, which may be due to crystallization, surface annealing, and deactivation of the catalyst as result of surface carbon deposition.

Differences between the catalytic properties of the nanostructured iron and of conventional supported catalysts are also observed in selectivities of hydrocarbon synthesis. Under our conditions, the major reaction products for both catalysts are short chain C_1 - C_4 hydrocarbons and CO_2 . Product distribution of hydrocarbons showed that at temperatures lower than 275°C, the silica-supported nanostructured iron catalyst shows higher selectivity towards long chain hydrocarbons (C_5), whereas the conventional supported iron shows no activity at these temperatures. At temperatures higher than 275°C, the reaction product distributions are similar for both types of catalysts.

Synthesis and catalytic studies of nanostructured Fe-Co alloys

$\text{Fe}(\text{CO})_5$ and $\text{Co}(\text{CO})_3(\text{NO})$ were chosen as precursors because of their high vapor pressures at modest bulk solution temperatures where they are still thermally stable. Solutions of $\text{Fe}(\text{CO})_5$ and $\text{Co}(\text{CO})_3(\text{NO})$ at various relative concentrations in dry decane were irradiated at 0°C with a high-intensity ultrasonic probe for 3 hours under argon. After irradiation, a black powder was formed, which was filtered and washed with dry pentane in the glove box. The composition of the Fe-Co alloys can be controlled simply by changing the ratio of solution concentrations of the precursors; any alloy compositions ranging from pure Fe to pure Co can be readily obtained.

The solid-solution nature of the alloys was confirmed by TEM-EDX results, which were made on different spots of the polycrystalline alloy powders. The EDX results show that the alloys are homogeneous on a nanometer scale. The original Fe, Co, and Fe-Co alloys produced by ultrasound are porous, coral-like agglomerates of few-nanometer sized clusters; they are structurally amorphous on the nm scale, as determined by XRD, electron-beam microdiffraction, and DSC. After heat treatment under H_2 gas flow at 400°C for 2 hours, all samples underwent an irreversible crystallization, as shown by both DSC and XRD. The XRD results show no peaks attributable to iron/cobalt oxide, iron/cobalt carbide or other iron/cobalt impurity phases. Pure Fe crystallizes to cubic (bcc) structure, pure Co crystallizes to cubic (fcc) and hexagonal (hcp) mixed structures. All the alloys that we have tested so far crystallize in the bcc structure, which is consistent with the known Fe-Co equilibrium phase diagram (14). Elemental analysis results show that nearly pure metal and alloys are produced. SEM at high magnification indicates that these materials are porous aggregates of small clusters of 10-20 nm particles. Surface electronic structures and surface compositions of the sonochemically prepared Fe-Co alloys were also examined by using x-ray photoelectron spectroscopy (XPS). The XPS measurements have been performed on heat treated samples before catalytic reactions. The electronic structures of the surfaces of these samples appear to be the same as the pure metals. The surface compositions of the alloys demonstrate some small enrichment of Fe over Co. Similar trends towards an iron-enriched surface have been reported by other researchers with other preparations using coprecipitation methods (15).

Catalytic studies of the sonochemically prepared Fe-Co alloys were made on the reactions of cyclohexane: i.e., dehydrogenation versus hydrogenolysis. These reactions provide a useful pair of structure sensitive catalytic reactions to probe the nature of the sonochemically prepared nanophase catalysts. All catalysts were treated under H_2 gas flow at 400°C for 2 hours before the catalytic studies. The catalytic activity (in terms of turnover frequency of cyclohexane molecules converted to benzene per surface Fe/Co atom per second) as a function of temperature is shown in Figure 3. Two kinds of products were formed during the

cyclohexane reaction: benzene was the only dehydrogenation reaction product and aliphatic hydrocarbons (mostly methane) were the hydrogenolysis reaction products. The catalytic selectivity (in terms of the percentage of benzene among all the reaction products) as a function of temperature is shown in Figure 4. The catalytic properties of the sonochemically prepared Fe, Co and Fe-Co alloys in the cyclohexane reaction exhibit interesting trends. First, they are all active catalysts for cyclohexane conversion: pure Co has the highest activity (albeit primarily for hydrogenolysis), pure Fe has the lowest activity, and Fe-Co alloys have intermediate activity between pure Fe and pure Co. Second, Fe-Co alloys generate much more dehydrogenation product (benzene) than pure Fe or Co. Third, the 1:1 Fe/Co alloy has both much higher dehydrogenation activities and selectivities at all reaction temperatures (250°C to 300°C) than the other alloys or pure metals. In the best cases, the selectivity for dehydrogenation approaches 100%. The origin of this dramatically improved selectivity is under further investigation.

CONCLUSIONS

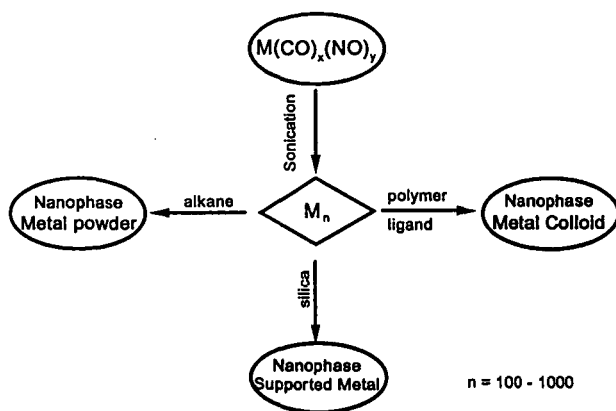
Sonochemical decomposition of volatile organometallic precursors in high boiling solvents produces nanostructured materials in various forms with high catalytic activities. Sonication of iron pentacarbonyl with silica in decane at 20°C generated supported amorphous nanostructured Fe on silica catalyst. The nanostructured Fe on silica catalyst showed higher catalytic activity for the Fischer-Tropsch synthesis compared to the conventional Fe/silica catalyst prepared by incipient wetness method. Sonochemical decomposition of Fe(CO)₅ and Co(CO)₈ in decane at 0°C generated nanostructured Fe and Co metals and Fe-Co alloys. The sonochemically prepared Fe-Co alloys have large surface areas relative to bulk metal even after heat treatment. We find very high catalytic activity for these Fe, Co, and Fe-Co powders for the dehydrogenation and hydrogenolysis of cyclohexane. The sonochemically prepared Fe-Co alloys show high catalytic activity for the dehydrogenation of cyclohexane to benzene, with 1:1 ratio Fe-Co alloys having selectivities as high as 100%.

ACKNOWLEDGMENTS

This work was supported by National Science Foundation. We thank Peggy Mochel, Vania Petrova, and the UIUC Center for Microanalysis of Materials, supported by the US Department of Energy, for their assistance in the electron microscopic studies.

REFERENCES

1. K.S. Suslick, *Science* **247**, 1439 (1990).
2. K.S. Suslick, in K.S. Suslick (eds.), *Ultrasound: Its Chemical, Physical, and Biological Effects*, VCH Press, New York, 1988, p. 123.
3. E.B. Flint and K.S. Suslick, *Science* **253**, 1397 (1991).
4. K.S. Suslick, R.E. Cline and D.A. Hammerton, *J. Amer. Chem. Soc.* **106**, 5641 (1986).
5. H. Weller, *Adv. Mater.* **5**, 88 (1993).
6. G.A. Ozin, *Adv. Mater.* **4**, 612 (1992).
7. S.C. Davis and K.J. Klabunde, *Chem. Rev.* **82**, 152 (1982).
8. A.S. Lisitsyn, A.V. Golovin, A.L. Chuvilin, V.L. Kuznetsov, A.V. Romanenko, A.F. Danilyuk and Y.I. Yermakov, *Appl. Catal.* **55**, 235 (1989).
9. H. Boennemann, W. Brijoux R. Brinkmann and T. Jousen, *Angew. Chem., Intl. Ed. Engl.* **129**, 273 (1990).
10. K.-L. Tsai, J.L. Dye, *J. Amer. Chem. Soc.* **113**, 1650 (1991).
11. K.S. Suslick, S.B. Choe, A.A. Cichowas and M.W. Grinstaff, *Nature* **353**, 414 (1991).
12. M.W. Grinstaff, M.B. Salamon and K.S. Suslick, *Phys. Rev. B* **48**, 269 (1993).
13. Dumesic, J. A.; Topsøe, H.; Boudart, M. *J. Catal.* **37**, 513 (1975).
14. T. Nishizawa and K. Ishida, *Bull. Alloy Phase Diagrams* **5**, 250 (1984).
15. M. Nakamura, B. J. Wood, P. Y. Hou, and H. Wise in *Proc. 4th Intl. Congr. Catal., Tokyo*, Kodansha Ltd., Tokyo, 1981, p. 432.



Scheme 1. Sonochemical synthesis of various forms of nanostructured materials.

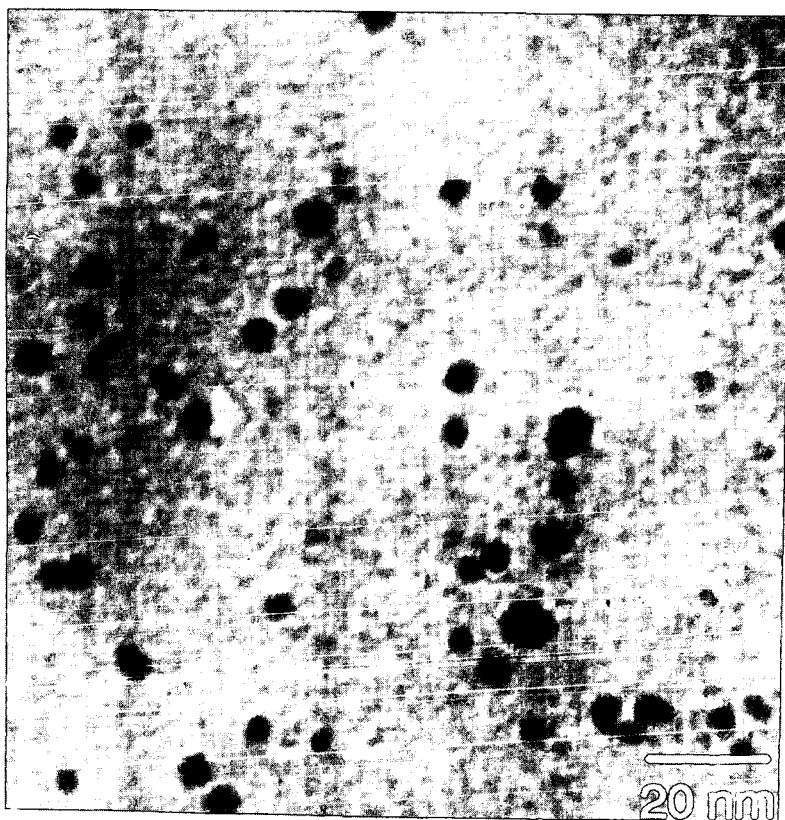


Figure 1. Transmission electron micrograph of nanostructured Fe/PVP, obtained on a Philips 420 electron microscope.

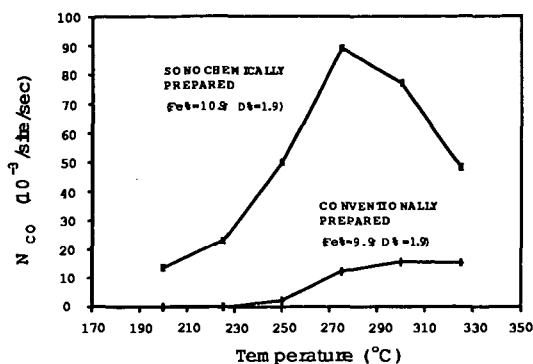


Figure 2. The catalytic activity for Fischer-Tropsch synthesis as a function of temperature. Silica-supported nanostructured iron catalyst prepared by ultrasonic irradiation of a decane solution of $\text{Fe}(\text{CO})_5$ slurried with silica (iron loading wt% = 10.94, and dispersion, D% = 1.85) compared to conventional silica-supported crystalline iron catalyst prepared by the incipient wetness method (Fe wt% = 9.91, D% = 1.86). H_2/CO = 3.48, 1 atm.

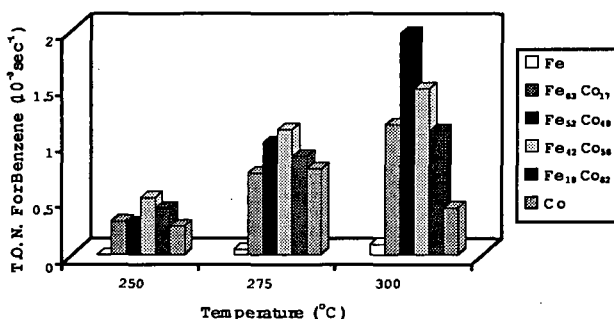


Figure 3. The catalytic activity of Fe, Co, and Fe-Co alloys for dehydrogenation of cyclohexane to benzene as a function of temperature.

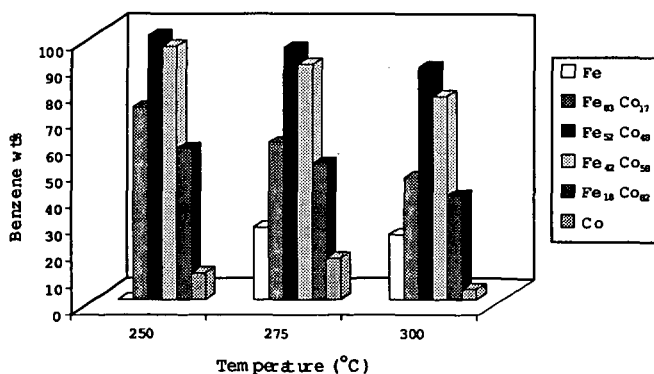


Figure 4. The catalytic selectivity of Fe, Co, and Fe-Co alloys for dehydrogenation versus hydrogenolysis of cyclohexane as a function of temperature.

THE EFFECT OF CATALYST DISPERSION ON THE ACTIVITY OF UNSUPPORTED MOLYBDENUM CATALYSTS

Anthony V. Cugini, Donald V. Martello, Donald Krastman, John P. Baltrus, Michael V. Ciccio, Elizabeth F. Frommell, and Gerald D. Holder*

U.S. Department of Energy/PETC, P. O. Box 10940, Pittsburgh, PA, 15236 (*University of Pittsburgh, Department of Chemical and Petroleum Engineering)

INTRODUCTION

Unsupported catalysts have received considerable attention for coal liquefaction. These catalysts have been introduced into coal liquefaction systems by impregnation of the coal, as water-soluble salts, as volatile metal carbonyls, as oil-soluble organometallics, as finely divided powders, and as mineral matter associated with the coal and/or solvent.⁽¹⁾ For the most part, the method of catalyst precursor addition affected the observed catalyst performance. Weller et al.⁽²⁾ found that, with ammonium heptamolybdate, coal impregnation resulted in higher coal conversions than physical mixing of the powder with coal. Others^(3,4) have also observed this result. Additionally, Derbyshire et al.⁽⁴⁾ found that the conditions used to dry the impregnated coal (removing the aqueous solvent used for solubilizing the catalyst precursor) affected the activity of the molybdenum. Joseph⁽⁵⁾ and Artok et al.⁽⁶⁾ reported that expanding the coal structure (by swelling during impregnation) improved the observed activity of the catalyst, possibly by allowing better contacting of the coal with the catalyst. Schlesinger et al.⁽⁷⁾ found that results approaching those of impregnated MoS₂ could be obtained by thoroughly mixing a powdered catalyst with the coal using a ball-mill.

The results from the study of Schlesinger et al. suggests that it is difficult to determine if the mode of catalyst addition is important because of enhanced coal/catalyst contacting or if the mode of addition affects catalyst dispersion (i.e. the physical properties, surface area and/or particle size) of the ultimate catalyst. Other studies⁽⁸⁻¹¹⁾ have shown the importance of catalyst dispersion in determining the activity of unsupported molybdenum catalysts. Related work⁽¹²⁾ demonstrated the importance of catalyst dispersion on iron catalyst activity.

The objective of this study was to decouple the coal/catalyst contacting and catalyst dispersion and to quantify the importance of both variables.

EXPERIMENTAL

Feedstocks: The coals selected for use in this study had similar composition, but quite different particle sizes. Analyses of these coals, DECS-6 and DECS-17 Blind Canyon bituminous coals from the Department of Energy Coal Sample Base at Pennsylvania State University, are summarized in Table 1. Ammonium heptamolybdate (AHM), MoS₂, ferric nitrate, and elemental sulfur were obtained from Fisher Chemical Co., tetrahydrofuran (THF), and ammonium tetrathiomolybdate (ATTM) from Aldrich Chemical Co. PANASOL[®], a mixture of alkylated naphthalenes, was obtained from Crowley Chemical Co.

Coal Impregnation: Coal was impregnated with aqueous AHM using an incipient wetness technique. In the present study, 10 g of coal was wetted with an aqueous solution containing 6% by weight of molybdenum as AHM. After standing for 0.5 h, the water was removed from the wetted coal by vacuum drying at 40°C to a constant (10g) weight of coal. In some experiments where the coal was swelled during impregnation, the amount of solution necessary for incipient wetness was augmented by THF in the ratio of 9:1 THF to solution. The coal/catalyst solution/THF mixture was left to stand overnight and vacuum dried to remove the water and THF.

Catalyst Penetration and Dispersion Measurements: When coal is impregnated with a catalyst precursor, the precursor penetrates each coal particle to a limited extent. The depth of penetration into the coal particle was measured by two methods; X-ray photoelectron spectroscopy (XPS) and energy dispersive spectroscopy/scanning electron microscopy (EDS/SEM). A model LHS-10, Leybold XPS was used to determine the concentration of Mo on the surface of impregnated coal particles. The penetration of coal by the precursor was estimated by comparing the surface concentration with the overall Mo concentration impregnated into the coal. Measurements of the Mo penetration into the coal particles were made using an ETEC Autoscan Model U-1 SEM. The X-ray maps obtained from the SEM had an analytical spatial resolution on the order of 1 μm^3 . These measurements were a direct check of the Mo penetration obtained from the XPS examinations.

Catalyst dispersion was characterized by transmission electron microscopy (TEM), SEM,

X-ray diffraction (XRD), and BET surface area. A JEOL 200CX TEM was used to obtain images of MoS_2 crystallites. Similarly, SEM was used to obtain catalyst images and X-ray maps of a larger size range than those obtained by TEM. XRD analysis of the MoS_2 was performed using a Rigaku computer-controlled diffractometer to estimate MoS_2 crystallite size. The XRD size estimate was confirmed by TEM examinations of the same material. BET surface area was measured using a Coulter OMNISORB 100 CX. Nitrogen adsorption was used for these measurements.

Liquefaction Studies: Experiments were conducted by adding 3.3 g of coal or impregnated coal to the 40-mL tubular microautoclave reactor with 6.6 g of PANASOL[®]. In experiments in which catalysts were used, 1000 ppm of Mo was added. The reactor was charged with the desired pressure of hydrogen and sealed. The pressurized reactor was then heated, either rapidly, 1-2 minutes, or slowly, 40 minutes, to the liquefaction temperature (425°C) in a fluidized sandbath. The liquefaction conditions were 425°C, 1000 psig H_2 (cold), added sulfur, and 0.5 h. Following the liquefaction period (0.5 h), the reactor was cooled and depressurized. Coal conversion was calculated from the solubility of the coal-derived products in tetrahydrofuran (THF) and in heptane as determined by a pressure filtration technique.⁽¹³⁾

Catalyst Preparation: Batches of powdered MoS_2 , for addition as a dispersed catalyst, were prepared in microautoclaves and 1-L autoclaves. The conditions used in these preparations were similar to the conditions used in the liquefaction studies. In the microautoclave, the precursor, aqueous AHM, powdered AHM, aqueous ATTM, or powdered MoS_3 , were added with PANASOL[®]. The conditions were 425°C, 1000 psig H_2 (cold), added sulfur, and 0.5 h (both slow and rapid heat-up of the reactor were tested). In the 1-L flow-through reactor the conditions used were 400 g PANASOL[®], 10000 ppm Mo (based on PANASOL[®]) as aqueous AHM (12% by weight) or aqueous ATTM (3% by weight), 2,500 psig, 4 SCFH of $\text{H}_2/3\%\text{H}_2\text{S}$, 400°C, and 0.5 h. In all cases the catalyst was recovered as the solids from a THF extraction of the reaction products.

RESULTS:

Catalyst Dispersion: MoS_2 samples were prepared with different average particle and/or crystallite sizes and surface areas. The size and surface area were varied by using different precursor types, heat-up rates, and reactor types. The XRD-determined crystallite size and surface area for the different MoS_2 preparations are shown in Table 2. Introduction of the precursors as aqueous solutions appeared to give higher levels of dispersion than the powdered precursors. The 1-L stirred autoclave resulted in significantly higher dispersion than the shaken microautoclaves and aqueous AHM in the 1-L autoclave resulted in higher MoS_2 dispersion than aqueous ATTM (by BET surface area but not by XRD). The catalyst powder produced in the 1-L autoclave had an elemental composition of 50 wt% C and 50 wt% MoS_2 . SEM and TEM analysis qualitatively confirmed the relative levels of dispersion determined by BET and XRD. TEM examination of the MoS_2 produced from AHM and ATTM in the 1-L autoclave provided some explanation for the discrepancy in surface area and XRD crystallite size for the two catalysts. For the MoS_2 from AHM, the TEM analysis indicated that the particles were less than 25 Å (single layers) and were poorly crystalline. For the MoS_2 from ATTM, the TEM analysis indicated that the particles were small (perhaps less than 25 Å) but there appeared to be a longer range structure of the carbonaceous material associated with the MoS_2 that may have accounted for the lower surface area.

Liquefaction tests were made using the various MoS_2 samples with different levels of dispersion. The results are shown in Figure 1. The 0 m²/g surface area cases in Figure 1 represent data for no catalyst added. It appears that there is a linear relationship between catalyst surface area and conversion to THF and heptane soluble products. A similar trend was observed in plotting coal conversion with respect to inverse crystallite size (Figure 2). For the high surface area MoS_2 , the inverse crystallite size was calculated based on single layer MoS_2 with a stack height of 6 Å. These results indicate that at a constant level of addition of MoS_2 , the physical properties of the MoS_2 were very important in determining the ultimate activity observed. Note that for the one case of MoS_2 from ATTM in the 1-L autoclave, the activity was higher than predicted on the basis of surface area and lower than predicted on the basis of inverse crystallite size.

Coal/Catalyst Contacting: The DECS-6 and DECS-17 Blind Canyon coal were physically mixed with MoS_2 , impregnated with AHM by incipient wetness, or impregnated with AHM by incipient wetness with swelling (using THF) during impregnation. The effect of the method of catalyst addition on liquefaction activity is shown in Figure 3. The selection of powdered MoS_2 for the physically mixed comparison was made based on evaluation of the dispersion of MoS_2

resulting from impregnation. The XRD analysis of MoS₂ resulting from impregnated AHM treated at liquefaction conditions indicates a crystallite size of 46 Å thickness to 103 Å width (46/103Å). Swelling had little effect on this size (47/90Å). The physically mixed MoS₂ powder used for comparison had a crystallite size of 25/77Å. The results presented in Figure 3 indicate that the method of catalyst addition influences the ultimate observed activity. One explanation for the enhancement in activity observed with the impregnation techniques is that these techniques result in penetration of the coal particle by the catalyst precursor. The penetration depths of catalyst into the coal for these cases along with the physically mixed cases are shown in Table 3. Also shown in Table 3 is the fractional volume of coal that is also occupied by the catalyst (calculated from the penetration depth). It is apparent from this table that impregnation results in enhanced penetration of the coal particle by the catalyst. EDS/SEM analyses of these samples directly confirmed the relative penetration depths calculated from XPS data. Figures 4 and 5 present coal conversion as a function of penetration depth and fractional volume of coal occupied by the catalyst. The results indicate that the coal conversion is not so much a function of the penetration depth as it is a function of the fractional volume of coal occupied by catalyst, essentially a function of the extent of contacting between coal and catalyst. However the most significant difference in activity occurred between physical mixing and impregnation. Subtle differences (at most) were observed between the two modes of impregnation.

CONCLUSIONS:

The results of this study indicate that for catalysts with similar properties (size and surface area), the mode of catalyst addition affected the observed performance. Better catalyst performance was observed with impregnation than physical mixing. Also, for similar modes of catalyst addition, increasing the catalyst dispersion by decreasing the catalyst particle size (or increasing the surface area) results in higher observed activity. The results suggest that any comparison of catalysts should account for differences in catalyst dispersion and the mode of catalyst addition.

DISCLAIMER:

Reference in this manuscript to any specific commercial product, process, or service is to facilitate understanding and does not necessarily imply its endorsement or favoring by the United States Department of Energy.

REFERENCES:

1. Derbyshire, F.J., Catalysis in Coal Liquefaction: New Directions for Research IEA CR/08 London, UK: IEA Coal Research, June 1988.
2. Chien, P.L., Chao, H., and Weller, S.W., *Ind. Eng. Chem. Proc. Des. Dev.*, **22**, pp 660-662 (1983).
3. Weller, S.W., *Proceedings: Fourth International Conference on the Chemistry and Uses of Molybdenum*, H.E. Barry and C.N. Mitchell, Ed., pp 179-186 (1989).
4. Derbyshire, F.J., Davis, A., Lin, R., Stansberry, P.G., and Terrer, M.T., *Fuel Processing Technology*, **12**, pp 127-141 (1986).
5. Joseph, J., *Fuel*, **70**, pp 459-464 (1991).
6. Artok, L., Davis, A., Mitchell, G.D., and Schobert, H.H., *Fuel*, **71**, pp 981-991 (1992).
7. Schlesinger, M.D., Frank, L.V., and Hiteshue, R.W., Bureau of Mines Report No. 6021 (1961).
8. Frety, R., Breyesse, M., Lacroix, M., and Vrinat, M., *Bull. Soc. Chim. Bulg.*, **93**(8,9), pp 663-672 (1984).
9. Busetto, L., Ianibello, A., Pincolini, F., and Trifiro, F., *Bull. Soc. Chim. Bulg. Proc. Des. Dev.*, **90**(12), pp 1233-1248 (1981).
10. Ratnasamy, P. and Leonard, A.J., *Journal of Catalysis*, **26**, pp 352-358 (1972).
11. Utz, B.R., Cugini, A.V., and Frommell, E.A., Novel Materials in Heterogeneous Catalysis, Baker, R.T., and Murrell, L.L., Ed., ACS Symposium Series No. 437 Chapter 27 (1989).
12. Cugini, A.V., Krastman, D., Martello, D.V., Frommell, E.F., Wells, A.W., and Holder, G.D., *Energy & Fuels*, **8**(1), pp 83-87 (1994).
13. Utz, B.R., Narain, N.K., Appell, H.R., and Blaustein, B.D., Coal and Coal Products: Analytical Characterization Techniques, Fuller, Jr., E.L., Ed. ACS Symposium Series No. 205, p. 225 (1982).

Table 1. Analyses of Feed Coals

	Blind Canyon, DECS-6	Blind Canyon, DECS-17
Proximate Analysis, wt% as received		
Moisture	4.73	3.7
Volatile Matter	42.4	45.0
Fixed Carbon	47.3	44.9
Ash	5.6	6.3
Ultimate Analysis, wt% moisture free		
Carbon	76.5	76.2
Hydrogen	5.9	5.8
Nitrogen	1.5	1.3
Sulfur	0.4	0.4
Oxygen (Diff.)	9.9	9.6
Ash	5.8	6.8
Sulfur Forms, wt%		
Sulfate	0.01	0.01
Pyritic	0.02	0.02
Organic	0.37	0.41
Average Particle Size, μm	397	84

Table 2. MoS_2 Physical Properties

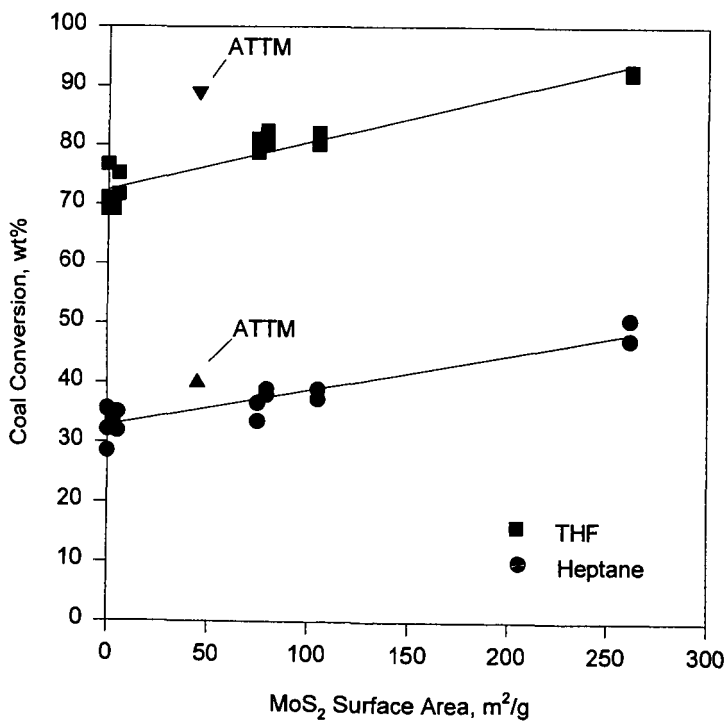
Precursor	Gas, Heat-up	Reactor Type	BET Surface Area, m^2/g	XRD Crystallite Size, \AA Height/Width
MoS_2	na	na	2.7	very ordered
AHM, Powdered	$\text{H}_2/\text{H}_2\text{S}$ slow	Microautoclave	na	very ordered
ATTM	H_2 fast	Microautoclave	79.5	26 / 78
ATTM	N_2 fast	Microautoclave	84.4	27 / 78
ATTM	H_2 slow	Microautoclave	74.9	30 / 81
MoS_3	H_2 fast	Microautoclave	104.8	25 / 77
AHM (aq)	$\text{H}_2/\text{H}_2\text{S}$ slow	Microautoclave	na	46 / 103
AHM (aq)	$\text{H}_2/\text{H}_2\text{S}$ slow	1-L Autoclave	262.0	--* / 25
AHM (aq)	$\text{H}_2/\text{H}_2\text{S}$ slow	1-L Autoclave	243.0	--* / 25
ATTM (aq)	$\text{H}_2/\text{H}_2\text{S}$ slow	1-L Autoclave	45.0	--* / 25

*001 line was not observed.

Table 3. Effect of Mode of Addition and Coal Particle Size on Penetration Depth and Percent of Coal Contacted.

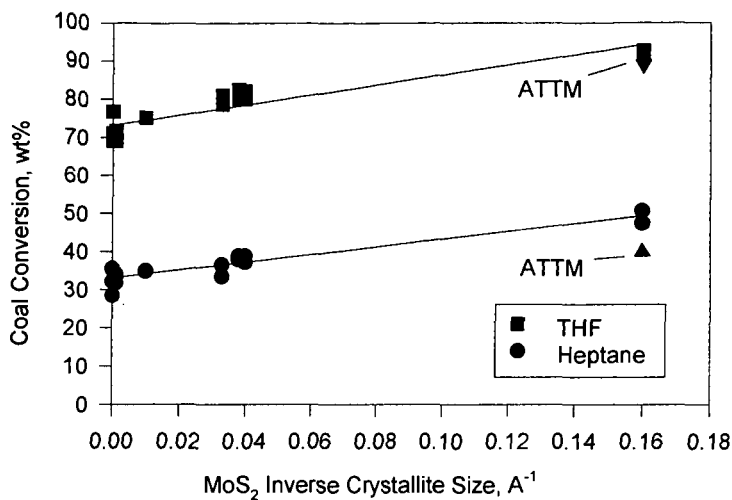
Particle Size, μm	Mode of Addition	Penetration Depth, μm	Percent of Coal Contacted, %
397	Physically Mixed	1	1.5
84	Physically Mixed	1	7.0
84	Aqueous Impregnation	4.7	29.7
397	Aqueous Impregnation	9.4	13.6
84	THF-Assisted Aqueous Impregnation	13.7	69.5
397	THF-Assisted Aqueous Impregnation	16.0	22.3

Figure 1. Effect of MoS_2 Surface Area on Blind Canyon Coal Conversion



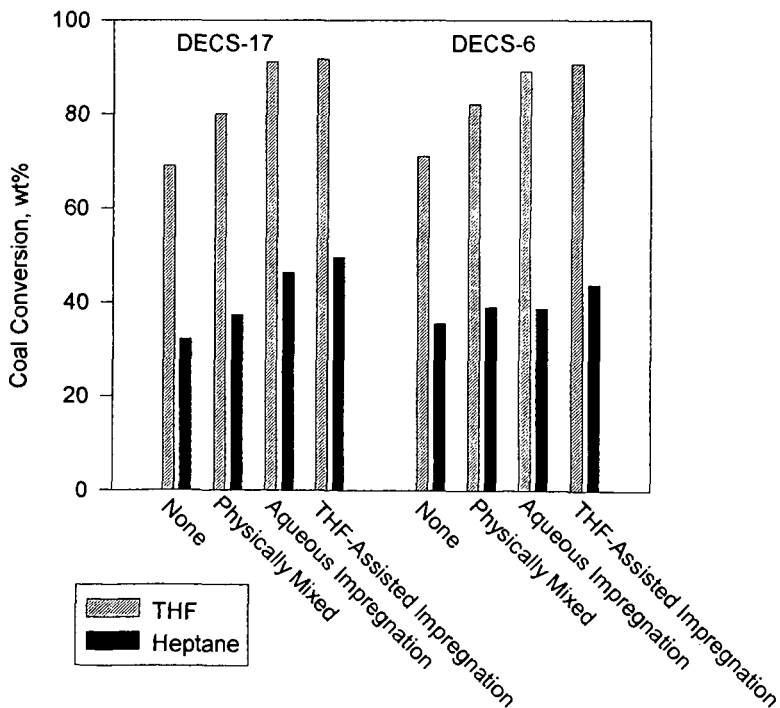
2:1 PANASOL to Coal, 425°C , 1000 ppm Mo, 1000 psig H_2 (cold) and 0.5 h

Figure 2. Effect of MoS_2 Inverse Crystallite Size on Blind Canyon Coal Conversion



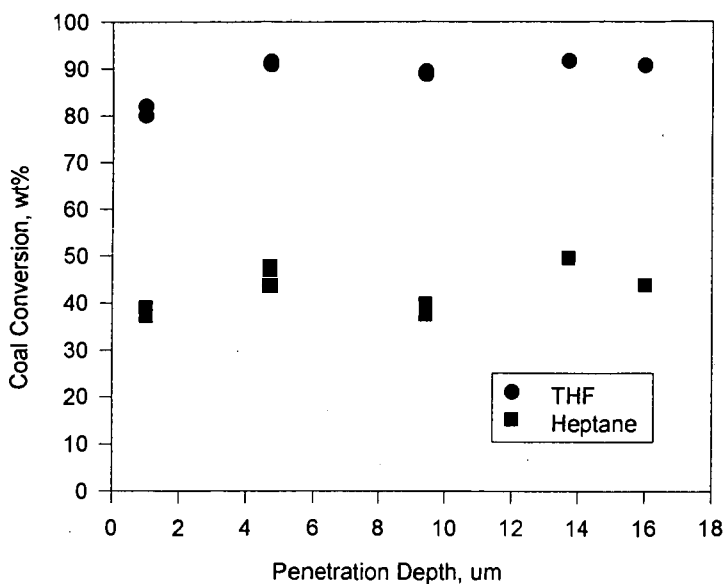
2:1 PANASOL to Coal, 425°C , 1000 ppm Mo, 1000 psig H_2 (cold), and 0.5 h

Figure 3. Effect of Method of Catalyst Addition



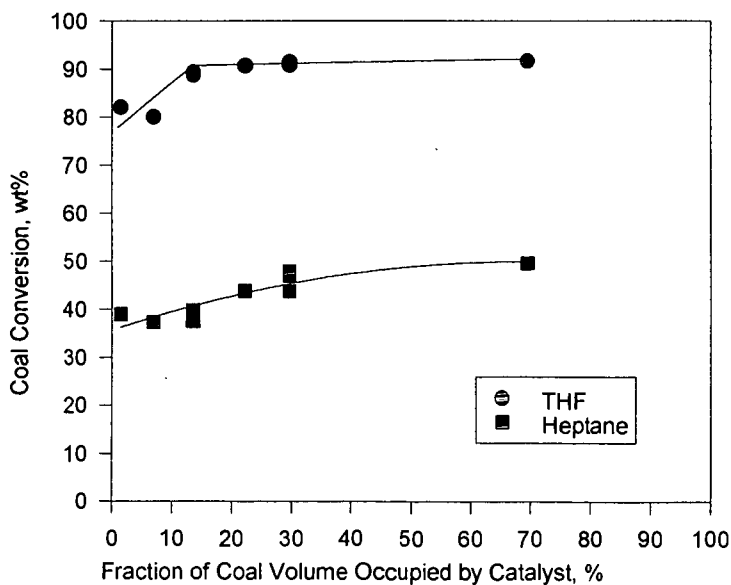
2:1 PANASOL to Coal, 425°C , 1000 ppm Mo, 1000 psig H_2 (cold), and 0.5 h

Figure 4. Effect of Penetration Depth on Blind Canyon Coal Conversion



2:1 PANASOL to Coal, 425°C, 1000 ppm Mo, 1000 psig H₂ (cold), and 0.5 h

Figure 5. Effect of Coal Contacted on Blind Canyon Coal Conversion



2:1 PANASOL to Coal, 425°C, 1000 ppm Mo, 1000 psig H₂ (cold), and 0.5 h

Preparation of Highly Dispersed NiMo Catalysts Supported on Carbon Black Particles of Hollow Spheres

Kinya Sakanishi, Haru-umi Hasuo, Isao Mochida, and Osamu Okuma^{*)}

Institute of Advanced Material Study, Kyushu University,

Kasuga, Fukuoka 816, Japan

^{*)} Polymer & Chemical Technology Lab., Kobe Steel, Ltd.,

Kobe, Hyogo 651-22, Japan

Abstract

One of unique carbon blacks, Ketjen Black(KB) which has extremely high surface area and low specific gravity, was selected as a catalyst support to prepare a highly dispersed NiMo catalyst for the hydrogenation of 1-methylnaphthalene(1-MN) using a magnetic-stirred autoclave of 50 ml capacity under the standard conditions of 380°C, 40 min, and 10 MPa H₂ reaction pressure. The catalyst, prepared from Mo dioxycethylacetone (MoO₂-AA) and Ni(OAc)₂(Ni acetate) in their methanol solution by successive impregnations of Mo(10 wt%) and Ni(2 wt%), provided the highest conversion of 84 % to methyltetralins. Combinations of metal salts soluble in organic solvent, impregnation solvents, and surface properties of carbon black are suggested to be very important for the preparation of highly active catalysts. The nitric acid treatment introduced a large number of oxygen functional groups to the carbon black to improve the dispersion of water-soluble metal salts. It is also noted that KB-supported NiMo catalysts showed much higher activity for the present hydrogenation than a commercial NiMo/Al₂O₃.

Introduction

NiMo and CoMo catalysts supported on alumina extrudates have been extensively applied to the petroleum refineries as hydrotreating catalysts. Alumina is believed one of the best supports because it has large surface area for high dispersion of metals and high mechanical strength for the utilization to the conventional fixed bed flow-reactors. However, such alumina-supported Mo-based catalysts often suffer coking and plugging problems due to the acidity of alumina and the limited activity for the heavy polyaromatic hydrocarbons.¹⁻³⁾ Hence, recently Ca-modified NiMo/Al₂O₃ and fine particle Mo catalysts used in dispersed phase as well as the modified aluminas of controlled surface properties have been developed for the suppression of catalyst deactivation due to the coke formation.⁴⁻⁶⁾

Titania and carbon supports have attracted much attention for the preparation of anti-coking Mo-based catalysts because of their moderate polarity and metal dispersion ability⁷⁻¹⁰. Carbon supported catalysts can be recovered after the reactions by gravimetric separation due to their low specific gravity and hydrophobic properties for phase separation^{11,12}.

In the present study, Ketjen Black(KB), one of unique carbon blacks with extremely high surface area and low specific gravity, was selected as the support for NiMo. Ketjen Black(KB) particles have hollow spheric structure which brings about their extremely high surface area of ca. 1000 m²/g for high dispersion of active species and low specific gravity for catalyst recovery.¹³ Fine sphere without pore may be most suitable for the catalyst support for the heavy hydrocarbon. Carbon blacks have been reported to exhibit some catalytic activity for hydrocracking reaction due to its positively charged surface and high surface area with functional groups.^{14,15}

Such KB-supported NiMo catalysts are one of the most promising catalysts which have the fairly large activity for hydrogenation and liquefaction at the least amount of catalyst with the function for the recovery by gravimetric separation.

Experimental

Some properties of Ketjen Black(KB) ED and JD used in the present study are summarized in Table 1. Ni, Mo-supported KB catalysts (NiMo/KB) were prepared by impregnating methods using Ni(NO₃)₂ or Ni(OAc)₂ as Ni salts, and (NH₄)₆Mo₇O₂₄, Mo(CO)₆ or Mo dioxycetylacetonate (MoO₂-AA) in water, methanol and their 9:1 mixture, or n-hexane according to the solubility of the salts. The catalyst precursors were dried at 120°C for 12 h in vacuo and presulfided in 5% H₂S/H₂ flow at 360°C for 3 h prior to the reactions. KB was pretreated in conc. nitric acid at 80°C for 1 h followed by filtration, repeated washing with water, and drying at 120°C in vacuo. The nitric acid-treated KB JD was abbreviated as KB JD-O, which was used for improved dispersion of metal species. A commercially available NiMo/Al₂O₃(KF-842) provided by Nippon Ketjen Co., was used for the comparison with the KB-supported NiMo catalysts.

1-Methylnaphthalene(1-MN; 1.0g), decalin(9.0g) and catalyst (5 wt% based on 1-MN) were charged into the autoclave of 50 ml capacity. Standard conditions for the hydrogenation were 380°C -40min and 10MPa H₂ of reaction pressure. The conversion to hydrogenated products of 1- and 5-methyltetralins and their selectivity were determined by GC and GC-MS to estimate the hydrogenation activity of the catalysts.

Results and Discussions

The hydrogenation activities of KB-supported NiMo catalysts are shown in Figure 1. KB JD which has a larger surface area of $1270 \text{ m}^2/\text{g}$ exhibited a little higher activity for 1-MN hydrogenation than KB EC($800 \text{ m}^2/\text{g}$). The nitric acid-treated KB JD (KB JD-O) provided its supported NiMo catalyst with higher hydrogenation conversion of 60 %, increasing the selectivity to 1-methyltetralin (1-MT). The nitric acid treatment of carbon black introduced oxygen functional groups, improving the dispersion of metal salts on the carbon black support.

Figures 2 shows the effects of the species of Ni and Mo salts using KB JD support on the hydrogenation activity. The Mo species were very influential on the catalytic activity in combination with $\text{Ni}(\text{NO}_3)_2$ and KB JD support.

The combination of MoO_4^{2-} AA with $\text{Ni}(\text{NO}_3)_2$ in methanol solvent improved the hydrogenation conversion upto 82% ,suggesting that the balanced solubilities of Ni and Mo salts in impregnation solvent may be very important for preparing the highly dispersed NiMo catalyst on KB.

The activities of KB-supported NiMo catalyst are compared with a commercial $\text{NiMo}/\text{Al}_2\text{O}_3$ catalyst(KF-842) in Figure 3. The KB-supported NiMo catalyst of the highest activity, prepared from the successive impregnations of MoO_4^{2-} -AA and $\text{Ni}(\text{OAc})_2$ in methanol supported on KB JD, provided the 1-MN conversions of 84% and 47% respectively by the catalyst amounts of 5 wt%and 1%,respectively. On the other hand, powdered the commercial $\text{NiMo}/\text{Al}_2\text{O}_3$ (60mesh pass) exhibited a lower conversion when 5 wt% of the catalyst was applied. The reaction rates of KB-supported and commercial NiMo catalyst under conditions of 380°C , 10MPa H_2 reaction pressure by 1wt% catalyst amount are $v = 1.7949 \times 10^{-4}$ and 4.1287×10^{-5} , respectively. The KB catalyst has about 4.4 times more active than that of the commercial catalyst (see Figure 4).

Figures 5 and 6 show the effects of reaction pressure and temperature on 1-MN hydrogenation for NiMo/KB and KF-842. The KB-supported NiMo catalyst exhibited sharp increase of activity by increasing pressure to 7.0MPa H_2 . Further increase of pressure increased moderately. In contrast, KF-842 did very moderate increase upto 10MPa.

The NiMo/KB showed significant activity at 320°C and increased its activity at higher temperature upto 360°C . Further higher temperature reduced the activity probable due to equilibrium limitation. KF-842required to show its significant activity.

Conclusion

KB supported NiMo was found very active for the hydrogenation of 1-methylnaphthalene, exceeding very much a commercial NiMo alumina catalyst of similar metal loading level. The activity at lower temperature and pressure should be noted.

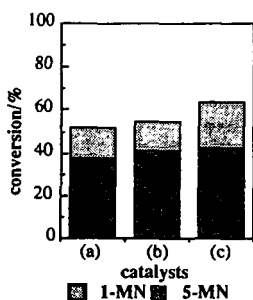
Kind and pretreatment of KB and supporting procedure were influential on the catalytic activity. The larger surface tends to give higher activity. The oxidation treatment was effective for the impregnation from the aqueous solution, while the impregnation from the organic solution gave the highest activity to the as-received KB with organic soluble salts of MoO_3 -AA and $\text{Ni}(\text{OAc})_2$.

References

- 1) Groot, C.K., de Beer, V.H.J., Prins, R., Stolarski, M., Niedzwiedz, W.S., *Ind. Eng. Chem. Prod. Res. Dev.*, 1986, 25, 522-530.
- 2) Hillerova, E., Vit, Z., Zdrzil, M., Shkuripat, S.A., Bogdanets, E.N., Startsev, A.N., *Appl. Catal.*, 1991, 67, 231-236.
- 3) Louwers, S.P.A., Prins, R., *J. Catal.*, 1992, 133, 94-111.
- 4) Kageyama, Y., Masuyama, T., *Proc. Int. Conf. Coal Sci.*, 1985, p.157-160.
- 5) Paradhan, V.R., Herrick, D.E., Tierney, J.W., Wender, I., *Energy & Fuels*, 1991, 5, 712.
- 6) Kim, S.I., Woo, S.I., *J. Catal.*, 1992, 133, 124-135.
- 7) Mochida, I., Oishi, T., Korai, Y., Fujitsu, H., *Ind. Eng. Chem. Prod. Res. Dev.*, 1984, 23, 203.
- 8) Japanese Patent, Showa 57-132547 (1982).
- 9) Duchet, J.C., van Oers, E.M., de Beer, V.H.J., Prins, R., *J. Catal.*, 1983, 80, 386-402.
- 10) Derbyshire, F.J., DeBeer, V.H.J., Abotsi, G.M.K., Scaroni, A.W., Solar, J.M., Skrovanok, D.J., *Appl. Catal.*, 1986, 27, 117.
- 11) Schmitt, J.L., Castellion, G.A., *US Patent* 3,997,473 (1976).
- 12) Schmitt, J.L., Castellion, G.A., *US Patent* 4,032,435 (1977).
- 13) Nelson, J.R., Wissing, W.K., *Carbon*, 1986, 24, 115-121.
- 14) Farcasiu, M., Smith, C., *Energy & Fuels*, 1991, 5, 83.
- 15) Farcasiu, M., Smith, C., *Prepr. ACS Div. Fuel Chem.*, 1990, 35, 404.

Table 1 Some properties of Ketjen Blacks

	KB EC	KB EC600JD
Surface area(m ² /g)	800	1270
Volatile matter(%)	0.5	0.7
pH	9.0	9.0
Particle size (nm)	30	30
Apparent density (g/l)	145	115
Ash (%)	0.1	0.1



Reaction conditions

Reaction temp.: 380°C
 Reaction press.: 10MPa
 Heating rate : 10°C/min
 catalyst : 5wt% (based on 1-MN, simultaneous
 impregnation from Ni(NO₃)₂ and (NH₄)₆Mo₇O₂₄)

catalysts support

- (a) KB EC
- (b) KB JD
- (c) KB JD-O

Fig.1 Effect of support species on 1-MN Hydrogenation(HYD).

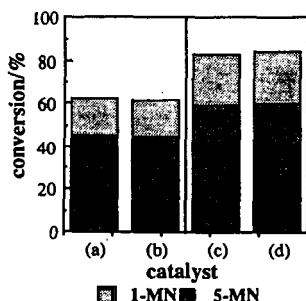


Fig.2 Effect of metal salts combination in organic solution on 1-MN HYD.

metal salts

- (a) Mo(CO)₆, Ni(NO₃)₂
- (b) Mo(CO)₆, Ni(OAc)₂
- (c) MoO₂-AA, Ni(NO₃)₂
- (d) MoO₂-AA, Ni(OAc)₂

support : KB JD

successive impregnation in methanol

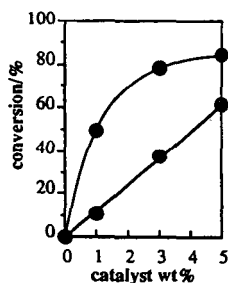
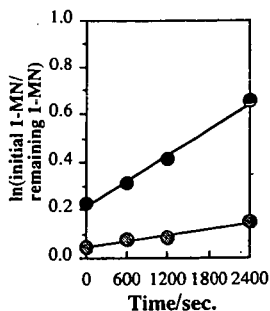


Fig.3 Effect of amount of catalysts on 1-MN HYD.

- KF-842 (60mesh under)
- Ni-Mo/KB JD
- (MoO₂-AA, Ni(OAc)₂)

(Other conditions are same as Fig. 1)



Reaction conditions

Reaction temp.: 380°C
 Reaction press.: 10MPa
 Heating rate : 10°C/min
 catalyst : 1wt%(based on 1-MN)

Ni-Mo/KB JD $\nu = 1.7949 \times 10^{-4}$
 KF-842 $\nu = 4.1287 \times 10^{-5}$

- KF-842 (60mesh under)
- Ni-Mo/KB JD
(MoO₂-AA, Ni(OAc)₂)

Fig. 4 Comparison of commercial NiMo and KB-supported NiMo catalysts in the hydrogenation of 1-MN

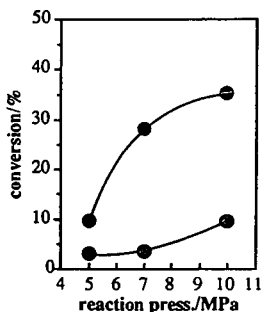


Fig. 5 Effect of reaction pressure on 1-MN HYD.

- KF-842 (60mesh under)
 - Ni-Mo/KB JD
(MoO₂-AA, Ni(OAc)₂)
- Reaction pressure : 5.0 ~ 10MPa
 Reaction Time : 40min

(Other conditions are same as Fig. 4)

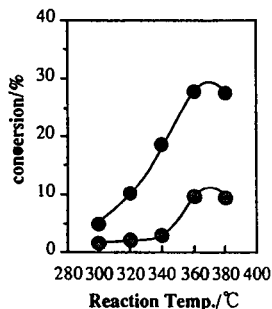


Fig. 6 Effect of reaction temperature on 1-MN HYD.

- KF-842 (60mesh under)
 - Ni-Mo/KB JD
(MoO₂-AA, Ni(OAc)₂)
- Reaction temp.: 300~380°C
 Reaction time : 40min

(Other conditions are same as Fig. 4)

The Activity of Nanoscale Iron Oxide for Model Compound Reactions

G. T. Hager, K. D. Greer, E. N. Givens, F. J. Derbyshire
Center for Applied Energy Research
University of Kentucky
3572 Iron Works Pike
Lexington, KY 40511-8433

Abstract

Iron based catalysts have long been known to enhance the conversion in a direct coal liquefaction process. Attempts to increase the moderate activity of these catalysts have focussed on reducing particle size, enhancing and maintaining dispersion, and modifying the structure by addition of promoters. Sulfated hematites have been reported in the literature to exhibit significant activity for low rank coal liquefaction. The use of promoter metals such as molybdenum and tungsten has been shown to further enhance the catalytic effect. The superacidity of these particles has been suggested as a possible explanation for their high activity. The purpose of this study was to ascertain the effect of various promoter metals, both individually and in combinations on different types of reactions commonly associated with coal liquefaction.

Introduction

Iron based dispersed catalysts have been utilized in direct coal liquefaction since the early 1900's, particularly for the liquefaction of low rank coals. Continuing efforts have been directed at improving the activity of these catalysts without significant increases in cost. These efforts have focussed on reducing the particle size, enhancing and maintaining the dispersion, and modifying the structure by addition of promoters.

Several studies have demonstrated the high activity of sulfated hematite for both coal liquefaction, and coprocessing of coal with a petroleum resid.^{1,2,3} The use of molybdenum or tungsten as a promoter metal further improved the activity of these particles.^{4,5} Other research has examined nickel, cobalt, tungsten, and molybdenum as promoter metals, both individually and in combination.⁶ Molybdenum produced the largest increase in activity for singly-promoted sulfated hematite. The influence of tungsten, when used in combination with molybdenum, was essentially additive while the combination of nickel or cobalt with molybdenum exhibited synergistic effects, resulting in enhanced conversions at low promoter loading.

The role of catalysts in coal liquefaction is obscured by the complexity of the coal itself. In order to more clearly understand the role of these promoter metals in enhancing the activity of sulfated hematite catalysts for coal liquefaction, they have been studied in the reactions of selected model compounds. The activity for cleavage of the sulfur bridges may be studied by the hydrodesulfurization (HDS) of benzothiophene. Similarly, the activity for cleavage of the etheric bond may be inferred from the hydrodeoxygenation (HDO) of diphenyl ether and the activity for nitrogen removal by the hydrodenitrogenation (HDN) of quinoline. Hydrogenation (HYD) activity of the catalyst may be studied by the conversion of naphthalene to tetralin.

Experimental

Reactions were carried out using 25 ml stainless steel microautoclave reactors. The reactors were loaded with 5 g of a 5 wt% solution of reactant in hexadecane. The catalysts were loaded at 5 wt% on a reactant basis and 0.017 g dimethyldisulfide (DMDS) was added in most runs. The reactors were purged and pressurized to 800 psig (cold) with hydrogen. The loaded reactors were placed in a heated fluidized sand bath at 385°C and agitated vertically at 400 cycles/minute to minimize any mass transfer constraints. The reactions were carried out for times of 15 to 60 minutes after which the reactor was quenched in a cool sand bath.

The reaction products were removed from the reactor by washing with tetrahydrofuran. A gas chromatograph (Hewlett Packard 5890 Series 2) using both a 30 m DB-5 and a 30m carbowax column was utilized to analyze the products of the reaction. The catalyst activity was determined by the rate of model compound disappearance.

The spent catalyst was collected and stored with the product to reduce oxidation from exposure to air. The major phases present in the catalyst particles were determined by X-ray diffraction (XRD) and the average particle diameter was estimated from the peak broadening using the Debye-Scherrer relationship.

Catalyst Synthesis and Characterization

The iron based catalysts used in this study were prepared using an aqueous precipitation technique. This method involves the coprecipitation of iron and a promoter metal in the presence of sulfate ions. In this study, urea was used to effect the precipitation of ferric ammonium sulfate (iron alum), following the method of Kotanigawa et al.¹ The promoter metal molybdenum was incorporated by addition of ammonium molybdate to the iron alum solution, as described previously.⁶ Ammonium nickel sulfate hydrate and cobalt sulfate hydrate were used to add nickel and cobalt, respectively. The precipitated catalysts were filtered and dried in an air flow oven overnight and then calcined in air at 475 °C for 30 minutes.

The promoted sulfated hematite catalysts were analyzed by a variety of techniques. The results of electron microscopy analysis have shown that the catalysts consist of a loose agglomeration of particles, with acicular shape and average dimensions of ~10x50 nm. Surface areas measured by nitrogen BET adsorption were found to be in the range of 100-200 m²/g. The addition of up to 10 wt% of molybdenum had little effect on the particle size and no apparent effect on the major phase identified by XRD. The XRD spectra of the as-formed catalysts indicate that the major phase is α -FeOOH, although the crystallinity was poorly developed. After calcination the major phase was clearly identified as α -Fe₂O₃.

Elemental analysis of the sulfated hematites indicated sulfur contents of 2-6 wt%. The results of metals analysis are shown in Table 1. Molybdenum is more easily added to the catalyst resulting in a higher concentration than nickel or cobalt. XPS studies have indicated that the molybdenum is present on the surface of the particles while nickel and cobalt are substituted for iron in the particles.⁶

Results

The results of the naphthalene hydrogenation studies are shown in Figure 1. All runs were conducted with an excess of sulfur present to assure complete sulfidation of the catalyst. The unpromoted sulfated hematite resulted in an increase in conversion of ~20% over the thermal baseline. Promotion by nickel and cobalt appeared to slightly inhibit the activity of these catalysts for the hydrogenation reaction. Molybdenum had a very positive effect, producing an increase in naphthalene hydrogenation of ~50% over the unpromoted sulfated hematite after 60 minutes. This result can be related to the high concentration of molybdenum and its well known hydrogenation properties. The data indicate that the catalysts experience an initial period of low activity before the activity begins to increase, as clearly displayed by the molybdenum promoted catalyst. This induction period may correspond to the conversion of the catalyst from the oxide phase to a sulfide phase. XRD spectra of the catalyst recovered from 15 minute runs indicate that pyrrhotite is the major phase present. The activity of the catalyst prior to conversion to the sulfide may be significantly lower than the activity after conversion. Studies at shorter times should help to elucidate the rate of activation the catalysts.

The catalysts followed a similar trend for the HDO of diphenyl ether, as shown in Figure 2. Unpromoted sulfated hematite caused a significant increase over the thermal runs giving a conversion of 40% at 60 minutes. Nickel and cobalt promoters were found to have little additional effect, but molybdenum produced a significant increase to 57% after 60 minutes. The major reactions appears to involve cleavage of one of the carbon oxygen bonds resulting in the formation of equal amounts of benzene and phenol with

some further hydrogenation to cyclohexane and cyclohexanol, respectively. Only the molybdenum promoted catalyst resulted in a slight (<5%) amount of oxygen removal.

Both oxide and sulfide forms of Co/Mo supported on alumina are known to exhibit high activity for HDN reactions⁷, which may help to explain the rapid reaction rates seen in the studies of quinoline HDN, shown in Figure 3. As observed in the previous reactions, the nickel and cobalt promoters had little effect on the activity of the sulfated hematite, and all three catalysts resulted in a significant increase in conversion over the thermal baseline. Again, the molybdenum promoted catalyst had the most significant effect on rate of quinoline conversion. The main product in all the reactions was 1,2,3,4 tetrahydroquinoline and very little HDN was observed for any of the catalyst.

It has been suggested that the superacidity associated with the sulfate groups chemisorbed on the surface of the hematite particles may explain some of the catalyst function.² This type of acidity should result in significant cracking of the hexadecane solvent used in this study. Since no significant increase in cracking was observed in these experiments, it would appear that the superacid sites are no longer present under reaction conditions.

Conclusions

Sulfated hematite catalysts appear to exhibit moderate activity for hydrogenation reactions. The use of nickel and cobalt as promoter metals had only slight effect on the activity of the sulfated hematite. Molybdenum promoted sulfated hematite showed significantly higher activity than the unpromoted catalyst. This agrees well with the results from coal liquefaction experiments. From these investigations it would appear that hydrogenation and ether cleavage are relevant catalyst functions in the liquefaction of a low rank coal.

Acknowledgements

The authors would like to gratefully acknowledge support for this project received from the United States Department of Energy under contracts DE-AC22-91PC91040.

References

1. Kotanigawa, T., Yokoyama, S., Yamamoto, M. & Maekawa, Y. *Fuel* **68**, 618-621 (1989).
2. Pradhan, V.R., Tierney, J.W., Wender, I. & Huffman, G.P. *Energy & Fuels* **5**, 497-507 (1991).
3. Pradhan, V., Tierney, J.W. & Wender, I. *ACS Preprint - Fuel* **36**, 597-604 (1991).
4. Pradhan, V.R., Herrick, D.E., Tierney, J.W. & Wender, I. *Energy & Fuels* **5**, 712-720 (1991).
5. Pradhan, V.R., Hu, J., Tierney, J.W. & Wender, I. *Energy & Fuels* **7**, 446-454 (1993).
6. Hager, G.T., Givens, E.N. & Derbyshire, F.J. *ACS-Division of Fuel Chemistry Preprints* **38**, 1087-1092 (1993).
7. Gates, B.C., Katzer, J.R., & Schuit, G.C.A. *Chemistry of Catalytic Processes*, McGraw-Hill, New York 464 pp (1979).

Table 1. Elemental Analysis of Promoted Catalysts.

Promoter Metal	Promoter Concentration (wt%)
Nickel	1.8%
Cobalt	2.0%
Molybdenum	8.0%

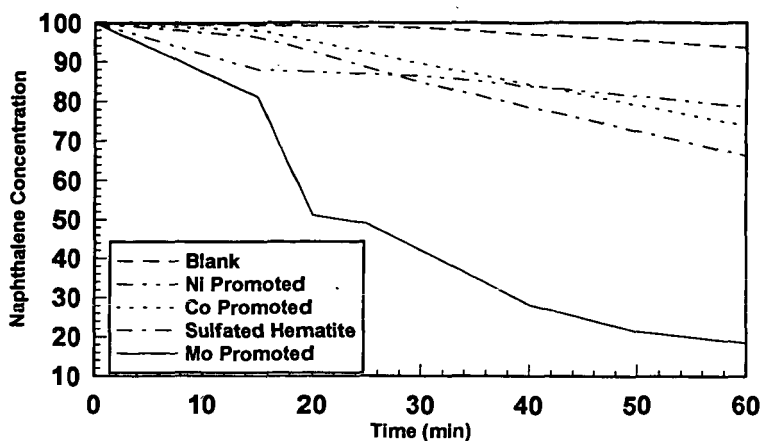


Figure 1. Hydrogenation of Naphthalene

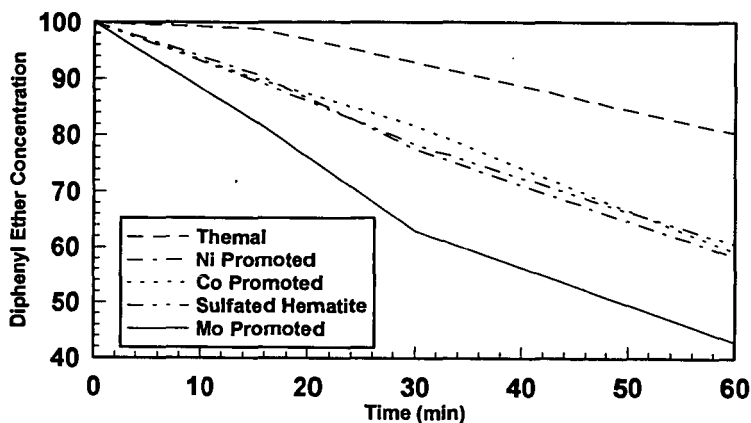


Figure2. HDO of Diphenyl Ether

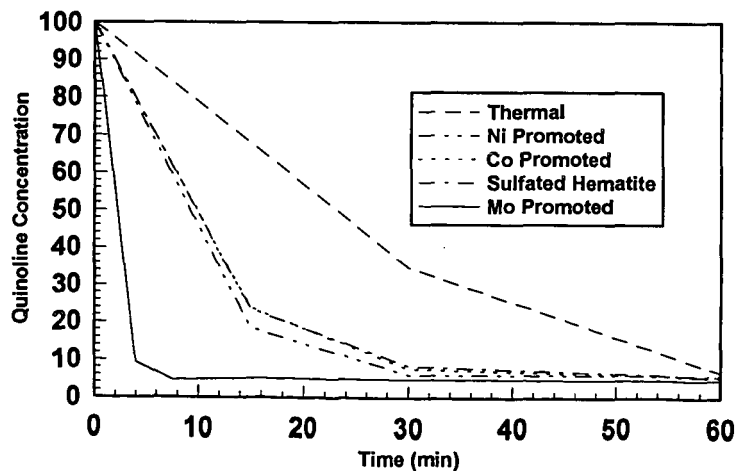


Figure 3. HDN of Quinoline